HYDRODYNAMICS AND GAS DISPERSION IN INDUSTRIAL FLOTATION CELLS

A thesis submitted to the
UNIVERSITY OF CAPE TOWN
in fulfilment of the requirement for the Degree of
MASTER OF SCIENCE IN ENGINEERING

by

DANIEL EGYA-MENSAH
BSc. (Metallurgical Engineering), UST, Kumasi

Department of Chemical Engineering
University of Cape Town
Rondebosch 7700
Cape Town
South Africa

August 1998

DECLARATION

I hereby declare that, unless indicated, all the work in this thesis was done by myself and that this dissertation has not been submitted to this or any other institution of learning in support of an application for any other degree or qualification.

D. Egya-Mensah

August 1998

ACKNOWLEDGEMENTS

My utmost gratitude goes to the Almighty God for His love, care and guidance throughout this project.

I would also like to acknowledge the following people and organisations for their support and assistance throughout my study:

Ashanti Goldfields Company, Ltd., Ghana, for supporting my studies;

Australia Mineral and Industrial Research Association (AMIRA) for the funding for this project;

Professor J.-P. Franzidis for his invaluable advice and guidance as my project supervisor;

Mr. Dave Allan Deglon for his constructive input as co-supervisor;

Mr. Bert Knopjes, Mr. Mike Valenta and Mr. Tony Streczynski, all of Lonrho Platinum Division, for their invaluable advice, interest and support during the experimental phase of this project;

Mr. Craig Jewell my project mate for his friendship, tolerance and assistance during the experimental phase of the project;

Mrs. Dee Bradshaw for her concern and encouragement;

Members of the Mineral Processing Research Unit for their help and assistance;

The entire staff and students of the Chemical Engineering Department for the friendliness and warmth; and

My family for their perpetual love, patience, encouragement and prayers.

SYNOPSIS

Solids suspension and gas dispersion studies were performed on a total of 40 industrial flotation cells of various types, sizes and duties in a Platinum Group Metal (pgm) concentrator in the North West Province of South Africa. The wide variety of cells studied included a Bateman 3-m^3 cell, Outokumpu 16-m^3 conventional and 50-m^3 TankCells, WEMCO 84, 120, 144 cells and WEMCO 144 with 164 mechanism and high-power motor.

The gas phase properties of bubble size, superficial gas velocity, air holdup and bubble surface area flux were used in characterising these cells. The bubble size was measured at six different locations in the cells using the UCT Bubble Size Analyser. The superficial gas velocity and gas holdup were measured similarly with other special designed devices. The bubble surface area flux, a new parameter for characterising the hydrodynamics and gas dispersion in flotation cells, was calculated from the ratio of the superficial gas velocity to the Sauter mean bubble size. The results of these measurements were analysed in terms of key variables including air flowrate, impeller speed and location in the cell.

The bubble size was found to increase with increasing air flowrate and decreasing impeller speed. Bubbles in the impeller zone were found to be smaller than bubbles in the quiescent zone due to significant bubble coalescence in this region. The bubble size was also found to be inversely related to the power consumption provided that this was expressed on an impeller-swept-volume basis.

The superficial gas velocity was found to increase with increasing air flowrate and impeller speed and was significantly affected by location in the cell. Differences in superficial gas velocities were observed at constant air flowrates and at different impeller speeds. This unexpected finding was attributed to differences in flow patterns in the cells.

Air holdup was found to be largely insensitive to changes in air flowrate and impeller speed in cells operating at their normal conditions. Differences in air holdup in the quiescent and turbulent zones were observed but these were more noticeable in smaller cells.

The bubble surface area flux in industrial flotation cells was found to be in the range of 50-60 $m^2/m^2/s$ irrespective of the type, size and duty of cell. However, it was observed that the bubble surface area flux could be varied by manipulating certain key cell variables such as the impeller speed and the air flowrate. The bubble surface area flux was found to increase with increasing air flowrate until reaching an optimum at sufficiently high air flowrates.

TABLE OF CONTENTS

CHAPTER 3 – BUBBLE SURFACE AREA FLUX: AN ALTERNATIVE WAY OF CHARACTERISING FLOTATION CELL HYDRODYNAMICS AND GAS DISPERSION

CHAPTER 4 - EXPERIMENTAL WORK

CHAPTER 5 - RESULTS AND DISCUSSIONS

LIST OF TABLES

LIST OF FIGURES

NOMENCLATURE

a	Specific Bubble Surface Area, mm^{-1}
A	Surface Area of Cell, m^2
A_b	Total Surface Area of Bubbles, mm^2
b	Impeller Height, m
B	Width of Wall Baffles, m
C	Clearance of Impeller from Bottom of Tank, m
D	Impeller Diameter, m
d_b	Arithmetic Mean Diameter, mm
d_P	Particle Size, m
d_{max}	Maximum Bubble Diameter, mm
d_S	Sauter Mean Diameter, mm
g	Acceleration Due to Gravity, m^2/s
h	Height of Clear Liquid, m
H	Height of Clear Liquid in the Tank, m
H_i	Height of Impeller From the Bottom of the Cell, m
Jg	Measured Superficial Gas Velocity, cm/s
J'g	Calculated Superficial Gas Velocity, (Q_g/A) cm/s
Jg_{1-6}	Average Superficial Gas Velocity for Locations 1-6, cm/s
k	First Order Flotation Rate Constant, s^{-1}
K	Constant that Depend on Particle Properties
m	Constant that Depend on Particle Properties
n_i	Number of Bubbles With Diameter d_i
N	Impeller Rotational Speed, rpm
N_1	Impeller Rotational Speed at which the 1-sec Criterion Occurs, rpm
N_c	Impeller Critical Speed for Gas Induction, rpm
N_{CD}	Impeller Critical Speed for Gas Dispersion, rpm
N_F	Impeller Rotational Speed in Flooding Regime, rpm
N_{Fr}	Froude Number, N^2D/g, Dimensionless
N_{js}	Critical Impeller Speed for Particle Suspension in Solid-Liquid System, rpm

N_{jsg}	Critical Impeller Speed for Particle Suspension in Solid-Liquid-Air System, rpm
N_p	Power Number in an Unaerated System, $P_L/\rho N^3D^5$, Dimensionless
N_{PG}	Power Number in an Aerated System, $P_{AL}/\rho N^3D^5$, Dimensionless
N_Q	Air Flow Number, Q_g/ND^3, Dimensionless
N_r	Impeller Rotational Speed for Recirculation, rpm
N_R	Impeller Rotational Speed for Onset of Gas Recirculation, rpm
N_{Re}	Reynolds Number, $ND^2\rho/\mu$, Dimensionless
$N\theta$	Mixing Time, Dimensionless
P	Particle Floatability
P_{AL}	Power Consumption in a Two-phase, Liquid-Air , Solid-Liquid Systems, W
P_{ALS}	Power Consumption in a Three-phase, Liquid-Air-Solid System,W
P_d	Probability of Particle Detachment
P_L	Power Consumption in a Single Phase Liquid System, W
P′	Static Pressure Head Above Impeller, N/m^2
Q_g	Air Flowrate, m^3/s
Q_L	Liquid Flowrate, m^3/s
r	Particle Radius, mm
r_m	Radius of Largest Flotable Particle, mm
s	Dimensionless Suspension Parameter
S	Impeller Peripheral Speed, m/s
S_b	Bubble Surface Area Flux, s^{-1}
S.G.	Pulp Specific Gravity
t_c	Pulp Circulation Time, s
T	Tank Diameter, m
v	Fluid velocity, m/s
V	Tank Volume, m^3
V_b	Average Fluid Velocity near the Bottom of the Tank for Downflow Turbine Impeller, m/s
V_L	Total Volume of Bubbles, cm^3
V_R	Average Gas Recirculation Velocity, m/s
V_s	Average Fluid Velocity near the Surface of the Tank for Upflow Turbine Impeller, m/s

V_T	Average Bubble Rise Velocity, m/s
V_w	Average Fluid Velocity near the Wall of Tank, m/s
W	Impeller Blade Width, m
We_c	Critical Weber Number, Dimensionless
X	Concentration of Solids, %

Cell Notations

PR1	Primary Rougher Cell Number 1
PR2	Primary Rougher Cell Number 2
PR3	Primary Rougher Cell Number 3
PR4	Primary Rougher Cell Number 4
SR5	Secondary Rougher Cell Number 5
SR6	Secondary Rougher Cell Number 6
SR7	Secondary Rougher Cell Number 7
SR8	Secondary Rougher Cell Number 8
PS9	Primary Scavenger Cell Number 9
BC	Bateman BQ30 (3-m^3) Cell
FC	WEMCO120 (8.5-m^3) Final Cleaner Cell
UC	WEMCO 164 (10-m^3) Unit Cell
PR	WEMCO 144 (16-m^3) Primary Rougher Cell
SR	WEMCO 144 (16-m^3) Secondary Rougher Cell
SC	WEMCO 144 (16-m^3) Scavenger Cell
TC	Outokumpu 50-m^3 TankCell

Greek Letters

α	Dimensionless Impeller Discharge Coefficient
γ_{mw}	Surface Tension Forces Between Mineral and Water phases
γ_{ma}	Surface Tension Forces Between Mineral and Air Phases
γ_{wa}	Surface Tension Forces Between Water and Air phases

ε_g	Gas Holdup, %
μ_w	Viscosity of Water, Pa s
μ	Viscosity of Pulp, Pa s
θ	Static Contact Angle at the Liquid/Solid Interface
ν	Kinematic Viscosity, m^2/s
ρ	Pulp Density, kg/m^3
ρ_L	Liquid Density, kg/m^3
ρ_S	Solid Density, kg/m^3
$\Delta\rho$	$\rho_S-\rho_L$,kg/m^3
σ	Surface Tension Forces, N/m
υ^2	Mean Square Velocity Over a Distance Equal to d_{max}, $m^{-2}s^{-2}$

Trademarks

WEMCO™ is a registered trademark of the EIMCO Process Equipment Company. It is denoted by WEMCO in the thesis.

SmartCell™ is the tradename of flotation cells designed and manufactured by EIMCO. It is represented as SmartCell.

TankCell™ is the tradename of flotation cells designed and manufactured by Outokumpu. It is denoted by TankCell.

CHAPTER 1
INTRODUCTION

1.1 BACKGROUND

Froth flotation is a physico-chemical process widely used in the mining industry to separate finely divided mineral particles from gangue material by contacting these fine particles with a plume of rising air bubbles. The process of flotation can be considered as an interactive engineering system involving many complex chemical and physical processes. Klimpel (1984) has related the response of the flotation process to chemical, equipment and operational factors. Much research work has been done in the chemistry of flotation but very little attention has been devoted to the physical aspects of the process, or to the effects of machine configuration on process performance.

Consequently, the actual processes that occur in the flotation machine are still not well understood, and this has led to a proliferation of flotation machines that are built on the basis of the manufacturer's perception of the process (Harris, 1976). In contrast, in the last few decades, extensive research work has gone into investigating both hydrodynamics and gas dispersion in sparged *chemical* reactors. Based on this work, recent investigations into mechanical flotation cells, as part of the AMIRA P9K project, have established a linear relationship between the first-order, flotation-rate constant and the hydrodynamic conditions in a flotation cell (Gorain *et al*, 1997). This work was done in a specially designed, portable, 2.8-m^3 cell. Different impellers were fitted to the cell in turn, and tests were conducted over a wide range of impeller speeds and air flowrates. Bubble sizes, gas holdup and superficial gas velocities were measured at six different locations in the cell and a parameter termed the bubble surface area flux[1] was calculated from these values. The bubble sizes were measured using the UCT Bubble Size Analyser, while the gas holdup and the superficial gas velocities were measured using other, specially designed devices. It had not been possible to do this work previously because the measurement techniques were not available. The findings of work suggest that there is little correlation between the first-order flotation rate constant and the usual, cell hydrodynamic and gas dispersion parameters like the bubble size, superficial

[1] Bubble surface area flux is related to bubble size and superficial gas velocity by the expression: $S_b = 6J_g/d_s$

gas velocity and gas holdup, when they are considered individually. However, when these cell parameters are combined to determine the bubble surface area flux, a very good linear relationship with the flotation rate constant is realised, and is found to be independent of impeller type. Thus, it appears that the bubble surface area flux is potentially a good criterion for characterising the hydrodynamics and gas dispersion properties of flotation cells.

The practical implication of this finding is that the bubble surface area flux is a very important parameter with regard to the selection, optimisation and scale-up of flotation cells. However, the work to date in this area has only been done in the specially manufactured, 2.8-m^3 cell, in which the air flowrate, impeller speed and other operating variables were properly controlled. It would be interesting and very useful to measure the bubble size, gas holdup and superficial gas velocity, and to determine the bubble surface area flux, in industrial flotation cells, to see how and whether these cell parameters vary with the cell size and type, the cell geometry and the duty of the cell. In other words, it would be valuable to investigate whether the above-mentioned variables, especially the bubble surface area flux, may be used to characterise industrial flotation cells.

1.2 OBJECTIVES

The aim of this project is to characterise the hydrodynamics and gas dispersion in industrial flotation cells on the basis of bubble size, gas holdup, superficial gas velocity and bubble surface area flux. The key questions that this project seeks to address are:

- What are the range of bubble sizes, gas holdups, superficial gas velocities and bubble surface area fluxes in industrial cells?
- Do bubble size, gas holdup, superficial gas velocity and bubble surface area flux vary much in different sections of the cell?
- Do bubble size, gas holdup, superficial gas velocity and bubble surface area flux vary with cell type, size, impeller type, duty, etc.?
- How can these cell parameters, especially bubble surface area flux, be varied or increased in a cell?

Previous work in the 2.8-m^3 cell, carried out in a zinc cleaner circuit, only looked at Agitair Pipsa, Agitair Chile-X, Dorr-Oliver and Outokumpu impellers. No data was obtained for WEMCO flotations cells, which constitute the largest proportion of industrial flotation cells. Another objective of this work therefore is to investigate a number of industrial WEMCO cells of different sizes, and compare their characteristics with those of other cells in the same circuit. The work also provides an opportunity to see how the cell characteristics and particularly the bubble surface area flux are affected in a platinum group metal (pgm) ore system, which is more complex than the zinc cleaner system.

1.3 SCOPE OF THE THESIS

The work presented in this thesis represents the findings of the hydrodynamics and gas dispersion studies performed on a variety of industrial mechanical flotation cells employed on platinum concentrators. The cells studied include a 3-m^3 Bateman cell, 4.2-m^3, 8.5-m^3, 10-m^3 and 16-m^3 WEMCO cells; 16-m^3 OK conventional and 50-m^3 OK TankCells. The bubble sizes, the gas holdups and the superficial gas velocities were measured in these cells, and from the results the bubble surface area flux was determined. This bubble surface area flux was then investigated as a parameter for characterising the hydrodynamics and gas dispersion in these cells.

Chapter 2 reviews available literature on the principles of flotation and the current understanding of hydrodynamics, gas dispersion and solids suspension in two and three phase systems. Due to inadequate information in the literature on flotation machines in the areas of design and operation, a classical chemical engineering approach has been chosen to elucidate the hydrodynamics, particle suspension and gas dispersion of mechanical flotation cells. Though the design of flotation cells differs in many respects from that of chemical reactors, the fundamental principles of design of some basic components common to both are discussed in the literature review. Consequently, in this thesis, It is proposed that the flotation cell can basically be regarded as a modified, three-phase chemical reactor.

In Chapter 3, the work of Gorain and co-workers leading to the development of the k-S_b relationship has been extensively reviewed. Chapter 4 includes a brief description of the ore,

the pulp, the chemical conditions and the flowsheets describing the different process routes at each of the two concentrators where the experimental work was carried out. The chapter concludes with details of the experimental techniques and procedures which were used for the work. The results are presented in Chapter 5 together with discussion and interpretation of the results. The thesis is concluded in Chapter 6 with some recommendations for future work.

All measurements for this thesis were performed on-site on two of Lonrho Platinum Division's platinum concentrators, Karee and Eastern Platinum, near Rustenburg in the North West Province of South Africa.

CHAPTER 2
LITERATURE REVIEW

2.0 INTRODUCTION

This chapter gives a review of the literature relevant to this thesis. The chapter commences with a discussion of the principles of flotation. Hydrodynamics, gas dispersion and solids suspension in two and three phase systems are also discussed in relationship to the flotation cell. The design of some basic components and the effects of some parameters of the flotation cell in relation to the standard chemical reactor are then presented. The chapter concludes with a brief description of some of the common types of mechanically agitated flotation cells in use today.

2.1 FLOTATION OVERVIEW

The essence of the froth flotation process is the concentration of different types of fine solid particles in a liquid-solid suspension by contacting the solids with upward moving air bubbles in a flotation machine. When the solids are exposed to chemicals (collectors), a condition is created that favours the attachment of a certain portion of the solids to the air bubbles. This selected portion is then collected in a froth phase stabilised by other chemicals (frothers) and subsequently removed from the flotation vessel.

Froth flotation has wide industrial applications in chemical, biological, environmental and mining processes. In the mining industry, it is the cheapest and the most extensively used separation method to separate minerals (gold, pgm, copper, zinc etc.) from gangue materials.

The principle of froth flotation is based on the utilisation of differences in the physicochemical surface properties of the particles of various minerals. On treatment with reagents, different particles acquire different surface properties; hence, their

abilities to attach themselves to gas bubbles differ significantly. In the concentrating of minerals by flotation, the part of the mineral that is to be extracted passes into the froth product, becoming the float fraction, while the other part remains in the pulp as the unfloated fraction. When the valuable minerals are separated into the froth product, the process is called direct flotation; when the gangue is drawn into the froth phase, it is called reverse flotation. At the end of the process, whichever fraction that contains the valuable minerals is called the concentrate while the other fraction is known as the tailings.

In froth flotation, air is blown through the pulp to which flotation reagents have been added. The mineral particles in the pulp which have water-repellent surfaces, i.e., those rendered hydrophobic, attach themselves to the air bubbles as they rise through the pulp and are carried to the surface. A mineralised froth layer, filled with mineral particles attached to air bubbles, is formed. Particles of the other minerals that are readily wetted by water (hydrophilic) do not stick to the air bubbles and remain in suspension in the body of the pulp.

A particle must be able to attach itself to a bubble and be lifted to the surface of the pulp for flotation to take place. The particles must be ground to a fineness that economically liberates most of the valuable minerals (typically about 80% of the mill product passes through a 75-micron sieve). This fineness of grind may also be required so that the mass of the largest particle does not overcome the adhesion force between the particle and the bubble, causing the particle to detach from the bubble and stay in the aqueous phase. The air bubbles can only stick to the mineral particles if they can displace water from the surface of the mineral. The process of water displacement can occur when the mineral is to some extent hydrophobic.

Most minerals are not sufficiently hydrophobic or hydrophilic in their natural state and so for flotation to be effective, reagents must be added to the pulp. One type of reagent, collector, is adsorbed on the mineral surfaces and renders them hydrophobic, thereby enhancing bubble-particle attachment. A second type of reagents, frother, assists in froth formation while a third type, regulator, is used to control the flotation process.

Regulators either activate or depress mineral attachment to the air bubbles or regulate the pH of the pulp. A detailed discussion of the types of flotation reagents and their functions is presented in the sections that follow.

2.1.1 Flotation Reagents

Flotation reagents ensure that the flotation process is highly selective and efficient. They vary significantly in composition, and include organic and inorganic compounds, water-soluble substances and other materials which are practically insoluble in water. Flotation reagents can be classified as follows:

2.1.1.1 Collectors

Collectors are organic compounds that act selectively on the surfaces of certain mineral particles. Collector action concentrates on the water-mineral interface, rendering the mineral particle hydrophobic through the adsorption of molecules or ions of the collector and thus ensuring the attachment of the particles to the air bubbles.

Under these adsorption conditions, the stability of the hydrated layer that separates the mineral particle and the adjacent air bubble is reduced to the level necessary for the formation of a solid-liquid-air contact when the particle comes in to contact with a bubble, and for attachment of the bubble in a short time interval.

Most collectors have complex molecular composition. They are asymmetrical in structure and consist of two parts - polar and nonpolar - that differ in properties. The nonpolar part of the molecule is a hydrocarbon radical that has practically no reaction with water and possesses remarkable water-repellent properties: These are due to the presence in the hydrocarbon radicals of extremely weak lateral residual van der Waals forces, whereas the bond forces within the hydrocarbon chains are strong. In contrast to the nonpolar part, the polar part of the molecule has a high

reactivity with water. A typical example of such a collector with a heteropolar molecular structure is sodium oleate. During adsorption of these collectors on the mineral surface the polar parts of the molecules are aligned towards the mineral surface and the nonpolar parts towards the water phase thereby rendering the mineral water-repellent.

Collectors are generally classified according to their ionisation properties, into anion or cation collectors. A general classification of collectors can be found in Appendix A.

2.1.1.2 Frothers

Frothers are surface-active substances which concentrate at the air-water interface, helping to keep the air bubbles dispersed and preventing their coalescence. They are heteropolar molecules with polar and non-polar groups. Frothers increase the stability of the froth by stabilising the mineralised bubble as it rises to the pulp surface, thus improving the conditions for mineral-particle attachment. Furthermore, frothers provide a sufficiently stable froth to prevent undue froth breakage and returning of the floatable particles to the pulp before the froth is removed. However, it is important that the froth breaks down rapidly enough once it has been removed from the flotation machine to prevent problems that may occur in froth pumping and other downstream operations (Kelly and Spottiswood, 1982).

A very important requirement of the frother is that it should not be adsorbed on the mineral particles. If the frother adsorbs on the mineral surface, it will interfere with the collector action and hence reduce the selectivity of the collector. On the other hand, some collectors such as long chain fatty acids do exhibit frothing properties (Wills, 1988). For good plant control, the overlapping of the functions of both the collector and the frother should be kept to the minimum.

Alcohols and glycol ethers are the most widely used frothers because of their inability to adsorb on to the mineral surfaces. The modern trend in the chemical

industries is towards the production of synthetic high molecular weight alcohol frothers of closely controlled composition to enhance proper plant control and performance. Examples of some widely used synthetic frothers are: 2-ethyl hexanol and methyl iso-butyl carbinol (MIBC).

2.1.1.3 Regulators

The main purpose of this class of reagents is to enhance the effect of collectors on mineral particles, so that the selectivity of the flotation process is increased. In the presence of the regulating agent, the collector activates only those minerals that are to be collected into the froth.

Some regulators act directly on the surface of a particular mineral, enhancing the subsequent interaction of this mineral with the collector by reducing the mineral surface hydration layer and thus improving the results of flotation (Glembotski, *et al.*, 1963). This class of regulating agents is referred to as activators. For example, copper sulphate is used as an activator in sulphide flotation. Activators are generally water soluble salts that readily ionise in solution and react with the mineral surface (Wills, 1988).

In other cases, the regulating agents are adsorbed onto the mineral surfaces, creating conditions that make them unfavourable for attachment by collectors. This phenomenon is called depression and the reagents responsible for it are called depressants. A wide range of depressants exists and their actions are complex and much more difficult to understand than those of the other flotation reagents (Wills, 1988). The inorganic electrolyte depressants, namely sodium sulphide, cyanide, lime and iron sulphate, are known to depress the flotation of gold and other precious metals by reacting with the metals to form an insoluble compound which coats the mineral surface, thus preventing collector attachment. Their use is therefore to be restricted on such metals plants. The use of organic depressants such as starch, tannin, quebracho, dextrin, etc. is advised in precious metal flotation. Since the organic depressants do not ionise in solution, they form colloidal deposits

on the mineral surfaces, preventing flotation in a similar manner to slime coating of mineral particles. They are not as selective as electrolyte depressants so when added in large quantities can depress all minerals (Wills, 1988).

Another class of regulators is called pH modifiers. These reagents produce an environment suitable for flotation of some minerals but unsuitable for others. They maintain a pulp ionic composition that enhances the reactivity and stability of some flotation reagents. Li and De Bruyn (1966) have suggested that the hydroxyl or hydrogen ion concentration and, for that matter, the pH, affects the electrical double layer and zeta potential of the mineral particles, and hence the hydration of their surfaces, and its impact on flotation is very significant. Lime, sodium carbonate (soda ash) and sulphuric acid are generally used to control pulp pH.

It is worthwhile to note that this classification of reagents is by no means conclusive. Many reagents perform more than one function and thus it is not enough to classify them in one group. Some collectors have the properties of frothers and some frothers possess some collector properties. A regulating agent which is a depressant under some conditions might be an activator under other circumstances. In view of this, it is more accurate to refer to the activating or the depressive effect of a particular regulating agent in a specific environment.

2.1.2 Physical Processes that occur in Flotation

2.1.2.1 Collision

As the bubble rises through the pulp, it will encounter particles of the ore and gangue, and, provided a particle is sufficiently hydrophobic, the bubble may collide with the particle following which attachment may occur. Although the mechanism of collision in such a highly turbulent system as the flotation cell is very complex, it is clear that a solid particle must have sufficient momentum to resist the tendency to follow the streamlines of the water that flow around the bubble. Fine particles do

not posses enough momentum to break away from streamlines and so move around the bubble without any contact.

2.1.2.2 Attachment

Following collision, the bubble surface is deformed from the impact and the water film separating the bubble and the particle is thinned until it eventually ruptures. The time period over which this happens is the induction time. Attachment usually occurs at the front of the bubble and the particles adhering to the surface will slide over the surface to the rear of the bubble by the relative motion between the bubble and the liquid. King, *et al.*, (1974) have produced striking photographic evidence of this sliding action. Sutherland and Wark (1955) have also shown photographs of galena particles, in single and aggregate forms, suspended from the rear of a bubble. Particles will therefore attach to the bubble if the induction time is smaller than the sliding time. Woodburn, *et al.*, (1971) have found that the induction time decreases with decreasing bubble diameter and a similar observation has been made by Dobby (1984). Klassen and Mokrousov (1963) have reported the influence of bubble diameter on contact angle, and have also pointed out that contact angle increases with decreasing bubble diameter. A mechanism postulated by Klassen and Mokrousov (1963) to explain this phenomenon is that the greater internal pressure of a smaller bubble causes a thinner, hydrated layer on the bubble surface thereby yielding a smaller induction time and a larger contact angle. Thus smaller bubbles increase the probability of bubble-particle attachment after collision with particles.

2.1.2.3 Detachment

Turbulence and gravitational forces that act on a particle adhering to a bubble have a considerable tendency to detach the particle from the bubble. Inasmuch as turbulence is crucial in inducing particle-bubble collision, excessive turbulence can have a serious, disruptive effect on particle-bubble aggregates. A fraction of the particles that successfully adhere after particle-bubble collision will be detached while the bubbles rise to the surface of the pulp. The probability of detachment can

therefore be seen as a function of the particle size and density, and the intensity of turbulence.

Woodburn, *et al.*, (1971) have reported their findings on the effects of particle size on detachment. Their results have shown that when the bubbles are suddenly accelerated, the large particles, due to their large inertia, lag behind causing a strain on the bubble which stretches until it finally results in the particle breaking off back into the pulp. They further have shown quantitatively that the probability of detachment, P_d, for a particle of radius, r, is given by;

$$P_d = \left(\frac{r}{r_m}\right)^{1.5} \qquad (1)$$

where r_m is the radius of the largest floatable particle in the pulp.

2.1.2.4 Particle-bubble aggregate transport

When a bubble reaches the froth-pulp interface, it does not rupture immediately, but remains beneath the froth for some time while the liquid film separating the two phases drains away gradually (Jameson, *et al.*, 1977). By bubble crowding effects, new bubbles rising into the froth zone arrive behind the one in question, pushing it further into the froth zone while still carrying its load of ore with it. The liquid film drainage and the rupture of bubbles with age cause some of the particles to return to the pulp in the cell. Solids enrichment is said to be enhanced in the froth phase as drainage continues (Klassen and Mokrousov, 1963). The froth is then transported, carrying its trapped particles, out of the flotation vessel. The rate at which froth is transported from the flotation vessel is dependent on a number of factors, principal of which are the rate of aeration, pulp chemistry and cell geometry.

2.1.3 Hydrophobicity and Contact Angle

Hydrophobicity in flotation refers to the ability of the mineral particle to repel water from its surface, while hydrophilicity refers to the opposite. A method of quantifying the degree of hydrophobicity of a mineral particle is by measuring the contact angle, θ, between the air bubble and the mineral particle. Figure 2.1 is a classical illustration of three-phase contact between water, an air bubble and a smooth ideal mineral surface.

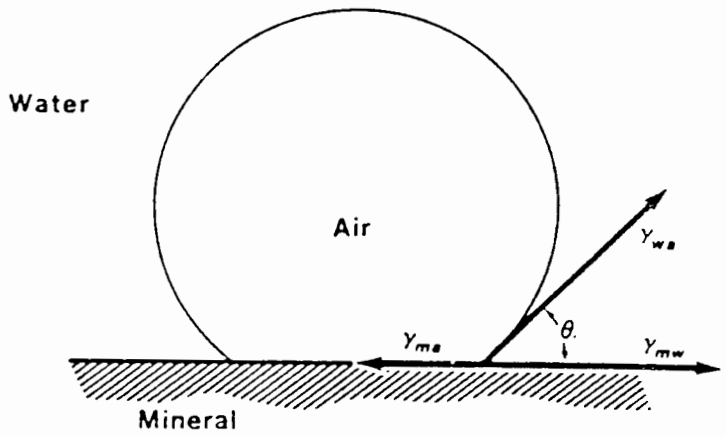

Figure 2.1: Idealised representation of three-phase equilibrim contact between air, water and mineral surface (from Kelly and Spottiswood, 1982).

As the contact angle increases, hydrophobicity increases. Hydrophobicity and contact angle phenomena have been widely reported by King (1982), Kelly and Spottiswood (1982) and Laskowski (1986).

Apart from a few minerals that are naturally hydrophobic to some extent (antimonite, graphite, molybdenite, etc.), the bulk of minerals must have artificial hydrophobicity created on their surfaces in order to float. A necessary condition for particle hydrophobicity according to Laskowski (1986) is:

$$\gamma_{ma} - \gamma_{mw} < \gamma_{wa} \qquad (2)$$

where, γ_{ma}, γ_{mw} and γ_{wa} are the tensions of the mineral-air, mineral-water and water-air interfaces respectively. Most minerals do not satisfy equation (2) but tend to satisfy more equation (3) below,

$$\gamma_{ma} - \gamma_{mw} > \gamma_{wa} \quad (3)$$

The main function of the collector is to act on the mineral in such a way that the factor ($\gamma_{ma} - \gamma_{ma}$) is reduced to satisfy equation (2), and thereafter hydrophobicity is said to be imparted to the mineral.

It is not the aim of this thesis to deal with flotation chemistry. Excellent papers are available in the literature that handle comprehensively the chemistry and surface reactions in flotation (King, 1982; Klimpel, 1984).

2.2 HYDRODYNAMICS IN AGITATED TANKS

A knowledge of the hydrodynamics in a gassed mixing tank is important in understanding the gas dispersion behaviour and solid suspension characteristics in the tank. It is also useful for predicting the design parameters concerned with mixing, velocity profiles, turbulence and mass transfer coefficients. The different flow patterns generated by the different types of conventional impellers - disk turbine, pitch blade and propeller - in a three-phase system are briefly discussed below as a prelude to understanding the hydrodynamics in flotation cells. A diagram of these impellers is shown in Figure 2.2.

2.2.1 Disk Turbine

The disk-style turbine (also known as the radial impeller) produces basically a radial flow pattern, the flow from the impeller comprising a high velocity component along the centre line and two convex systems, one along the top of the blades and the other

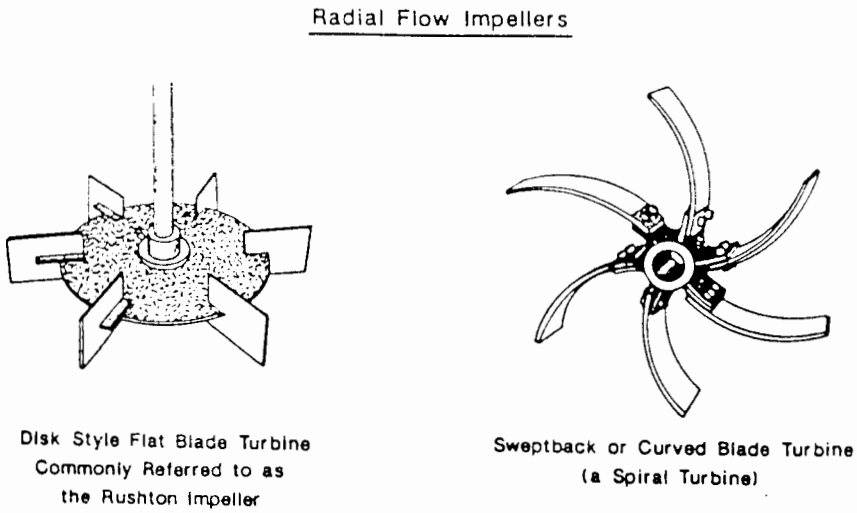

Figure 2.2: Turbulent impellers (from Tatterson, 1991).

along the bottom of the blades, as in Figure 2.3. Further away from the blades, the organised vortices and the center-line flows are disrupted causing significant increase in turbulent velocity fluctuations. Mixing therefore occurs where discharge streams from the impeller blade are disrupted by the flow from the bulk of the tank.

Mujumdar, *et al.*, (1970) measured turbulence parameters in an agitated tank using a disk- style turbine. They reported that the mean velocity was inversely proportional to the distance from the impeller tip and that the ratio of the mean velocity to the impeller tip speed was independent of the impeller rotational speed. A local maximum in the root-mean-square (r.m.s.) velocity fluctuations was found at some distance from the impeller. Beyond this point the fluctuation decreased as the wall was approached. The energy dissipation spectra showed a peak at the blade passing frequency. The rate of energy dissipation showed a similar trend, increasing with distance from the impeller and then decreasing as the wall was approached.

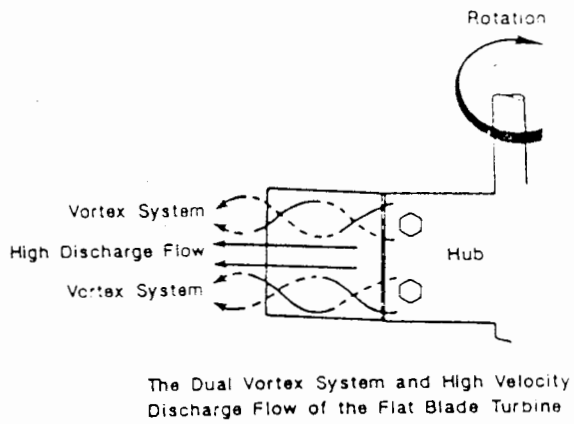

Figure 2.3: Flow systems from radial flow impeller (from Tatterson, 1991).

In addition to the radial velocity component, the flat disk turbine generates a tangential velocity component (Figure 2.4) which is almost equal and opposite at the impeller tip to the radial velocity, though the tangential component decreases more rapidly along the radial distance from the impeller. Radial flow impellers are mostly used for high shear applications such as air dispersion. They consume a high degree of power as compared to the other types of impellers.

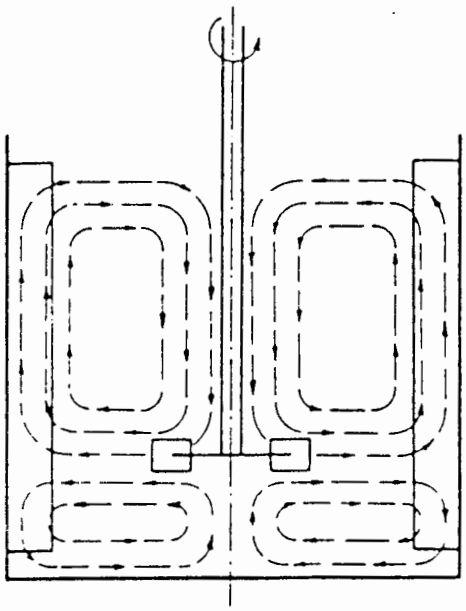

Figure 2.4: Flow pattern generated by radial flow impeller (from Joshi, *et al.*, 1982)

The liquid pumping capacity, Q_L, of all impellers can be correlated by the equation:

$$Q_L = \alpha N D^3 \tag{4}$$

where N = impeller rotational speed

D = impeller diameter

and 'α' is a dimensionless discharge coefficient which is a function of the impeller type and geometry. Values for 'α' have been provided by various researchers (Uhl and Gray, 1960; Betrand, *et al.*, 1980).

The fluid velocity near the wall is given by (van der Molen and van Mannen, 1978):

$$V_W = 0.53\left(\frac{D}{W}\right) ND \left(\frac{D}{T}\right)^{7/6} \tag{5}$$

where W = impeller blade width and T = tank diameter.

This equation also gives an approximate value of the fluid velocity in the bulk of the tank. The r.m.s. velocity has been observed to have two components, a periodic component near the impeller and a random fluctuating component that is dominant at a certain radial distance from the impeller. The r.m.s. fluctuating velocity in the impeller region is about 50-70% of the average fluid velocity and 5-15% in the bulk of the tank (Joshi, *et al.*, 1982).

2.2.2 Pitch Blade Turbine

The pitch-blade turbine impeller, also known as the axial flow turbine, mainly generates axial flow with the radial flow only proportional to the projected blade area (Figure 2.5). Levins and Glastonbury (1972) have studied the discharge velocities of fluid from the tip of the impeller. They have found that the tangential and radial velocities are comparable in magnitude, with the vertical velocities about twice the radial velocity components. The axial-flow impeller is known to produce more flow than the radial flow impeller at the same power input. Therefore it possesses greater power economy than the radial impeller.

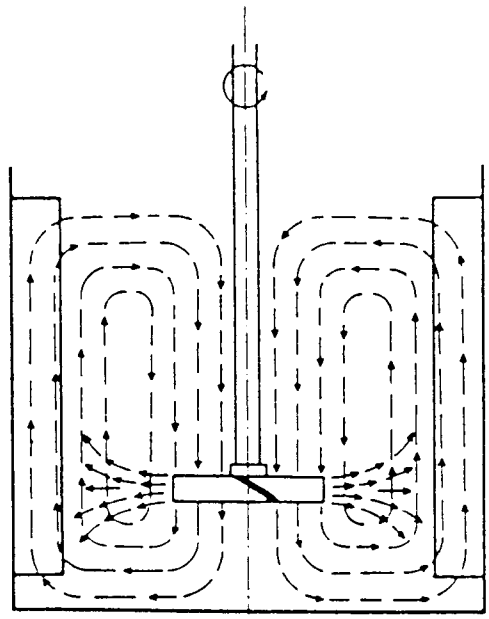

Figure 2.5: Flow pattern generated by axial flow impeller (from Joshi, *et al.*, 1982).

The average velocities near the surface of the liquid for the upflow, pitch-blade turbine and near the bottom of the tank for the downflow turbine have been correlated as follows (Joshi, *et al.*, 1982):

For upflow pitch blade turbine,

$$V_s = 0.78ND\left(\frac{D}{H - H_i}\right) \tag{6}$$

and for downflow pitch blade,

$$V_b = 0.78ND\left(\frac{D}{H_i}\right) \tag{7}$$

where H = height of the clear liquid in the tank

H_i= height of the impeller from the bottom of the cell.

2.2.3 Propeller

A typical flow pattern generated by a propeller is shown in Figure 2.6. The propeller produces mainly axial flow. The position at which the maximum velocity occurs depends on the pitch of the impeller blade. The cross sectional area of the flowing stream from the impeller does not depend on the impeller speed and is only a function of the vertical distance from the impeller plane. It can therefore be inferred that the extent of entrainment is not a function of the impeller speed, but at high impeller speeds the discharge velocity only increases, increasing the discharge flowrate. The average velocities near the liquid surface and near the bottom of the tank for the upflow and downflow impellers, which are practically the same as the velocity in the bulk of the tank, are given by (Joshi, *et al.*, 1982):

For upflow,

$$V_s = 0.65ND\left(\frac{D}{H - H_i}\right) \tag{8}$$

For downflow,

$$V_b = 0.65ND\left(\frac{D}{H_i}\right) \tag{9}$$

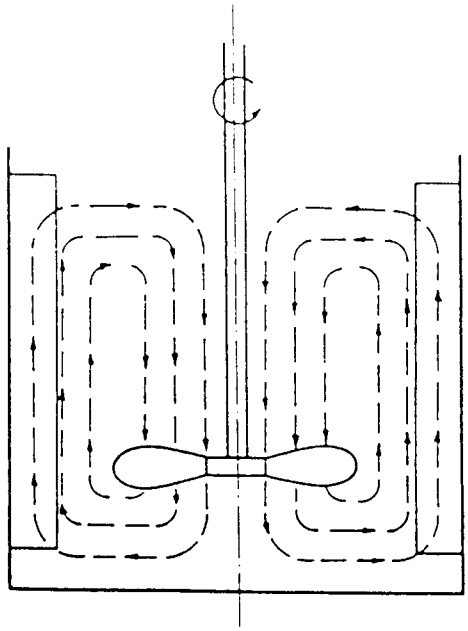

Figure 2.6: Flow pattern generated by propeller (from Joshi, *et al.*, 1982).

2.3 GAS DISPERSION IN AGITATED TANKS

2.3.1 Gas dispersion mechanism

When gas is introduced into an agitated tank, a number of processes occur. The gas is broken into small bubbles and spread into the entire tank by means of the flow pattern that is generated by the action of the impeller. It is known that when liquid flows over a solid body, vortices are formed. In an agitated tank, vortices are generated at the low pressure regions behind the impeller into which gas accumulates to form ventilated gas cavities which are responsible for the dispersion of gas. Rennie and Valentin (1968) were among the first to demonstrate with photographs showing the presence of trailing vortices behind the blades of a rotating impeller.

Van't Riet and Smith (1973), using a rotating camera in a single-phase flow, established that the circumferential velocities in the vortices are approximately the same order of magnitude as the impeller tip speed. They then concluded that at such speeds, substantial centrifugal forces existed in the flow that significantly affected gas dispersion. Gas dispersion in a mechanically agitated tank can be said to be a function of the air flow number ($N_Q=Q_g/ND^3$) and the Froude number ($N_{Fr}=N^2D/g$). The air flow number is defined as a dimensionless parameter relating air transfer (Qg) to the rotor dimension (D) and rotor speed (N). The Froude number is the ratio of the pressures resulting from the centrifugal forces and hydrostatic pressure on the rotor. The power number, $N_p=P/N^3D^5\rho$, is also defined as the ratio of fluid resistance to inertial forces. Detailed definitions of these quantities are given in sections 2.3.10 to 2.3.12 below.

Though the sparged system is not directly related to flotation in mechanically agitated cells, the discussion below involving a sparged tank has been included to elucidate the mechanisms involved in such a tank with respect to power consumption, flow patterns and flow regimes. The method of air circulation in mechanical flotation cells is similar to that in sparged systems. The following summarises the explanation by Rewatkar, *et al.*, (1993) of the dispersion of gas and its influence on power in a sparged system as illustrated in Figure 2.7.

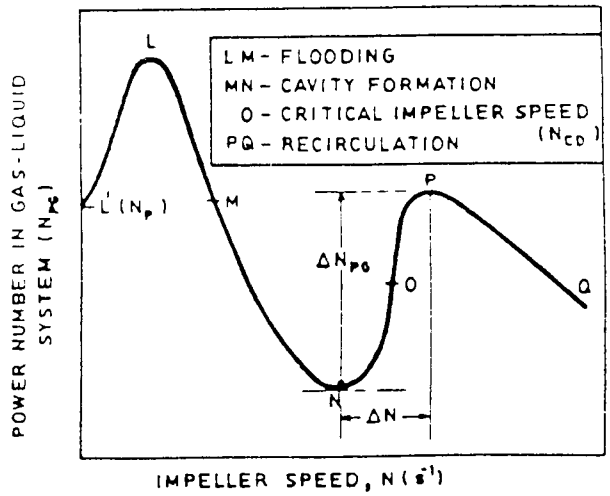

Figure 2.7: Variation of power number with impeller speed in a liquid-gas system (from Rewatkar, *et al.*, 1993).

When gas is introduced into a system with a stationary impeller, by means of a sparger located beneath the impeller, a flow pattern develops similar to that which occurs in a bubble column. Liquid flows develop because of the non-uniform gas holdup in the radial direction. The high gas holdup in the area of the agitator directly above the sparger, coupled with the low holdup near the wall, create a pressure difference that results in a pressure driving force for liquid flow. The circulation is directed upwards in the centre and downwards near the wall. When the air is introduced close to the wall, the direction of the fluid motion is reversed, downward in the central region and upwards near the wall (Rewatkar, *et al.*, 1993).

When the impeller is started it generates a liquid flow opposite in direction to that generated by the sparger. At low impeller speed the liquid flow is dominated by the air flow. The gas bubbles generated by the sparger rise vertically through the impeller region without any disruptions. The torque required for starting the impeller is much greater than in the case of ungassed liquid (point L) resulting in higher power consumption (Figure 2.7). The increase in power consumption depends on the gas flow. At a certain critical speed, the flows generated by the impeller and the sparger are comparable. Above this critical speed, the impeller action takes over and the behaviour of the tank is controlled by the impeller.

Variation in power number occurs along the curve LM. As the speed increases along the curve LM, the flow generated by the impeller increases continuously and presents an increasing resistance to the gas flow. The gas holdup increases and reduction in power number occurs along the curve LM. The impeller does not generate enough flow in this region compared to the sparger and the mixing process is controlled by the gas. No bubble breakup by the impeller action occurs and the impeller is said to be flooded. LM is called the flooding region.

The impeller rotation generates a low pressure region behind the impeller blades. At a certain impeller speed, the reduction in pressure is sufficient to hold the gas in the low pressure region against the buoyant force of the bubbles. The gas forms a cavity behind the impeller. Cavity formation starts from M on the curve; the cavity formed increases in size as the impeller speed increases along the curve. The cavity reaches its maximum size at N. Because of the cavities formed, the intensity of eddy motion behind the impeller decreases and turbulent energy dissipation is reduced. Impeller power consumption is reduced and mixing time is increased.

At impeller speeds beyond N, the shear stress field generated by the impeller is sufficiently strong to break up cavities. As the impeller speed increases along NP, the cavity sizes are reduced continuously by bubble breakage and, consequently, the power number increases steadily. At point O, liquid circulation generated by the impeller is sufficiently strong to disperse the gas to the bottom of the tank. The impeller speed at this point is called the critical speed for gas dispersion, N_{CD}. Beyond P, the liquid circulation produced by the impeller increases continuously and bubbles become entrained in the downflow. Initially only small bubbles are entrained but as the speed of the impeller increases large bubbles are caught in the trail as well. Gas holdup increases along PQ, resulting in reduction in pulp density in the impeller region and a steadily decreasing power number. This region is called the circulation regime.

2.3.2 Cavity Formation

Surfaces of discontinuity are said to be formed as a fluid flows past a solid body, separating at the edge and giving a dead space behind the body. As discussed in the previous section, the region behind the blade of an impeller is normally at a pressure below that of the surrounding fluid. If air is admitted to the impeller region, it is sucked into this space to form the observed air cavity. In the absence of bleed air, and if the relative velocity between the impeller and the fluid is sufficiently large, cavitation occurs when the reduced pressure is lower than the vapour pressure of the fluid, and a vapour filled cavity is formed (Grainger-Allen, 1970).

2.3.3 Types of Air Cavity

Different types of cavities have been identified to form behind the blades of the impellers. Van't Riet and Smith (1973) have identified four types of cavities that form behind the impeller blades of a disk-style turbine, i.e., vortex, clinging, large and 3-3 cavities. They have also found that the type of cavity formed depends on the impeller rotational speed, air flowrate and the flow pattern in the tank. Nienow and Wisdom (1974) have confirmed van't Riet's observation. Figure 2.8 shows the types of cavities observed by Nienow and Wisdom.

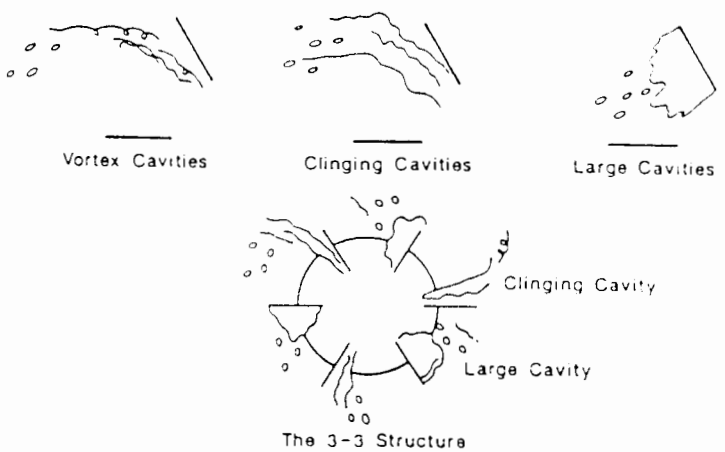

Figure 2.8: The different types of cavity systems (from Tatterson, 1991).

The study of the various cavities in gas dispersion is important because of their effects on the power draw, the liquid pumping capacity of the impeller, the liquid hydrodynamics around the impeller, the gas dispersion and the mass transport.

At low impeller speeds, the buoyant force of the bubbles exceeds the centrifugal forces of the fluid and the gas will not be captured by the vortices. At high impeller speeds, gas will be drawn into the vortices to form cavities from which the gas dispersion will be effected. Nienow and Wisdom (1974) and Bruijn, *et al.*, (1974) have carried out extensive research on gas cavities, correlating the type of cavity formed with the air flow number and the Froude number.

These authors have found that at low air flowrate, with air flow number $N_Q < 0.01$, gas is captured by the vortex systems to form vortex cavities (Figure 2.8). Vortex cavities are the least desired because of the low quantity of gas dispersed. At high air flowrate, with air flow number $N_Q > 0.03$, large cavities are formed behind the impeller blades. The gas dispersion in the large cavities has been found to be ineffective because the pressure in the cavity is not low enough for effective bubble capture due to the relatively low impeller speed. The pressure in the large cavity is nearly equal to the static pressure near the leading edge of the blade (Bruijn, *et al.*, 1974).

It is therefore not enough to correlate these types of cavities on the basis of the air flow number only; the Froude number must be incorporated. It has been found that the impeller speed at which the large cavities are formed is given by the Froude number, $N_{Fr} \geq 0.1$. At a high air flowrate and $N_{Fr} < 0.1$, the impeller will not be able to disperse the gas and large bubbles will escape from the large cavities due to large buoyancy forces of the bubbles. This condition is known as flooding (Bruijn, *et al.*, 1974).

Between the vortex cavity and the large cavity regimes, a clinging cavity or a 3-3 cavity occurs. The 3-3 cavity comprises an alternating system of three large and three clinging cavities, and has been found to be the most important of all the cavity types identified because of its superior gas handling capability. Smith (1985) has noted that for the 3-3 cavity formation, $N_{Fr} > 0.045$. More recently another type of cavity, the ragged cavity,

has been discovered by Nienow and Ulbrecht (1985). This was considered to be essentially large cavities formed behind the impeller blades under flooding conditions. At extremely high gas rate and impeller speed, the gas dispersion process becomes impossible to observe and the exact mechanism is, therefore, unclear.

2.3.3.1 Effects of cavity type on power

The vortex cavity was found to have an insignificant effect on power draw (Bruijn, *et al.*, 1974). At higher air rate, the clinging cavity formed caused a reduction in power draw to about 80% of ungassed power. Large cavities reduced power to about 40-50% of ungassed power. Consequently, it can be inferred that the power draw by impellers in a gassed system depends very much on the type of cavities formed behind the blades of the impeller.

2.3.3.2 Effects of cavity type on liquid circulation

Large cavities block the radial outflow of liquid from the impeller and reduce the radial liquid velocities in the bulk of the tank and hence recirculation of both gas and liquid to the impeller. For clinging and vortex cavities, liquid circulation appears unaffected by the presence of the gas. There is an increasing trend in mixing and circulation times as the air rate is increased. This condition is confirmed in section 2.4.1 under the discussion of mixing times in gassed systems.

2.3.3.3 Effects of surfactants on cavity type

Bruijn, *et al.*, (1974) have found that bulk liquid properties such as viscosity and density are important in determining the cavity shapes and flow regimes but changes in surface tension and dissolved solute do not affect the types of cavities formed. However electrolytes and other surfactants cause a reduction in bubble size by decreasing the surface tension forces between the continuous liquid phase and

the bubbles, and thereby increase the number of bubbles in recirculation to the impeller.

2.3.3.4 Effects of geometry on cavity type

The effects of geometry can be linked to power studies because rapid reductions in power draw as a function of air flow number, N_Q, indicate the formation of large gas cavities and poor gas dispersion. The number of impeller blades affects the type of cavity formation (Bruijn, *et al.*, 1974). More blades provide higher gas handling capacity and better gas dispersion and liquid mixing. A 12-blade impeller has more than three times the gas handling capability of a 6-blade impeller. This observation has also been made by Calderbank (1956).

Van't Riet, *et al.*, (1976) have studied gas dispersion for different impeller blade geometries including concave and convex impeller blades. The concave impeller was found to have a superior gas handling capacity at lower power cost.

2.3.4 Flow Map

A flow map as shown in Figure 2.9 has been presented by Warmoeskerken and Smith (1985) to describe the three flow regimes corresponding to the cavity types, viz. vortex and clinging, 3-3 structure and large or ragged cavities (see Figure 2.8). The presence of these regimes gives rise to three distinct transition lines: A to B, B to C, and A to C. The discussion in this section and the ones that follow is limited to disc-style turbine impellers only, since the features and principles of operation of flotation cell impellers are more closely related to these than to any other type of impellers.

The A-B transition is from vortex clinging cavities to large-ragged cavities of flooding. This is characterised by the drastic drop in power and the lower liquid pumping rate as the large cavity zone is approached. The large cavities are more streamlined behind the

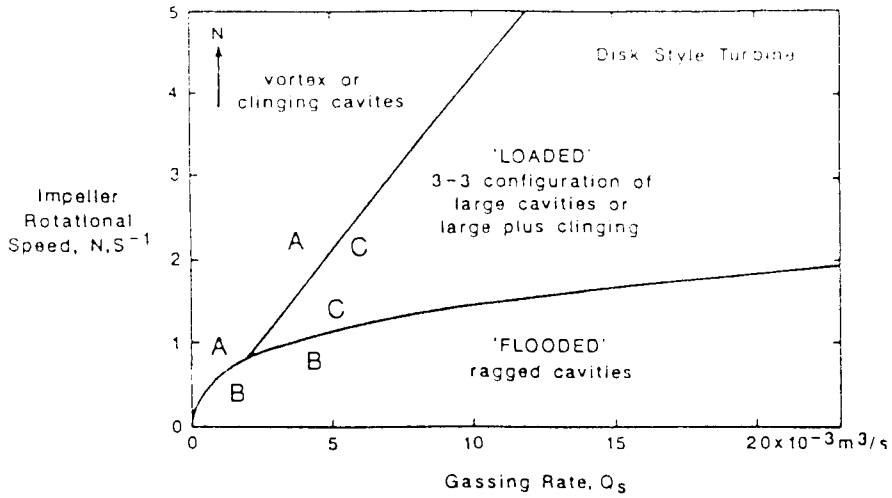

Figure 2.9: Cavity formation map for a 1.2 m diameter vessel (from Warmoeskerken and Smith, 1985).

impeller blades and this accounts for the lowering of power in zone B, while large cavities are known to obstruct liquid pumping.

The B-C transition occurs between the large cavities and the 3-3 cavity structure. It was observed that there is an increase in power as the flooding region is approached. The probable cause for this observation is that the 3-3 structure has more streamline effect, reducing the drag on the impeller blades.

The A-C transition is between the 3-3 structure and the clinging-vortex. The transitions A-B, B-C, A-C, were found to be independent of the system, whether coalescing or non-coalescing. This agrees with the fact that cavities were not affected by changes in surface tension.

2.3.5 Recirculation of Gas

The amount of gas recirculated is important in chemical and biological processes, where high gas recirculation results in longer residence times of air bubbles in the system. This is beneficial when high oxygen utilisation is required, especially in the

bio-oxidation processes. The onset of gas recirculation in a gassed, stirred reactor is largely determined by the impeller rotational speed and the air flow number. Consequently, the impeller speed required for the initial onset of recirculation of gas becomes important. The discussion in this and the following sections is for disk-style turbines only, for same reasons as stated in section 2.3.4.

This condition of high gas recirculation is, however, not desirable in the flotation process. In recirculation, the bubbles become largely confined to the flow loop around the impeller, decreasing their chances of colliding and adhering to particles in the bulk of the flotation cell. It is therefore important to know the operating regime that induces recirculation of gas in the flotation cell so as to avoid it in the process.

Relating the average recirculation velocity, V_R, for a single phase liquid to impeller speed and impeller and tank diameters, the impeller speed for the onset of recirculation can be quantified. Holmes, *et al.*, (1964) found the following relationship:

$$V_R = \frac{cND^2}{T} \tag{10}$$

where c is a constant and N, D and T have meanings defined under section 2.2.1.

For the recirculation of the gas the bubble rise velocity, V_T, must be less than or equal to the recirculation velocity of the fluid, hence

$$V_T < \frac{cND^2}{T} \tag{11}$$

If the rise velocity of bubbles is assumed constant, i.e. $V_T = K$, and proportional to the recirculation velocity, then the rotational speed for the onset of recirculation (Greaves and Kobbacy, 1981) is given by the empirical relationship:

$$N_R \alpha \frac{T^{0.97} Q_g^{0.13}}{D^{2.34}} \tag{12}$$

The rotational speed is affected by the air holdup. The greater the gas holdup the more difficult it is to circulate gas bubbles through the impeller region because of longer circulation paths for the gassed liquids. Small bubbles behave as fluid particles and are in continuous recirculation. Recirculation of gas results in lower power draw since the impeller receives more gas than induced or sparged. This is likely to lead to the formation of large cavities behind the blades of the impeller, a phenomenon which has already been discussed in section 2.3.3.

2.3.6 Flooding Transition

Flooding is defined as the flow regime where the impeller cannot disperse the gas properly, while flooding transition is the regime between flooding and good gas dispersion conditions. Greaves and Kobbacy (1981) have derived a correlation for the impeller speed in the flooding transition as:

$$N_F = 1.52\left(\frac{T^{0.2}Q_g^{\,0.29}}{D^{1.74}}\right) \tag{13}$$

where N_F = impeller rotational speed at flooding.

2.3.7 Complete Dispersion

The complete dispersion regime refers to the condition where the gas is dispersed throughout the tank. Nienow, *et al.*, (1977) have studied the condition for complete gas dispersion in a tank stirred by a disk-style turbine. The impeller rotational speed, N_{CD}, at which this occurs has been correlated and expressed as:

$$N_{CD} = \frac{4Q_g^{\,0.5}T^{0.25}}{D^2} \tag{14}$$

where the constant 4 has the units of $m^{0.25}s^{-0.5}$

For the different types of impeller studied, Chapman, *et al.*, (1983a, b, c) found that the standard disk-turbine showed the lowest N_{CD}, but at the highest power cost.

2.3.8 Bubble Breakup

Until recently, the concept of bubble formation in mechanical flotation cells had been more guess work than reality. It was perceived by some researchers as a process of shearing large bubbles into smaller ones between the rotor and the stator. Taggart (1951) was among the early researchers to dismiss this concept by effectively demonstrating the process of bubble dispersion by a rotating impeller without the use of a stator.

Research work by Rennie and Valentin (1968), Grainger-Allen (1970), van't Riet and Smith (1973) and Bruijn, *et al.*, (1974) have revealed that bubble formation by a rotating impeller is due to the attachment of air cavities to the trailing edge of the impeller blade which is a low pressure region. Bubbles are then formed by vortex shedding from the tail of the cavities due to turbulence in the pulp generated by the impeller. The stator blades only serve to distribute the bubbles by deflecting them horizontally from the impeller blades, but do not shear large bubbles into smaller ones.

The theoretical prediction of the size of bubbles formed in shear flow due to the rotation of the impeller is extremely difficult due to the complexity of the flow involved. However, in turbulent flow conditions as in stirred vessels, the forces that control the bubble size can be identified as the inertial forces due to the dynamic pressure fluctuations and the surface tension forces that resist the deformation. Hinze (1955) suggested that a bubble would break up if the ratio of the inertial and surface tension forces, expressed as the Weber number, exceeded a critical value. The critical Weber number, We_c, is given as;

$$We_c = \rho \upsilon^2 d_{max}/\sigma \qquad (15)$$

where υ^2 is the mean square velocity difference over a distance equal to the maximum bubble diameter (d_{max}) that is stable against breakup by turbulence. ρ and σ are the density and surface tension of the continuous phase respectively.

2.3.9 Bubble Coalescence

Bubble coalescence in simple terms is the conjugation of bubbles into larger ones. As a common occurrence in flotation cells, coalescence has a detrimental effect on bubble mineralisation and froth stability. Bubble sizes to a large extent are dependent on the degree of coalescence occurring in the cell. Where the rate of coalescence is high, pulp aeration deteriorates and with it the flotation process as a whole. In flotation cells this problem is minimised with the addition of optimum quantities of frothers.

Bubble coalescence is directly dependent on the number of bubbles present in a unit volume of the pulp and the rise velocities of the bubbles. The greater the number of bubbles the greater the probability of their collision and coalescence. Bubbles with high rise velocities possess enough kinetic energy to coalesce on impact. The presence of frother reduces bubble size and bubble rise velocity, thereby reducing the tendency to coalesce. Levich's (1962) explanation for this observation is that, due to the reagent adsorbing at the air water interface, the bubble behaves like a rigid sphere. Without frother, bubbles develop enlongated tails that reduce the hydrodynamic resistance on them. The bubbles therefore rise with high ascent velocity, increasing the chance of coalescence on impact.

The mechanism of coalescence has been attributed by (Lessard and Zieminski, 1971) to the thinning and rupture of the liquid film between adjacent bubbles. Another school of thought has explained the process in terms of a bubble wake draft mechanism (Preen, 1961) in which bubbles are believed to coalesce when they are drafted into the wakes of other bubbles.

Additionally, bubble-bubble and bubble-particle interactions serve as an impediment to further reduce the bubble rise velocity. As the solids concentration of the pulp increases, the bubble velocity decreases, but at very high pulp densities, ascent velocities increase again due to channelling of large bubbles through the pulp. However, a dynamic equilibrium is rapidly established between the processes of bubble breakage and coalescence and bubble size characteristics then remain approximately constant.

No known models have been constructed to quantify bubble coalescence accurately due mainly to the inadequate understanding of the mechanisms involved. However, a rough means of quantifying coalescence would be by comparing bubble size and gas holdup values, obtained from reliable estimation techniques, with experimental values.

2.3.10 Air flow Number

For geometrically similar mechanisms, the fluid flow leaving the rotor has a velocity proportional to ND. The surface area from which the flow leaves is proportional to D^2. The fluid volume thus leaving the rotor is proportional to ND^3. The dimensionless air flow number ($N_Q = Q_g/ND^3$) is thus the ratio of air flow to the fluid flow leaving the rotor (Fallenius, 1979). At a given air flow rate, the dispersion of the air into fine bubbles by the rotor requires a sufficient amount of fluid flow. The air flow number gives a measure of this amount of air. Above a certain minimum value of N_Q, air dispersion is inadequate. Therefore the largest amount of air that can be dispersed can be scaled up with the air flow number.

The air flow number also characterises the air-to-fluid ratio of the primary jet leaving the rotor. In the cell space this ratio is different, although it is proportional to the air flow number of the pumping jet if the size of the bubbles remains constant. If this condition is fulfilled, the air flow number can also be considered to characterise the air content of the cell.

The air flow number is also useful for characterising suspension in aerated systems. For a given range of particles size fractions, stable suspension is possible for N_Q less than a critical value. At the critical value the suspension will begin to sediment. This phenomenon is further discussed in section 2.5.4. Arbiter, *et al.*, (1969) have shown that geometrically similar cells of different sizes can be scaled up once the following condition is satisfied:

$$N_Q = Q_g/ND^3 = \text{constant} \quad (16)$$

However, the above equation is not valid if the ratio between the size of the mechanism and that of the vessel is not constant.

2.3.11 Power Number

The impeller power number, $N_p = P/N^3D^5\rho$, is a dimensionless constant defined as the ratio of fluid resistance to inertial forces. The power number expression does not however account for the impeller geometry. Arbiter, *et al.*, (1969) have suggested the need to incorporate a dimensionless constant from the dimensions of the impeller to account for this discrepancy. The power in rotational machinery is generally related to the net change in the tangential velocity component imparted to the fluid by the impeller. Hence the power number in flotation machines reflects the flow straightening characteristics of the shrouds, baffles, stators and tank on the pulp emanating from the impeller. There are significant differences in power numbers in cells of the same type but of different sizes, and differences that are far greater in cells of different types. Differences in power numbers result from the lack of geometric similarity among the cells of the same type, a consequence of the desire of the manufacturers to satisfy several flotation criteria by distorting geometrical scaling. However, constancy of power number has been observed over a range of system sizes that are geometrically similar (Rushton, *et al.*, 1950). Therefore if power number is to be used as a scale-up criterion, strict adherence to geometrical scaling must be observed.

For a fully baffled mixing system, N_p is found to be a function of the Reynold's number, N_{Re} ($N_{Re}=ND^2\rho/\mu$). As has been shown by Rushton, *et al.*, (1950), a plot of N_p versus N_{Re} reduces all data for a fully baffled system to the same curve for geometrically scaled systems. When $N_{Re}>10^4$ (full turbulence), N_p is constant. Strictly, this correlation refers to geometrically scaled equipment. Cell and impeller geometries vary as a function of size not only between manufacturers but even within the same types. For non-geometrically scaled equipment, N_p versus N_{Re} curves for different sizes are different. A study of the factors affecting the N_p and N_{Re} correlation requires the evaluation of the geometrical dimensionless ratios to account for the power and Reynolds numbers.

2.3.12 Froude Number

A condition for scale-up is that the gas dispersion at corresponding points in two different cells must be the same. At these points, it is presumed that the Froude numbers ($N_{Fr} = N^2D/g$) of the rotors are equal. Equal Froude numbers mean that the ratio between the pressure caused by the centrifugal forces and the hydrostatic pressure difference is the same in both cases.

For example, in the mechanisms of Outokumpu flotation cells, one condition that holds for similar operations from the standpoint of air dispersion is that:

$$N^2D = \text{constant.} \qquad (17)$$

As the speed of rotation increases from a low value, the air dispersion zone extends downwards from the upper parts of the rotor, and for the optimum N_{Fr}, the air is dispersed from the entire rotor envelope. With further increase in the speed of rotation above this optimum value, a greater proportion of air is dispersed from the lower points of the rotor.

2.4 MIXING

Mixing or the degree of turbulence in a flotation cell can affect the rate of flotation considerably. Adequate mixing promotes bubble-particle contact and adhesion but too much turbulence detaches particles from the aggregates. By a similar reasoning, too little turbulence will not provide enough kinetic energy for effective particle-bubble collision and attachment.

Mackenzie and Matheson (1963) have found that the rate of flotation for a given range of particle size increased with increasing impeller speed. Kirchberg and Topfer (1965) have varied the impeller speed in a subaeration cell and determined that the recovery increased to a peak and then decreased as the turbulence in the pulp increased. This was due to the detachment of the particles from bubbles as the turbulence intensity increased with increased agitation. The effect of mixing and pulp turbulence on flotation has been investigated further by Bogdanov, *et al.*, (1965). They discovered that the time of flotation required for a given recovery was reduced with an increase in pulp flow rate in a continuous cell. This observation was explained by the fact that an increase in the pulp flowrate causes a reduction of pulp impoverishment, which results from excessive mixing.

A number of methods of measuring the mixing efficiencies have been suggested. Different criteria have been used to decide the degree of mixing or homogeneity and based on these results, empirical correlations have been proposed for the prediction of the dimensionless mixing time "Nθ" for different types of systems (Holmes, *et al.*, 1964; Khang and Levenspiel, 1976).

2.4.1 Mixing Time

Joshi, *et al.*, (1982) have proposed a method of calculating mixing time on the basis of liquid circulation velocity for both gassed and ungassed systems. They have based their

method on a formula used earlier by Joshi (1980) to calculate the average liquid circulation velocity based on mixing time and the maximum length of circulating loop.

McManamey (1980) has established the dependence of mixing time on impeller speed, impeller/tank aspect ratio, impeller clearance from the tank bottom and impeller blade width. He has used the average liquid circulation velocity and maximum loop length to explain the effects of the various parameters mentioned above.

The model used by Joshi, *et al.*, (1982) was based on the assumption that:

- Mixing time is directly proportional to the longest loop length, which depends on impeller type and position (Figure 2.10);

- Mixing time is inversely proportional to the average circulation velocity near the wall (radial impellers) or near the surface or tank bottom (axial impellers);
- Mixing time is equal to 5 times the circulation time (Holmes, *et al.*, 1964); and

- Flow is fully turbulent and the dimensionless quantity (S/ND) is constant, where S is the peripheral speed of the impeller.

2.4.1.1 Flat blade turbine

The velocity near the tank wall for a standard flat blade turbine can be calculated from equation (5) on page 18.

As can be seen from Figure 2.10, the longest loop is 'abcda' or 'abefa' depending on the position of the impeller. Hence the longest loop length is (aH+T) where 'a' is equal to 1 when the impeller is situated centrally or equal to 1.33 when H_i is equal to H/3 and so on.

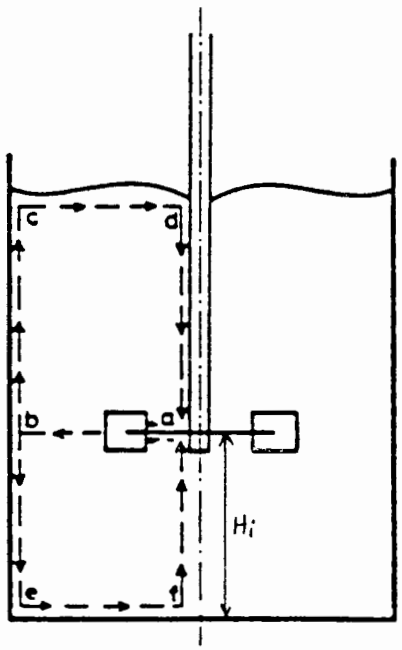

Figure 2.10: Length of longest circulation path in the case of disk turbine (from Joshi, *et al.*, 1982).

The circulation time, t_c, is given by:

$$t_C = \frac{Length\ of\ the\ longest\ loop}{average\ circulation\ velocity} \tag{18}$$

For a standard flat blade turbine the power number, Np = 5. Hence,

$$t_C = \left(\frac{aH + T}{0.53ND\left(\frac{D}{W}\right)\left(\frac{D}{T}\right)^{7/6}} \right) \tag{19}$$

and from section 2.4.1, $N\theta = 5t_c$

$$\therefore\ N\theta = 9.43\left(\frac{aH + T}{T}\right)\left(\frac{T}{D}\right)^{13/6}\left(\frac{W}{D}\right) \tag{20}$$

Similar derivations based on the circulation model have been proposed for mixing times with pitch blade turbines and propeller impellers (Joshi, *et al.*, 1982).

2.4.1.2 Mixing time in the presence of gas

The flow behaviour of aerated fluid is similar in many respects to unaerated liquid flow in an agitated tank, except that the mixing times under aerated conditions are prolonged by some 20-30%. Liquid pumping capability of the impeller is reduced, while circulation and mixing times are increased because of the gas cavities and aeration.

Following previous work by Joshi, *et al.*, (1982), Pandit and Joshi (1983) have derived a correlation for mixing times in gas-liquid dispersion based on the circulation model. Applying Hughmark's correlation for aerated power ratio and combining with equation (18), the mixing time for aerated pulp based on the circulation model has been correlated as:

$$N\square = 20.41\left(a\frac{H}{T}+1\right)\left(\frac{T}{D}\right)^{13/6}\left(\frac{W}{D}\right)\left(\frac{Q}{NV}\right)^{1/12}\left(\frac{W^2D^4}{gWV^{2/3}}\right)^{1/15} \qquad (21)$$

where V and W are liquid volume and blade width respectively and 'a' as in equation (20) is a variable which depends on the length of recirculation loop; it is equal to unity for a centrally located impeller as in this scenario.

2.5 SUSPENSION OF SOLIDS

The importance of particle suspension in a three-phase system cannot be overemphasized. In flotation cells particle suspension and dispersion are critical to the recovery of mineral particles. Sun and Zimmerman (1950) have shown that mineral recovery in flotation cells increases with suspension height within the limit of turbulence intensities that do not disrupt the bubble-particle aggregates.

One of the functions the impeller performs is to suspend solid particles so that they may encounter the air bubbles. A considerable amount of work has been published on three-phase systems in stirred tanks but the main emphasis has usually been on the reaction

kinetics; there is very little consideration given to the solids suspension mechanisms involved. One of the early works to deal with the interaction of aeration and suspension of solids in the field of froth flotation was that of Arbiter, *et al.*, (1969). They noticed that a drastic sedimentation of suspended particles occurred if a critical air flow number was exceeded. The results of their work are however difficult to relate directly to standard three-phase chemical reactors, since the impeller and shroud geometry used in flotation cells is very different from that found in these reactors. The sudden drop in power ratio with introduction of air was attributed to particles blocking the suction ports of the impeller, which is unlikely to occur in an unshrouded system. They also noted that sedimentation was achieved gradually with increase in gas rate. It could be inferred from their work that:

- Aeration causes a decrease in power consumption; and
- Particle sedimentation is closely associated with this power drop.

It is obvious that, if agitation is not strong enough, as a result of reduction in mixing power, particles will settle out at the bottom of the tank, preventing any effective particle-bubble contact.

The principle underlying the mechanism of solids suspension in flotation cells is difficult to understand. Recently, much research work has been done into the suspension characteristics of particles in solid-liquid-air systems. In the sections which follow, an attempt has been made to elucidate the understanding of the mechanism of solids suspension in flotation cells by first analysing the phenomenon in two-phase systems (solid-liquid, liquid-gas systems) and then extending the analysis to solid-liquid-gas systems.

2.5.1 Solid-Liquid Systems

Particle suspension in a mixing tank is a function of the hydrodynamics of the fluid medium. The hydrodynamics in turn depend on such parameters as the characteristics of the impeller, impeller speed, impeller power, cell geometry, particle characteristics,

etc., (see section 2.2 above). Increasing the speed of the impeller generates fluid motion which has a resultant rise velocity in the upwards direction. If the fluid rise velocity is greater than the particle settling velocity, the particle will be suspended.

Zwietering (1958) has proposed that a complete suspension is achieved if no particles remain motionless at the bottom for more than 1 second. An important parameter in solid-liquid suspension systems is the critical impeller speed (Njs) at which the particles are completely suspended. Many models have been developed to predict the Njs for different systems and under different conditions, but Zwietering's correlation still remains the most useful in estimating Njs (Chapman, *et al.*, 1983a, b, c). His empirical expression for Njs is given as:

$$Njs = s\nu^{0.1}d_p^{0.2}(g\Delta\rho/\rho_L)^{0.45}X^{0.13}D^{-0.85} \quad , \qquad (22)$$

where s = dimensionless suspension parameter,

ν = kinematic viscosity (m^2/s),

d_p= particle size (m),

g = acceleration due to gravity (9.81 m/s^2),

ρ_L= density of liquid (kg/m^3),

ρ_s= density of solid (kg/m^3),

$\Delta\rho = \rho_s - \rho_L$ (kg/m^3),

X = concentration of solids (%), and

D = impeller diameter (m).

Below Njs, the total surface area of the solid particles is not available for processing as the tendency of some of the particles to settle at bottom of tank is high, thereby reducing their surface areas available for contact.

The concept of complete suspension differs considerably from the state of complete dispersion or homogeneous suspension, except in cases where the particles are very fine; but homogeneity of suspension is not a critical requirement for most three-phase

system operations. However, in dealing with solid-liquid systems it is important that the two conditions of complete suspension and complete dispersion are differentiated.

The complete suspension state has also been studied by Schubert (1985). He found that the speed of the agitator at which the one second criterion (N_1) occurs can be related to the power number as follows:

$$N_1 = K(N_p\rho)^{-m}, \qquad (23)$$

where K and m are constants that depend on particle properties.

A more general correlation relating Zwietering's result to the Froude and Reynolds numbers and other geometric ratios has been proposed. Under similar pulp conditions, Zwietering (1958) has shown that the impeller tip speed, S, required for complete suspension of solids is related to the impeller diameter D by:

$$S \alpha D^{0.15} \qquad . \qquad (24)$$

Pavlushenko, *et al.*, (1957) have studied the requirements for complete dispersion, and their result can be shown to be similar to equation (24) with the diameter term raised to the power 0.4. A common scale-up criterion (Weissman and Efferding, 1960) proposes maintenance of constant power intensity and so if power number, geometrical ratios and solids concentration are constant, then the impeller peripheral speed can be shown to be proportional to the impeller diameter raised to the power of 0.33.

To prevent sedimentation of particles in a suspension, the vertical pulp velocity must exceed the particle sedimentation velocity. The pulp stream issuing from the impeller must have sufficient velocity to prevent sedimentation in the most distant parts of the cell. Since velocity decays with distance, the impeller discharge velocity must increase with system size.

Even when suspension appears to be complete, a decreasing density gradient is usually evident from top to bottom. This observation is supported by the theory of isotropic turbulence applied to suspensions, which predicts that the solids concentration in a suspension decays exponentially with height (Arbiter, *et al.*, 1969).

2.5.1.1 Suspension height

Weissman and Efferding (1960) have reported suspension data can be described by a power intensity rule. They found that for given pulp conditions and constant geometrical ratios, the suspension height is directly proportional to the power intensity.

A correlation was also derived by Arbiter, *et al.*, (1969) which predicts the suspension height with operational parameters including power, particle properties and tank and impeller geometry.

$$\frac{h}{T} = q\left(\frac{T}{D}\right)^{a}\left(\frac{C}{D}\right)^{b}\left(\frac{P_{AL}}{W}\right)^{e} X^{Z}, \qquad (25)$$

where h is the height of suspension-clear water interface and values of the constants q, a, b, e and z from different flotation systems as found by Arbiter, *et al.*, (1969) are given in Appendix B. The other parameters have their usual meanings.

Equation (25) indicates that suspension characteristics can be improved by increasing the clearance of the impeller from the tank bottom, without a corresponding increase in power requirements. This is however not always the case, as different flotation cells behave differently at different clearances. With the Denver machines, for instance, any adjustment to the impeller/tank clearance must be made with caution as beyond a certain C/D value, solids begin to settle. Reducing the clearance can also lead to low suspension height that again can result in sedimentation.

The effect of tank size on suspension must be considered in relation to power consumption. In the absence of solids, power consumption is generally independent of tank size. With the presence of solids in suspension, decreasing the tank size increases power consumption. For Denver and WEMCO machines, it also lowers the suspension height as well, but for the Agitair machine, the suspension height is raised. This behaviour is reflected in the negative exponent of T/D in the Agitair correlation as shown in Appendix B.

Weissman and Efferding (1960) have also reported increasing suspension height with decreasing tank size in a fully baffled tank, as with the Agitair machine. While the other flotation machines have stators, the Agitair is a baffled system.

In terms of particle suspension, axial flow impellers are found to be more effective than radial flow impellers. Axial flow impellers produce higher flow but lower turbulence than the radial impellers (Nagata, 1975). This suggests that the enhanced drag forces resulting from the higher volumetric pumping rate of the axial flow impellers are primarily responsible for suspension. An alternative reason might be that the path length between the impeller and the point from which particles were last suspended is less for an axial impeller than for a radial impeller, reducing the probability of turbulent eddies decaying. Axial impellers require higher speeds to perform a given suspension duty and it is only their low power numbers that make them energy-efficient.

2.5.2 Liquid-air systems

Previous researchers (Oyama and Endoh, 1955) have studied power consumption in mixers with air sparged through different size nozzles. They have found that due to the non-uniform distribution of air in the tank, the power reduction is far less than it would be if the air was evenly distributed in the tank. It was suggested that the decrease in power consumption is largely due to the low density of the pulp in the immediate vicinity of the impeller, which is different from the average pulp density of the bulk. Unfortunately, no known device has been developed for power measurement in the

bulk of the liquid. The probable reasons for these differences in liquid densities are first, the distinct trend of decreasing bubble concentration with distance from the impeller, and second, the large number of bubbles that are trapped in circulation in the impeller region.

Various workers (Costes and Couderc, 1988; Okamoto, *et al.*, 1981) have reported that the local rate of energy dissipation varies with location, being very high near the impeller zone and smaller in the bulk of the tank. Furthermore, van't Riet and Smith (1973) and Saleemi (1986) have shown that bubble breakup in a stirred tank occurs in the impeller zone and that in a non-coalescence system the sizes of the bubbles are preserved, but a decrease in bubble population is observed with distance from the impeller region. A more recent report (Barigou and Greaves, 1992) has confirmed the non-uniformity of bubble size distribution in a mixing tank. Therefore it is more rational to use energy dissipation rate in the impeller zone to predict the bubble sizes and other gas dispersion characteristics (Parthasarathy, *et al.*, 1991). Similar views have been expressed by Calderbank (1967).

Oyama and Endoh (1955) have suggested that the rate of decrease of power number at a given air flowrate describes the gas dispersion ability of the impeller. Thus as the power number drops rapidly due to an increase in the quantity of gas in the impeller region, the pumping rate and dispersion capability of the impeller also drop suddenly. In the turbulent regime where power number remains constant, their data were well correlated by the power ratio P_{AL}/P_L (where P_{AL}=power in an air-liquid system and P_L=power in an ungassed system) and the air flow number, N_Q. Figure 2.11 shows the variation of the power ratio as a function of the air flow number for the Denver and the Agitair laboratory flotation machines, confirming the findings of Oyama and Endoh (1955).

Another important parameter in liquid-gas systems is the critical impeller speed for complete gas dispersion. This critical speed is defined differently by many researchers, but in simple terms, it is the minimium impeller speed to just completely disperse the gas to all parts of the vessel. Westerterp, *et al.*, (1963) correlated the minimum impeller

peripheral speed required for effective gas dispersion for different types of impellers and different sizes of tanks based on surface tension measurements. The difficulty in making these measurements made their correlation quite unpopular.

Nienow, *et al.*, (1977) have also correlated the minimum impeller rotational speed for complete gas dispersion based on the air flowrate and the impeller and tank diameters as given in equation (14).

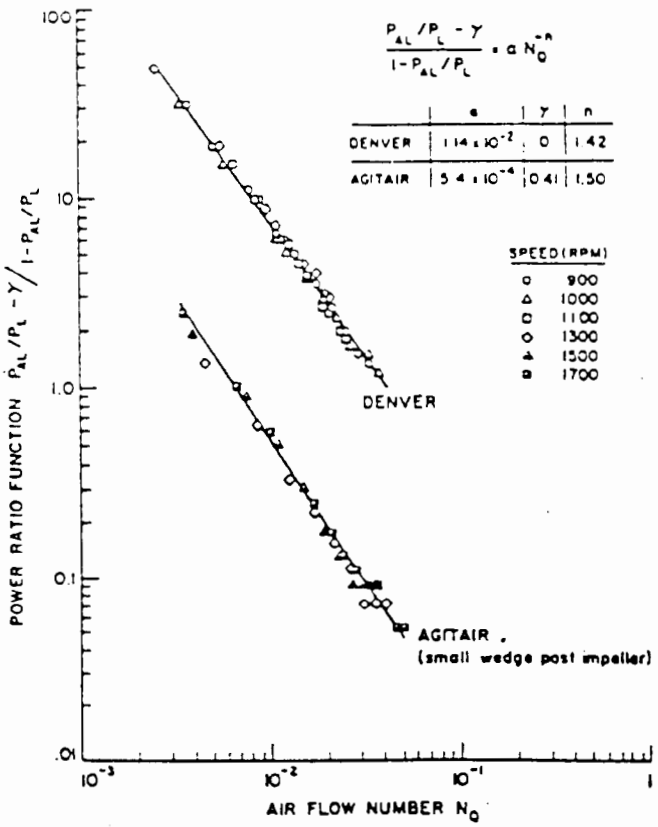

Figure 2.11: Power ratio function versus air flow number correlation for laboratory Denver and Agitair flotation machines in air-water system (from Arbiter, *et al.*, 1969).

2.5.3 Air-Liquid-Solid Systems

Many studies on three-phase systems have been accomplished as parts or extensions of two-phase studies. The basic problems of the two-phase systems appear in the three-phase systems with the additional complications of the changing flow behaviour because of the presence of a third phase.

Although the conditions of the two-phase systems may not match perfectly well, they may be merged into a set of conditions for a three-phase system. In the gas-liquid systems, the quantities of interest are mass transfer, gas recirculation, minimum impeller speed for complete gas dispersion, etc. In solid-liquid systems, particle suspension characteristics with respect to the impeller speed, power consumption, etc., are typically of greatest interest.

By combining the equations from two-phase systems, one may obtain a description of a three-phase system of gas, liquid, and solids that adequately defines gas dispersion and solids suspension. The available correlations that provide operating conditions for two-phase systems are often used in three-phase systems. The assumption made is that the third phase does not alter the flow behaviour significantly from the two-phase behaviour. For some processes, two-phase correlations are adequate; in others, the results can be very misleading. However, correlations for three-phase systems are developing.

Introduction of air into a solid-liquid system brings into play the effects of both solid-liquid and liquid-air systems considered earlier on. The impeller power consumption as well as the ability of the machine to suspend particles is reduced drastically. The apparent reduction in the fluid density in the area of the impeller is a probable cause of the reduction in power consumption. With the air entrainment, the pumping capacity and hence the fluid velocity from the impeller are reduced below the critical velocity required to suspend the particles. These effects are worse in the presence of frothers.

Figure 2.12 shows the power ratio versus air flow number correlations as observed in a laboratory-scale Denver flotation machine for a solid-water-air system.

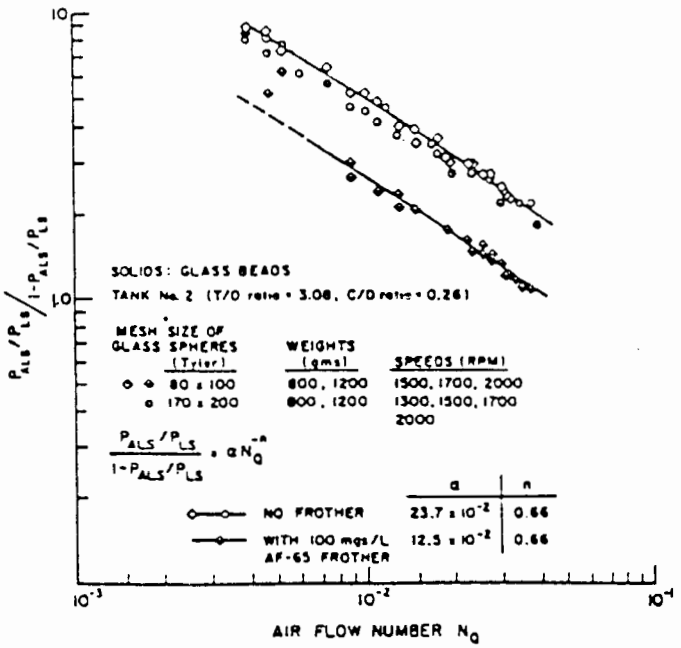

Figure 2.12: Power ratio functions versus air flow number correlation for laboratory Denver flotation machines in air-water-solid systems (from Arbiter, *et al.*, 1969).

A comparison of Figures 2.11 and 2.12 shows that the power ratio versus air flow number curves are similar in the two and three-phase systems. The analysis of an air-liquid system can therefore be used to estimate the behaviour of an air-liquid-solid system fairly well. Similarly, an equation developed to correlate power ratio and air flow number in air-liquid systems holds equally well for solid-liquid-gas systems (Arbiter, *et al.*, 1969).

2.5.4 Suspension of solids in flotation cells

Despite the similarities that exist between flotation and other three-phase-processes, the flotation process is very different in many respects. The flotation cell configuration is far from that of chemical reactors, whose designs may in almost all cases be described in terms of a generic standard, as detailed in section 2.6.2, below. The processes that

occur in these systems are therefore not exactly the same. For example, the fact that a quiescent zone is required at the top of the flotation cell, so that a stable froth may be established, means the agitator must be located almost at the bottom of the tank. This also means that the flow pattern generated during flotation will be very different from that in a standard chemical reactor.

An adequate state of suspension is essential in a flotation cell if the cell is to function properly. Good suspension enhances the chances of bubble-particle collision and attachment, thereby improving the process of flotation. It is not practical in flotation cells to achieve a complete state of suspension, in which all the particles are in suspension, as proposed by Zwietering's criterion. A small layer of settled solids covering the bottom and the corners of the cell is often observed, apparently due to the low turbulence in these cell spaces. A very high level of turbulence is required in the flotation cell to produce complete suspension of solids. This will have a detrimental effect on flotation in that the rate of detachment of bubble-particle aggregates will be high. Flotation results are essentially dependent on the magnitude of turbulent dissipation.

The maintenance of complete suspension in the flotation cell requires a great deal of energy, and this represents a considerable cost especially when large cells are involved. A stationary layer of solids on the bottom of the cell is not detrimental as long as it does not interfere with the flow pattern in the cell. This small layer of solids is actually seen as beneficial since it forms a wear-preventing layer on the bottom of the cell.

Extensive experimental work by Arbiter, *et al.*, (1969) has contributed much to the understanding of the behaviour of solids in air-liquid systems. Some of these findings may be summarised as follows:

- With a narrow size range of suspended solids, solids settle rapidly as a certain critical air flow number is attained. With a wider range of particles sizes, solids settle relatively slowly at the critical air flow number. The finer sizes settle first and the coarse fraction settles slowly even at the critical air flow number. This

implies that decreasing the critical air flow number reduces the sedimentation of the coarse particles.

- In some of the machine designs, complete sedimentation occurs at the critical air flow number, accompanied by a sudden drop in power number. The Agitair flotation machines display this behaviour.

- The critical air flow number decreases as the particle size and the solids concentration decrease.

- The design of some self-aerating machines (i.e., WEMCO) is such that their critical air flow number is above the normal operating range.

- The rate of air flow induced by self-aerating machines is a function of solids concentration, particle size, impeller submergence, frother concentration, tank size and the impeller clearance from the bottom of the tank.

2.6 FLOTATION MACHINES

The flotation process dates back to nearly a century ago and it might be expected that the design of the machines used would have reached a high level of perfection. Unfortunately, this is not so. The design of flotation cells still remains empirical and their application is often a matter of experience combined with judgement and a certain amount of prejudice.

Flotation machines in use today can generally be described under three main categories, according to method of aeration employed. This categorisation, given in Table 2.1, is definitely not exhaustive because a good number of the flotation machines found in the mining industry today are hybrids of these groups.

Table 2.1 Classification of flotation machines according to the method of aeration.

Type of machines	Aeration method	Design feature
1. Mechanical	Pulp aerated by mixers of various designs	1. Radial bladed impeller 2. Special impeller 3. Squirrel cage
2. Pneumatic	Pulp aerated by compressed air	1. With porous mats (fixed or movable) 2. Airlift (internal elevator)
3. Pressure variation	Pulp aerated by reducing pressure to evolve gas from solution	1. Vacuum (reducing pressure above pulp to below atmospheric) 2. Compressor (with the discharge of pulp found under pressure)

Many of the machines described in this section were introduced only experimentally, and found little long-term application in industry. Others were installed at one or a few sites, and were not adopted by other users. However, all are described to provide a complete picture of the wide variation in both proposed and proven flotation machines.

2.6.1. Pneumatic Flotation Machines

This class of machines has no impeller and relies on compressed air for aeration and agitation of the pulp. It consists of elongated columns or deep troughs. Pulp flows from one end and air is induced from the other by means of an external pump or blower, through pipes or some form of porous mats. The Column cell, the Flotaire and the Leeds column are examples of this class of flotation machines.

2.6.1.1 Column flotation cell

The Column flotation cell is the most widely used of the pneumatic flotation machines. Although its invention dates back to early 1960s, it has only in the last decade gained any industrial recognition.

The Column flotation cell is a tall column into which conditioned pulp is fed about a fifth of the way down from the top (Figure 2.13). Air is blown into the column through a diffuser or spargers at the base, and wash water is fed at the top. Concentrate overflows the top of the column and tailings discharge from the bottom. The column has the advantage of producing high grade concentrates, through the controlled addition of wash water. It is clear that the quiescence of the collection zone promotes stability of particle-bubble aggregates, which are easily broken in the more turbulent environment of the mechanically agitated flotation cells.

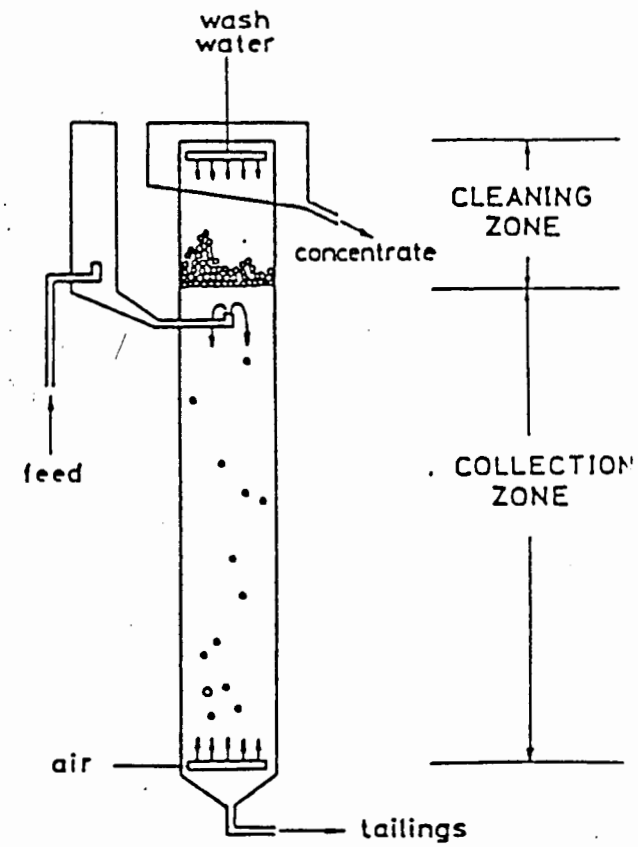

Figure 2.13 Column flotation cell (from Jameson, 1994).

2.6.2 Pressure Variation Machines

This class of flotation machines is still the basis of the most widely used separation method in waste water clarification. Although widely used in mineral recovery in the earliest days of flotation, this class of flotation machines has almost disappeared from use today.

2.6.3 Mechanical Flotation Machines

The most widely used class of flotation machines is characterised by a mechanically driven impeller which agitates and disperses air into the pulp. The distinguishing feature of mechanically agitated flotation machines is the high degree of turbulence in the pulp. The high intensity of contacting between particles and bubbles promotes the recovery of relatively fine particles, while the good solids suspension capability results in high recovery of coarse material.

There is a wide range of mechanical flotation machines in use in the mining industry, ranging from newly developed to old, modified designs. The new designs are usually said to address some specific technical advantages (better air dispersion, fine particle flotation, better mixers, etc.), while the old designs are modified with the objective of reducing cost and complexity.

In recent years, the trend has been towards the construction of larger machines to compensate for the diminishing grades of ore. A brief description of some of the common types of mechanical flotation machines is given below. In particular, the WEMCO, Outokumpu and Bateman machines, from which measurements were taken for this work, are discussed in more detail.

Figures 2.14 and 2.15 depict the tank and impeller geometries of some of the machines described below.

2.6.3.1 Aker flotation machine

The Aker flotation machine, designed and constructed in Norway in the late 1970s, has not enjoyed much international recognition. Its use is confined to domestic applications in Norway in the treatment of a variety of sulphide ores, upgrading of iron ores and quartz-feldspar separation processes.

The machine is basically a rectangular tank (Figure 2.14) with no baffles and a relatively small diameter impeller. Vertical plates fitted between mechanisms are responsible for restricting pulp flow between the cells and for reducing undesirable turbulence at the froth zone. Air is drawn down the hollow impeller shaft and distributed via slots on the low pressure side of the blades of the unidirectional impeller. The rotor comprises a number of vertical, rectangular blades covered with polyurethane (Figure 2.15). The design and lining of the impeller enhances flexing and permits the impellers to be started even under loaded conditions, as may happen during unplanned shutdowns. The lining also has an added advantage of preventing scale formation that would otherwise block the air outlets. The overall design criteria of the Aker flotation machine are aimed at achieving high air dispersion capacity and good solids suspension, and at the same time maintaining a quiescent froth zone.

2.6.3.2 Booth flotation machine

The Booth flotation machine was designed and built by the Booth company of the U.S.A. It is a self-aerated machine with a shallow tank and possesses two impellers (Figure 2.15). An upper impeller, very close to the pulp level, is responsible for aeration, while a lower, axial-flow propeller, at the bottom of the shaft, keeps the solids in suspension. The tank has a truncated, rectangular cross-section (as can be seen in Figure 2.15) with no baffles. It contains between mechanisms vertical plates, which dampen the turbulence in the froth zone as well as constricting pulp flow between cells.

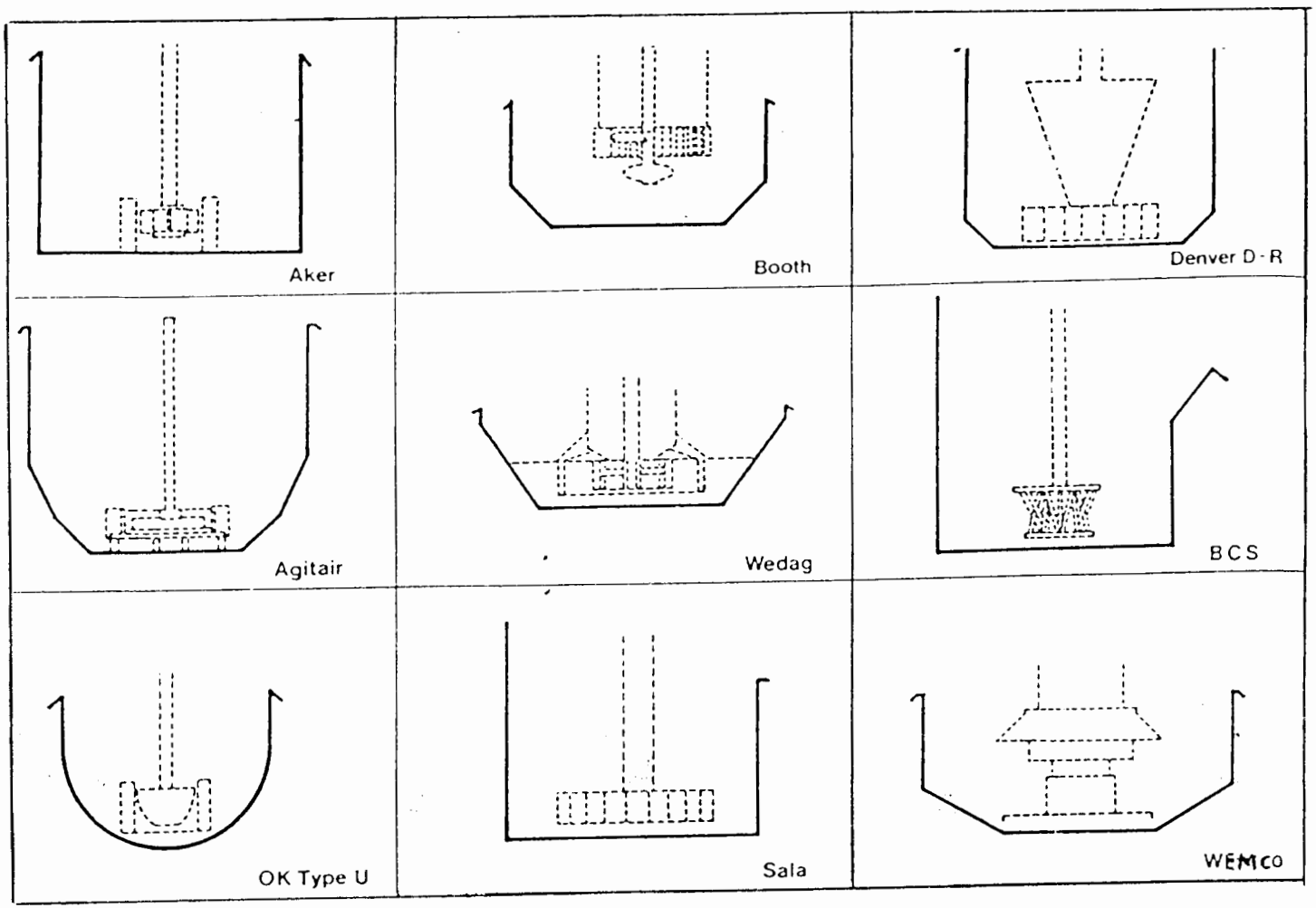

Figure 2.14: Cell Tank Geometries in Typical Open Flow Mechanical Flotation Cells (Young, 1982).

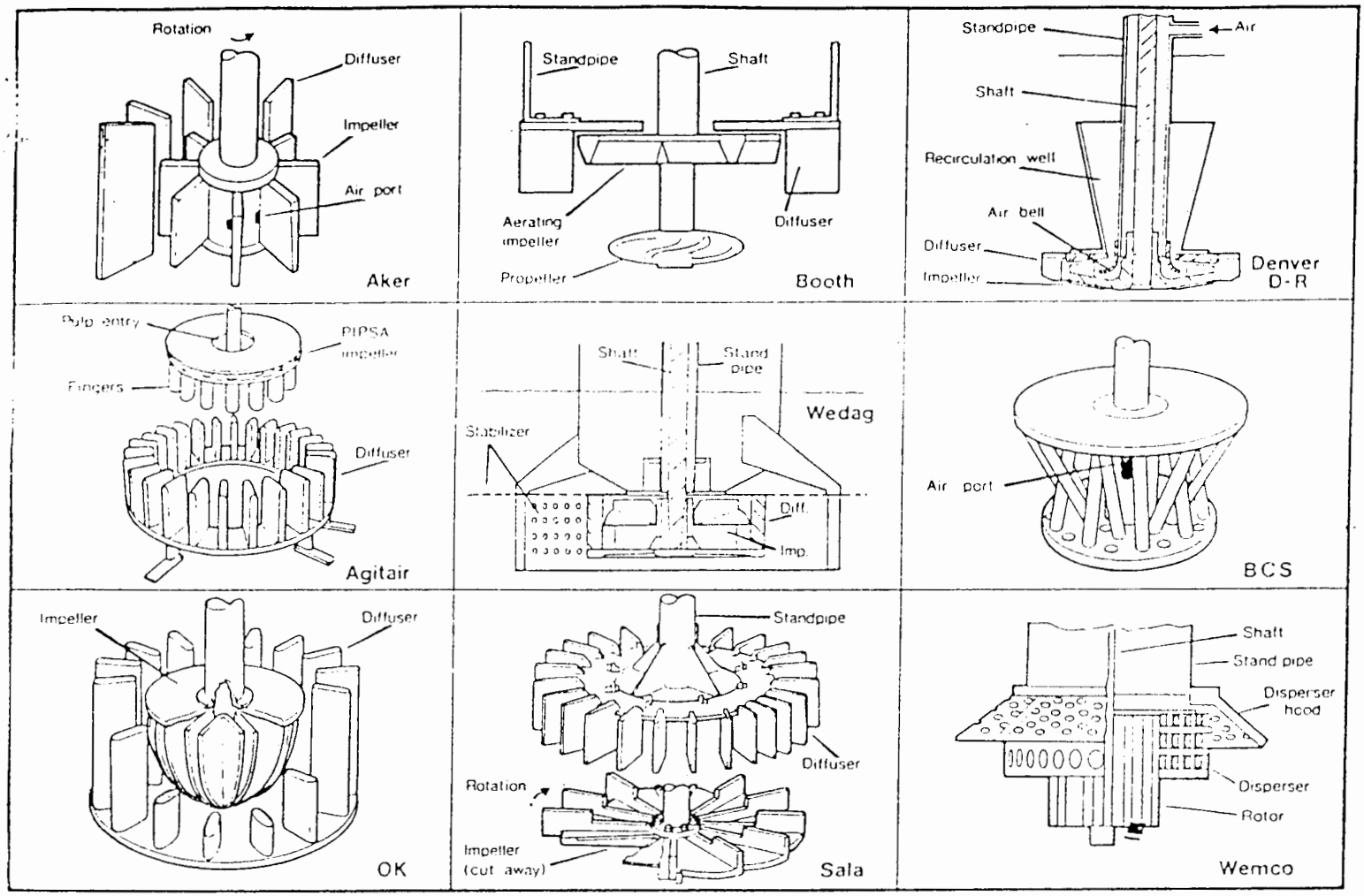

Figure 2.15: Impeller Geometries in Typical Mechanical Agitated Cells (Young, 1982).

During operation, the lower propeller draws the pulp up the centre of the machine and pumps it into the aerating impeller, which in turn discharges the pulp towards the tank walls and inwards across the base. An air hood opened to the atmosphere encloses the aerating impeller and communicates with the pulp chamber by a small annular opening around the shaft.

This machine is claimed to produce adequate turbulence for particle-bubble contact, a quiescent froth phase and a high aeration capacity because of the use of double impellers. The Booth machine, however, has a high-power consumption compared with the other mechanical flotation machines. The absence of provision for regulating the air flow is seen as a major drawback to the design, as the control of air is considered by many to be an extremely important criterion for tuning the performance of flotation cells. Some of the early installations were rougher and scavenger circuits on Kennecott Copper Concentrators.

2.6.3.3 *Denver flotation machine*

This class of flotation machines was produced by Denver Equipment Division of Joy Industrial Equipment Co., in the U.S.A. Only the single mechanism D-R cells have been manufactured recently; a double mechanism machine was produced years ago.

The design of the smaller cells, below 2.8-m^3, has changed little since their introduction. Froth paddles and spitzkasten are present to provide quiescence near the froth zone. The larger cells have now been equipped with cast polyurethane impellers, diffusers and air bells or hoods. They are also truncated rectangles in cross-section (Figure 2.14), without spitzkasten but with internal baffles to reduce undesired turbulence. Removable vertical plates are provided between the mechanisms, extending only a short distance below the pulp level, which serve to control the flow of pulp between the cells and to stabilise the froth. The sand discharge dart valves, which regulate the discharge of tailings, have been changed from downward flow to upward flow to minimise the chances of sanding.

The applications of the Denver D-R machine cover a wide range of commodities (coal, copper, gold, etc.) and applications (roughing, scavenging, cleaning, etc.), and several design variations have been introduced. For example, it is claimed by the manufacturers that the coal machine has a specially-developed smaller impeller and a low power consumption to handle the low density pulp typical of the coal industry. Large installations are found in the Philipines mining industries.

2.6.3.4 Agitair flotation machine

The Agitair flotation machines, developed by Galigher Company of the U.S.A., have enjoyed wide acceptance over a broad spectrum of the mining industry. In the original form, cells with multiple spindles were produced but modern advances in engineering have revolutionised the wide range of their products for economic benefits. The original Agitair impeller, which was found to be hardly successful functionally, has been replaced by the newer designs of the Chile-X and the Pipsa impellers (Young, 1982).

The Chile-X impeller has a smaller number of larger fingers than the standard impeller and the Pipsa is essentially the Chile-X unit with a closed impeller 'pump' on its upper surface. This 'pump' draws pulp down the shaft and expels it radially. Air is sucked down the hollow shaft and dispersed by the fingers of the impeller into bubbles that are moved out radially and axially into the bulk of the pulp.

The Pipsa impeller is reputed to give the best solids suspension and has consequently been adopted as the standard impeller for the new brand of Agitair machines. Incorporated in this new design is a smaller, circular stabilizer that is very similar to the stabilizers in the Aker and Outokumpu machines. The new machines are slightly deeper and are truncated rectangular tanks featuring a "double break" to prevent sanding (see Figure 2.14). The presence of vertical plates between cells constrains pulp flow to the impeller region and baffles minimise the turbulence in the froth zone.

The Agitair design and trade name are now owned by EIMCO. Most recent sales have been in Australia and South America.

2.6.3.5 *Wedag (Humboldt) flotation machine*

This group of flotation machines originates from Germany and was designed specifically for coal flotation, although it is suitable for treating mineral slurries containing no coarse particles (Young, 1982). Like the Agitair, the Wedag machine has undergone a total overhaul in design. The tank now assumes a trapezoidal shape (Figure 2.14) for all the different size ranges, and punched plates are used as baffles, in the form of a horizontal plate over the diffuser and a large cylinder around the diffuser. A row of paddles is present to remove the usually heavily-loaded froth as is typical of coal flotation systems.

The mechanism, however, essentially remains unchanged. Pulp is drawn in from above and below and thrown horizontally through the diffuser. Air is drawn down a standpipe concentric with the impeller shaft. Interchangeable throat rings can be fitted to the two pulp entry ports in the diffuser body to control the pulp flow through the impeller, and the control of air flowrate is by a variable constriction at the air inlet.

A new impeller, the "multiple wobble" (Figure 2.15), consists of a number of vertical, radial vanes connected by tilted disc sectors, each alternative sector tilted in the opposite sense. The impeller is of a shallow, self-aerating design and the tank depth is restricted by the ability of the impeller to induce adequate airflow.

2.6.3.6 Outokumpu flotation machine

Outokumpu Oy is a Finnish company that manufactures the Outokumpu (OK) range of flotation machines. The OK impeller, like the Minemet impeller, is a radical departure from the flat turbine impellers seen in the other types of flotation machines. The rotor has the shape of a half sphere and consists of a number of

narrow, vertical slots that communicate with the air passage in the hollow shaft. Each slot tapers downwards and the top of the rotor is closed by a horizontal disc. With the rotation of the impeller, the pulp is accelerated in the slots and expelled near the point of maximum diameter; this pulp is replaced by fresh pulp that enters the slots near the base. The impeller thus acts like a pump, drawing in pulp from the base of the cell and expelling it upwards. Air is blown down the shaft and mixed into the pulp by the pumping action of the impeller. The air drawn in is discharged from the upper two-thirds of the rotor height; the lower one-third does not disperse air but only functions as the suction side of the rotor by pumping slurry. The impeller is surrounded by a circular stator. The shape of the impeller is said to prevent sanding of the impeller during shutdowns, and to enable easy start-up under load.

The direction of the pulp flow outside the mechanism is towards the tank walls and upwards, which effectively maintains adequate turbulence in the entire cell space and thus intensifies the collision of bubbles and particles. In spite of its size, the rotor acting as a powerful pump can maintain even quite coarse particles in suspension throughout the cell (Fallenius, 1975). Figure 2.16 is a diagram of a typical OK impeller showing the inflow of the pulp to the rotor and the outflow of pulp and air from the rotor.

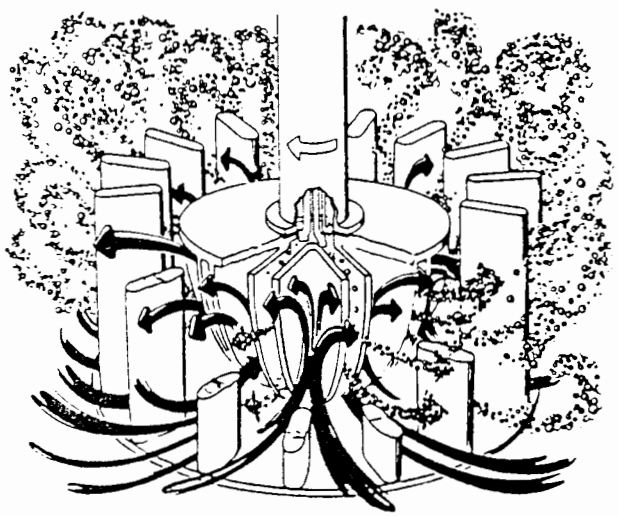

Figure 2.16: Pulp and Air flow around the rotor and stator of OK Cell (from Kelly and Spottiswood, 1982).

Smaller cells up to 8-m^3 are usually baffled and are rectangular in shape while larger sizes are U-shaped, usually without baffles. The U-shape contributes substantially to the hydrodynamic performance of the mechanism.

The requirements of the mechanism of a large flotation machine are considerable. For example, the OK 16-m^3 has been designed and sized so that particle suspension is effectively maintained throughout the cell and also the rotor is able to disperse a large amount of air, some 15-25 m^3/min, into fine bubbles.

The OK flotation cell has a wide application in the flotation of sulphides and ores of iron, clays, tin and tungsten and pgm. It is also used widely in hydrometallurgical processes as a gas dispersion agitator. In Figure 2.16, the separate paths for the introduction of air and slurry to the mantle of the rotor can be seen. The rotor is formed deep so that its diameter is kept moderate and the dispersion surface still remains sufficient. A deep rotor however disperses air effectively only when the air is introduced deep down its lower section (Fallenius, 1975).

To improve performance, several derivatives of the original OK designs have emerged. The OK TankCells, cylindrical in shape, are claimed to show better performance than conventional cells in producing high concentrate grades and superior selectivity. The large sizes of the TankCells, up to 160-m^3, translate into the use of fewer cells, and lower maintenance and operating costs compared with the conventional cells. Recent installations are found on the Karee Concentrator in South Africa, the Mt Keith nickel mine in Western Australia and the Ashanti Goldfields mine in Ghana.

2.6.3.7 WEMCO flotation machine

WEMCO flotation machines, manufactured by the EIMCO Process Equipment Company and its agents worldwide, are the largest group of flotation machines in the mining industry today. Their success can be attributed to the simplicity of the original design, which provides good air dispersion, together with good marketing

techniques and engineering services. There is hardly any evidence to show that the dominance of WEMCO machines is due to their superior performance in flotation over the other types of flotation machines. However, WEMCO machines operate reliably over a wide range of variations in feed grade and pulp density, and are considered by many a good choice because of this.

Figure 2.17a shows the mechanism of a WEMCO cell. It consists of a star-shaped rotor (1) suspended in the pulp between a draft tube (3), at the bottom of the cell, and a standpipe (2) at the top of the cell. The draft tube sits on the false bottom (7). The rotor is surrounded by a disperser (4), which is a cylindrical shell having a series of holes through which the three-phase mix can pass.

In operation, the impeller rotation generates a vortex in the pulp that extends from the interior midpoint of the standpipe, through the rotor, down to the top region of the draft tube. The resulting vacuum, generated in the core of this vortex, induces air through the air-inlet duct (6) into the interior of the rotor. Air flowing between the rotor vanes is mixed with pulp. These are simultaneously circulated, by the rotor, from the bottom of the vessel through the draft tube to the rotor.

The three-phase air-pulp mixture leaves the rotor blades with a dominant tangential momentum vector that is turned to the radial direction. This creates further mixing, as the flow passes through holes of the disperser (Figure 2.17b). The floatable particle-air bubble aggregates separates from the rest of the pulp by rising toward the top of the cell. The hood (5) baffles the flow leaving the disperser, to provide a quiescent zone in the vicinity of the froth.

All the individual mechanism elements are important in influencing the flotation cell hydrodynamic patterns, but the rotor is the most important. It is the key parameter in the determination of air transfer and liquid circulation capacity of the mechanism. Air ingestion and liquid circulation capacity is also determined by rotor speed and submergence in the pulp. Rotor submergence is defined as the vertical

distance between the top of the rotor and the pulp surface when the rotor is not in operation.

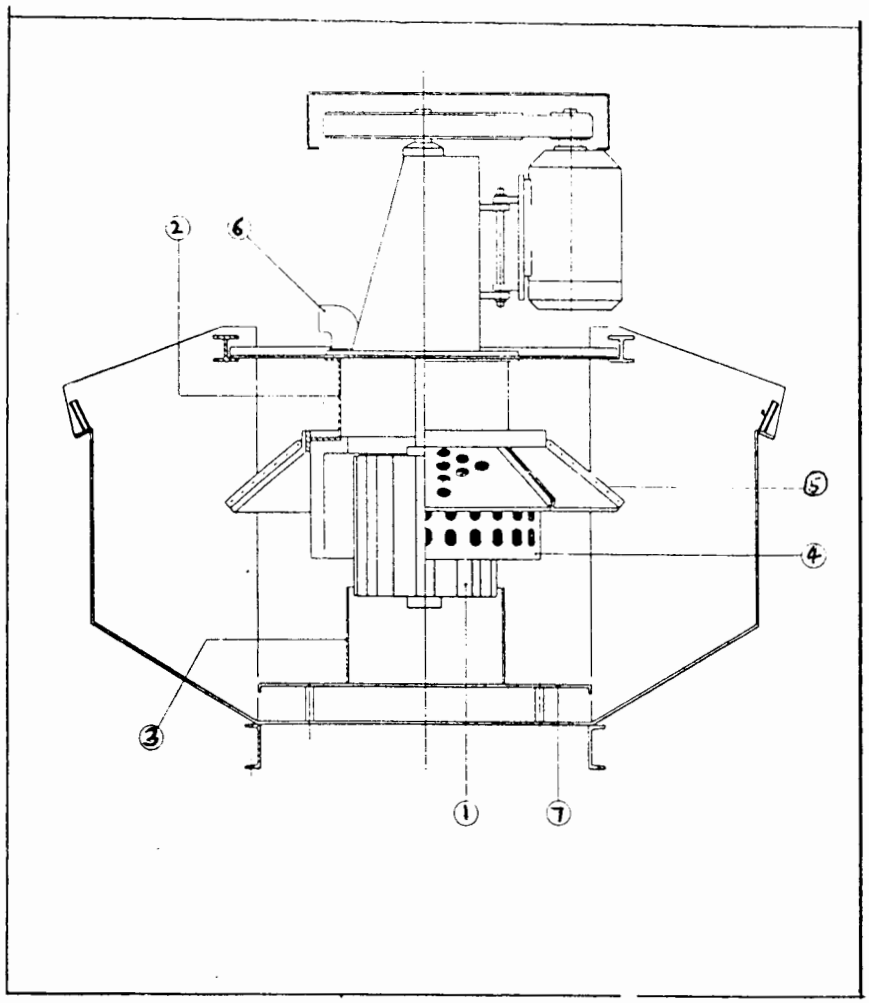

(a)

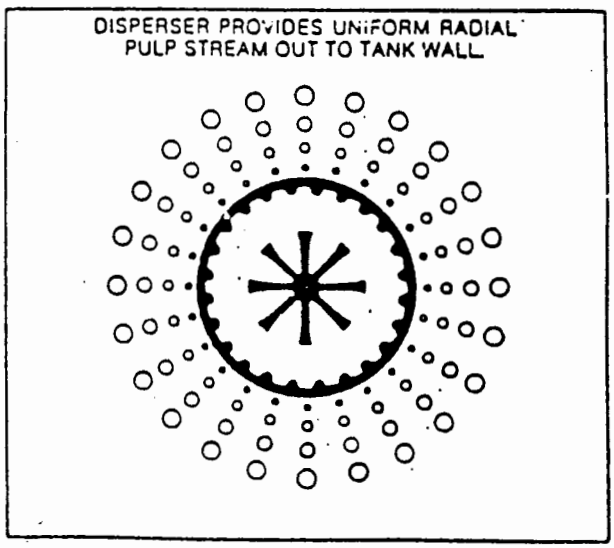

(b)

Figure 2.17: (a) WEMCO Cell, (b) Pulp and Air outflow from Mechanism (Eby, 1972).

Similar to the OK TankCells, the WEMCO SmartCell flotation machines have been developed more recently with the aim of optimising the flotation recovery, concentrate grade and operating cost over the existing range of conventional WEMCO flotation machines. The new SmartCell machine, as in Figure 2.18, employs the WEMCO 1+1 mechanism, which is said to have been reconfigured to produce improved performance, while retaining the aeration mechanism of the 1+1. Induced air provides efficient aeration, and mechanical simplicity and capital economy are some of the benefits envisaged

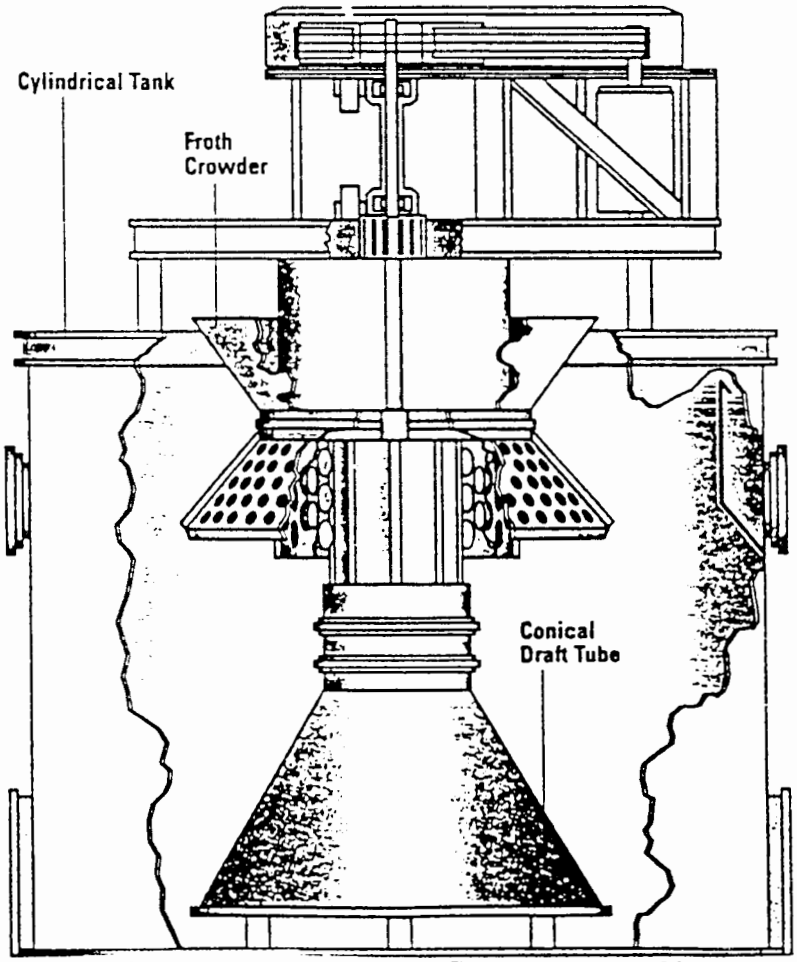

Figure 2.18: WEMCO SmartCell Flotation Machine.

The key features of the SmartCell include a cylindrical tank, conical draft tube and froth crowder. The cylindrical geometry is said to improve mixing efficiency and air dispersion because all points in the cell are at equal distance from the rotor discharge. The uniformity of the mixing in the SmartCell is confirmed by the stability of the froth seen on the surface of the cell. The conical draft tube improves

pumping, circulation and solids suspension compared to the conventional cells. Short circuiting is said to be reduced and bubble-particle contact opportunities are increased with positive impact on metallurgical performance. A froth crowder, which is not used in the conventional cells, accelerates solids transport across the cell surface, reducing the residence time in the froth phase and the air input required for froth transport.

2.6.3.8 Minemet (or BCS) flotation machine

The Minemet Industrie of France are the manufacturers of the Minemet or BCS group of flotation machines, popular mostly in the French speaking world. The peculiarity in this class of machines lies in the fact that it has neither baffles nor stators, and the impeller is of original design as the OK impellers.

The Minemet crossbar impellers consist of two series of circular bars forming two opposite cones on a common vertical axis (see Figure 2.15). The bars are mounted between two horizontal discs of different diameters; the lower disc being about three quarters the diameter of the upper. The lower disc has perforations for partial recirculation of pulp. The height of the impeller is about half the diameter of the top disc. The impeller provides for thorough mixing of the pulp and air dispersion. The efficiency of the impeller is related to the arrangement of the bars, providing differential peripheral speeds. Pulp is drawn into the lower parts of the impeller and expelled upwards. The impeller does not sand up on shut down and can be restarted under full load. The tank is rectangular with a small spitzkasten to accomodate the large froth paddles. Vertical plates separate the cells and help in retaining the froth and controlling the pulp flow to the impeller zone.

Minemet machines were used for floating sulphides, base-metal oxide ores, phosphates, etc. The impeller speed is adjustable to suit the application; the high speeds give a high air dispersion and solids suspension at the expense of greater power consumption. Maintenance is however very simple and rapid.

2.6.3.9 Sala flotation machine

Sala International AB, Sweden, are the manufacturers of the Sala flotation machine. The Sala AS series are the current products and are evidently different in design from earlier series. The design emphasises radial mixing more than vertical and it is said that natural stratification in the pulp is beneficial to the flotation process. The impeller is a flat disc with vertical, radial blades on both surfaces, and the disc is cut back behind the trailing edge of the blade. The upper blades expel air blown down the standpipe, and the lower blades expel slurry from the central base area of the tank. These two flows mix in the cut out areas of the disc and the aerated slurry is then expelled through the circular stabilizer of fairly conventional design.

It is useful to note some of the constraints of the design as below:

- an unusually large impeller diameter in relation to the tank size is required to prevent sanding in the corners of the cell;
- the clearance under the impeller is critical for good agitation; and
- the impeller is unidirectional.

However, Sala cells are acclaimed for exceptional ability to:

- disperse air into very closely sized fine bubbles which are suitable for fine particle flotation; and
- perform air dispersion and pulp circulation independently, by the upper and lower impeller surfaces; therefore the change in the pulp flow characteristics does not change the air dispersion achieved by the impeller.

The tank is rectangular (Figure 2.14) with no internal baffles and with vertical plates between mechanisms to restrict pulp flow to the impeller zone. Sala cells are used in the processing of base metals, iron ores, coal and industrial minerals.

2.6.3.10 Bateman flotation machine

The Bateman flotation machine is a novel machine developed by Bateman Equipment Limited and Metquip (Pty) Limited of Australia, in 1993. It consists of a U-shaped open tank with an impeller connected to a solid drive shaft (Figure 2.19). Air is forced down the cell through a standpipe surrounding the shaft into an open impeller. A hood, with baffle plates projecting downwards to form a stator, is connected to the bottom of the standpipe.

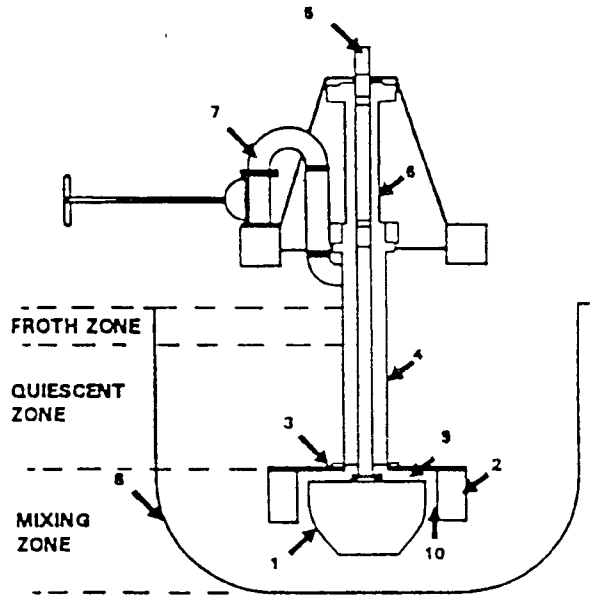

1. IMPELLER
2. STATOR BLADE
3. STATOR HOOD
4. STAND PIPE
5. SHAFT
6. BEARING ASSEMBLY
7. AIR CONTROL
8. TANK
9. HOOD GAP
10. CONTACT AREA

Figure 2.19: Bateman Flotation Cell (from Bezuidenhout, 1995).

During operation, air cavities are formed behind the blades of the impeller as it rotates. The impeller edge shears the air into fine bubbles which are radially dispersed through the stator vanes. The shape of the Bateman cell impeller is very similar to that of the OK cell. The open pumping characteristics of the parabolic impeller are the result of the pressure drop upwards along the height of the impeller.

Air dispersion capacity is determined by the proportion of the impeller volume occupied by the air. The horizontal hood of the stator assembly has a horizontal baffling effect on turbulent pulp flow emanating from the mixing zone. This enhances the relative tranquillity in the quiescent zone above the hood plane thus improving the separation of the hydrophilic particles from the bubble-attached hydrophobic particles. The horizontal stator hood protects the impeller from settled solids during a shutdown, ensuring the rotor does not get "bogged" so that it can easily be restarted. The low power consumption for particle suspension is assisted by the suspended impeller, which unlike the conventional designs does not hinder the upward flow of solids into the impeller. A 3-m^3 cell is found on the Karee

Platinum Concentrator and versions of 38-m^3 cells have been installed on Goldfields of South Africa's Northam Platinum plant on the Bushveld Complex north of Johannesburg, all in South Africa.

The relatively shorter blades reduce the total baffling, contributing to lower operating power requirement. The open-topped impeller design enhances high pumping capacity of the impeller allowing operation at relatively low rotational speed while maintaining dense particle suspension capability. Sizes ranging from 3-100-m^3 are available for various industrial applications. The smallers cells are usually employed in cleaner circuits while the large ones are designed for rougher circuits. The Bateman flotation machines have proved very efficient in the flotation of pgms, graphite and base metals.

2.6.3.11 Dorr-Oliver flotation machine

Dorr-Oliver flotation cells, until recently, were manufactured and owned by Dorr-Oliver Company Ltd. They are now owned by Svedala Company Ltd. The Dorr-Oliver cells are produced in a variety of sizes, all claiming to have low power consumption. A number of its design features are said to account for this feat. One is the design of the stator (Figure 2.20), which possesses legs to lift it clear of the bottom of the tank and thereby eliminates the effect of baffling in the lowest

circulating zone. Another is the rotor's vortex profile; large pumping channels produce a positive radial flow pattern, as well as allowing a large portion of the rotor blades to assume the role of air dispersion. The Dorr-Oliver and the Outokumpu machines are similar in many respects; whereas most "traditional" flotation machines are basically agitators, the Dorr-Oliver and Outokumpu machines are essentially pumps due to their vortex-shaped rotors. The Dorr-Oliver is, however, claimed to be an improvement on the Outokumpu machine in that the double wall has been eliminated to maximise pump chamber volume. Also, the stator blades on the Dorr-Oliver machine have been eliminated in the lower area of the cell to avoid throttling the suction of the "pump".

Air is supplied to the cell via a hollow shaft that leads directly to an air chamber contained in the rotor itself, before passing into the pumping channels. The rotor's high pumping efficiency disperses large volumes of air, when compared with turbine-type rotors. The air pockets created during rotation on the trailing face of each blade provide a large slurry interface. The vortex profile circulates more pulp through the rotor, effectively dispersing more air. Directional slurry flow and extra rotor depth disperse fine air bubbles across almost the entire cross-sectional area, and in the lowest region of the cell. Recent installations include the Dumagami and Inco gold mines in Canada and the Elders gold mine in Australia.

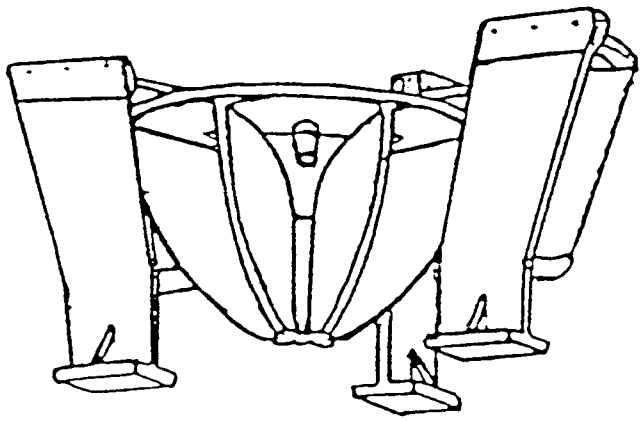

Figure 2.20: Dorr-Oliver Impeller (from Gorain, *et al.*, 1995a).

2.7 MECHANICAL FLOTATION CELLS

2.7.1 Design Criteria

The design of flotation cells is often a matter of experience combined with judgement and a certain amount of prejudice rather than design from a detailed analysis based on first principles (Young, 1982).

Flotation machines are designed to produce maximum recovery of valuable minerals, at high product grades and the lowest possible cost. These machines are therefore designed such that the following objectives can be achieved simultaneously from the cell:

- maintenance of particles in suspension,
- dispersion of air into small bubbles in the slurry,
- creation of adequate conditions for bubble-particle contact,
- creation of quiescent conditions in the froth zone of the cell,
- ensuring that particles entering the cell are removed relatively easily into the concentrate and tailings streams,
- ensuring easy start-up after stoppages due to breakdowns, power outages, etc.,
- ensuring that cell geometries fit easily into circuits (in series configurations), and
- provision for easy removal of froth.

Since the flotation machines can be regarded as three-phase chemical reactors in which three-phase contacts are responsible for separation of the solid phases, their general design criteria will be discussed along the lines of standard chemical reactors. In this section, the critical components of the reactor such as tank geometry, volume and impeller systems are discussed.

2.7.2 Tank geometry

Mixing tanks have appeared in all shapes and sizes in various spheres of chemical and metallurgical engineering applications. However, it was not until the last few decades that a standard geometry was produced to govern the design of reactors. Figure 2.21 shows a standard reactor with tank diameter T, impeller diameter D, impeller blade width W, off-bottom impeller clearance C, liquid height H, and wall baffles of width B. For easy referencing, all dimensions are based on the tank diameter, particularly for scale-up purposes.

It is important to note that the standard geometry as described in Figure 2.21 is not standard for all processes that occur in a tank. The flotation process uses tank geometries far different from the standard geometry so described. In view of the different functions they perform and the high solids content of the pulp encountered in them, relative to chemical reactors, flotation cells are normally shaped in such a manner that dead spots are reduced to a minimum and turbulence is prevalent in all sections of the cell.

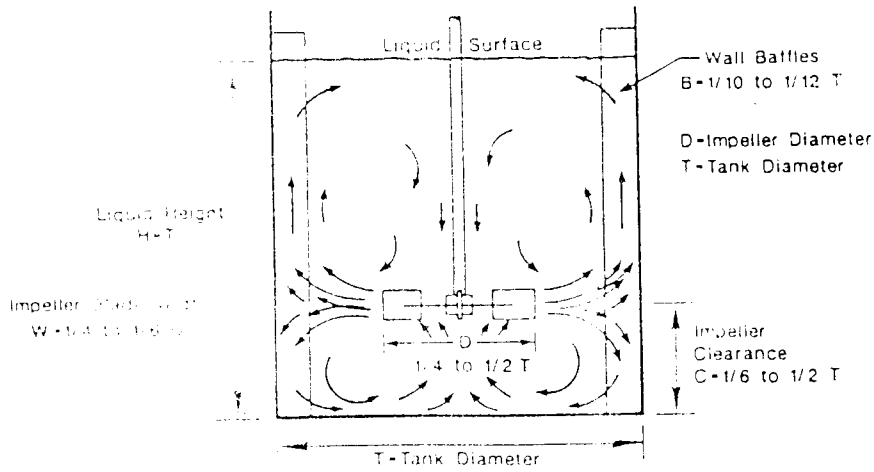

Figure 2.21 Gross flow pattern for a radial flow impeller showing standard tank geometry (from Tatterson, 1991).

Another important distinguishing feature is the provision of a facility for easy transfer and collection of froth from the flotation cells. Flotation cells are therefore developed in various forms and shapes - rectangular, cylindrical, U-shaped, etc., designed to achieve the above- mentioned objectives, but do not generally show a wide variation in shape within the given types.

Baffles are often considered an integral part of a chemical reactor. They are sited in the path of flow of slurry to disturb or redirect the flow. The most common types are wall baffles, with widths usually expressed as a percentage (e.g. 10%) of tank diameter. However, other types of baffles exist in the form of disk baffles suspended on the impeller shaft. The presence of baffles in the tank increases the power consumption and reduces the solid body rotation of the pulp, a condition which is undesirable in flotation or any mixing processes (Tatterson, 1991). In flotation cells, special types of baffles in the form of stators are largely used.

Modern flotation cells are arranged in series or in parallel to each other. In the series configuration, the cells are usually shaped and partitioned into two or more cells for easy interconnection and also to ease pulp flow along the bank. Partitions may be omitted in the case of free-flow or hog-trough design. Machines of the same type usually possess a clear resemblance but often do not show much geometrical similarity in the different size ranges.

The bottom edges and corners of most flotation cells are truncated to enhance agitation. This is usually prominent in machines that have shallow impeller submergence and smaller impeller-to-tank diameter ratios. The corners of rectangular cells provide some baffling effect and complete truncation can result in swirl of pulp in the cell.

Surface truncation is also provided in some designs in the form of crowder or deflector plates that assist the forward flow of concentrate, thereby minimising the air input required for froth mobility.

2.7.3 Tank volume

Data collated for about twenty families of flotation machines (Harris and Lepetic, 1966) have shown that the effective volume, V, and the tank diameter, T, can be described by a simple correlation:

$$V = kT^n \quad (26)$$

k and n are constants and are characteristic for a given type. Values of n and k differ by manufacturer but have all been found to lie in the ranges $2 < n < 3$ and $0.6 < k < 1.3$, with typical values of $n = 2.6$ and $k = 0.9$. Practically, the significance of n can be explained as follows: n=2 represents a constant pulp level while n=3 is interpreted as the presence of a striking geometrical similarity (Harris and Lepetic, 1966).

2.7.4 Impeller Design

The impeller is the single component that displays the widest range of difference in design in the flotation cell. It is often described as the "heart" of the flotation machine. The main functions of the impeller are to create fluid motion in the cell, and to disperse air into small bubbles to all parts of the reactor.

Impellers used in the chemical industry are generally defined according to the mixing regime employed, i.e. laminar or turbulent flow regime. Hixson and Baum (1942) have classified impellers in the turbulent flow regime into axial and radial flow impellers. Further classification of impellers by Weetman and Oldshue (1988) is based on the duty of the impeller, whether it is a flow, pressure or shear impeller. Impellers with large pumping capacity are called flow impellers, those that work against pressure gradients are pressure impellers and the class that produce shear are shear impellers. Flotation machine impellers generally produce radial flows so their behaviour is very similar to the radial flow impellers used in chemical reactors.

Knowledge of the power drawn by a rotating impeller is of vital importance for the design of a chemical reactor. The performance of mechanically agitated contactors is governed by the power characteristics, which are directly related to the operating cost. It has been shown by Uhl and Gray, (1966), Joshi, *et al.*, (1982) and Oldshue, (1984) that, for a given process, the impeller performance per unit power consumption depends very much upon the impeller design. A lot of work has been done over the last few decades in an attempt to optimise the impeller design in order that maximum performance and economy are achieved.

Tatterson, *et al.*, (1980) have studied extensively the flow generated by pitched blade turbines. Ali, *et al.*, (1981) have also studied liquid dispersion mechanisms in agitated tanks using pitched blade turbines. Recently, Pandit and Joshi (1983) and Raghava Rao, *et al.*, (1988a, 1988b, 1988c, 1989a, 1989b) have studied in greater detail solid suspension, gas dispersion and liquid-phase mixing in solid-liquid, gas-liquid and gas-liquid-solid systems using different types of impellers. They found that the pitched blade turbine, down-flow (PTD) was the most energy-efficient among the impeller types studied.

The study was taken a step further by Rewatkar, *et al.*, (1990), who investigated the contributions of the different geometric parameters of the PTD impeller on power consumption. The effect of the blade angle, blade width, impeller diameter, hub size, blade thickness, impeller clearance, liquid height and vessel size on power consumption were studied to a large extent. Some of the findings, which are generally applicable to the other types of impellers, are summarised in the sections below.

2.7.4.1 Effect of impeller clearance

The biggest effect of the impeller clearance is on the power consumption. When the impeller is far from the bottom of the cell, the liquid flow changes direction continuously so that the downward flow changes direction to flow along the base, horizontal to the tank, before it starts to rise along the sides of the wall. As the impeller clearance decreases, the change in direction becomes more sudden as the

flow hits the base and more energy is dissipated. At the smallest clearance, all the kinetic energy is dissipated. Hence, the power number is found to increase significantly with decreasing impeller clearance.

2.7.4.2 Effect of impeller diameter

As the impeller diameter is increased, the power consumption is found to increase as well. One of the reasons purported to account for this phenomenon is that the increase in impeller diameter increases the impeller blade width and the radial component of the liquid velocity is thus increased. The axial component, because of the high velocity, changes direction twice before it rises along the sides of the wall. Much energy is dissipated during these changes in direction.

A second possible reason is attributed to the high form energy dissipated due to the larger blade sizes. A third reason could be that the high radial velocity opposes the axial component rising along the tank wall. All of these reasons may account to some degree for the high power number in the large impeller scenario.

2.7.4.3 Effect of impeller blade angle

The blade angle has a strong influence on the power number. The blade angle refers to the angle the blade subtends to the horizontal. For a given impeller of fixed diameter and blade width, the projected blade width increases with an increase in the blade angle. Due to the low projected blade width, less form dissipation of energy occurs behind the impeller blade and therefore, for example, a PTD with a blade angle of 30 degrees consumes less power than a blade angle of 45 degrees.

Another observation is related to the liquid velocity and turbulent intensity. It is found that increasing the blade angle up to 60 degrees increases the average liquid velocity and the turbulence intensity in the tank. This trend ceases to hold at blade angles greater than 60 degrees, because large angles alter the nature of the impeller stream through the generation of a stronger trailing vortices behind the blades. At

90 degrees blade angle, the flow is completely radial. The increased form dissipation and higher turbulence results in a higher power number.

2.7.4.4 Effect of blade width

The effect of impeller blade width has been studied indirectly as the ratio of the impeller width (W) to the diameter (D) (Uhl and Gray, 1966). It has been found that, for a given impeller angle and clearance, the power number increases almost linearly with the impeller blade width. An increase in the blade width increases the form dissipation energy, and also increases the radial component of the fluid flow far above the axial component. At very large widths, the flow pattern is almost completely radial and higher form energy is dissipated. Ranade and Joshi (1989) observed that the effect of changes in blade width is not as significant as changes in the blade angle in smaller tanks.

2.7.4.5 Effect of number of blades

The power number increases with an increase in the number of blades. This is because with an increased number of blades, form dissipation increases and turbulence intensity increases as well. It therefore follows from the previous discussion that a higher power number results. It has been observed by Raghava Rao, *et al.*, (1989a) that the performance improves considerably in gas dispersion and solids suspension when the number of blades is increased.

2.7.4.6 Effect of blade thickness

The effect of blade thickness on power consumption is not very significant as compared with other parameters. The slight increase in power number with an increase in blade thickness is due to edge effects of the impeller blades.

2.7.5 Flotation cell impellers

A subaeration flotation machine is required primarily to perform the functions of particle suspension and aeration. The manner in which pulp and air interact with the impeller is perceived differently by the different manufacturers (Harris, 1976). This accounts for the differences in design among the various makes of subaeration machines.

In one case, the aim of the manufacturer is to maintain separate flow of air and pulp, presumably in order to attain optimum design for each function. This is the principle underlining the design of the Outokumpu flotation impeller. In another case, the aim is to mix pulp and air in the eye of the impeller, as exemplified by the Denver design. Other designs fall between these extremes. In all cases air-pulp contact occurs at the impeller periphery and beyond. Pulp is ejected in the high-pressure region at the leading edge of the blade, while bubbles are created in the low-pressure region at the trailing edge of the blade; to a certain extent their flow paths must separate.

While the design of impellers in flotation cells departs largely from the standard chemical engineering design criteria, they are suited for their specific environments and there is some degree of similarity among the different manufacturers. Some of the special characteristics of flotation impellers are pointed out in the sections that follow.

2.7.5.1 Impeller-cell aspect ratio (D/T)

Different designs exhibit an almost constant impeller per cell ratio for the different-sized cells of the same type. Harris, *et al.*, (1975) have found that most fell in the range from 0.4 to 0.5; in the cases of the Denver, a constant value of 0.5 was maintained in the different size ranges. The smallest aspect ratio observed by Harris *et al.*, (1975) was 0.25 for the family of WEMCO cells.

2.7.5.2 Impeller aspect ratio (b/D)

The aspect ratio of an impeller is the ratio of its height (b) and diameter (D). Harris and Lepetic (1966) have reported that the impeller aspect ratio of all the flotation cells measured lay in the range 0.15 to 0.9, with Denver impellers showing the smallest ratio and the WEMCO the highest. Thus the WEMCO cells employ the largest impeller aspect ratio but the smallest impeller/cell aspect ratio.

2.7.5.3 Number and types of blades

The number of blades for the turbine impellers varies from four to 16. Blades are usually perpendincular to the direction of rotation to maximize radial pulp flow. There exist however, different forms and orientation of impeller blades: Minemet uses pairs of posts set to cross at an angle to enhance vortexing, and curved impellers as in the Mekhanobr have been manufactured (Harris, 1976).

The old versions of the Booth machine use both an impeller and a propeller to optimise gas dispersion and solids suspension simultaneously. Except for the Humboldt, all impellers are symmetrical in the horizontal axis so that direction of rotations can be reversed to extend the useful life of the impeller.

2.7.5.4 Impeller clearance

Clearance is the distance between the impeller and the bottom of the cell and has been found to have a significant effect on the general flow patterns and power consumption in the flotation cell. Axial flow impellers, placed close to the tank bottom, will discharge radially. The optimum clearance suggested by Chapman, *et al.*, (1983a, b and c) for a six-bladed, disc-turbine impeller is one-quarter of the tank diameter (C = T/4). This distance has been found to enhance particle suspension and has also been recommended as the optimum for gas dispersion.

2.7.6 Other features

Many features have been incorporated by various manufacturers into the design of flotation cells, which have the overall advantage of getting around problems like the incidences of solids bogging impellers on shut downs, especially unplanned stoppages resulting from power outages or other engineering failures. For example, the WEMCO and Aker impellers are manufactured with pliable materials that enable them to flex in response to high loads.

In the Outokumpu and the Minemet designs, the size of the lower section of the impeller is smaller than the upper section to obviate start up problems. This is as a result of the lower torque required to disperse the settled solids by the smaller diameter at the base of the impeller.

The provision of hoods around the impeller in some designs can be helpful in holding enough air to fluidise the settled solids, thereby putting less strain on the impeller. It is quite common for impellers to be covered with wear-resistant material (polymer) to minimise wear by coarse particles and tramp metals, thereby prolonging their useful lives.

2.7.6.1 *Draft Tube*

A draft tube is a tube in which the impeller is positioned to create a strong axial flow in chemical reactors. Its main functions are to enhance uniform mixing in the cell especially in wide and tall vessels in which the mixing effect of the impeller is minimal at remote distances from it, and also to aid air induction into the reactor. The diameter of the draft tube is usually slightly larger than the impeller diameter.

The draft tube concept is not popular in many flotation cells types. However all WEMCO cells employ this concept in their designs.

2.6.6.2 *Stator*

The stator is a stationary ring of vanes placed around the perimeter of the impeller to redirect the impeller discharge flow, hinder the formation of solid body rotation and create a quiescent zone in the upper sections of the cell. The effect of the stator on flotation performance is still not fully understood. While some manufacturers claim that the impeller/stator clearance is important and so provide wear plates to offset wear, others like EIMCO maintain a substantial clearance to minimise the effect of wear. There are, however, still other designs in which stators are completely absent. At one time, the stator was erroneously perceived as responsible for breakage of air bubbles in a flotation cell. Grainger-Allen (1970) has shown that the stator does not aid in breaking of bubbles (see section 2.3.8).

Stator blades close to the impeller direct bubbles radially outwards towards the walls of the cell, improving air dispersion and increasing aeration capacity. Reduction in the clearance between the rotor and the stator increases the aeration and the power consumption but decreases the specific power consumption.

2.7.7 Method of aeration

The method by which air is admitted into flotation machines depends on whether the machine is self-aerated or supercharged. The self-aerated machines usually have standpipes, terminating in hoods or shrouds covering the impeller. The supercharged cells often have standpipes, hollow impeller driveshafts, nozzles or spargers below the impeller, and are supplied with air by compressors and blowers.

It has been found that the chances of solids settling in flotation machines increase as the size of the mechanism increases (Harris, *et al.*, 1975). This is due to the interference of the mechanism with the flow pattern in the tank. It is therefore important that in designing a flotation machine, the air entry method and the size of the mechanism

should be as small and simple as possible to minimise interference with the pulp flow pattern.

2.7.7.1 Self-aerated machines

Since the amount of air induced into the self-aerated reactors is a function of the design parameters and the operating conditions, it is important that the principle of air induction is investigated further in order to identify the important factors for the purposes of optimisation.

Schlichting (1968) has shown that for an ideal, frictionless fluid with density ρ, the pressure at any point in the fluid obeys the Bernoulli equation:

$$d\left(\frac{\rho v^2}{2}\right) + d(P') = 0 \qquad (27)$$

When the impeller is at rest, the value of P′ on the impeller is equal to the static head above it. When the impeller speed is increased, from zero, the value of P′ decreases according to the equation above. At a certain critical speed, the value of P′ becomes equal to the pressure in the gas space above the liquid. Further increase in the impeller speed creates a driving force for the flow of gas. Sawant and Joshi (1979) have shown that the value of the critical speed (Nc), is given by:

$$N_c = \left(\frac{0.21gH}{D^2}\right)\left(\frac{\mu}{\mu_w}\right)^{0.11} \qquad (28)$$

2.7.7.2 Effect of liquid density

Joshi and Sharma (1977) have shown that the rate of gas induction is practically independent of the liquid density. On the basis of equation (27), it may appear contradictory that the liquid density has no effect on the rate of gas induction. However it may be argued that, although the static pressure may increase with the

increase in liquid density, the resistance to the flow of gas due to a greater static head of liquid ($H\rho_L g$) and, therefore, the minimum impeller speed required for the onset of gas induction, remain unaffected.

2.7.7.3 Effect of impeller speed

When the impeller speed is increased beyond the critical speed, gas induction begins. It is obvious from equation (28) that the rate of gas induction increases with an increase in impeller speed. An increase in the impeller speed enhances greater liquid flow in the radial direction, increasing the driving force which results in an increase in gas induction.

2.7.7.4 Effect of impeller diameter

Sawant and Joshi (1979) have established that the critical impeller speed (N_c) is inversely proportional to the square of the impeller diameter (D) and that the gas flowrate, Q_g, varies as D^3. They correlated the gas induction rate with the impeller speed and impeller diameter for an air-water system and obtained the following equation:

$$Q_g = 0.0021(N^2 - Nc^2)^{0.75} D^3 \quad . \qquad (29)$$

2.7.7.5 Effect of impeller submergence

An increase in the liquid height above the impeller, H, increases the resistance for the flow of gas because of a higher static pressure. The critical impeller speed therefore increases with an increase in the liquid height as suggested by equation (28).

2.7.7.6 Effect of viscosity

Zundelevich (1979) has shown that the rate of gas induction varies linearly with the liquid flow, Q_L by the relation:

$$Q_g = nQ_L \quad . \tag{30}$$

More recently, Sawant and Joshi (1979) have derived a relationship between gas flow and fluid viscosity as follows:

$$Q_g \alpha \mu^{-0.12} \quad . \tag{31}$$

It can therefore be concluded that an increase in the liquid viscosity decreases the liquid pumping capacity of the impeller and the decrease in Q_L results in a reduction of the rate of gas induction.

2.7.8 Scale-up Criteria

It is not presently possible to specify a unique criterion that must be obeyed in the scale-up of flotation cells. However, it is possible to suggest plausible scale-up factors in the light of existing flotation cell data. The flotation cell must be able to fulfil several functions simultaneously. It is required among other things to mix the cell contents, suspend solids, circulate the cell contents through the impeller zone without short-circuiting, draw and disperse air, and permit a stable froth to be formed. The necessary conditions for any of these functions must be such that they are not detrimental to the others; ideally, all should be scaled to achieve an optimum together. In scaling up of flotation cells, the main dimensionless groups which are considered are; the Froude number, the power number and the air flow number (Fallenius, 1979). These dimensionless quantities have already been defined in section 2.3. In addition to these groups, the turbulence and suspension criteria described below have also been suggested as useful scale-up criteria (Fallenius, 1979).

However, all these criteria are in one way or another not adequate in providing accurate scale-up between cells of different sizes because the conditions governing their applications are not usually satisfied in full. For example, for the Froude number, the power number and the air flow number to provide any meaningful scale-up between different sizes of cells, strict adherence to geometrical similarity is a crucial requirement. But geometrical similarity in flotation cells is a rare occurrence even within cells of the same make. To be valid, the suspension criteria require equal particle type and size in the different sizes of cells, while the turbulence criteria require equal turbulence intensity. It is hardly ever possible for these "ideal" conditions to be met satisfactorily and therefore these and other limiting conditions make the use of conventional methods neither very practical nor reliable in scaling up flotation cells.

2.7.8.1 Turbulence Criteria

Turbulent flows in the flotation cell affect particles and the formation of bubble particle aggregates through the turbulent fluctuation of velocity. The forces acting on the particles and bubbles and on particle-bubble aggregates will be equal in magnitude in cells of different sizes if the difference in turbulent velocity has the same value. This requires that the energy dissipations be the same when the kinematic viscosities are the same. When viscosities and surface tension forces are constant, the bubble size is found to be dependent on the difference in turbulent velocity in the dissipative range. This in turn means that a condition for the scale-up of these phenomena for cells of different size is that the fluctuation of the turbulent velocity is the same.

2.7.8.2 Suspension Criteria

Adequate suspension is a basic requirement in a flotation cell if the cell is to function properly, and for any meaningful scale-up purposes. Only when properly suspended can mineral particles adhere to air bubbles and be floated. This can be obtained when the absolute value and the direction of the velocity components prevailing at corresponding points in different cells are the same. At such

corresponding points, the viscous and gravitational forces acting on the particles, bubbles and particle-bubble aggregates are the same, provided that their sizes are the same. This similar state of suspension assumes that the solid content, mineralogical composition, and grain size distribution are the same at the corresponding points in the suspension.

Extensive research work has been done in the area of suspension by Zwietering (1958), Nienow (1968) and Nagata (1975). These results have shown that the same state of suspension can be achieved in mixers of similar type but of different sizes. Unfortunately, none of this work involved mixers in which the stator surrounded the rotor, as in most flotation cells. The results with the stator are expected to be the same; slight differences could possibly occur. Air flow was, however, not considered in their analysis of suspension.

2.8 FLOTATION CIRCUITS

Commercial flotation is carried out as a continuous operation in a series or bank of cells. This increases the residence time, allowing ample opportunity for particle-bubble attachment to occur. The residence time of particles in a bank of cells typically ranges from 5 to 15 minutes, though it may be much longer (up to several hours). The rate at which the particles float will depend on particle composition, pulp density, particle size and degree of turbulence in the cell. The arrangement of a number of cells in series allows for the collection of different products from the various cells. For example, liberated particles float more rapidly than composite particles, so a high grade concentrate can be collected from the first few cells in a bank, and concentrate from the remaining cells can be collected as a middling product.

A wide range in circuit variations, unique to the specific requirements of individual applications, exist. The number of flotation cells in a row varies greatly, from 15 or more to as low as three or four, depending on the flotation kinetics, economics, and plant space considerations. A simple circuit is illustrated in Figure 2.22. The series of

rougher and scavenger flotation might take 10 minutes whereas cleaner flotation may only take about 3 minutes.

The product from the scavenger stage and/or the tailings from the cleaner stage are usually low grade because of locked or composite particles and physically entrained gangue minerals. It may also contain free valuable mineral particles, present due to physical entrainment, odd shape or size or surface contamination. In many industrial plants these low-grade products are retreated after a regrind stage which further liberates the material, making it more amenable to additional flotation. The details of the regrinding practice depend largely on the ore characteristics. For example the presence of composites in any concentrate (such as the rougher concentrate) in any great number would dictate whether the concentrate is sent for regrinding.

2.9 SUMMARY

Most of the research into the operation of mechanical flotation cells has been based on qualitative or empirical considerations and has often not included a full fundamental consideration of the fluid mechanisms and hydrodynamics involved. Though manufacturers of the different types of flotation cells may have developed useful correlations through in-house research programmes, these are often specific to their applications and interests only. This chapter has provided a comprehensive review from classical, chemical engineering sources of the fundamentals of the hydrodynamics and gas dispersion in mechanically agitated vessels relevant to flotation cells. The conclusions of this review will now be summarised.

Hydrodynamics in an agitated tank are largely influenced by the geometry of the impeller and the vessel. Useful correlations exist for determining the fluid flowrate and velocity for the different types of impellers, usually based on the impeller speed and dimensions.

Gas dispersion in mechanically agitated tanks can generally be characterised by two dimensionless quantities; the air flow and Froude numbers. These quantites are in turn functions of the impeller characteristics. In stirred tanks, therefore,

cells that produce the initial concentrate is called the ROUGHER stage. Quite often the grade of concentrate produced from the rougher stage is not sufficiently high and must be further processed through CLEANER and RECLEANER stages. The tailings from the rougher stage, which can still contain considerable valuable particles, may be retreated through a SCAVENGER stage. This maximizes the opportunity for recovering the valuable minerals.

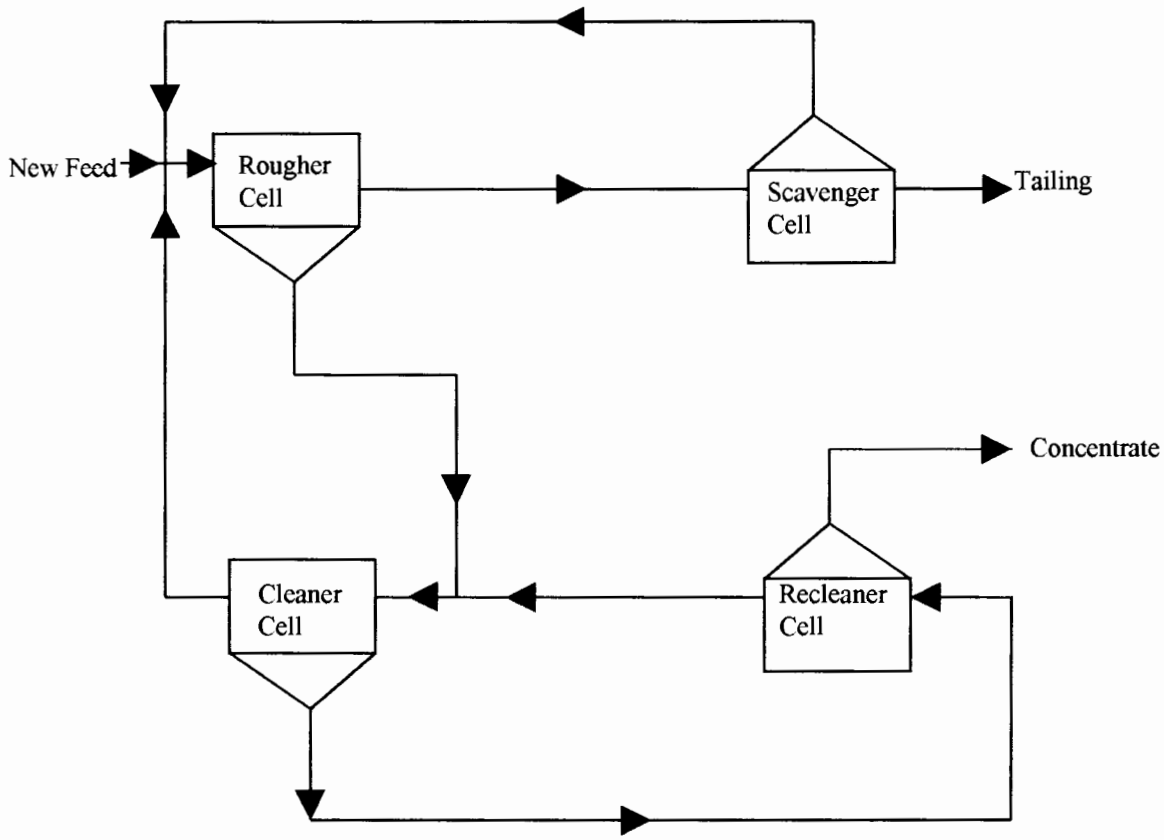

Figure 2.22: Standard Flotation Circuit

In general, the rougher-scavenger duty seeks to achieve high floatable specie recovery while the cleaner-recleaner duty is to achieve high product grade. The rougher-scavenger stages of the flotation circuit are usually given higher reagent dosages and long flotation times than the other stages in the process. On the other hand, the cleaner

The above observations were found to be directly applicable to the operation of mechanical flotation cells. Therefore similar research work aimed at optimising and scaling-up can be very instructive in analysing the performance of these cells. The traditional methods of scaling-up flotation cells have involved the use of the power number, the air flow number, turbulence and suspension criteria and the Froude number. The air flow number is applicable to cells in which the size of the rotor is in a fixed ratio to that of the vessel. The power number can reasonably be applied to systems which bear geometrical similarities. The turbulence factor ensures that similar conditions are preserved in scale-up as far as the hydrodynamics in flotation cells are concerned. Constant Froude number means that the pressure distribution on the surface of the rotor is similar in mechanisms of different sizes, and that conditions inside the rotor are similar.

A large number of events are known to occur in the flotation cell, and it is evident that even more factors can be found which should be taken into account in scale-up. Although the scale-up methods discussed above have good theoretical background and are applicable to a number of systems, they are difficult to apply to flotation systems as they fail to account for the multitude of different impeller and tank geometries that are in use.

It is therefore imperative that an alternative way of characterising flotation cell hydrodynamics be found that can adequately address these issues. The bubble-surface-area-flux (S_b) approach recently proposed by Gorain, *et al.*, (1995a, b; 1996; 1997) appears to address this problem, and is described and discussed in detail in Chapter 3. Unlike the traditional methods, the bubble-surface-area-flux approach is independent of the cell and the impeller geometries, and is a function

only of the hydrodynamics and gas dispersion characteristics in the flotation cell. It has been found that this new approach is a very useful scale-up criterion since it eliminates the geometrical discrepancies encountered in the traditional methods of scaling-up hydrodynamic and gas dispersion performance in flotation cells.

CHAPTER 3

BUBBLE SURFACE AREA FLUX (S_b) - AN ALTERNATIVE WAY OF CHARACTERISING FLOTATION CELL HYDRODYNAMICS AND GAS DISPERSION

3.0 INTRODUCTION

In the operation of mechanically agitated flotation machines, the dispersion of gas into small bubbles has been identified as the most important hydrodynamic process which is controlled by the air flowrate and the impeller speed (Sun and Zimmerman, 1950).

The traditional method of characterising flotation cells using dimensionless quantities such as the air flow number, power number, Froude number, etc. does not provide adequate characterisation criteria. For example, for the air flow number to be used with any appreciable accuracy, the different-sized cells of the same make must have the same geometrical similarity in the ratio of the impeller-to-tank dimensions. Since it is usually difficult for manufacturers to maintain these ratios in their design, characterising flotation with these quantities leaves much to be desired.

A new way of characterising flotation cells - based on the bubble surface area flux - has been proposed by Gorain, *et al.*, (1997). The bubble surface area flux is related to the three gas phase properties in a flotation cell, viz. bubble size, gas holdup and superficial gas velocity. Gorain, *et al.*, (1997) found that these properties could not be related individually to the metallurgical performance expressed in terms of the first order flotation rate constant, k, but when they were combined to determine the bubble surface area flux, they could be related extremely well with k. Consequently, Gorain, *et al.*, (1995a, b; 1996; 1997) proposed that the bubble surface area flux could be used as a characteristic measurement of the hydrodynamic conditions in a flotation cell that had a determining effect on flotation performance.

Unfortunately, all of the Gorain's work (Gorain *et al.*, 1995a, b; 1996, 1997) has been carried out using specially designed and constructed pilot flotation cells, ranging from 60 L to 2.8-m^3 in volume. No such work has been done on industrial-size cells. It is one of the main objectives of this thesis to characterise a number of industrial cells of different types, sizes and duties, by determining the bubble surface area flux, and to find out how bubble surface area flux varies from one cell to another.

This chapter describes and discusses the work of Gorain, *et al.*, (1995a, b; 1996, 1997). Bubble size, gas holdup, superficial gas velocity and the factors that affect them together with the concept of the bubble surface area flux are described in detail. The chapter ends with a discussion of the observed relationship between k, the flotation rate constant, and the bubble surface area flux.

3.1 BUBBLE SIZE

The mean diameter of a distribution of bubbles of different sizes can be expressed in any one of the several ways. The simplest, the arithmetic mean d_b, is defined by:

$$d_b = \frac{\sum_{i=1}^{i=n} d_i}{n} \quad , \tag{32}$$

where, d_i =Equivalent spherical bubble diameter, and
n =Sample size.

The arithmetic mean is appropriate for describing many physical processes that refer to the "mean" value of a population. In the flotation process, however, the main function of the bubbles is to collide with particles and carry the values into the concentrate. The size factor of interest here is not the bubble diameter, but the bubble surface area. Thus the probability of a collision between a bubble and a particle is directly proportional to the area presented by the bubble.

An appropriate representation of the mean bubble diameter which reflects the surface area is the Sauter mean diameter d_S, which is simply the diameter of the bubble with the same area to volume ratio as the whole bubble population. The Sauter mean bubble diameter can be expressed mathematically as:

$$d_S = \frac{\sum_{i=1}^{i=n} d_i^3}{\sum_{i=1}^{i=n} d_i^2}, \qquad (33)$$

$$d_S = \frac{6V_L}{A_b}, \qquad (34)$$

where, V_L =Total volume of bubbles (mm^3), and

A_b = Total bubble surface area (mm^2).

In practical terms the variation of the Sauter mean diameter from the arithmetic mean diameter gives an indication of the spread of the bubble sizes in a distribution. For bubbles of a uniform size, the Sauter mean diameter is the same as the arithmetic mean diameter. However, when there are differences, the Sauter mean is larger than the arithmetic mean because the former is more influenced by larger bubbles. This occurs because the area of individual bubbles increases in proportion to d_b^2 but the number of such air bubbles must decrease in proportion to $1/d_b^3$ (Jameson and Allum, 1984). Both the specific area and the rate of production of surface area decrease with increasing bubble size. Therefore, a small bubble size with large, total bubble surface area would be expected to increase the probability of collision and attachment between bubbles and particles in the flotation systems - with an increase in expected rate of recovery.

3.1.1 Factors affecting bubble size

The factors affecting bubble size in a mechanical flotation cell can be classified as physical and chemical. The physical factors include air flowrate, power input, impeller speed, pulp density, viscosity and particle size, while the chemical factors

include the frother type and concentration, pH, ionic strength and temperature. The focus of this thesis is on the effects of the physical factors. They were variables manipulated in the course of the experiments while the chemical factors were held constant.

3.1.1.1 Effect of air flowrate

As is evident from Figure 3.1, an increase in air flowrate at a constant impeller speed and chemical conditions leads to a considerable increase in bubble size. The increase in bubble size with air flowrate is related to the decrease in pulp turbulence: The shear forces that are responsible for shearing of the cavities into small bubbles are reduced. Grainger-Allen (1970) and Jameson (1984) have attributed similar observations to the increase in the size of air cavity formed behind the impeller blades. This increase has the effect of forming streamlines behind the blades, leading to reduction in turbulence and power consumption.

The data in Figure 3.1 were obtained by Gorain, *et al.*, (1995a) in a 2.8-m^3 flotation cell fitted with four different impellers in turn, and operated at a variety of air flowrates and impeller speeds. The ore treated was a bleed from the zinc cleaner feed stream at the Hellyer Concentrator in Tasmania, to which collector and frother had already been added. Bubble size was measured using the UCT Bubble Size Analyser (Tucker, *et al.*, 1994); measurements were made in six different locations in the cell, and the data in Figure 3.1 represent the average of the measurements at the six locations for each set of experimental conditions studied.

Figure 3.1 also shows that bubble size is sensitive to the type of impeller. Of the different types of impeller studied, Gorain, *et al.*, (1995a) found that the Outokumpu produced the smallest bubble size at each air flowrate, followed by the Dorr-Oliver. The pumping capacity of an impeller is related to the total surface area of the blades. It follows that if the number of blades and the blade width of the impeller are increased, there is an increase in the radial velocity of

the slurry and hence the pumping action of the impeller (see equation (5) in Chapter 2) is increased. This results in the production of smaller bubbles. This probably explains why the bubbles produced by the Outokumpu and Dorr-Oliver impellers are smaller than those produced by the Agitair type of impellers.

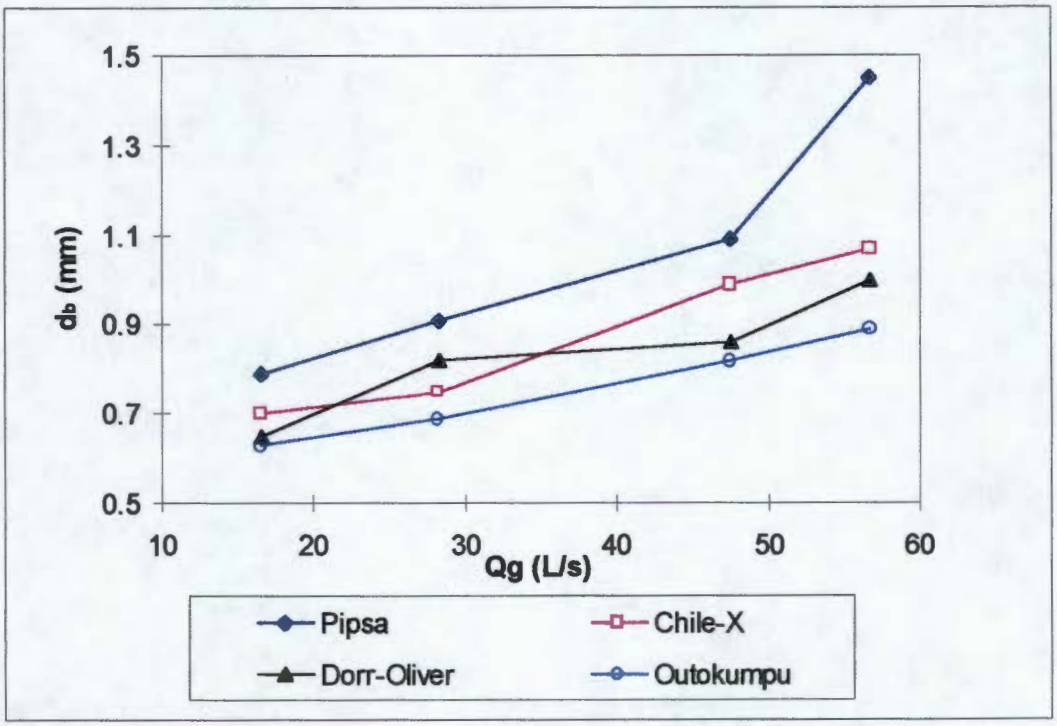

Figure 3.1: Effect of air flowrate (Qg) on mean bubble size (d_b) produced by different impeller systems at constant impeller speed (after Gorain, *et al.*, 1995a).

3.1.1.2 Effect of impeller speed

Increase in impeller speed at constant air flowrate will result in a decrease in the bubble size as demonstrated by Gorain, *et al.*, (1995a) in Figure 3.2. At low impeller speed, the shear forces generated by the impeller blades moving through the slurry are weak, resulting in the production of large bubble sizes.

As the impeller speed is increased, the shearing effect increases and the air is sheared into smaller bubbles. A similar observation has been made by Grainger-Allen (1970) in explaining the vortex-shedding phenomena.

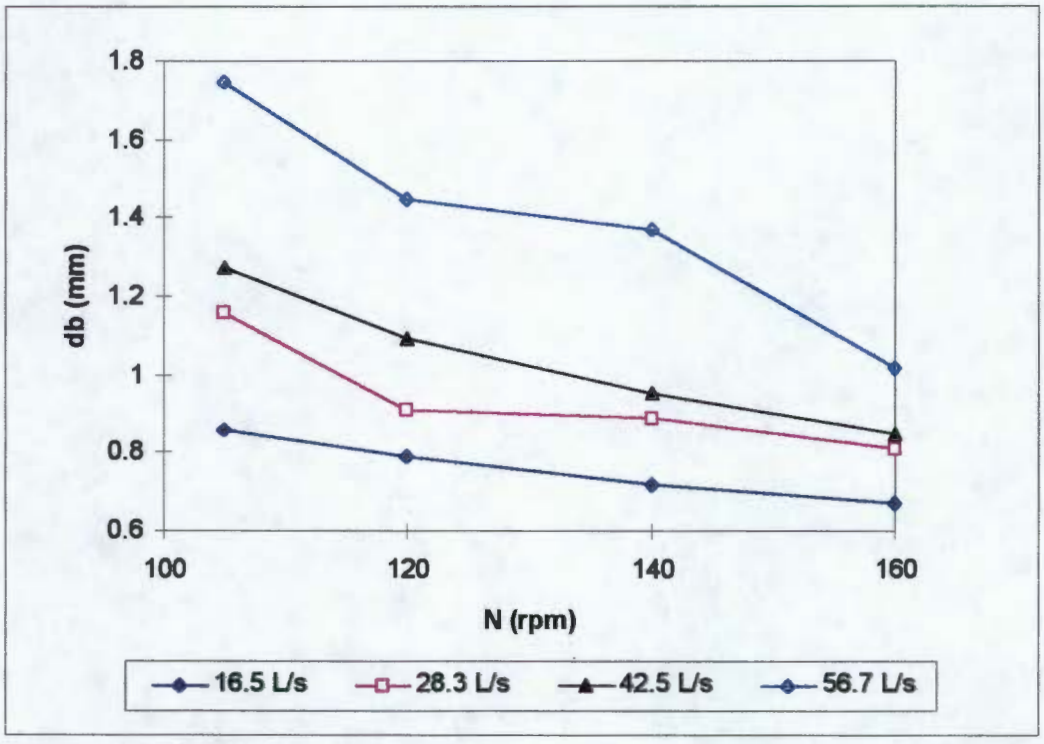

Figure 3.2: Effect of impeller speed (N) on mean bubble size (d_b) produced by the Pipsa impeller (Gorain, *et al.*, 1995a) at four different air flowrates.

3.1.1.3 Effects of pulp density, viscosity and particle size

The effects of pulp density, pulp viscosity and particle size have been studied by O'Connor, *et al.*, (1990). They found that decreasing the pulp density, which is equivalent to a decrease in viscosity, decreases the size of bubbles produced. This they suggested was due to the faster formation of liquid film at the points of bubble formation, leading to the production of smaller bubbles.

O'Connor, *et al.*, (1990) have found that decreasing the particle size resulted in a reduction in the size of bubbles formed in the flotation cell as shown in Table 3.1

Table 3.1 Effect of Particle size on Bubble Size (from O'Connor, *et al.*, 1990).

Particle size	Mean bubble Dia. (mm)	Standard dev. (mm)
Unsized	3.08	0.89
+106 μm	4.00	1.22
+75-106μm	3.63	1.10
+53-75μm	3.15	0.97
+38-53μm	2.95	0.86
-38μm	2.71	0.79

3.1.1.4 Chemical effects

The effect of the chemistry of the flotation pulp on bubble size may be summarised as follows:

- ***Frother***

Tucker, *et al.*, (1994) have shown that frother addition has a significant effect on bubble size. They have also shown the effects of different types and concentrations of frother on bubble size. There was a sharp decrease in bubble size in frother concentrations up to 20 ppm, with the effect being more significant in some frother types. The frother type and concentration became less important once a certain minimum dosage is attained (around 20 ppm).

- ***Pulp pH and ionic strength***

pH has been found to have an insignificant effect on bubble size (Tucker, *et al.*, 1994). Any observed changes in bubble size on addition of pH modifier to the pulp are attributed to the changes in the ionic strength of the pulp rather than a change in pH.

- ***Pulp Temperature***

An increase in the temperature of the pulp leads to a decrease in the bubble size, as has been shown by O'Connor, *et al.*, (1990). This effect is most likely to be due to the decrease in viscosity with an increase in temperature, the effect of which has been discussed above.

3.2 SUPERFICIAL GAS VELOCITY

The superficial gas velocity (Jg) is the volumetric flowrate of bubbles through the flotation cell per unit cross-sectional area of the cell. It can be defined as:

$$Jg = Q_g/A \quad , \qquad (35)$$

Where, Q_g = Air flowrate into the cell, (m^3/min), and
A = Cross-sectional area of the cell, (m^2).

This is the average superficial gas velocity. Different values of Jg can be measured at different locations in the cell. Schubert, *et al.*, (1982) have pointed out that differences in superficial gas velocity at different locations give an indication of the air dispersion characteristics in the cell. Uniformity of the superficial gas velocity values indicates a good distribution of air in the cell and, conversely, a wide variation in the superficial gas velocity values signifies poor gas dispersion. An easy diagnostic characteristic of flooding in a cell, for example, is that higher superficial gas velocity values in the cell are detected around the impeller region. Gorain, *et al.*, (1996) have shown flooding conditions in the flotation cells in their work from superficial gas velocity measurements and have also proposed a "dispersion index" which may be used to compare the measured superficial gas velocities with those calculated from equation (35), thereby giving an indication of the quality of gas dispersion throughout the cell.

3.2.1 Factors that affect superficial gas velocity

Gorain, *et al.*, (1996) studied the effects of air flowrate, impeller speed and impeller type on superficial gas velocity in the 2.8-m^3 flotation cell. The Jg measurements were carried out in the same circuit and under similar conditions as the bubble size measurements described above, using a modified version of a device developed by Jameson and Allum (1984). Gorain, *et al.*, (1996) measured the Jg at six different locations in the cell and the average of the six measurements at each condition was taken as the average Jg in the cell under those conditions. The data in Figures 3.3 and 3.4 are based on the average Jg values in the cell at the various conditions.

It was observed that in most cases, the superficial gas velocity increased with air flowrate, but was not affected by impeller speed at constant air flowrate. These two conditions are illustrated in Figures 3.3 and 3.4. The effect of impeller design on the superficial gas velocity can also be seen from Figure 3.3, in which the results obtained using the Outokumpu and the Dorr-Oliver impellers were distinctly different from those using the Agitair type of impellers (Pipsa and Chile-X). The differences in the superficial gas velocity between the two groups can be related to the differences in their capacities to disperse air effectively, which in turn is influenced by the impeller geometries as can be seen from Figure 2.16.

Figure 3.4 depicts the effect of impeller speed on superficial gas velocity for the Dorr-Oliver impeller, at four different air flowrates. The superficial gas velocity did not vary with impeller speed at the lower air flowrates; at the highest air flowrate the behaviour of the curve can be attributed to poor air dispersion due to flooding.

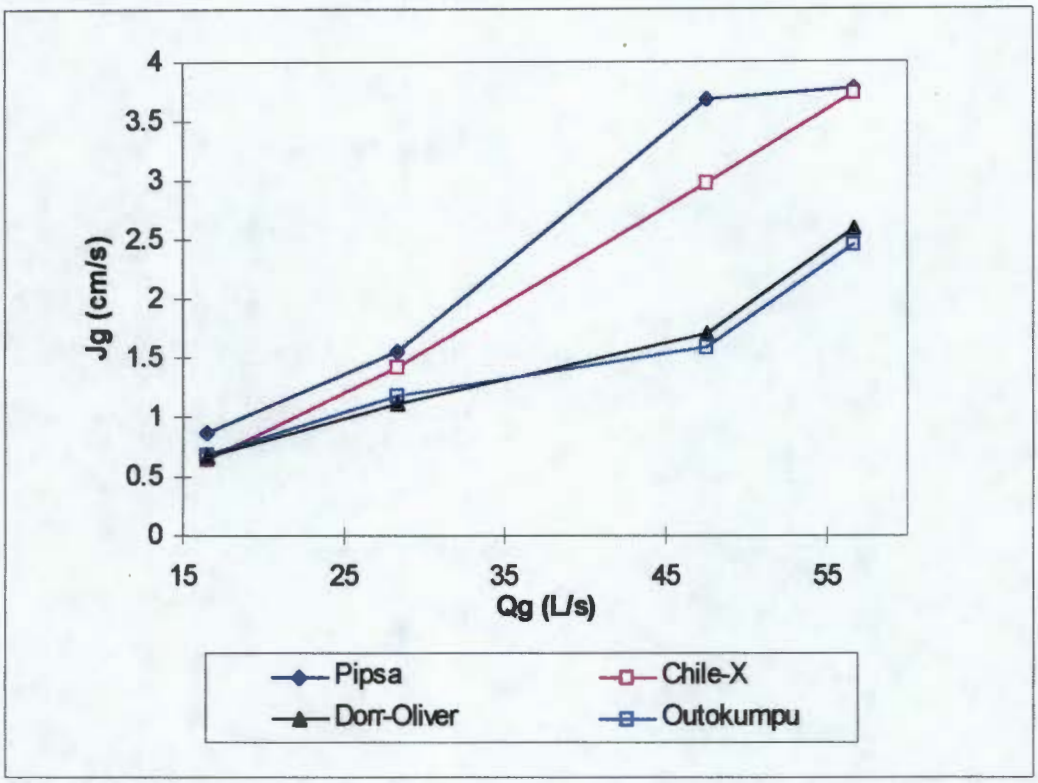

Figure 3.3: Effect of air flowrate (Qg) on superficial gas velocity (Jg) produced by different impellers at constant impeller speed (from Gorain, *et al.*, 1996).

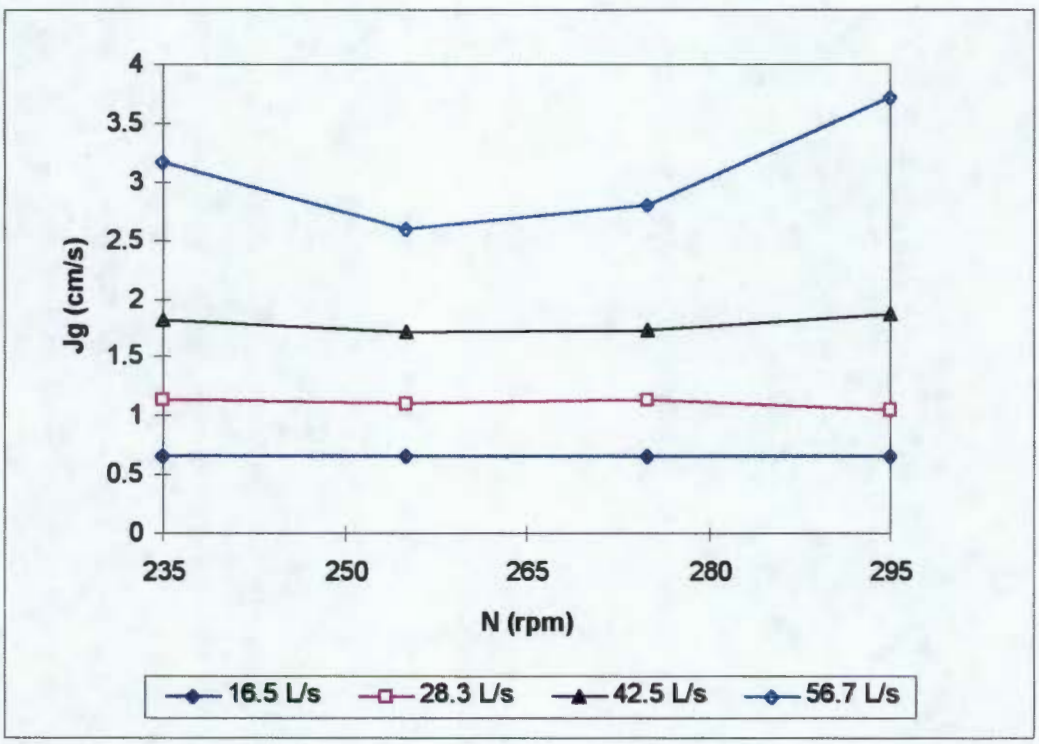

Figure 3.4: Effect of impeller speed (N) on superficial gas velocity (Jg) produced by the Dorr-Oliver impeller at four different air flowrates (from Gorain, *et al.*, 1996).

3.3 GAS HOLDUP

The gas holdup is the volume fraction of gas (usually air) in the pulp. In general, the larger the gas holdup, the more bubbles there are available in the cell to float the ore. The holdup by itself is not a sufficient description of the bubble population, because the voids may exist as one large bubble or many small ones. The gas holdup together with the bubble size and superficial gas velocity provide a very useful measure of gas dispersion in flotation cells. Until the development of the holdup measuring device (Jameson and Allum, 1984), gas holdup measurement in flotation cells was almost impossible because of the flow, turbulence and other conditions that make the use of simple measurement methods used in chemical reactors inapplicable. The instantaneous encapsulation of pulp by this new device has made gas holdup measurement in flotation cells possible. Gorain, *et al.*, (1995b) have measured the gas holdup using this device in the same circuit and in similar conditions as the bubble size and superficial gas velocity measurements. The measurements were done at six different locations at the different conditions. The values reported in Figures 3.5 and 3.6 are the averages of the six values for each set of conditions.

3.3.1 Factors that affect air holdup

The effects of air flowrate, impeller speed and impeller type on gas holdup have also been studied by Gorain, *et al.*, (1995b). Their general observations may be summarised as follows:

3.3.1.1 Effect of air flowrate

An increase in air flowrate increases the air holdup in the cell (Figure 3.5). It can also be seen from this figure that each impeller has a different ability to produce air holdup. The highest air holdup produced, in the Outokumpu cell, can easily be attributed to the small bubbles produced by this impeller type. The small bubbles produced in the Outokumpu cell have small rise velocity, resulting in high residence times in the cell and consequently high air holdup

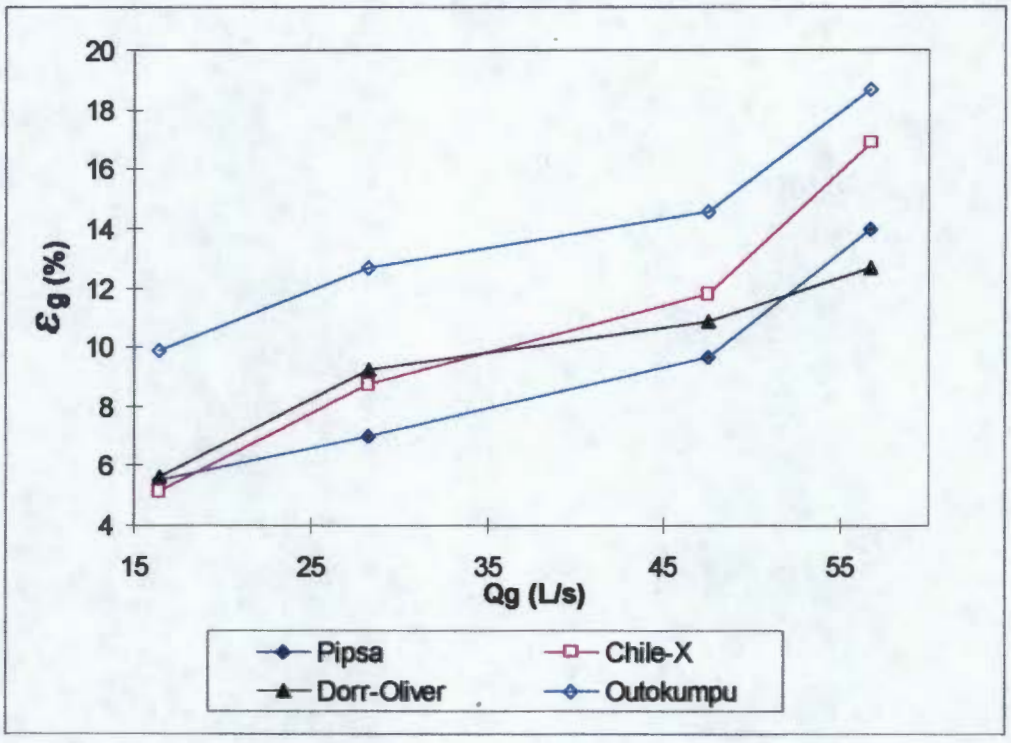

Figure 3.5: Effect of air flowrate (Qg) on air holdup (Εg) produced by different impellers at constant impeller speed (from Gorain, *et al.*, 1995b).

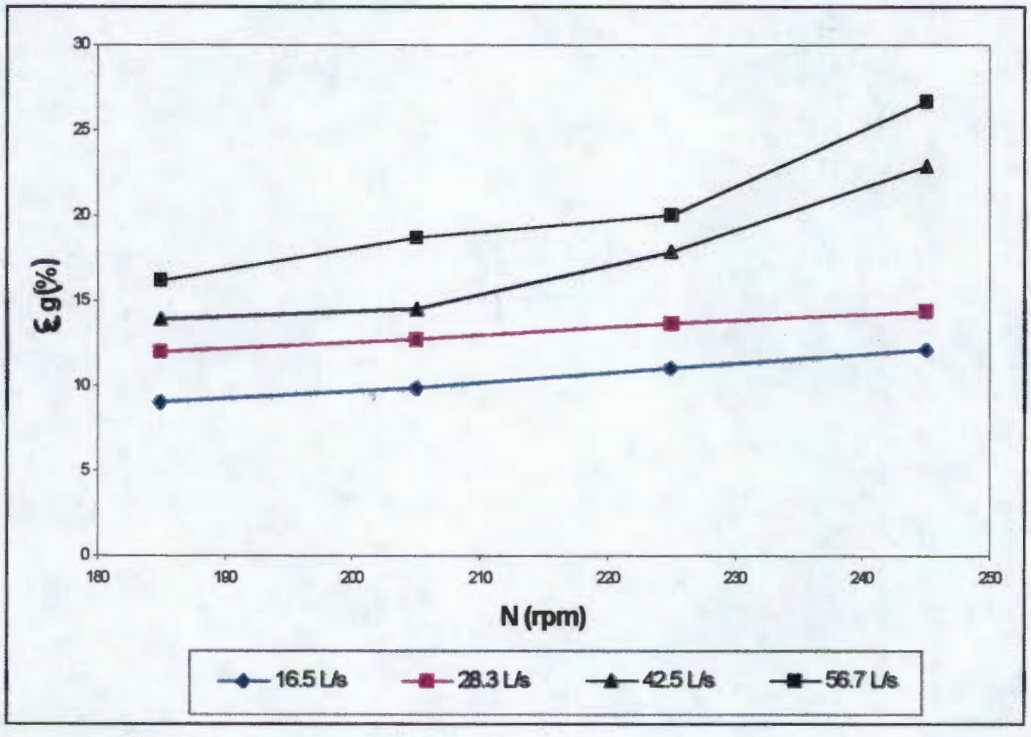

Figure 3.6: Effect of impeller speed (N) on air holdup (Εg) produced by the Outokumpu impeller at four different air flowrates (from Gorain, *et al.*, 1995b).

3.3.1.2 Effect of impeller speed

As is obvious from Figure 3.6, increasing the impeller speed at constant air flowrate will increase the air holdup. This behaviour is explained by the fact that, at higher impeller speeds (see Figure 3.6), the smaller bubbles produced have lower rise velocity, resulting in a longer residence time in the cell.

3.4 BUBBLE SURFACE AREA FLUX

The bubble surface area flux is defined as the rate of production of bubble surface area in the cell per unit of cell surface area. Bubble surface area flux is expressed mathematically as (Jameson and Allum, 1984):

$$S_b = \frac{aJ_g}{\varepsilon_g}, \qquad (36)$$

where, S_b = Bubble surface area per unit volume of pulp, m^2/m^2sec,

J_g = Volumetric air flowrate, (m^3/s) per m^2 of cell cross-sectional area,

ε_g = Gas holdup, m^3 air/m^3 pulp, and

a = Total bubble surface area per unit cell volume, (m^2/m^3).

If it is assumed that bubbles are spherical and uniform, then equation (36) above can be rewritten as:

$$S_b = \frac{6J_g}{d_s}, \qquad (37)$$

As part of the work described in the preceding sections, carried out in the zinc cleaner circuit at the Hellyer Concentrator in Tasmania, Gorain, *et al.*, (1997) tried to relate the metallurgical performance in the 2.8-m^3 flotation cell to the three

hydrodynamic properties that characterise gas dispersion, viz. bubble size, gas holdup and superficial gas velocity. These cell characteristics individually did not show much correlation with the first order flotation rate constant, k. However, when they were combined to determine the bubble surface area flux, S_b, a good correlation was found between k and S_b , which was independent of the impeller size and type. The R^2 value for the three different types of impeller systems is 0.94. Figure 3.7 shows the k-S_b relationship for the different types of impellers used in the 2.8-m^3 testwork in the zinc cleaner circuit at the Hellyer Concentrator in Tasmania.

Figure 3.8 shows similar results for a 250 L cell fitted with different impellers and tested with 5 cm froth depth at the Scuddles Concentrator in Western Australia. The R^2 value for all the impellers is 0.92. It is obvious from both Figures 3.7 and 3.8 that for a given ore type and chemical conditions, the k-S_b relationship holds well for different types of impellers and cell volumes.

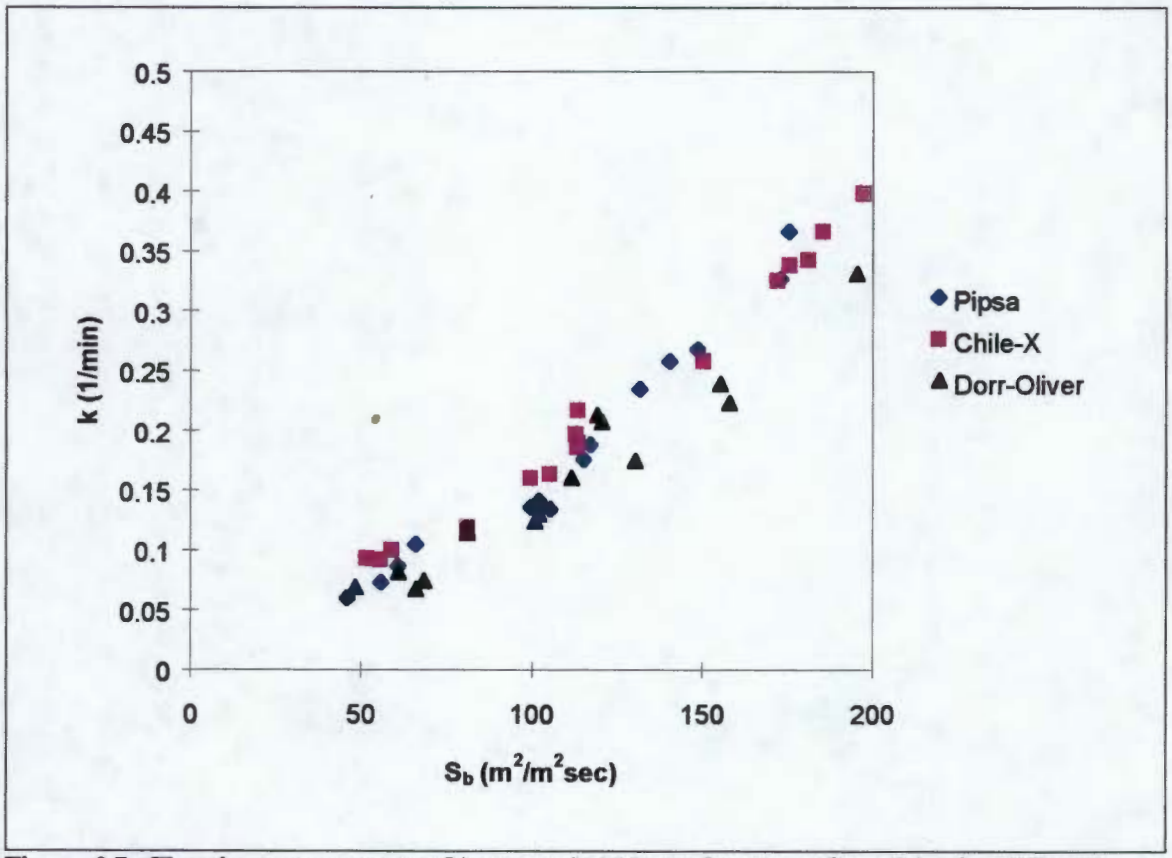

Figure 3.7: Flotation rate constant (k) versus bubble surface area flux (S_b) for different impeller systems in a 2.8m^3 pilot cell (Gorain, *et al.*, 1996).

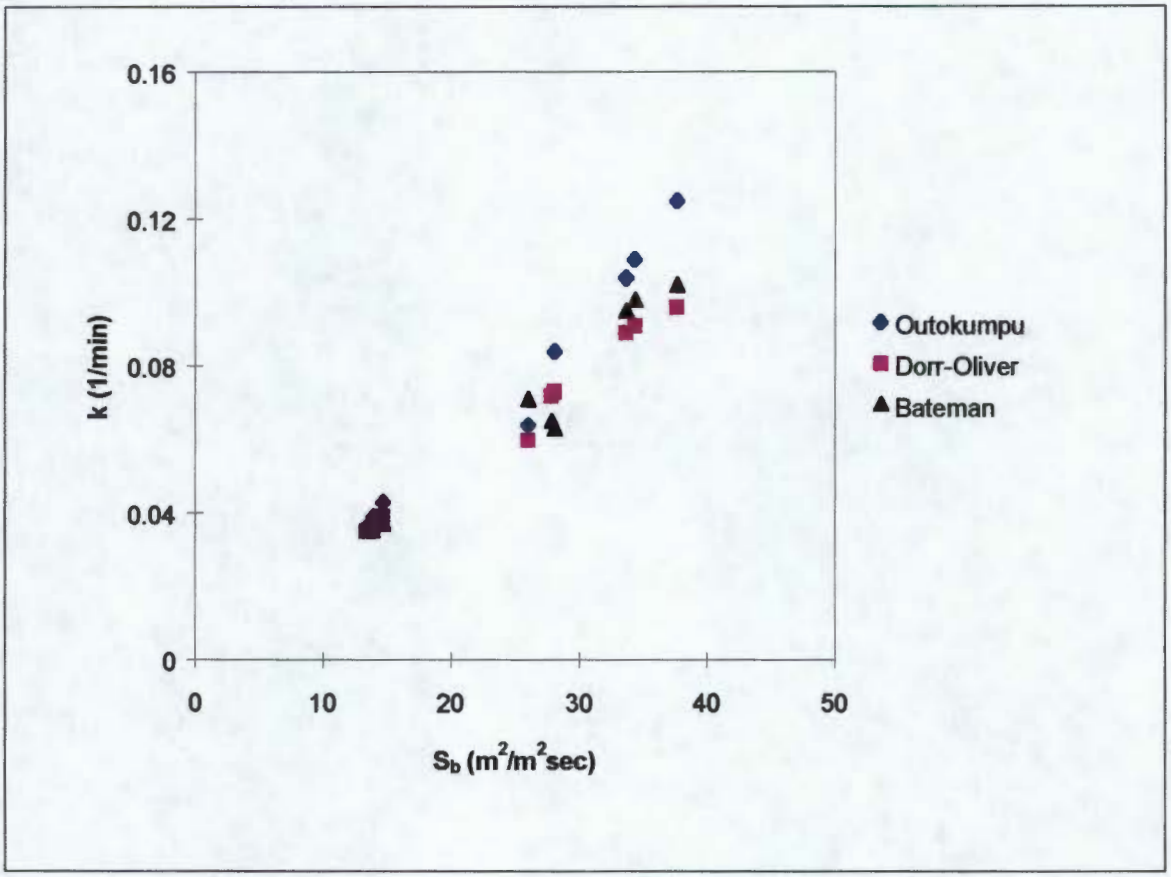

Figure 3.8: Flotation rate constant (k) versus bubble surface area flux (S_b) for different impeller systems in the 250 L cell at 5 cm froth depth for the Scuddles Test (from Gorain, *et al.*, 1996).

When data from the work of other researchers (O'Connor and Mills, 1994; Diaz-Penafiel and Dobby, 1994; Vera, 1995), using different flotation systems and conditions, were processed, an apparently good linear correlation between k and S_b was found in each case (Figure 3.9). This relationship had previously not been noted by these researchers. Figure 3.9 also indicates that, in at least one case, the linear relationship between k and S_b is different in a different flotation system.

Mathematically, the k-S_b relationship is expressed as:

$$k = P*S_b + Z \qquad (38)$$

where, P =Proportionality constant which is a function of ore type and pulp chemistry and Z is a constant (usually zero, but sometimes less than zero).

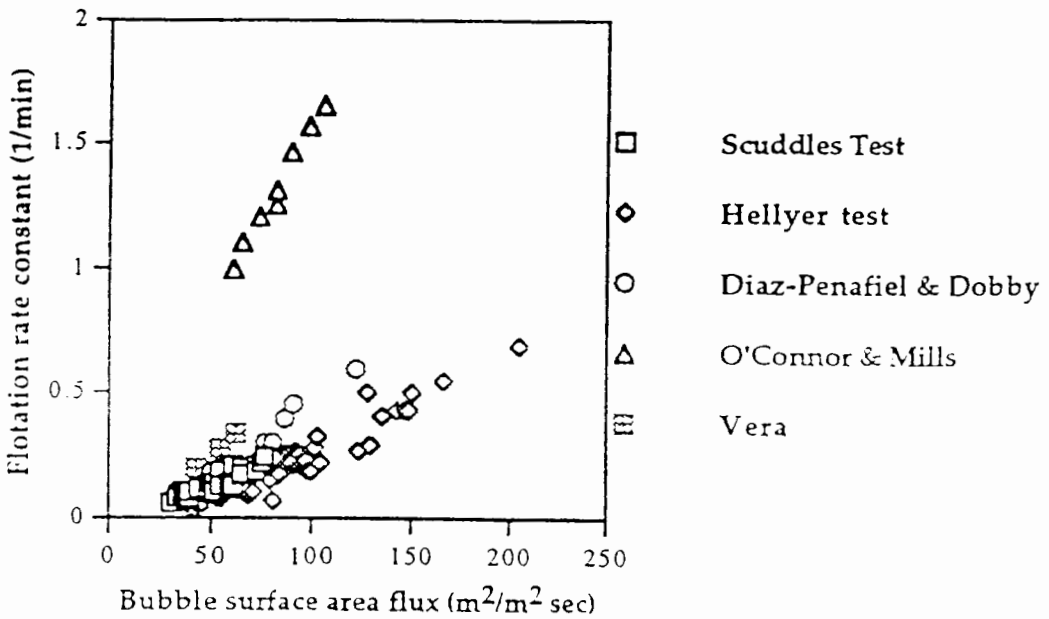

Figure 3.9: k - S_b relationship applied to data of O'Connor and Mills (1994), Diaz-Penafiel and Dobby (1994), Vera (1995) and Scuddles and Hellyer Tests (from Gorain, *et al.*, 1996).

3.4.1 Factors that affect the k-S_b relationship

This relationship implies that if the same bubble surface area flux is created in different cells, then the same kinetics would be expected from each cell as long as the ore type and the chemical conditions remain constant. The bubble surface area flux is a new and very important way of characterising the hydrodynamics and gas dispersion in flotation cells, as it has a determining influence on flotation performance.

In later work, Gorain, *et al.*, (1996) have found the slope of the k-S_b relationship to be sensitive to the froth height in the cell. This fact is adequately illustrated in

Figures 3.10 and 3.11, where the effect of froth depth on the k-S_b relationship is shown for the Dorr-Oliver and Outokumpu impellers tested in the 2.8-m^3 cell. This work was carried out in the zinc cleaner circuit at the Scuddles Concentrator in Western Australia. From the graph it was quite obvious that there was a good correlation (high R^2 values) between k and S_b at all the different froth depths, and the influence of froth depth on the kinetics was also clear. It was found that at low froth depths the kinetics of the cell were generally high and so the slope of the line was found to be greatest. At the greatest froth depth of 45 cm, the slope of the line recorded the lowest value. This trend was similar in the other impeller types.

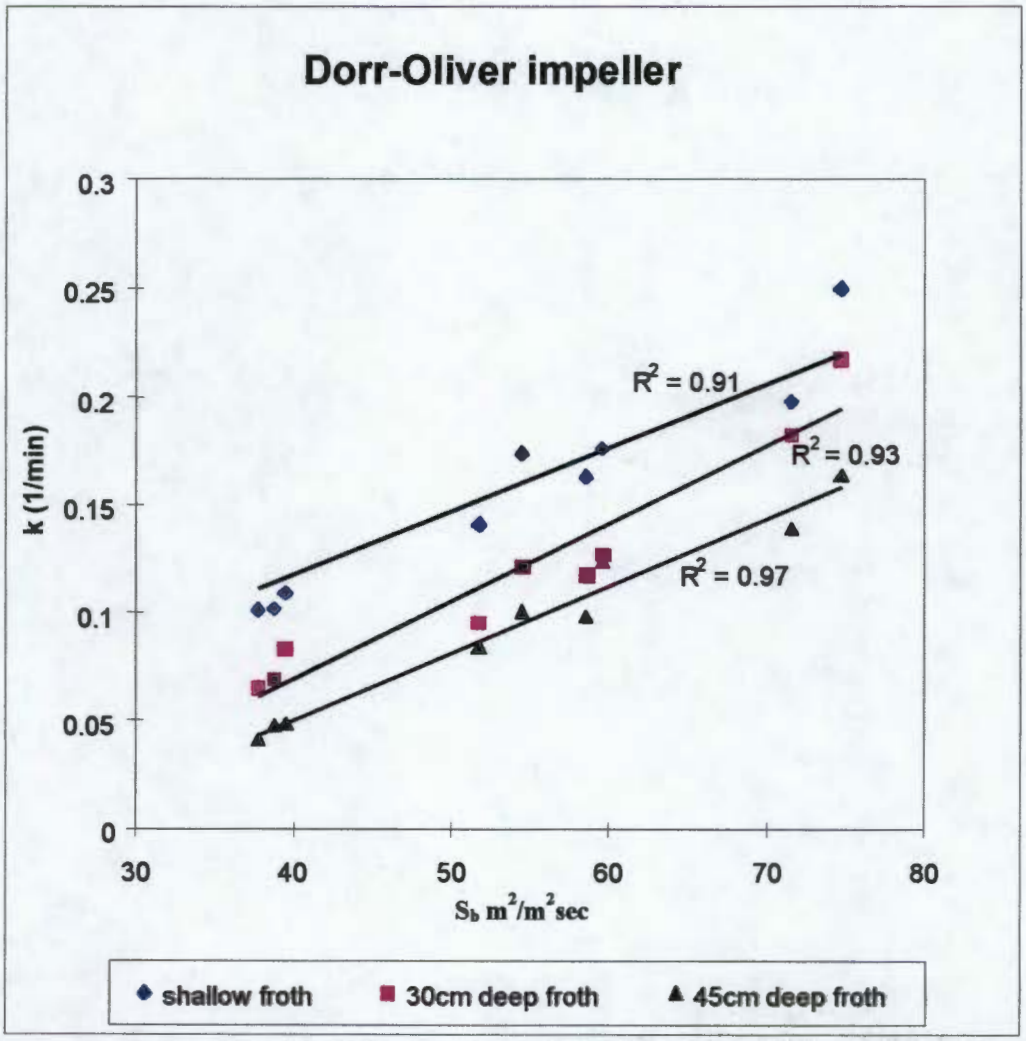

Figure 3.10: The effect of froth depth on k-S_b relationship for Dorr-Oliver impeller (after Gorain, *et al.*, 1996).

It has further been shown (Gorain, *et al.*, 1996) that when the k was plotted against S_b for data obtained in two different sizes of cells (250 *l* and 2.8-m^3) operated on the same feed at constant froth residence time, all the points lay on a common straight line. This observation suggests that the k-S_b relationship could be a potential criterion for flotation scale-up and design. Though scale-up of flotation cells falls outside the scope of this thesis, it is being explored by another MSc student working on a similar project using pilot and industrial scale flotation cells.

To date, the k-S_b relationship and the other subsequent findings have been developed in specially designed 250 *l* and 2.8-m^3 cells in which the cell parameters, viz. air flowrate and impeller speed were properly controlled and in which the pulp feed was very consistent, being zinc cleaner feed. It will be interesting and important to see how these findings can be applied to real large industrial size flotation cells treating a more complex ore as exists in the South African platinum industry. This therefore forms the basis of this thesis.

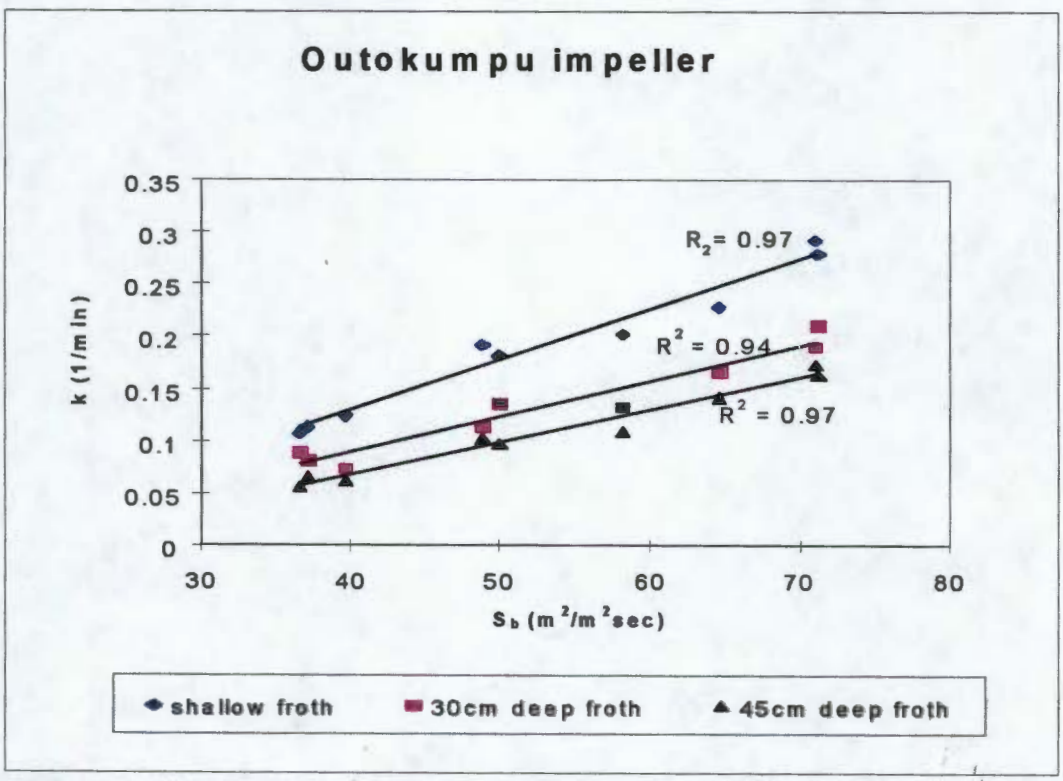

Figure 3.11: The effect of froth depth on k-S_b relationship for Outokumpu impeller (after Gorain, *et al.*, 1996).

CHAPTER 4
EXPERIMENTAL WORK

4.0 INTRODUCTION

The experimental work for this thesis was carried out on a platinum concentrator in the North West Province of South Africa. South Africa is the world's largest producer of platinum, and the concentrators employ chiefly WEMCO flotation cells.

This chapter starts with a brief description of the geology of the Bushveld Complex, where the main pgm ores - the Merensky and the UG2 reefs - are found in South Africa. This is followed by descriptions of the two concentrators at which the experimental work was performed. The pulp properties and reagent suites are briefly mentioned. The chapter concludes with a description of the types of cells investigated in the work, the variables studied, a description of the experimental techniques used and the procedures followed.

4.1 ORE DETAILS

4.1.1 Geology of the Bushveld Complex

The Merensky Reef and the UG2 chromitite layer, which constitute the source of pgm ore to the plants studied in this thesis, occur as distinct, persistent layers within the gigantic intrusive known as the Bushveld Complex, occupying an area of about 40,000 km^2 in the central Transvaal (Hochreiter, *et al.*, 1985). The Bushveld Complex is the world's largest, layered complex, comprising about 80% of the world's stock of platinum reserves. The Merensky and the UG2 layers have a proven reserve of 1360 million ounces (42.3 million kilograms) of platinum. The UG2 layer is located in the layer between 20 and 370 m below the Merensky Reef.

The formation of the Bushveld Complex is believed to be a result of a magmatic event in which large volumes of molten rock from the earth's mantle were injected into the

higher, crustal rocks of the Transvaal some millions of years ago. This injection is said to have happened in pulses of magma, each of which differs subtly from the preceding one. Some differentiation of the individual layers may have taken place as different minerals crystallised out at different temperatures, and the net result of these processes is that the Bushveld Complex became stratified into distinct, compositional units (Figure 4.1). A general trend is observed, with high temperature rock types, rich in magnesium, in the lower zones of the Bushveld Complex, to low-temperature siliceous and iron-rich rocks at the top.

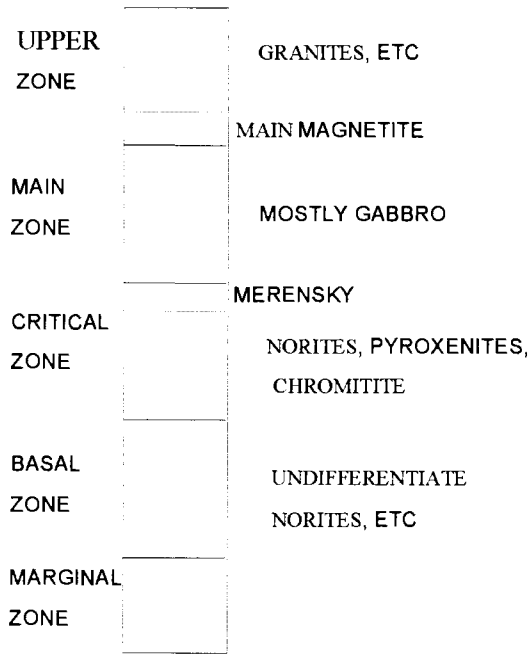

Figure 4.1: Generalised stratigraphy of the Bushveld Complex (after Willemse and Von Gruenewalt, 1969).

The Critical Zone, consisting of a series of chromitite layers within pyroxenite in the lower portion and a series of cyclically repetitive triplets of chromitite, pyroxenite and norite in the upper sections, forms the most important region in terms of the pgm. The Critical Zone is divided, according to the chromitite layer, into Lower Group, Middle Group and Upper Group, and further subdivided into LG1, LG2, etc. for the Lower Group chromitites, MG1, MG2, etc. for the Middle Group chromitites, etc. (Figure 4.2).

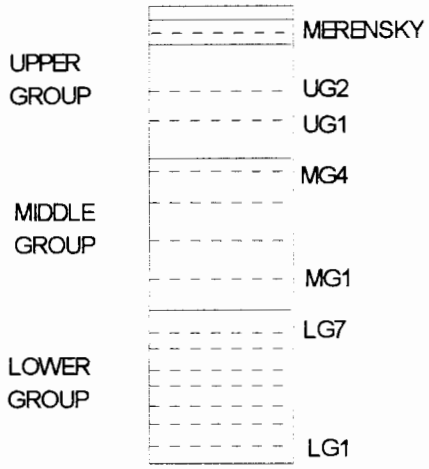

Figure 4.2: Stratigraphy of the Critical Zone.

There are no fewer than 13 of these chromitite units in the Critical Zone. Throughout the Bushveld Complex, only one of these, the UG2, carries any significant platinum values. Near the top of the Critical Zone, there is evidence to suggest that conditions leading to formation of another chromitite-pyroxenite-norite triplet occurred at some time. The pyroxenite is very prominent but the chromitite is poorly developed. This zone is the Merensky Reef.

Above the Merensky Reef is the final chromitite-pyroxenite layer, the Bastard Reef, whose chromitite is also poorly developed or completely absent in many places. It is virtually non-platiniferous. Above the Bastard Reef, the norites in the Critical Zone give way to gabbrous members of the Main Zone, which appear to represent a new and compositionally different infusion of magma into the Bushveld Complex ore mineralogy. The gabbrous layer is known to play a very important role in the flotation characterisation of the floatable particles.

Table 4.1 shows the characteristics of the Merensky and the UG2 ores. It is clear from the table that the processing (grinding, floating, etc.) of these two types of ores will be different, as their properties differ in many respects. The UG2 ore for instance requires a fine grind to allow any appreciable liberation of the mineral values to be achieved while coarse grinding will invariably suffice for the Merensky ores.

Table 4.1: Characteristics of pgm ores used in the testwork.

Merensky	**UG2**
Less than 1% chromite content	Approximately 27% chromite content
Found in pyroxenite layer	Found in chromite layer
Up to 20% talc content	Less than 5% talc content
Large sulphide grain size	Small sulphide grain size
High sulphide grade	Low sulphide grade
S.G. 3.0-3.2	S.G. 3.6-4.0
Bond Work Index of 19 kWh/t	Bond Work Index of 13 kWh/t

4.2 A DESCRIPTION OF THE CONCENTRATORS

4.2.1 Eastern Platinum Concentrator

The Lonrho Platinum Division operates a pgm plant, Eastern Platinum Ltd, which is located between Rustenburg and Brits in the North West Province of South Africa. UG2 ore is treated in this concentrator. Figure 4.3 shows the flowsheet of the grinding and flotation plant at Eastern Platinum at the time that the testwork was carried out.

The plant consists of primary and regrind ball mills and four stages of flotation. This is known as the MF2 circuit (mill-float, mill-float). Regrinding of the primary rougher tailings is necessary since a large proportion of the metal sulphides and pgm in UG2

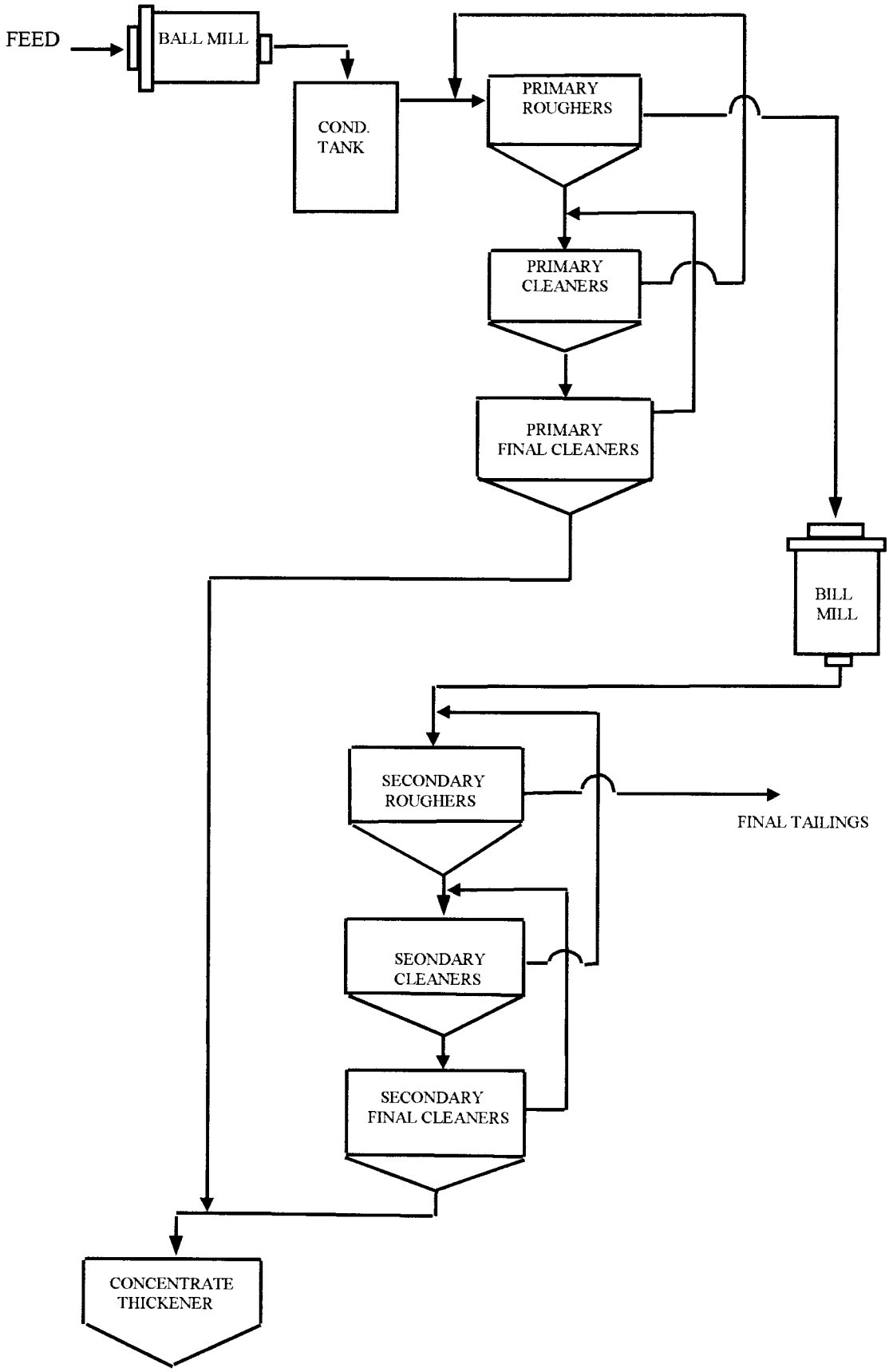

Figure 4.3: Flowsheet of pgm flotation plant at Eastern Platinum.

ore are found locked up in fine silicate grains. As can be seen from Figure 4.3, there are WEMCO 144 cells in the primary rougher banks and the secondary rougher banks. The primary cleaner banks and the secondary cleaner banks each consist of WEMCO 84 cells. The final primary and secondary cleaners each consist of WEMCO 84 flotation cells. The concentrates of the first and second cleaners are fed to the final cleaners, while the tailings of the final cleaners are fed to the first cleaners (for both the primary and secondary circuits). The concentrate from the final cleaners is thickened and transported by truck to the smelter.

The concentrator has two similar process streams with identical flow sheets. These two streams are called the A and B streams. The B stream is similar to the A stream described above except that OK 16 cells are used for the roughing duties only. Each stream employs two milling stages - the primary and regrind milling.

4.2.2 Karee Concentrator

The second Lonrho plant at which experimental work was carried out for this thesis is at Karee. The ore for the Karee Concentrator is from both the UG2 and Merensky reefs of the Bushveld Complex. The precious minerals in the Merensky ore are found in relatively abundant and large, sulphide grains as can be seen from Table 4.1. The Karee plant was designed to treat Merensky ore which requires only one-stage-milling (the MF1 system) to liberate the pgms for floating. Regrinding and secondary flotation of the Merensky and UG2 ore blend is not used, so the MF1 milling stage is still maintained. The flowsheet for the flotation circuit of the Karee concentrator has been reviewed over the years to address the value of regrinding, but Figure 4.4 represents the existing circuit at the time of the test.

Conditioned pulp is introduced into the serial configuration of three OK 50-m^3 TankCells at the head of the roughing circuit. The tails from the OK 50 cells then flow to three, successive banks of cells, the primary and secondary roughers and scavengers, while the concentrate is cleaned in a 10-m^3 WEMCO unit cell. A unit cell, also called a

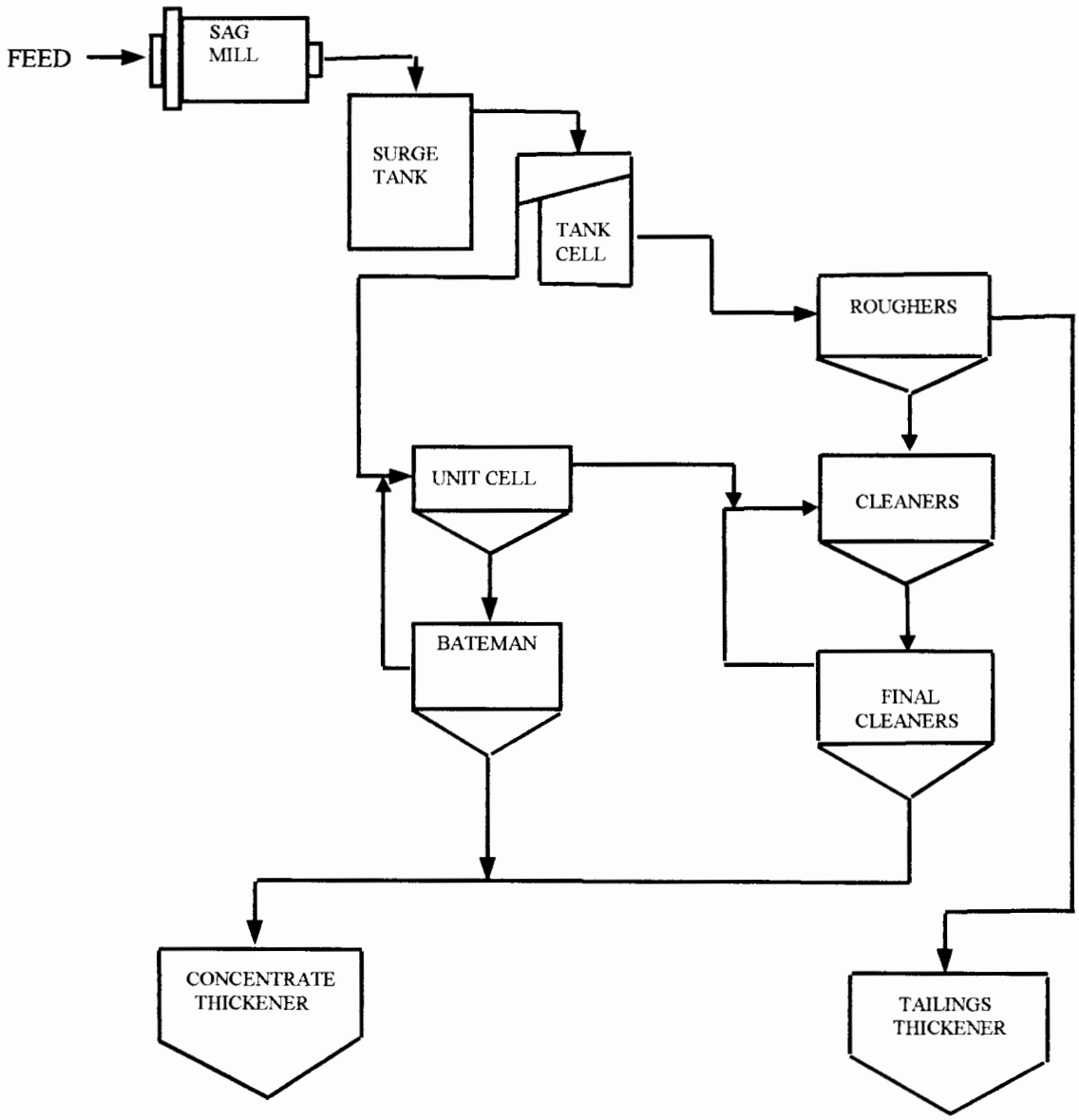

Figure 4.4 Flowsheet of pgm flotation plant at the Karee Concentrator.

flash flotation cell, is designed to allow for recovery of dense mineral particles before they become overground in the milling circuit, or increase the circulating load in a circuit. It is usually employed in the cyclone underflow stream which feeds the regrind circuit. Concentrate from the roughers undergoes cleaning in two banks of 8.5-m^3 WEMCO cleaner cells, before it is finally cleaned in a third bank of two WEMCO final cleaner cells.

A 3-m^3 Bateman cell produces the final concentrate, from the froth product of the unit cell. The final concentrate from the two sources, i.e. the 3-m^3 Bateman and the 8.5-m^3 WEMCO final cleaner cells, is thickened before trucking to the smelter. The tailings from the rougher banks is also thickened, and disposed of to the tailings dam.

4.3 DETAILS OF CELLS AND VARIABLES MEASURED

The variety of flotation cell types, sizes and duties in Karee and Eastern Platinum Concentrators made them very suitable for this kind of work. Over the course of the experimental programme, a total of 40 flotation cells, with volumes ranging between 3 and 50 m^3, and operating in a variety of applications, were characterised. Details of the flotation cell types, volumes and application are given in Table 4.2, together with a list of the manipulated variables. Among the cells measured were two types of OK 50-m^3 TankCells with different mixing mechanisms - the Multi-mix and Free-flow systems. Diagrams showing the differences in the rotor/stator arrangements, their flow patterns and a few characteristic properties are given in Figures 4.5 and 4.6.

The other types of impellers involved in this work are shown in Figure 2.16. The dimensions of these impellers are given in Table 4.3.

Table 4.2: Characteristics and conditions of flotation cells studied.

Cell type	Volume (m^3)	Duty	Manipulated Variables
Bateman BQ 30	3	Final Cleaner	nil
WEMCO 84	4.2	Cleaner Recleaner Final Cleaner	nil nil nil
WEMCO 120	8.5	Cleaner Final Cleaner	nil nil
WEMCO 120	10	unit cell	nil
WEMCO 144L WEMCO 144D WEMCO 164	16 16 16	Rougher Rougher Rougher	air flowrate, motor, air flowrate air flowrate
OK 16	16	Rougher	air flowrate
OK 50 TankCells (Multi-mix and Free-flow)	50	Rougher	air flowrate

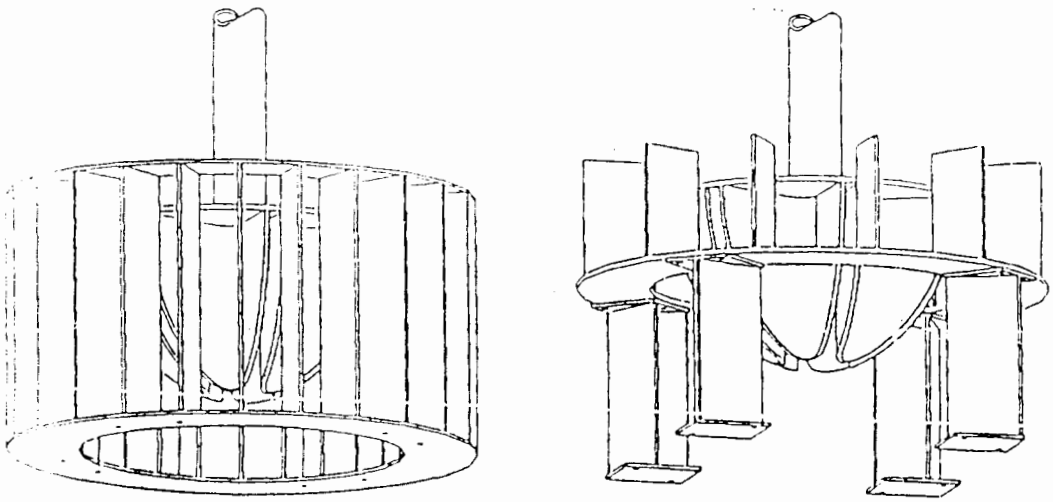

Figure 4.5: Multi-mix and Free-flow impellers (Lindegger, 1993).

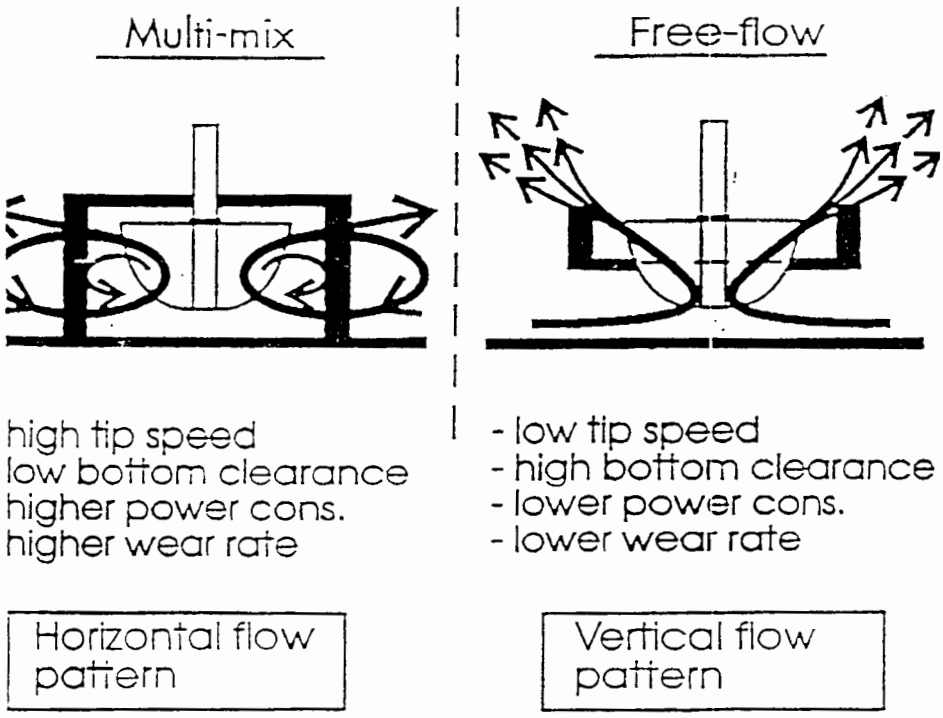

Figure 4.6: Flow pattern in Multi-mix and Free-flow impeller systems (Lindegger, 1993).

Table 4.3: Impeller types and their dimensions.

Impeller type	Impeller height (m)	Impeller diameter (m)
Bateman BQ 30	0.314	0.488
WEMCO 84	0.406	0.406
WEMCO 120 WEMCO 120 (mod)	0.559 0.762	0.559 0.762
WEMCO 144	0.660	0.660
WEMCO 164	0.762	0.762
OK 16	0.450	0.750
OK 50 Tank cell	0.630	1.050

4.4 DESCRIPTION OF LOCATIONS OF MEASUREMENTS

The main objective of this thesis was to characterise the gas dispersion characteristics of the flotation cells under investigation. Accordingly, the physical measurements taken in each cell were the bubble size distribution, the gas hold-up, the pulp specific gravity and the superficial gas velocity. The locations in the cells where measurements were taken have been denoted by the numerals 1,2,3...6 as shown in Figure 4.7. The locations were selected to lie in a plane parallel to the froth launder and roughly midway between the agitator and cell lip. The upper locations 1, 2 and 3 were chosen relatively close to the pulp-froth interface to measure the conditions in the quiescent zone. The lower locations 4, 5 and 6 were selected in the impeller region to measure

equivalent conditions in the turbulent zone. Other measurements and readings taken included air flowrates, impeller rotational speed and current draw.

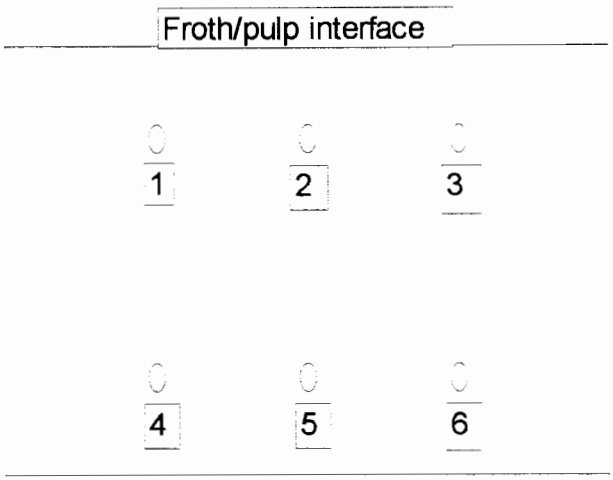

Figure 4.7: Schematic representation of the locations of measurements in the cell.

Measurements were performed at all six locations for the majority of the conventional cells. For the OK 50-m^3 TankCells, only one location was used for measurement owing to structural limitations caused by the presence of the froth crowder. A hole was cut in the froth crowder through which the cell was accessed for measurement. The location of measurement in the OK 50-m^3 tank cell was at a depth of approximately 1.4 m below the pulp-froth interface. Because of time constraints, only locations 2 and 5 were measured in some of the cells in a bank.

4.5 EXPERIMENTAL DETAILS

4.5.1 Bubble Size Distribution Measurement

Bubble size distribution was measured using a UCT Bubble Size Analyser (Figure 4.8) fitted with a bubble sampler. A detailed description of the apparatus and the procedure is given in Tucker, *et al.*, (1994) and Gorain, *et al.*,(1995a). Three lengths of PVC tubes of 0.5, 1 and 2 m of 20 mm inside diameter enabled easy measurements to be taken at both the lower and upper locations.

For most cells, measurements at the upper locations 1, 2 and 3 (see Figure 4.7) were taken with the 0.5 m tube while at the lower locations 4, 5 and 6, the 1 m tube was used. For greater depths, as in the OK 50-m^3 TankCells, the 2 m tube was used. The bubble sampler, the PVC pipe, the capillary and the electronic detector assemblage were clamped to a piece of channel iron which traversed the top of the cell. Measurements were taken at different locations by sliding the unit on the channel iron. The channel iron also made it possible to maintain the probe at constant depths, regardless of the location across the cell.

After each change in the input variables, about 20 minutes of equilibration time were allowed before measuring the bubble size distributions. In the UCT Bubble Size Analyser, bubbles from the flotation cell are drawn through a bell-shaped glass capillary and into a burette through a detector head. Bubbles are transformed into cylinders in the capillary. Within the detector head, two pairs of light emitting diodes (LED) measure changes in intensity of the light as each bubble passes through. This difference in intensity is derived from the difference in the refractive indices of water and air. These two pairs of detectors are used to measure the time it takes for the ends of each "cylinder" to pass. The analyser converts the time into bubble volume. The total bubble volume captured in the burette, together with the length and velocity readings, are used by the computer software to generate the mean bubble diameter, mean bubble volume and mean total bubble surface area. The values for each bubble are also recorded.

Three measurements were performed per location and set of conditions. Approximately 4000 bubbles were sampled per measurement. The average of the three measurements was used to calculate the Sauter mean bubble diameter, which is the parameter used in the calculation of the bubble surface area flux.

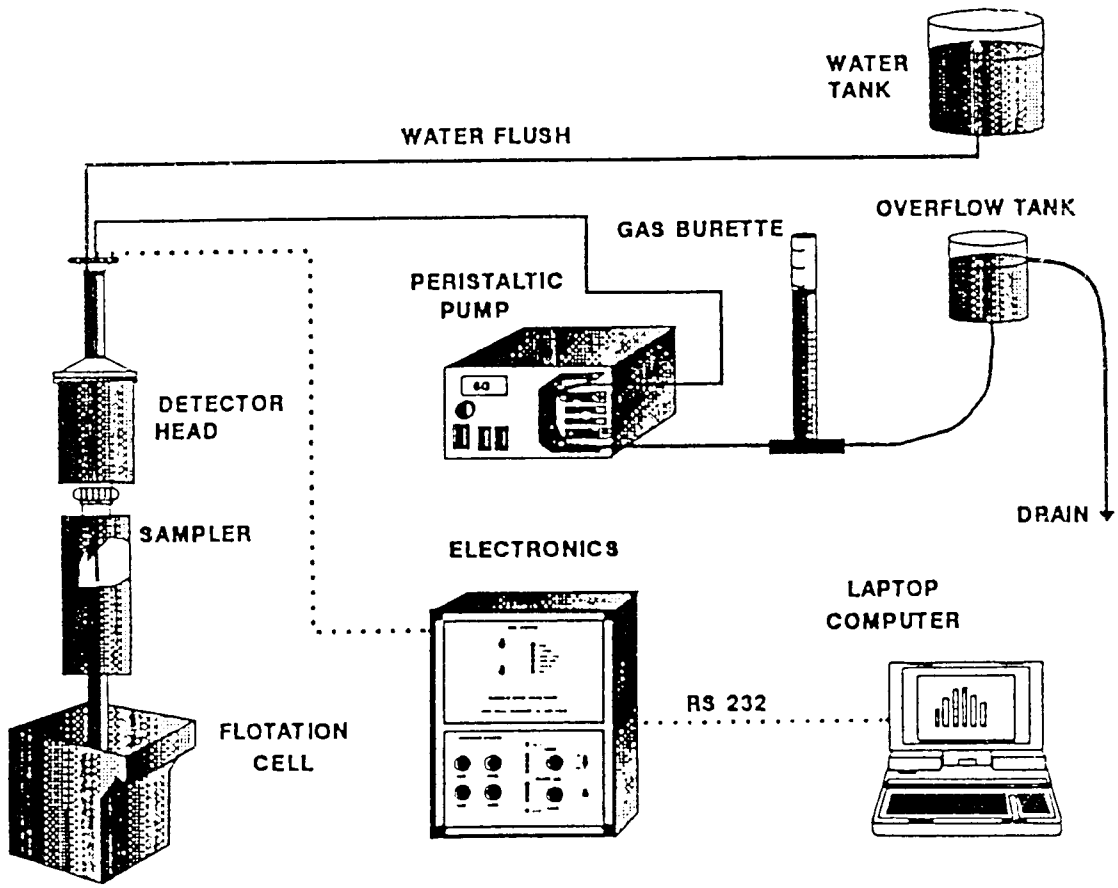

Figure 4.8: UCT Bubble Size Analyser (from Tucker, *et al.*, 1994).

4.5.1.1 Reproducibility

An important characteristic of good experimental technique is high reproducibility of results. The mean bubble sizes were therefore checked for reproducibility for three successive measurements in some of the cells at the same location and conditions. Very good reproducibility was found in the quiescent locations (1, 2 and 3) as illustrated in Figure 4.9, but it was not as good in the turbulent locations (4, 5 and 6). The good reproducibility obtained (especially in the quiescent zone) may be attributed partly to the reliability of the UCT Bubble Size Analyser and in part to the large number of bubbles that were measured (in excess of 4000 bubbles per measurement).

Table 4.4 shows the standard deviation of bubble size measurements in a WEMCO 144 cell with a 164 mechanism. As is obvious from this table, the deviation in bubble sizes in the impeller zone was much greater than in the quiescent zone. This is largely due to the higher degree of turbulence that exists in this part of the cell. While the average standard deviation in the upper section of the cell was found to be less than 2%, the corresponding value in the impeller region was quite substantial, above 10%. A similar trend was observed in the other cells (see Table C25 in Appendix C).

Table 4.4: Reproducibility of the UCT Bubble Size Analyser.

Location	Bubble dia. mm			S.D., mm
	run 1	run 2	run 3	
1	1.13	1.12	1.10	0.02
2	1.00	1.02	1.04	0.02
3	1.01	1.02	1.02	0.01
4	1.15	1.03	0.95	0.10
5	1.07	0.88	1.10	0.12
6	1.25	1.14	1.00	0.13

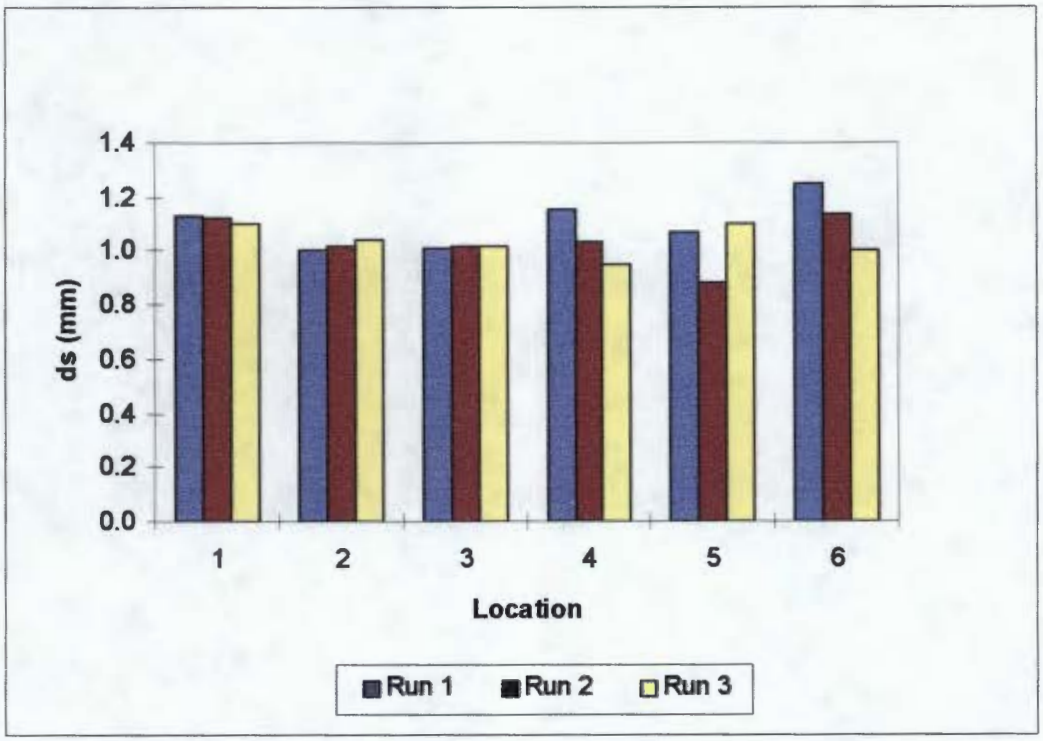

Figure 4.9: Reproducibility of bubble size measurements.

4.5.2 Superficial Gas Velocity Measurement

The procedure for the measurement of the superficial gas velocity was similar to that used for the bubble size distribution measurements. The measuring equipment was similar to that used by Gorain, *et al.*, (1996). The instrument consisted of a 0.5 m long transparent graduated plastic tube (20 mm inside diameter) which was screwed onto the different lengths of PVC tubes described in section 4.5.1. At the bottom of the PVC tube were a pneumatic pinch valve and air and water inlet valves, while at the top of the transparent tube was an air outlet valve that was opened to allow trapped air to escape while the tube was being filled with water, as illustrated in Figure 4.10.

The tube was immersed vertically in each flotation cell and supported so that the pinch valve was just at the intended location of measurement. The pinch valve was closed and the water and air valves opened to fill the tube with 50 ppm solution of frother. The

significance of the frother solution was to minimise the chances of bubbles coalescencing as they rose up the tube. When the tube was full, both valves were closed and the pinch valve was opened to allow air from the cell to rise up the tube displacing water. The time for the air-water interface to traverse a known distance (30 cm) was noted and from this information, the superficial gas velocity was calculated in cm/s.

Two measurements were performed at each location under the same conditions, with an average of 100 ml of air being collected over time intervals from 30 and 120 seconds, depending of the type of cell under investigation. The average of the two measurements was used in the calculation of the bubble surface area flux. The procedure was repeated for all the different variables used in the test.

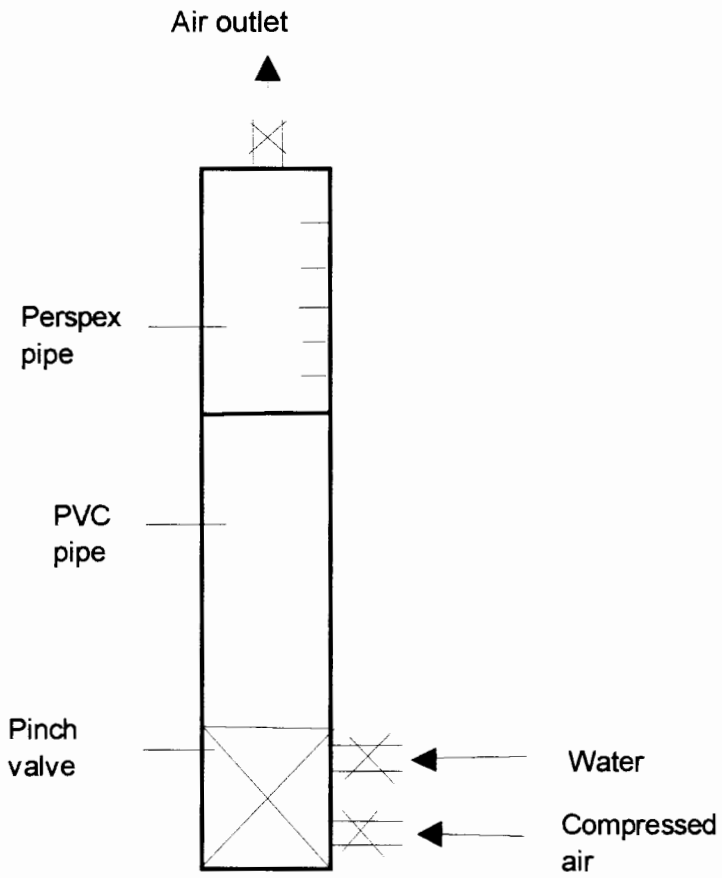

Figure 4.10: The superficial gas velocity measuring equipment.

4.5.2.1 Reproducibility

Reproducibility of Jg measurements is illustrated in Table 4.5 with data obtained from the WEMCO 144 high power cell at an air flowrate of 7.5 m^3/min (see Table C26 in Appendix C). The relative errors between the measurements at each location are reasonably low; an indication of a high reliability of the Jg measuring device used in the experiment.

Table 4.5: Reproducibility of superficial gas measurements.

Q_g m^3/min	Location	t1 s	t2 s	Jg1 cm/s	Jg2 cm/s	R.E. cm/s
7.51	1	59	60	2.03	2.00	0.02
	2	61	61	1.97	1.97	0.00
	3	57	61	2.11	1.97	0.07
	4	64	64	1.88	1.88	0.00
	5	68	69	1.76	1.74	0.01
	6	63	61	1.90	1.97	0.04

t1, t2 = Times in test 1 and 2 respectively for the air-water interface to fall within the marked points on the perspex tube

Jg1, Jg2= Corresponding superficial gas velocities for t1 and t2

[2]R.E. = Relative Error

Q_g = Air flowrate

4.5.3 Gas Holdup Measurement

The gas holdup in the cells was measured using a vacuum-activated plunger (Figure 4.11) similar to that used by both Jameson and Allum (1984) and Gorain, *et al.*, (1995b). It was made up of a 40-mm diameter cylinder with two plungers attached to a common central rod. This assembly was hooked to a long handle that permitted fairly

[2] Relative Error=Jg1-Jg2/(Jg1+Jg2)/2

deep submergence in the cells. Each plunger had an O-ring on it to ensure an air-tight fit when it moved within the cylinder.

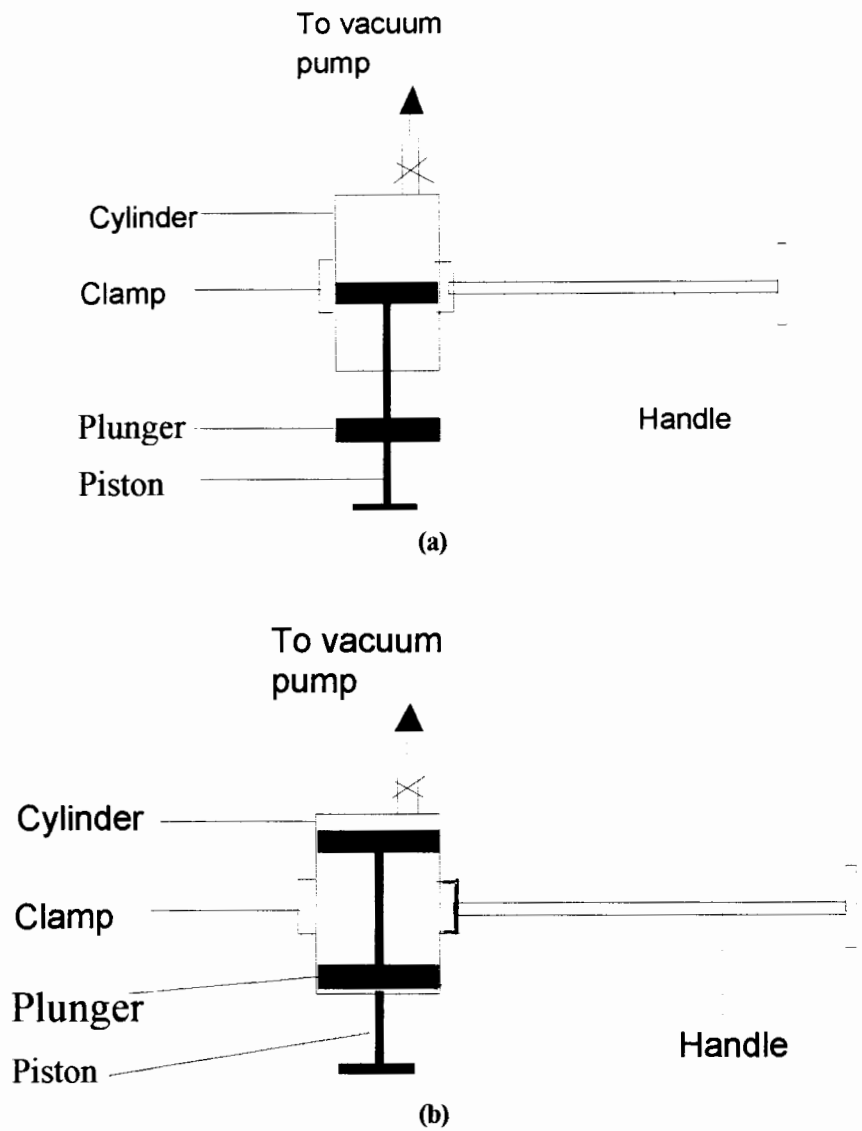

Figure 4.11: Gas hold up measuring device.

To start with, the upper plunger was pulled out of the cylinder as shown in Figure 4.11a. The cylinder was immersed at the required location in the cell and the vacuum was activated. The plungers were then drawn into the cylinder instantaneously, trapping a volume of the aerated pulp between the plungers as shown in Figure 4.11b. The cylinder was then removed from the pulp and the vacuum turned off. The cylinder's contents were emptied into a measuring cylinder by pulling out the plungers, allowing the trapped air to escape into the atmosphere. Four measurements were performed per

location with approximately 0.50 *l* of aerated pulp being collected per measurement. The total volume and mass of the four samples were used to calculate the gas holdup and the pulp density respectively at each location. Since the value at each location represents the average of four measurements, no separate repeatability checks were carried out.

4.5.4 Impeller Rotational Speed Measurement

The speed of the impeller was measured in the test cells using an optical tachometer. This was done by applying a reflective tape provided with the instrument on a vane of the mechanism pulley. The tachometer was activated and the sensor shone on the reflector as the impeller rotated. The impeller speed in rpm was recorded on the display of the instrument. The results obtained compared well with those estimated from the ratios of the pulley diameters.

4.5.5 Air Flowrate Measurement

The air flowrates to the OK 50-m^3 TankCells and the Bateman cell were measured by means of orifice plates fitted in the air feed pipe to the cells, with their output read from a computer in the control room. The air flowrates to the conventional OK 16 cells were calculated from the air velocity measured in the feed pipe with a hot wire anemometer. With the internal diameter of the pipe known, the air flowrate could then be computed. The air flowrate measurements of a few of the OK 16 cells were ignored as they were beyond the detection limit of the anemometer used, but it was not allowed for any air adjustments to be made on those cells.

Some of the WEMCO cells had neither air control valves nor air feed pipes. Air flowrates were measured by partially covering the air inlet orifice with a piece of plate and placing a vane anemometer over the uncovered part of the orifice to measure the speed of air into the cell. By moving the plate to change the orifice opening, the air

velocity at different air flowrates was measured. With a knowledge of the orifice diameter, the air flowrate to the cells was calculated. The air velocities into the cells with control valves were measured at different air flowrates by changing the position of the valves. The average of three measurements was recorded for each valve position. Details of the calculation of the air flowrates can be found in Appendix F.

4.5.6 Power Measurement

The current drawn by the motors was noted while the mechanisms ran with the cells empty (no load) and when the cell was in normal operation. The power consumption was estimated by subtracting the current drawn by the motor with the cell mechanism running free from that with the mechanism running under load. A power factor of 0.92 was used in the relevant equation.

Power consumption was calculated for the entire volume of the pulp and the impeller swept volume. A brief background of power measurement techniques and equations have been given in Appendix E.

CHAPTER 5
RESULTS AND DISCUSSION

5.0 INTRODUCTION

The results of the experiments are contained in this chapter, together with a discussion of the significance of these results. The bulk of the results can be found in Appendix C. The data relevant to a particular discussion have been extracted from the Appendix and are fully discussed under the appropriate sections in this chapter.

The results are discussed under three main categories. Section 5.1 discusses the solids suspension characteristics in flotation cells. In this section, the effects of different variables such as air flowrate, impeller speed and location on solids suspension in the different cells and circuits are considered.

Section 5.2 looks at gas dispersion in single cells. The effects of different variables such as air flowrate, impeller speed, mechanism size, and location in cell on the gas dispersion parameters like bubble size, superficial gas velocity, gas holdup and bubble surface area flux in the individual cells are discussed.

In section 5.3, the gas dispersion characteristics of the different types of cells are compared. The focus of this section is to see how gas dispersion varies between cells in the same and different circuits, and between cells of different sizes and applications, resulting from different reagents suites, solids concentration and so on.

The section ends with a discussion of some useful findings of this work, and their relevance to the classical, chemical engineering literature.

5.1 SOLIDS SUSPENSION

The aim of this part of the investigation was to find out how well particles are dispersed in typical industrial flotation cells. The focus of this section is not to

investigate whether particles were completely suspended, in conformity with Zwietering's 1-sec criterion (see section 2.5.1), but to determine the concentration profile of suspended particles in flotation cells of different sizes, types and under different modes of operation. Just complete suspension refers to the state in which all the particles are in motion and no particle remains on the base of the tank for more than a short period of time, usually 1-2 seconds. The suspension condition in flotation cells is different from the criterion described above.

A dip stick was used to probe the floor of a number of the cells while they were in operation and a small bed of settled solids was detected, with an even thicker bed in the corners of the cells. In the literature, much of the work pertaining to particle suspension is related to the minimum agitator speed for solids suspension in a three-phase system, N_{jsg}, or the specific power required to achieve this condition. The N_{jsg} and the specific power for these cells were not determined, but it was obvious that their perormance would fall below the minimum required for complete suspension.

In these experiments, samples of the pulp were taken at different locations in the cells using the air holdup measuring device (see section 4.5.3). The S.G. of the pulp was determined by dividing the mass of the sample by its volume. The effects of changing air flowrate and impeller speed were investigated. The results obtained for the different types, sizes and duties of cell studied are given in Tables C1-C13 in Appendix C.

5.1.1 Effect of air flowrate

As was observed in section 2.3 of the literature review, the introduction of air into a solid-liquid system reduces the liquid pumping velocity of the impeller in the cell, affecting both solids suspension and dispersion. This effect is even more pronounced as the air flowrate is increased and above a certain air flowrate, solids begin to settle. This usually coincides with a drastic drop in the cell power. Figure 5.1 shows the S.G. of pulp in the OK 50-m^3 TankCells (the "Free-flow" and the "Multi-mix" mechanisms), measured at 1.4 m below the froth. The measurement was made by

fitting an extension on to the gas holdup measuring device described in section 4.5.3. Each point in Figure 5.1 is the average of four samples. The air flowrates were read from the Distributed Control System (DCS) in the operator's control room, measured by an orifice plate.

As can be seen from Figure 5.1, there was a significant decrease in the S.G. of the pulp with increasing air flowrate. The most likely reason for this would be that with the introduction of air into a two-phase system as in flotation cells, the liquid pumping capacity of the impeller is considerably reduced. The liquid circulation velocity is no longer sufficient to keep the dense particles in suspension and so these dense particles either settle to the bottom of the cell or are suspended near the cell bottom and below

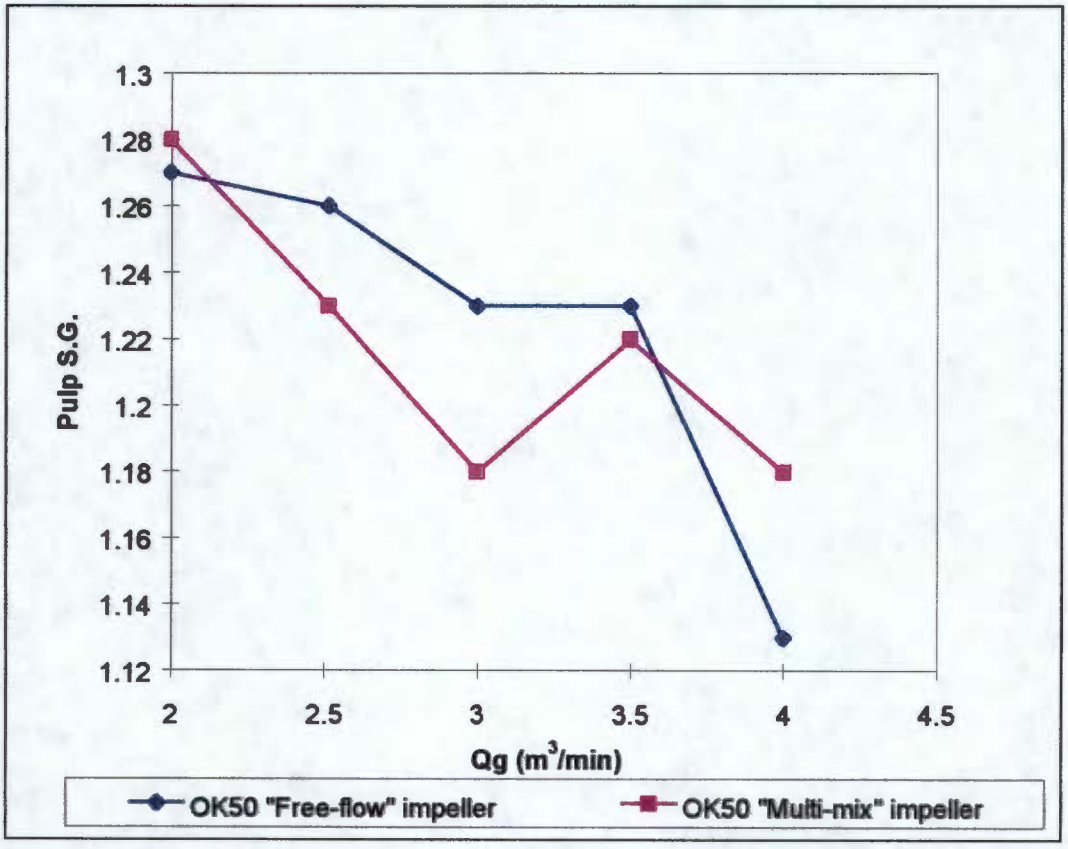

Figure 5.1: Pulp specific gravity (S.G.) at different air flowrates (Qg) in OK 50-m^3 TankCell.

the impeller. The pulp S.G. decreased significantly as the air flowrate was increased (Figure 5.1). To minimise the problem of particle settlement, the critical impeller speed for particle suspension in a flotation cell must always be kept considerably

higher than in a similar system that is suspending the same mass of solids in a two-phase, liquid-solid system.

The general trend of pulp S.G. was found to be similar in both the "Multi-mix" and the "Free-flow" OK 50-m^3 TankCells. An unusually high S.G. was observed at the air flowrate of 3.5 m^3/min in the case of the "Multi-mix" cell. The WEMCO 144 standard power cell showed a similar trend (Figure 5.2). The data of the pulp S.G. for these cells can be found in Tables C3, C4, C7 and C11 of Appendix C.

5.1.2 Effect of impeller speed

The formation of ventilated cavities behind the impeller blades, and the associated decrease in the shaft power and the pumping capacity upon addition of air, play a crucial role in aerated systems and can lead to a partial settling out of solids. Consequently, increased impeller speeds are required in order to maintain solids suspension in aerated systems such as flotation cells. At very high aeration rates, flooding can cause a complete loss of liquid pumping and gas dispersion with the consequence of solids settling out.

As evident from Figure 5.2, when the WEMCO 144 cell was operated with a standard (45 kW) motor, the suspension state was unsteady as the air flowrate was increased. Pulp S.G. generally decreased as the air flowrate was increased. Samples of pulp were taken at each of six different locations in the cell as shown in Figure 4.7, and each point represents an average S.G. of four samples. However, in the same cell, when the speed of the impeller was increased by replacing its motor with a 90 kW motor, the average S.G. in the cell was found to be almost uniform. This implies that with the 90 kW motor, increasing the air flow within the range shown did not result in any difference in the liquid pumping and solid suspension characteristics within the cell. Whether the high level of agitation found in the 90 kW WEMCO cell is desirable is a question that needs to be investigated further. It is general knowledge that excessive turbulence creates instability of the particle-bubble aggregates and adversely affects the stability of the froth phase as well. On account of this, samples were taken

alongside these measurements for kinetic studies of the cells. It is expected that, using those data, this question will be addressed when that phase of work is completed. However, that subject is beyond the scope of this thesis. It is part of another student's thesis being carried out in parallel with this work.

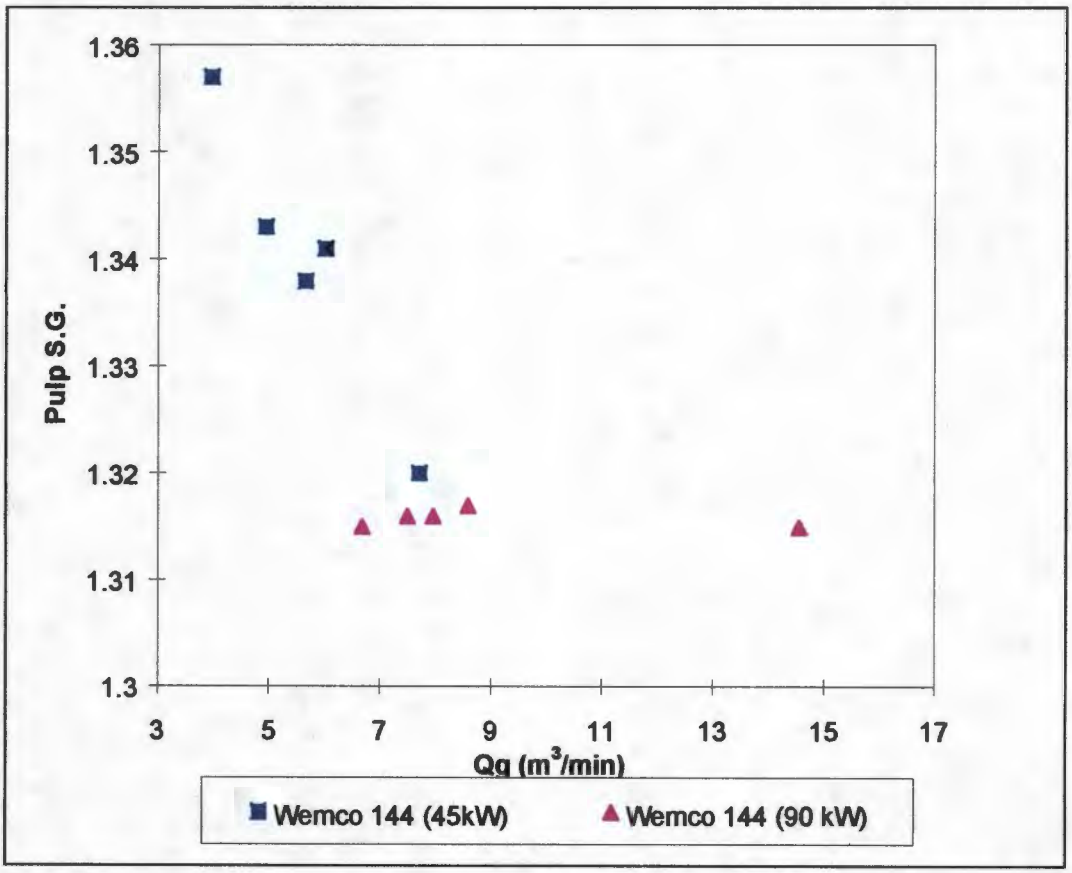

Figure 5.2 Average pulp specific gravity (S.G.) in WEMCO 144 cells at different operating conditions.

5.1.3 Effect of location

It is obvious from Figure 5.3 that there is a suspension gradient in the WEMCO 144 rougher flotation cell. The difference in the pulp densities between the upper and lower locations in the cell is clear. Pulp S.G. of the order of 1.32 and 1.16 were measured in the lower and upper sections of the cells, respectively (see Tables C3 and C4 in Appendix C). These observations are in agreement with other findings in the

literature. It has been shown by Shamlou and Koutsakos (1989) in a two-phase solid-liquid system that the radial distribution of solids above the impeller is remarkably uniform provided $N>N_{js}$. Other researchers (Barresi and Baldi, 1987) have also shown that the concentration of solids in a suspension is a function of height and that a maximum concentration usually occurs just above the impeller.

Above this maximum concentration region, these researchers observed an exponential decay of concentration with height. They also observed that for a given impeller speed, when complete suspension is achieved, the distribution of solids becomes better if the particle size and concentration of solids are small. This explains why an almost linear graph was observed in the WEMCO 120 cleaner cell (Figure 5.3) which handles pulp of low solids concentration (S.G. of 1.05) and small particle size. In the rougher cells, with a higher pulp density (S.G. of 1.32) and a relatively larger particle size, there was a clear distinction of densities in the impeller and quiescent regions of the cell.

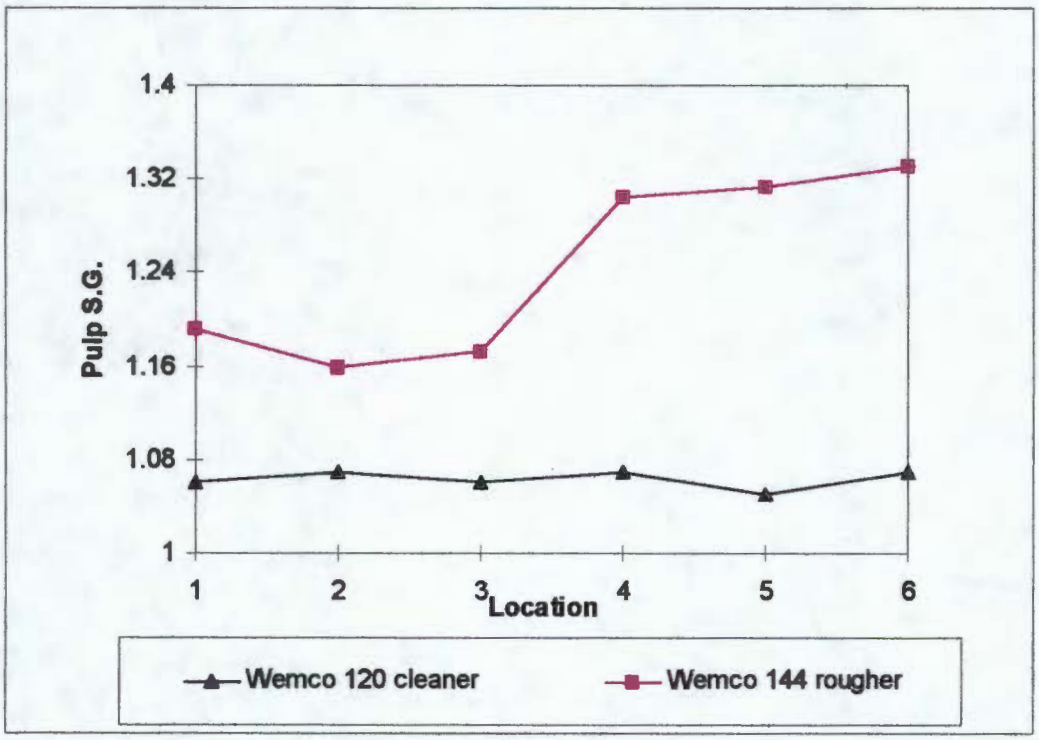

Figure 5.3: Pulp specific gravity (S.G.) profile in WEMCO 120 and 144 cells.

5.1.4 Summary

Generally, the specific gravity of the pulp in the cells was found to decrease as the air flow rate to the cells increased. There was a clear solids concentration profile in the cells with axial distance from the impeller. The concentration was found to be greatest in the impeller region and to decrease as the surface of the cell was approached. This profile was found to be quite prominent in cells treating large particle sizes and high solids concentration (viz. roughers) but insignificant in cleaners treating pulp with low solids concentration and finer particles. By increasing the impeller speed, the problem of segregation of solids in the flotation cells was reduced significantly.

5.2 GAS DISPERSION - CHARACTERISATION OF SINGLE CELLS

Gas dispersion in flotation cells is the central theme of this thesis. In this section, the results of the investigation into the gas phase properties such as bubble size, gas holdup and superficial gas velocity in cells of different size, type and duty are discussed in detail.

Each of the gas dispersion properties mentioned above is discussed in this section in terms of how it is affected by variations in air flowrate, impeller speed and location in the cells. The discussion in this section is limited to individual cells only. In the next section (5.3), these characteristics are compared for the different sizes, types, duties of cells and the positions of these cells in the circuit.

5.2.1 Gas holdup

The air holdup in a flotation cell is the volume fraction of gas in the pulp. It is believed that the greater the air supply to the cell, the more air holdup there will be and the more the air bubbles that are available for flotation. It has, however, been shown that in the flotation cell this is not wholly true, as holdup does not increase infinitely with air flowrate, but is a function of other factors that are discussed in the

sections that follow. Unless otherwise stated, the air holdup values discussed below refer to the average of the values measured at all the six locations in the cells. Results of gas holdup measurements in the cells studied are given in Tables C1-C18 in Appendix C.

5.2.1.1 Effect of air flowrate

The effect of air flowrate on air holdup is shown in Figure 5.4 for the various types of cells described below. The range of air flowrates to all the cells studied was restricted to a narrow range around their normal operating ranges. The lower air flowrates limits were chosen to avoid tripping the impeller motors on overload current, and the upper limits such that excessive turbulence was prevented. For the WEMCO cells there was no maximum air flow limitations as some of the mechanisms were without air control valves. The air holdup in different cells varies differently with air flowrate. The individual behaviour exhibited by each of these cells is discussed in the sections below.

(a) WEMCO 144 cell (standard and high-power motor)

Detailed results of the air holdup investigation in the WEMCO 144 cell operated with a standard and high-power motors may be found in Tables C3 and C4 in Appendix C. Within the range of air rates studied, no significant change in air holdup was observed in the WEMCO 144 standard cell, but in the high-power cell a slight increase in holdup was observed with increase in air flowrate (Figure 5.4). In the standard cell, holdups of between 8 and 10 % were measured but did not appear to follow any definite order as a function of air flowrate, while in the high power cell holdups of between 15 and 18 % were measured corresponding to the lowest and highest air flowrates respectively. The slight increase in air holdup with air flowrate in the high power cell might be due to the smaller sizes of the bubbles produced in it, compared to those in the standard cell. This suggests that the bubble dispersion in the standard cell may not be good enough in the range of air flowrates at which the tests were conducted (4-8 m^3/min).

(b) OK 16-m³

Air holdup appeared to be unaffected by air flowrate in the OK 16-m³ cell as can be seen from Figure 5.4. Though the graph contains data for the various cells measured at different depths, it is only intended to show the trend in air holdup with air flowrate for each cell, and should not be used to compare air holdup values in different cells. The trend shown by the OK 16-m³ cell is very similar to that in the WEMCO standard cell, possibly for the same reason. It is worth noting that the OK 16-m³ cell operates at a much higher air flowrate (10-16 m³/min) than the WEMCO 144 standard (4-8 m³/min) to produce almost the same air holdup (10-11% and 8-10% respectively). The results of the air holdup measurements in the OK 16-m³ cell may be found in Tables C7 and C8 in Appendix C.

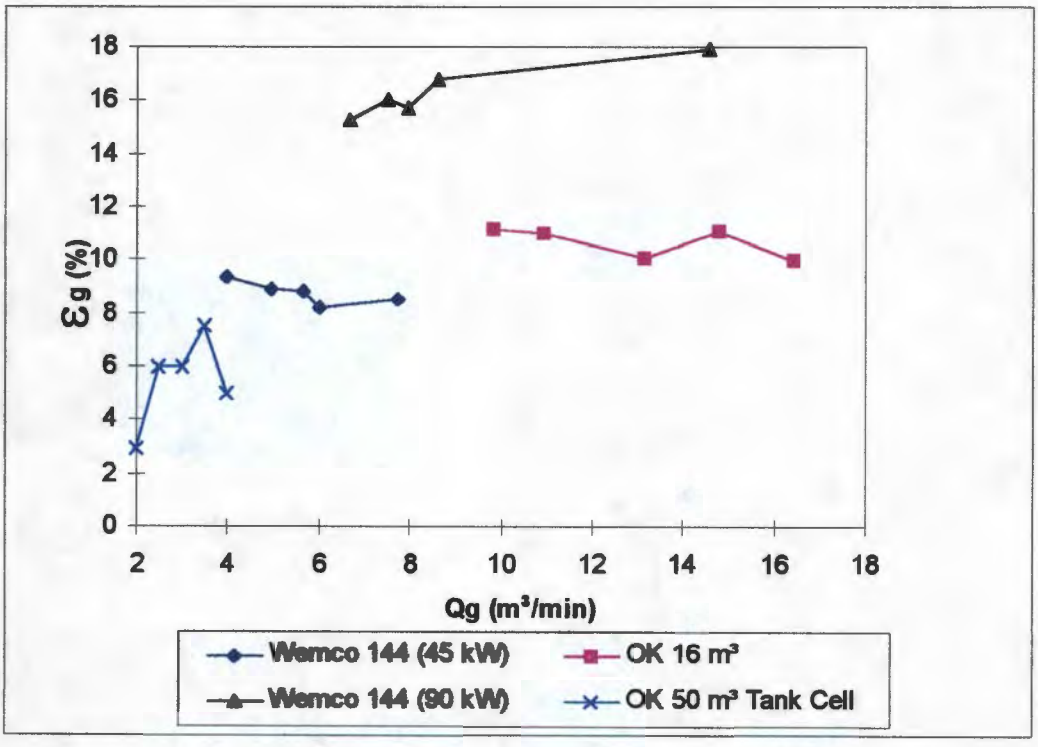

Figure 5.4: Gas Holdup (Εg) at different air flowrates (Qg) in the WEMCO standard and high-power cells, and the OK 16 m³ conventional and 50 m³ TankCells.

(c) OK 50-m³ TankCell

The results of the air holdup measurements in the OK 50-m³ TankCells may be found in Table C11 in Appendix C. The air flowrates in the TankCells were the lowest of all the cells - only 2-4 m³/min. In the OK 50-m³ TankCells a distinct trend of increasing gas holdup with increase in air flowrate was obvious at very low air flowrate as seen from Figure 5.4. At the highest air flowrate however, a drop in the holdup was observed. There was a substantial difference in the air holdup between the "Multi-mix" and "Free-flow" impellers in the two OK 50-m³ TankCells (Figure 5.5), although their aeration rates were the same. It is interesting to note the commonality in their trends, as shown in Figure 5.5.

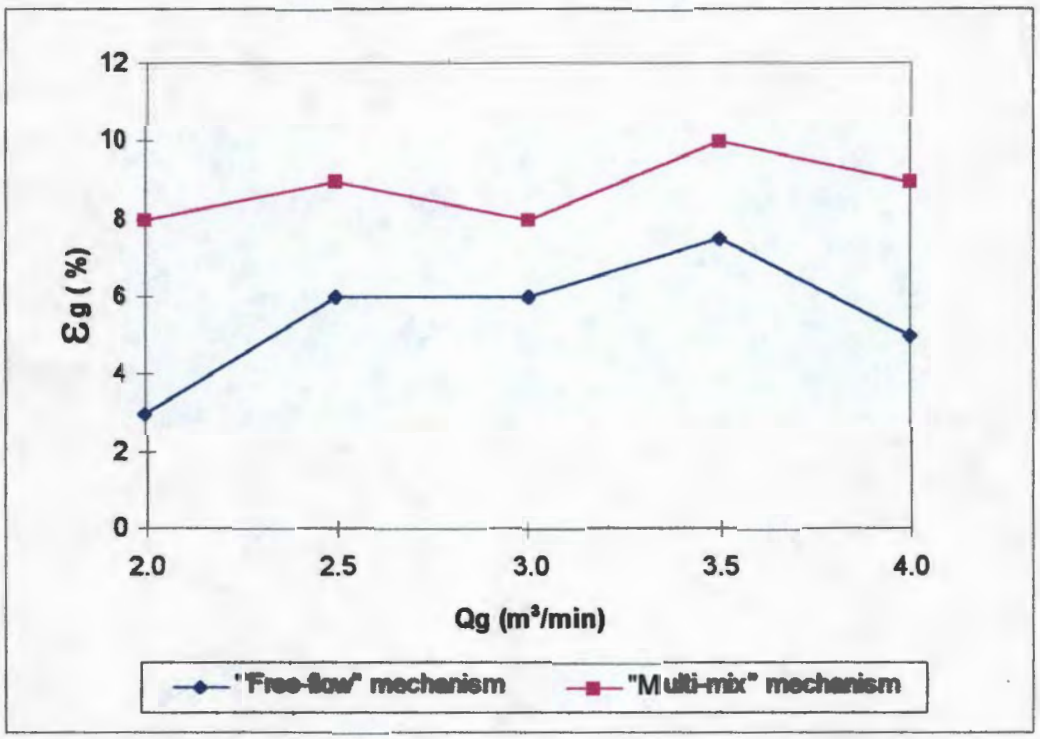

Figure 5.5: Air Holdup (Eg) at different air flowrates (Qg) in the OK 50-m³ "Multi-mix" and "Free-flow" impeller systems.

The most likely reason for this behaviour in the two TankCells is that different flow patterns are generated in the mechanisms as shown in Figure 4.6 in Chapter 4. Also the "Multi-mix" cell produces a higher pulp circulation velocity by virtue

of its greater impeller rotational speed. A lot of the small bubbles with lower buoyant forces are trapped within the circulation loop around the impeller leading to an increase in the residence time of bubbles compared with the "Free-flow" mechanism cell. Hence a higher air holdup is likely in the "Multi-mix" cell.

The air holdup increases with air flowrate in both cells. However, there seems to be a drop in the air holdup at the highest air flowrate of 4 m^3/min. This suggests that there is likely to be a threshold value in the region of 3.5 m^3/min beyond which gas dispersion in the OK 50-m^3 TankCells is no longer so effective. It is interesting to note that the normal operating air flowrate of about 3.5 m^3/min to these TankCells, as recommended by the manufacturers, corresponds to the maximum holdup observed in this work.

5.2.1.2 Effect of impeller speed and power input

It has been shown that air holdup increases with impeller speed or impeller power, if all other physical and chemical parameters in the cell are constant (Gorain, *et al.*, 1995b). The effect of impeller speed and impeller power on air holdup was studied for the WEMCO 144 standard and high-power cells and the OK 50-m^3 "Multi-mix" and "Free-flow" impeller cells in this work. The results are presented Tables C11 and C14 in Appendix C and are discussed in the sections that follow.

(a) WEMCO 144 cell (standard and high-power motor)

As discussed in Chapter 3, increasing the impeller speed increases the air holdup in flotation cells. Figure 5.6 shows the effect of impeller power on air holdup at similar air flowrates for the WEMCO 144 cells. It is seen that the high-power cell with the impeller rotating at 220 rpm produced about twice the air holdup as the standard cell with impeller rotating at 172 rpm at similar air flowrate of about 6-8

m^3/min. The data[3] for Figure 5.6 are found in Table C14. The most probable reason for this is that the high-power cell produced smaller bubbles, as will be seen in section 4.2.2.6 under the effect of power on bubble size. The smaller bubbles have lower rise velocities. The consequently longer residence times in the cell cause the air holdup to increase.

(b) OK 50-m^3 TankCell

The effect of impeller speed on the air holdup in the OK 50-m^3 TankCells may be seen in Figure 5.7, although the interpretation is complicated by the fact that the results are for different impeller types. Data for Figure 5.7 are found in Table C11.

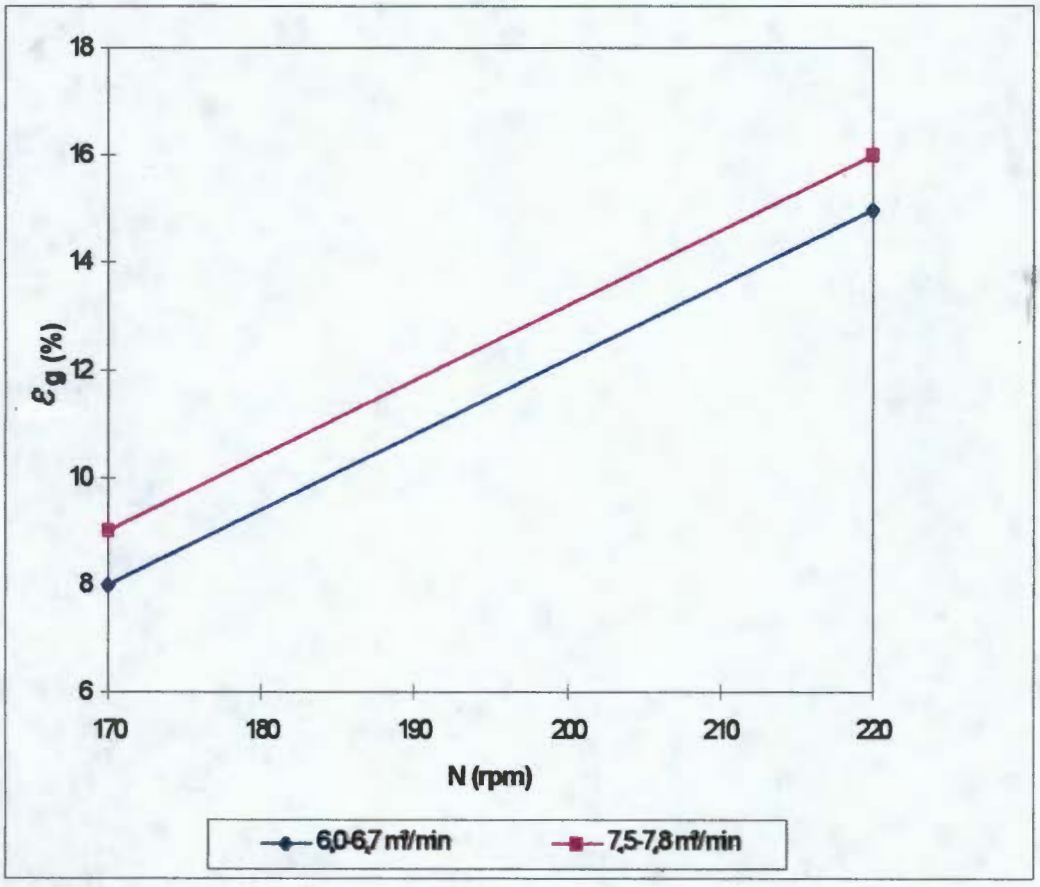

Figure 5.6: Effect of impeller speed (N) on air holdup (εg) in WEMCO 144 cells.

[3] The data for Figure 5.6 are correspond to the air holdups within the indicated air flowrates. There are only two data points on each graph but have been joined by a straight line to emphasise the trend and not the linearity.

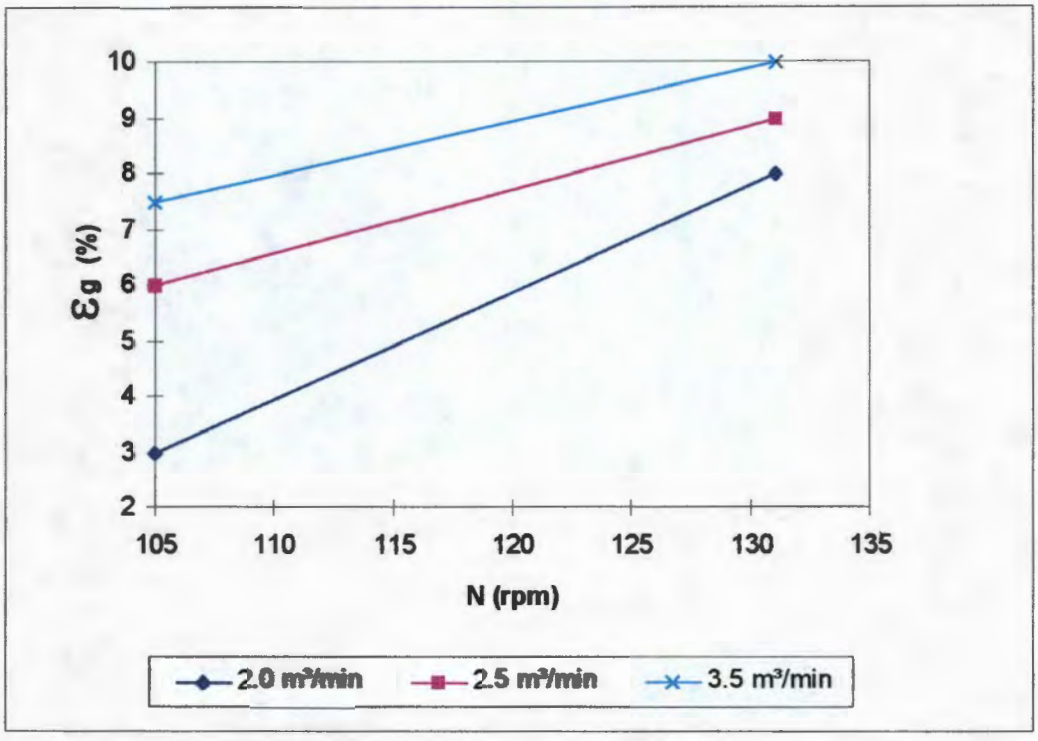

Figure 5.7: Effect of impeller speed (N) on air holdup (εg) *in* OK 50-m³ TankCells.

For clarity, the data points have been joined by straight lines. The graph shows the results obtained with the "Multi-mix" impeller rotated at 131 rpm and the "Free-flow" impeller at 105 rpm at three air flowrates. The "Multi-mix" impeller operating at the higher speed was found to produce a greater air holdup than the "Free-flow" impeller operated at the lower speed. The differences in the air holdup in the two cells may be attributed to the differences in the flow pattern in each cell. A large proportion of the relatively smaller size bubbles produced by the higher speed "Multi-mix" impeller system are retained by a higher pulp recirculation, hence the higher holdup compared to the lower speed, "Free-flow" impeller system.

5.2.1.3 Effect of location

The effect of location on air holdup is depicted in Figure 5.8 for the WEMCO standard and high power cells and the OK 16-m³ cell. The corresponding data can be found in Tables C3, C4 and C7 in Appendix C. The graphs were plotted by

using the averages of the quiescent and turbulent zones at the indicated air flowrates in each of the cells. As with the previous charts, the straight lines only serve to pair data points together.

(a) WEMCO 144 cell (standard and high-power motor)

As is evident from Figure 5.8, the average air holdup in the high power cell is greater in the impeller zone than in the quiescent zone. This is consistent with observations made by Gorain, *et al.*, (1995b). It will be seen in the discussion under section 5.2.2 (see Figure 5.12) below that large bubbles occur in the upper sections of the cell owing largely to bubble coalescence, which results in higher rise velocities of the bubbles in this region of the cell. Bubbles thus leave the cell at a relatively faster rate with a shorter residence time in the upper sections of the cell. In constrast, smaller bubbles observed in the lower regions of the cell possess lower rise velocities. This results in a longer residence time in the impeller zone hence a greater air holdup.

The standard cell did not show any difference in air holdup between the upper and lower sections of the cell. The air holdup in both sections was at 8.2% as may be seen in Figure 5.8 (the single point represents two points). This may be due to the fact that the size of the bubbles does not show much change in the cell. Bubble coalescence may not be very prominent in this cell compared to the high power cell owing to less turbulence in the cell and less air intake. The turbulence intensity and bubble population have been identified to have considerable effect on the degree of bubble coalescence in a flotation cell (Glembotski, 1963).

(b) OK 16-m^3 cell

Figure 5.8 also shows the average air holdup profile in the OK 16-m^3 cell in the lower and upper sections of the cell. It is clear from the graph that the holdup is greater in the lower than in the upper regions of the cell. The effect is similar to the trend observed in the WEMCO high power cell. Similar trends of lower air

holdup in the turbulent regions of the cell, and higher in the quiescent regions have been reported in literature (Gorain, *et al.*, 1995b). However, the air holdup in the OK 16-m^3 cell is much smaller than in the WEMCO 144 high power cell at similar air flowrate. This is probably due to better air dispersion into smaller bubbles in the latter cell.

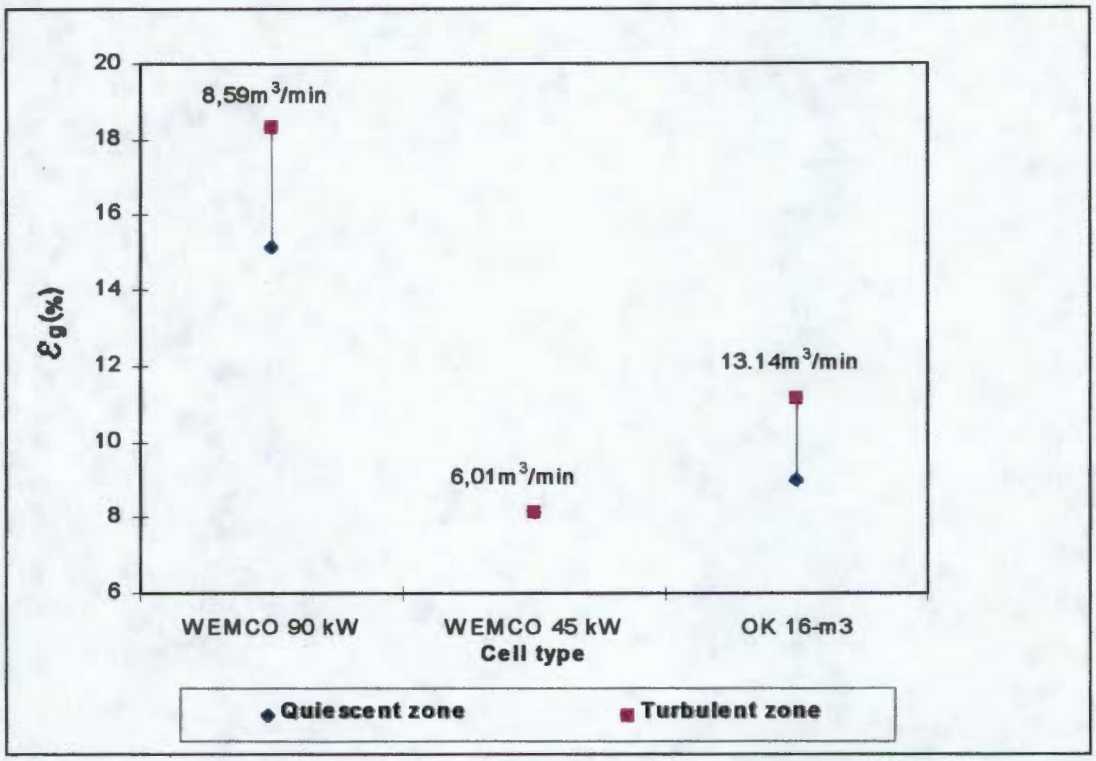

Figure 5.8: Air holdup (Εg) at different locations in the OK 16-m^3 and WEMCO 144 standard and high-power cells.

5.2.1.4 Summary

Gas holdup is known to be one of the most important quantities in evaluating the effectiveness of gas dispersion, and solids suspension in any three-phase system and particularly the flotation cell. As can be deduced from the discussion above, air holdup in the flotation cells is affected by the air flowrate, the impeller speed and the location in the cells. Air flowrate did not seem to have much effect on air holdup in the conventional cells operated under their normal operating conditions. In the standard WEMCO cell, location in the cell (quiescent zone versus turbulent zone) did not influence the holdup much, while this was significant in the OK

16-m^3 cell. Impeller speed, which is a reflection of the power input, was however identified as affecting air holdup significantly in all the cells.

Unfortunately not many universal correlations have been developed with the capacity to predict air holdup within the three-phase system to a high degree of reliability. Most of the existing correlations are based on variables which are themselves difficult to predict. There is a general lack of insight as to the variables required for generating these correlations. Improvements could be made in these correlations if it were possible to incorporate in them the factors that determine the flow and gas dispersion characteristics. Very little work has been done in developing correlations for air holdups that are based on flow regimes, although Warmoeskerken and Smith (1985), Smith (1985) and Barigou and Greaves (1992) have produced correlations based on flow which show great potential in predicting air holdup in such systems.

It is very likely that a useful correlation could be developed to predict air holdup in flotation cells on the basis of power or impeller speed and air flowrate. Though this does not form part of this thesis, the development of such a correlation as a continuation to this work is highly recommended.

5.2.2 Bubble size

The role of bubble size in flotation is very important due to its effect on the kinetics of the process. Consequently, the sizes of bubbles and their distributions in the flotation cells were measured to elucidate the effects of the different variables on bubble sizes in the cells.

5.2.2.1 Mean and Sauter mean bubble diameters

This section highlights the differences in arithmetic mean and Sauter mean bubble diameters as obtained in the results. The arithmetic mean bubble size is important in gas-phase literature since it is the quantity that is mostly used in relating

reaction kinetics to air bubbles in three-phase systems. The Sauter mean diameter on the other hand is important in determining the bubble surface area flux. It is often regarded as the mean of the area presented by all the air bubbles and therefore it is a better representation of the air bubble distribution than the arithmetic mean size. Hence it is the characteristic property that has been used in this thesis in the calculation of the bubble surface area flux.

In agreement with the discussion in Chapter 3, the Sauter mean bubble diameters measured in this work were found to be much bigger than the arithmetic mean bubble diameters because of the influence of the large bubbles on the former property. These differences can be seen in Table C1 in Appendix C. The Sauter mean diameters of the bubbles were found to be on average about 1.4-1.6 times the arithmetic mean bubble diameters (see Figures C1 and C2 in Appendix C). Similar differences were noticed between the Sauter and arithmetic mean bubble diameters, in a number of industrial cells measured by Jameson and Allum (1984). The significant differences between these two quantities, according to Jameson and Allum (1984), occur because the bubbles are not well dispersed in the flotation cells measured. When there is good dispersion of bubbles in a cell, the Sauter and the arithmetic mean bubble diameters will be close. In fact, good air dispersion indicates that the size distribution of bubbles is narrow.

Details of the method for calculating the Sauter mean bubble diameter from the experimental data using the total bubble surface area, S, and volume, V, are given in Appendix C. The computer programme "Bubpro", used with the UCT Bubble Size Analyser, produces a summary sheet showing the total bubble surface area, total bubble volume, the mean bubble diameter and the standard deviation of the bubble size distribution.

5.2.2.2 Bubble size distribution

The "Bubplot" programme of the UCT Bubble Size Analyser computer software package was used to plot the distributions of the arithmetic mean bubble size, as

measured in different locations, and at different air flowrates and impeller speeds. Measurements were made in the WEMCO 144 high-power cell and the OK 10-m^3 and 50-m^3 TankCells. These plots are shown in Figures 5.9 - 5.11 below.

Some striking differences exist in bubble sizes within the cells at different air flowrates, impeller speeds and locations. Figure 5.9(a) shows the average of the bubble size distribution in a WEMCO 144 high-power cell at locations 4, 5 and 6 while Figure 5.9(b) is that for locations 1, 2 and 3. It can be seen from Figure 5.9(a), that a narrow, apparently lognormal distribution with a small mean bubble size occurred in the lower locations (4, 5, and 6) near the impeller. In the upper locations of the quiescent zone, further from the impeller, a broader, apparently lognormal distribution was observed, but with a larger mean bubble size (Figure 5.9(b)). The bubbles close to the impeller are relatively smaller and have a narrower size distribution, probably because of the high shear forces responsible for breaking of bubbles in this region. As the axial distance from the impeller increases, the bubble shearing action decreases and bubble coalescence is more likely to occur. This is especially true in the region close to the froth layer, because of bubble crowding. This results in the wider range of sizes in the bubble size distribution found in the quiescent zone.

It is also seen that the distribution of bubble sizes in the upper locations (1, 2 and 3) are shifted more to the right. This implies that more of the bubbles in the upper locations exceed 0.6 mm diameter than in the corresponding lower locations. Similar observations have been made by Barigou and Greaves (1992) in an air-water system using a Rushton turbine impeller. It was shown that bubble size distributions vary considerably with both axial and radial distance from the impeller.

The effect of increasing air flowrate on the bubble size distribution is illustrated in the case of the OK 50-m^3 TankCells in which the distributions at two different air flowrates are noted. From Figure 5.10, it can be seen that different bubble size distributions were found at different air flowrates.

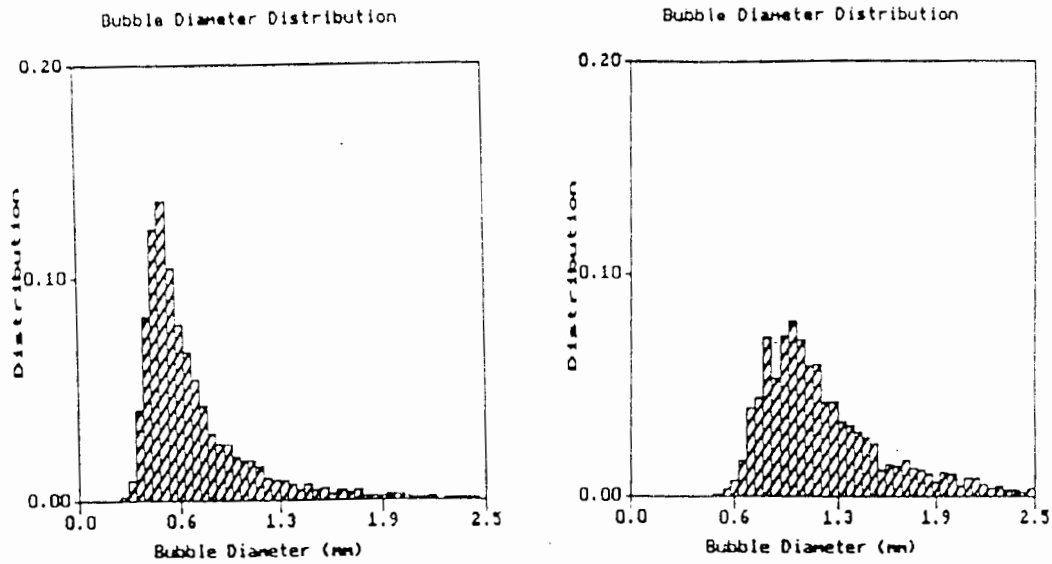

(a) (b)

Figure 5.9: Mean bubble diameter distribution at different locations in WEMCO 144 (90 kW motor) flotation cell, (a) impeller zone (b) quiescent zone.

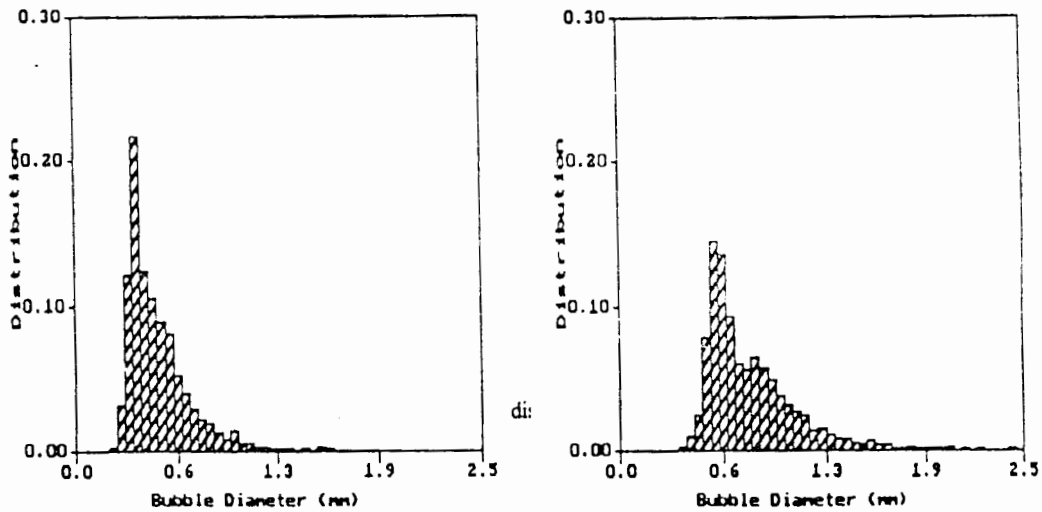

(a) (b)

Figure 5.10: Mean bubble diameter distribution at different air flowrates in OK 50-m^3 TankCell, (a) 2.0 m^3/min (b) 3.5 m^3/min.

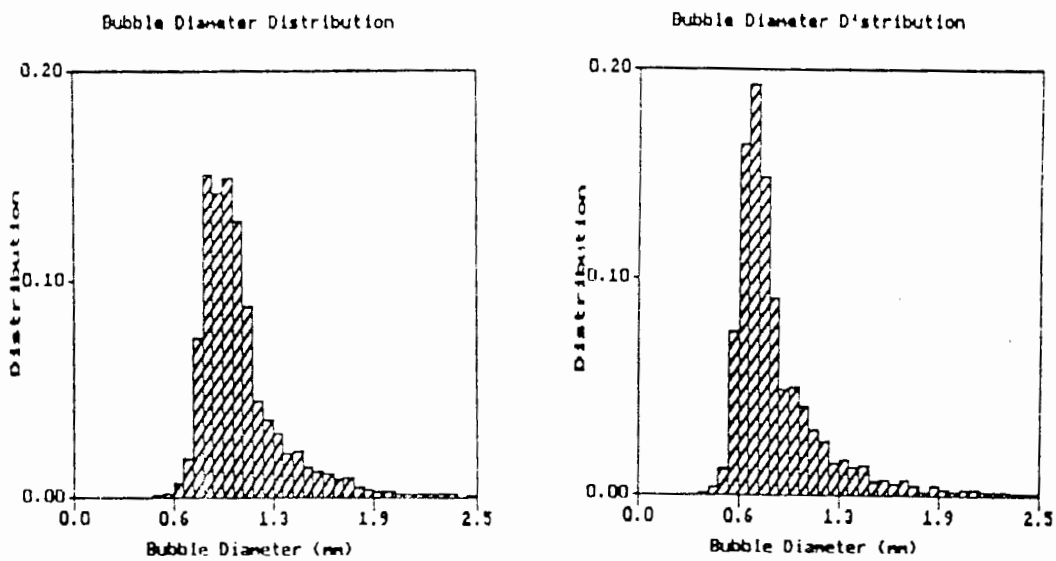

(a) (b)

Figure 5.11: Mean bubble diameter distribution at different impeller rotational speeds in OK 10-m^3 flotation cell, (a) 145 rpm (b) 180 rpm.

The bubble sizes shown represent the averages of six measurements at 1.4 m below the froth-pulp interface. A comparison of the distributions at the different air flowrates shows a trend similar to that seen in Figure 5.9. At lower air flowrates, the distribution is narrower and shifted to the left; it tends to shift to the right as the air flowrate is increased. At lower air flowrates, the proportion of bubbles with diameters smaller than 0.6 mm is greater and this ratio reverses as the air flowrate increases; the ratio of smaller bubbles decreases and that of the larger bubble increases as the air flow rate increases. This observation is consistent with findings by Gorain, *et al.*, (1995a).

A similar effect can clearly be seen for different impeller speeds in the OK 10-m^3 TankCell, as shown in Figure 5.11. (These observations were made in a different concentrator than those shown in Figures 5.9 and 5.10). At 180 rpm impeller speed smaller bubbles were produced and so the distribution was narrower than at 145 rpm. The reason for this observation is discussed in section 5.2.2.4 below.

5.2.2.3 Effect of air flowrate

Figure 5.12 below illustrates the effect of air flowrate on the Sauter mean bubble size for the WEMCO 144 standard and high-power cells, and for the OK 16-m^3 cell and OK 50-m^3 TankCells. The figure shows a general trend of increasing Sauter bubble diameter with air rate in all the cells studied. However, the manner of change differed in each cell. Data may be found in Tables C3, C4, C7 and C11 while the individual behaviours of bubble sizes in the cells are discussed further in the sections below.

(a) WEMCO 144 cell (standard and high-power motor)

Figure 5.12 shows an increase in Sauter mean bubble size with increasing air flowrate for both the standard and the high-power WEMCO 144 cells. It also shows that the rate of increase in bubble size is very rapid at the lower air flowrates and lower impeller speeds in the standard cell. In the WEMCO 144 cells

(the standard and high-power motors), the bubble sizes were measured three times each at six different locations using the UCT Bubble Size Analyser (see section 4.5.1). The values on the graph represent the averages of these measurements at the different air flowrates. As the air flowrate increases, the rate of increase in bubble size decreases and at very high air flowrates, the bubble size graph levels off or show a decrease. In the WEMCO 144 standard cell for example, at the highest air flowrate of about 7 m^3/min, a decrease in Sauter mean bubble size is observed. The decrease in the size of bubbles at higher air flowrate could be due to the measurement of the small bubbles from the tail end of the impeller blades only, as the bulk of the air is lost through flooding. A similar observation was made by Gorain, *et al.*, (1995a).

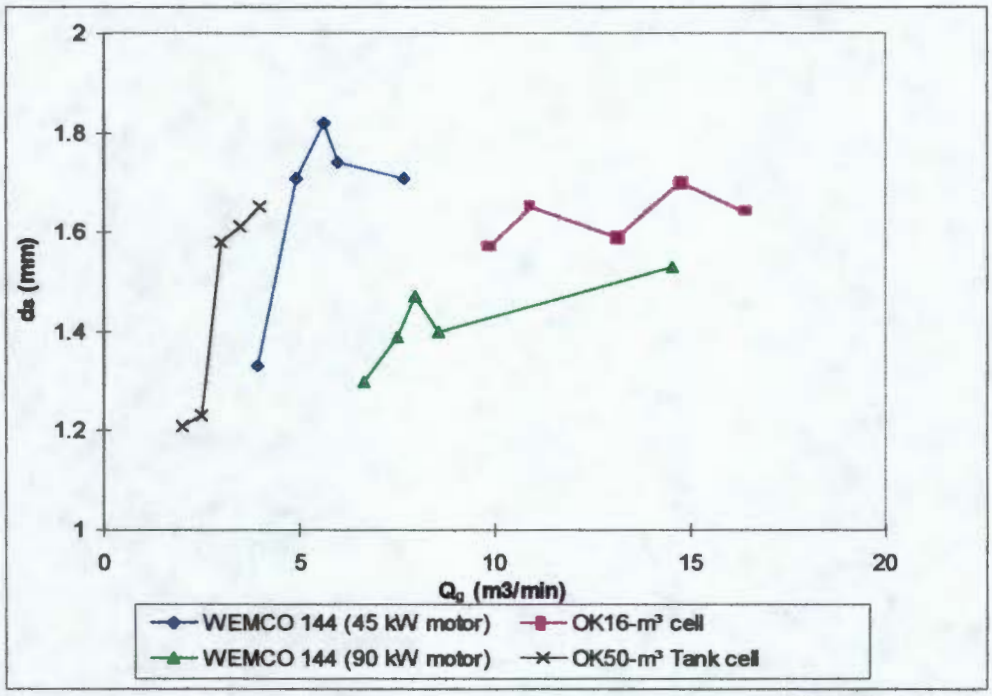

Figure 5.12: Sauter mean bubble diameter (d_S) at different air flowrates (Q_g) for the WEMCO 144 and OK cells.

At low air flowrate, the smaller Sauter mean bubble sizes suggests that the impellers are efficient in dispersing the air into small bubbles. As has been pointed out in section 2.3, an increased aeration rate forms large air cavities that tend to blind the impeller blades, thus decreasing pumping capacity. Lower pumping capacity means lower turbulence, resulting in lower forces that shear bubbles. The

efficiency of the impellers therefore decreases, resulting in generation of large bubbles.

As the air flowrate is increased further, larger bubbles are produced until a point is reached after which no great difference in bubble size is observed with increased air flowrate. This phenomenon of unchanging bubble size at high air flowrates can be explained by the fact that at such high air flowrates, the Sauter mean diameter is unaffected by and is usually even independent of the impeller speed, because an equilibrium is established between coalescence and dispersion. Similar views have been expressed by Barigou and Greaves (1992).

In the WEMCO 144 high power cell, Sauter mean diameters of 1.3-1.5 mm were measured with the aeration rates of 6-15 m^3/min. It can be noted from Figure 5.12 that with the same air flowrates of 6-8 m^3/min, the Sauter mean bubble diameters produced in the high power cell were less than those in the WEMCO 144 standard cell (see also section 5.2.2.4 below). Thus, the high-power cell could produce smaller bubbles than the standard power cell at more than twice the air flowrate. The Sauter mean bubble sizes in the WEMCO 144 standard power cell fell within a relatively wider range from 1.3 to 1.9 mm, even though the air flowrate available for investigation ranged only from 4-8 m^3/min.

(b) OK 16-m^3 cell

As in the WEMCO cells, the Sauter mean bubble sizes in the OK 16-m^3 cell were found to increase with increase in aeration rate, but more slowly, as can be seen from Figure 5.12. The actual values of the Sauter mean diameters were greater than those for the high-power WEMCO cell for all values of air flowrate. The format of measurements was similar to that for the WEMCO cells described above. In the OK 16-m^3 cells, within the air flow range of 9.9-16.5 m^3/min, Sauter mean bubble sizes of 1.42-2.12 mm (Table C8 in Appendix C) were measured. This was considerably larger than the ranges found in the WEMCO cells. At low air flowrates, the range of bubble sizes produced was quite narrow but the spread

increased significantly as the air flowrate was increased. At very high air flowrates in some cells, bubbles with Sauter mean diameter of 2.05 mm were measured near the surface of the cell, while bubbles as small as 1.28 mm were detected in the impeller regions of the cell at the same time.

(c) OK 50-m^3 TankCells

The size of bubbles produced in the OK 50-m^3 TankCell appears to be very sensitive to the air flowrate. Figure 5.12 shows Sauter mean bubble diameter versus air flowrate for the OK 50-m^3 "Free-flow" impeller cell. With aeration rates of 2-4 m^3/min, Sauter mean bubble diameters ranging from 1.2-1.6 mm were produced, similar to those found in the OK 16-m^3 and the WEMCO standard cells. The small bubble sizes produced are due to the low aeration rate, and also to the design of the OK 50-m^3 TankCells which has a froth crowder to enhance its operation at such low air flowrates.

5.2.2.4 Effect of impeller speed

(a) WEMCO 144 cell (standard and high-power motor)

The provision of two motor sizes - 45 and 90 kW - for the WEMCO 144 cell provided the opportunity for assessing the effect of varying impeller speed on bubble size. Measurements were taken on the WEMCO 144 standard cell with the standard motor (45 kW); measurements were then repeated with the high-power motor (90 kW). Apart from the impeller speeds, all the other variables in the cells remained virtually the same. With the high-power motor the impeller rotated at 220 rpm and induced about twice as much air as with the standard cell motor which rotated the impeller at 172 rpm. The ranges of aeration rate for the two impeller speeds overlap at 6.0-8.0 m^3/min allowing a quantitative comparison of the resulting bubble sizes (Figure 5.13). In this range, the differences in bubble size can be attributed to the difference in impeller speeds alone, as all other cell parameters were the same. Though this graph is plotted at only two impeller

speeds, it shows a trend of decreasing bubble size with increasing impeller speed for the WEMCO 144 standard and high-power cells. A similar trend has been noted by Gorain, *et al.*, (1995a) for different types of impellers. They have found that increasing the impeller speed at the same air flowrate produce smaller sizes of bubbles (see section 3.1.1 in Chapter 3).

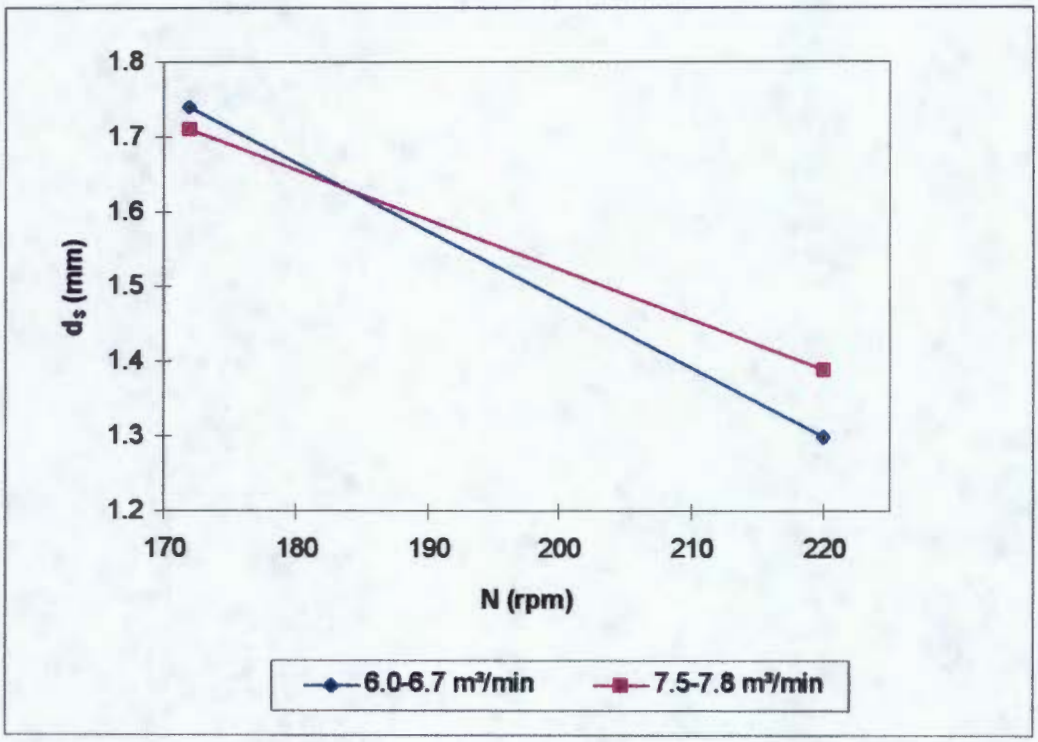

Figure 5.13: Sauter mean bubble diameter (d_S) at different impeller speeds (N) in WEMCO 144 cells.

(b) OK 50-m³ TankCell

A more detailed analysis of the effect of impeller speed on bubble size can be made from the data measured in the OK 50-m^3 TankCells, which were both supplied with the same amount of air while their impellers were rotated at different speeds (Figure 5.14). Figure 5.14 was generated from Table C11 in Appendix C. Again, the lines are only to show a trend and not linearity. The "Multi-mix" mechanism was rotated at 131 rpm, and the "Free-flow" mechanism impeller was rotated at 105 rpm. The trends were generally similar except for air flowrate of 3.0 m^3/min, which showed a slight deviation. As has been mentioned

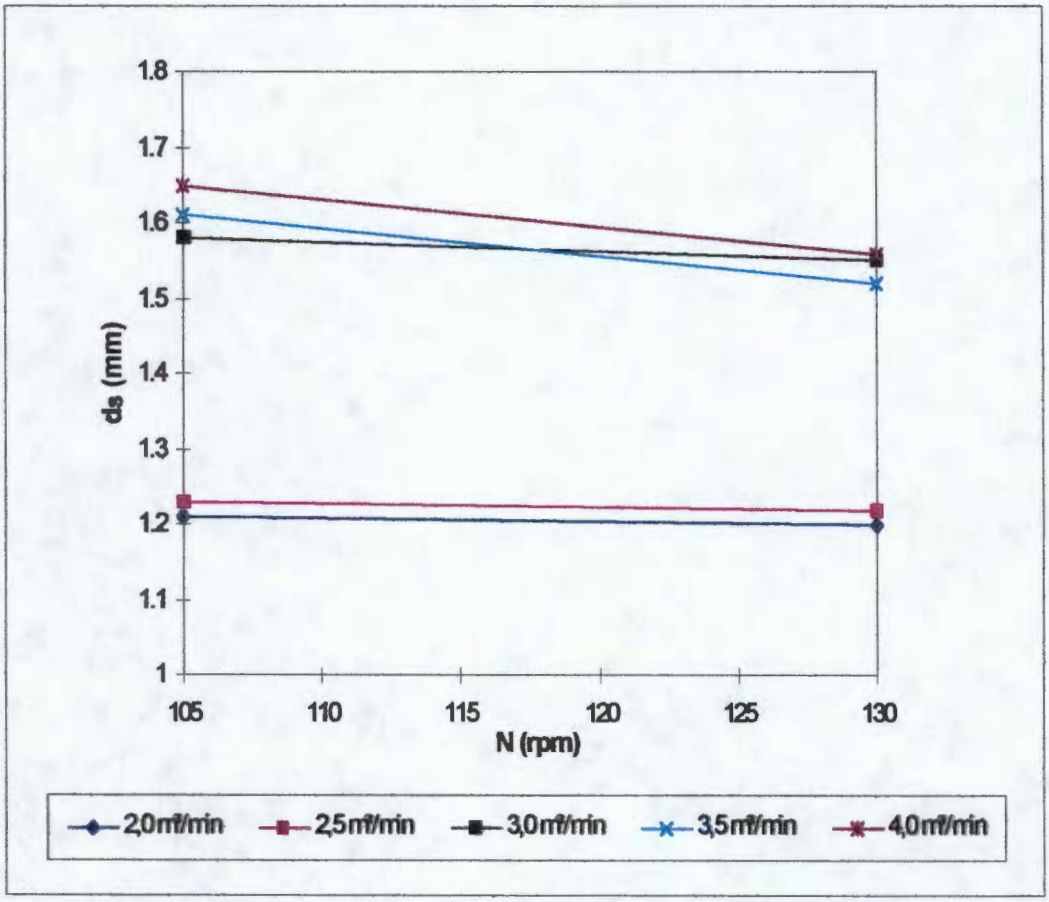

Figure 5.14: Sauter mean bubble diameter (d_S) at different impeller speeds (N) in OK 50-m^3 TankCells.

earlier, these graphs are only for quantitative analysis. At higher air flowrates, the "Multi-mix" mechanism, driven by a higher power motor, produced slightly smaller bubbles than the "Free-flow" with lower impeller speed. However, the difference in bubbles size was only 5% at the normal operating air flowrate of around 3.5 m^3/min to the cells. The slight difference in bubble sizes in the two cells is probably due to the higher shear forces resulting from higher turbulence intensities in the "Multi-mix" system than in the "Free-flow" system.

5.2.2.5 Effect of location

The effect of location in the cell on the sizes of bubbles measured is clearly illustrated in Figure 5.15, for the WEMCO 144 (standard and high-power motor) and OK 16-m^3 cells. In general, at the indicated air flowrates in each cell, smaller bubbles were found in the impeller zone, while larger bubbles were measured in

the quiescent zone. Again, the lines are only intended to pair the data points and not to show a functionality. Data on bubble sizes at each location may be found in Tables C1-C10 in Appendix C. The average bubble size in the quiescent and turbulent zones were used in generating Figure 5.15.

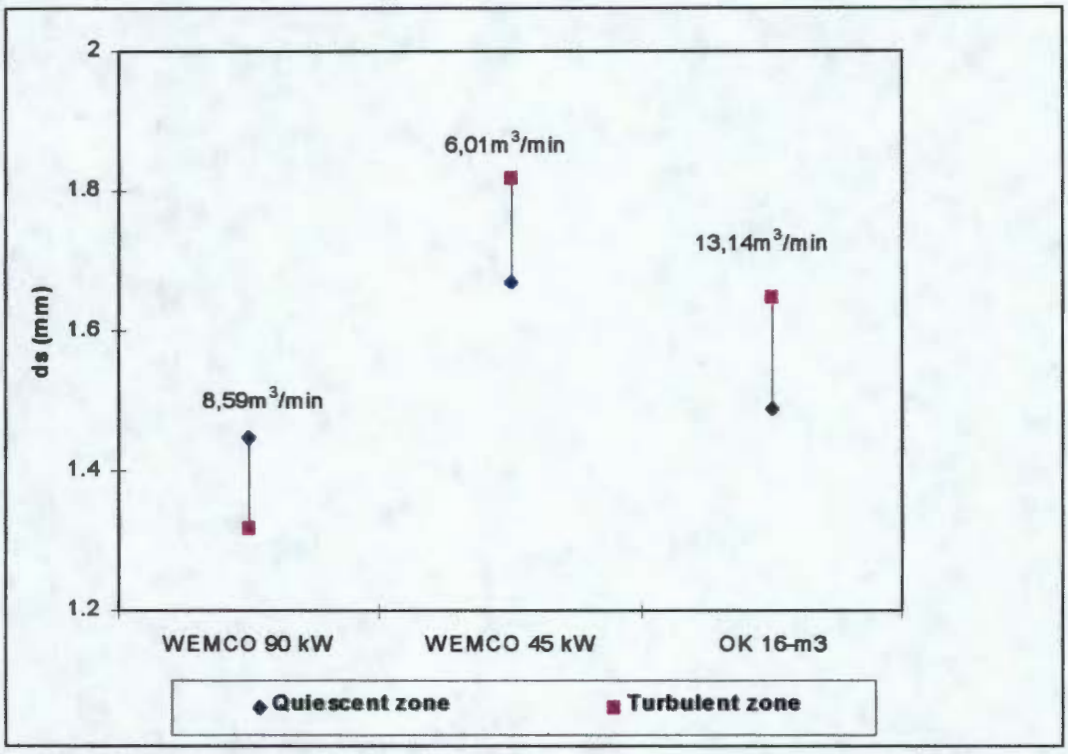

Figure 5.15: Sauter mean bubble diameter (d_S) at different locations in WEMCO 144 standard and high-power and OK 16-m^3 cells.

(a) WEMCO 144 cell (standard and high-power motor)

The effect of location on the Sauter mean bubble sizes in the WEMCO 144 cells is shown in Figure 5.15. It is evident from this figure that the Sauter mean bubble size varies with axial distance from the impeller region in both WEMCO 144 cells. While smaller bubbles were found at the lower locations (4, 5 and 6) close to the impeller region, relatively larger bubbles were observed in the upper locations (1, 2 and 3) away from the impeller. The lower locations lie in the zone where the turbulence intensity, responsible for shearing of air into small bubbles, is very high; hence small bubble sizes are found in this region. The larger bubble sizes found in the upper locations may be attributed mainly to coalescence as the bubbles rise through the pulp to the upper sections of the cell. Similar

observations have been made by Barigou and Greaves (1992) and Gorain, *et al.*, (1995a). Barigou and Greaves have shown that differences exist in bubble sizes with both radial and axial distance from the impeller in a coalescent system. The work by Gorain, *et al.*, showed an increase in bubble size as the surface of the cell was approached.

Another possible reason for this observation is that the high pulp densities typical of flotation cells make the hydrostatic pressure difference between the upper and lower locations quite significant, affecting the respective sizes of the bubbles at these locations (Glembotski, *et al.*, 1963). It is argued that the typical frother concentrations in flotation cells make the effect of bubble coalescence minimal, and the increase in bubble size near the surface of the cell is ascribed to the effect of the decrease in head of pulp.

(b) OK 16-m^3 cell

As is evident from Figure 5.15, the bubble sizes in the impeller region of the OK 16-m^3 cell are smaller than those found in the quiescent region. This observation is similar to the findings in the WEMCO 144 cells and the reasons for this observation are likely to be the same as those given above.

The difference in bubble sizes at the different locations is further illustrated by the bubble size distribution histograms presented in Figure 5.9. It can be seen that near the impeller the distribution is skewed more towards the left, indicating that the proportion of smaller bubbles is large in this location. With increasing axial distance from the impeller, the distribution is shifted to the right, towards the large bubble sizes, probably for the reasons discussed in section 5.2.2.2 above.

5.2.2.6 Effect of power input

Figure 5.16 shows the power-Sauter mean bubble size relationship in the WEMCO 144 cell with a 90 kW motor. The changes in power dissipation were a

result of the changing air flowrate into the cell since there was no facility available on site to vary power to the cells directly. It may be argued that the changes in bubble size could be attributed to the changes in air flowrate but they could equally be attributed to the effect of power on bubble size. On the basis of Figures 5.13 and 5.14, which show different bubble sizes within similar air flow ranges but different power inputs, translated into different impeller speeds, it may be inferred that a variation in power could produce the changes in bubble sizes observed in Figure 5.16. As the air flowrate was increased, the power consumption decreased. This effect of power on bubble size is discussed in more detailed in section 5.4. below. Similar trends were observed in the OK 16-m^3 cell but no trend was seen in the WEMCO 144 standard cell, probably because of the narrow range of air flowrates at which it was operated. The current draw at each air flowrate was noted as described in section 4.5.6 in Chapter 4, from which the power was calculated using equation (61) in Appendix E. The data can be found in Table C15-C18 in Appendix C. It is evident from this figure that power input to the flotation cell has a considerable effect on the sizes of bubbles produced.

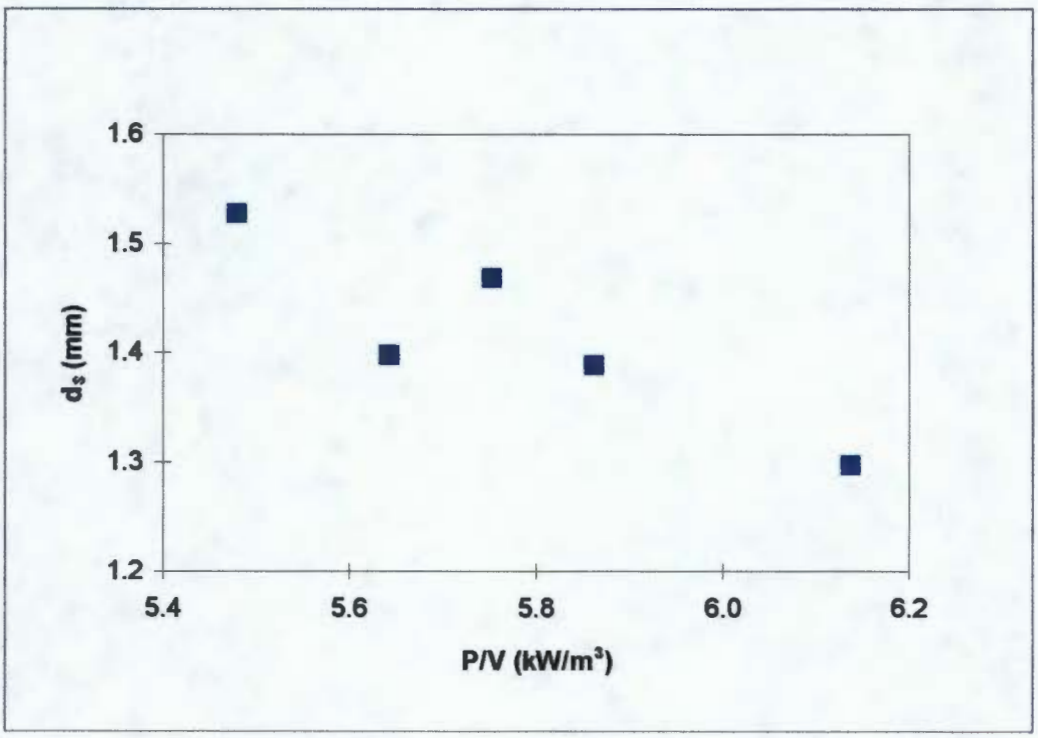

Figure 5.16: Effect of power input (P/V) on Sauter bubble diameter (d_S) in the WEMCO 144 high-power cell.

5.2.2.7 Summary

Bubble size measurements were made in the industrial flotation cells, varying from 16-m^3 to 50-m^3 in size and performing different duties. The bubble size distributions appear to be lognormal, as has been shown by other researchers (Barigou and Greaves, 1992) using different methods of measurements. This corroborates the reliability of the measuring technique of the UCT Bubble Size Analyser used in this work.

The arithmetic bubble diameters measured in the different types, sizes and duties of cells and operating under various conditions were found to lie well within the range 0.5 - 1.3 mm (Sauter mean diameter of 1.1 - 2.6 mm). These results do not differ much from the bubble size measurements of Jameson and Allum (1984) made using a photographic method in industrial flotation cells in base metal concentrators. The arithmetic mean diameters of the bubbles they measured were in the range 0.24-1.57 mm (0.53-1.77 mm for Sauter mean diameters).

From the discussions above, it can be concluded that the key physical factors affecting the sizes of bubbles in a flotation cell under normal operation are the air flowrate and the power input or the impeller rotational speed. Bubble size is known to be one of the crucial factors that influences the performance in flotation cells; thus a correlation for its prediction would be highly valuable. Unfortunately, unlike for column cells, very little success has been achieved in terms of finding a suitable correlation for predicting bubble sizes in mechanical flotation cells, owing to the high turbulence that occurs in them.

5.2.3 Superficial gas velocity

The superficial gas velocities in the flotation cells were measured using the method outlined in section 4.5.2. The measurements are given in Appendix C. Each superficial gas velocity value is the average of two readings per location. The values of the superficial gas velocity were all found to fall between 1.05 cm/s and 2.76 cm/s

for all the different types, sizes and duties of cells and the various conditions of the tests. It is notable that the superficial gas velocity values measured in this work are all within the limits reported by Harris (1976) of 1-3 cm/s for industrial flotation cells. Below is a discussion of the effects of some of the factors affecting the superficial gas velocities in the cells.

5.2.3.1 Effect of air flowrate

The superficial gas velocity is defined as the volumetric flowrate of air through a cell, divided by the cell's cross-sectional area. Air flowrate should therefore have a direct influence on the superficial gas velocity in flotation cells. The extent to which superficial gas velocity (in the OK 16-m^3, the OK 50-m^3 TankCell and the WEMCO 144 cells) varies with air flowrate is shown in Figure 5.17 and discussed in the sections that follow. It is important to note that Figure 5.17 is intended to show only the trend between the superficial gas velocity and air flowrate in the different cells. Data for this graph can be found in Tables C3, C4, C7 and C11.

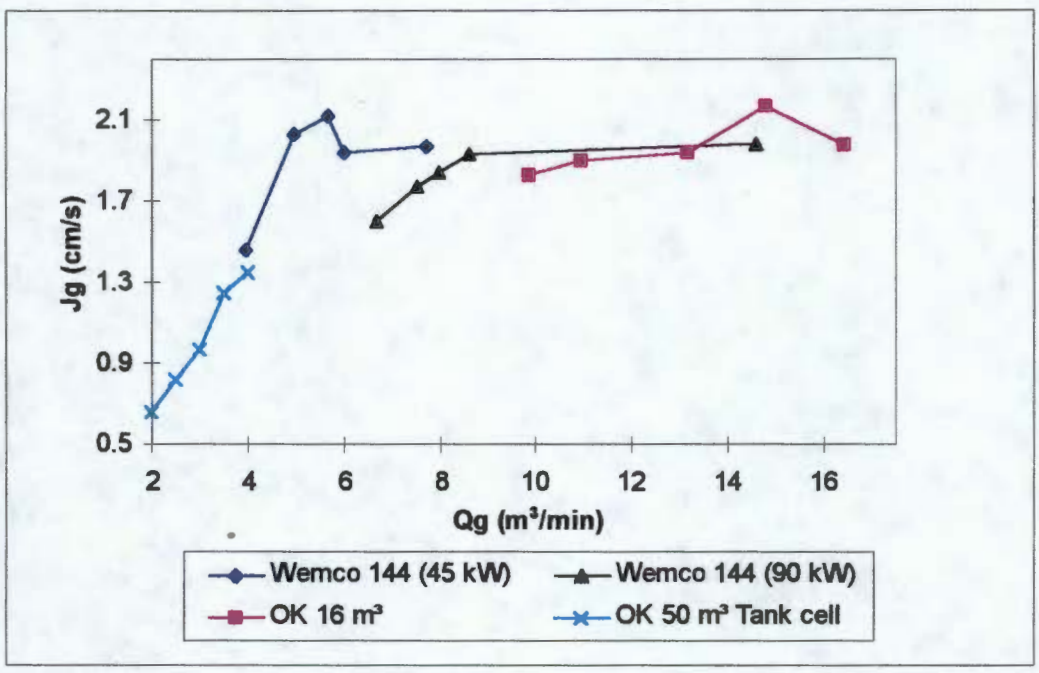

Figure 5 17: Superficial gas velocity (Jg) at different air flowrate (Qg) in OK 16-m^3 and WEMCO 144 standard and high power cells.

(a) WEMCO 144 cells (standard and high-power motor)

It is obvious from Figure 5.17 that the superficial gas velocity increased with increasing air flowrate for each of the cells investigated and that the manner of increase depended very much on the cell characteristics. Thus the graphs of the WEMCO standard and high-power cells show a significant difference by virtue of their differences in impeller speeds and air flowrates. It is quite clear from this figure that at low air flowrate there is a prominent rise in superficial gas velocity in each of the two cells. The increase tends to level off as the air flowrate increases, and with further increase in air flowrates there is a decline in the superficial gas velocity in the WEMCO 144 standard cell. This behaviour suggests that beyond certain air flowrates, the WEMCO 144 cell impeller is no longer capable of dispersing all the air into small bubbles, resulting in some of the air being lost out of the cell as large bubbles around the impeller (flooding). This would result in a decrease in apparent superficial gas velocity in spite of the increase in air flowrate, as there could be a possible starvation at the locations where the measurements were taken in the cell. It is interesting to note the similarities between the superficial gas velocity curves and the Sauter mean bubble diameter curves (see Figure 5.12). The maximum superficial gas velocity and Sauter mean bubble diameter occur at the same air flowrate.

The air flowrate required in the standard WEMCO 144 cell to produce the maximum superficial gas velocity was around 6 m^3/min. There was a slight drop in superficial gas velocity above this air flowrate and the most likely reason for this observation is similar to that discussed for the WEMCO 144 high-power cell, discussed in the next paragraph. Most of these WEMCO 144 standard cells were operated at air rates in excess of 7 m^3/min. It has been a general philosophy in the plants that more air to the cells results in better performance, although "better performance" is not usually clearly defined. From these data, it would be useful to consider controlling the air flowrate to these cells by the provision of control valves or other means, to a flowrate in the region of 6 m^3/min, the value which appears to produce the maximum superficial gas velocity. It must, however, be

emphasised that the maximum air flowrate for optimising superficial gas velocity could be different for even similar cells operating under different conditions because of the effects of physical and chemical variables on gas dispersion (O'Connor, *et al.*, 1990).

In the WEMCO high-power cell, the maximum superficial gas velocity seems to occur at an air flowrate between 9 and 14 m^3/min. There could possibly be a specific air flowrate at which maximum superficial gas velocity was produced in the high-power cell, however this could not be determined in this work because of the constraints encountered in measuring the air flowrate between these limits. It is important that this work be pursued in order to determine the maximum air flowrate required to maximise the superficial gas velocity in the high-power cell.

(b) OK 16-m^3 cell

The OK 16-m^3 conventional cell also seemed to show a maximum superficial gas velocity at about 15 m^3/min of air flowrate. As shown on Figure 5.17, one of the superficial gas velocities measured at an air flow greater than 15 m^3/min in the OK 16-m^3 appeared to show a decline in the trend. This may indicate that a threshold air flowrate of about 15 m^3/min exists for the production of optimum superficial gas velocity, all other parameters being equal.

There is a possibility that the flooding transition in the OK 16-m^3 cell occurs above this air flowrate but due to the presence of froth, it was not possible to make any visual investigations to confirm this suspicion. However, it has been reported elsewhere (Fallenius, 1975) that the best flotation performance for a set of OK 16-m^3 cells at the Hammaslahti Mine occurs at air flowrates of about 15 m^3/min. This correlation is interesting, especially because the determinations were made in two different flotation systems.

Referring again to Figure 5.12, it can be seen that the maximum bubble size was measured at the air flowrate of 15 m^3/min, at which the maximum superficial gas velocity was also found to occur. This air flowrate incidentally falls within the

manufacturer's suggested design range of 15-25 m^3/min (Fallenius, 1975), but just barely.

(c) OK 50-m^3 TankCell

Unlike the other cells, the OK 50-m^3 TankCells showed a consistent increase in superficial gas velocity as the air flow was increased from 2-4 m^3/min. This suggests that in this aeration range the impeller was capable of effectively dispersing the air supplied to the cell and that very little if any air left the cell undispersed because of flooding. The lower superficial gas velocities (0.6-1.35 cm/s) measured in them were attributed to the low aeration rates at which they were operated. As shown in Figure 5.18, there was a significant difference in superficial gas velocity between the "Multi-mix" and "Free-flow" impellers as the air flowrate increased.

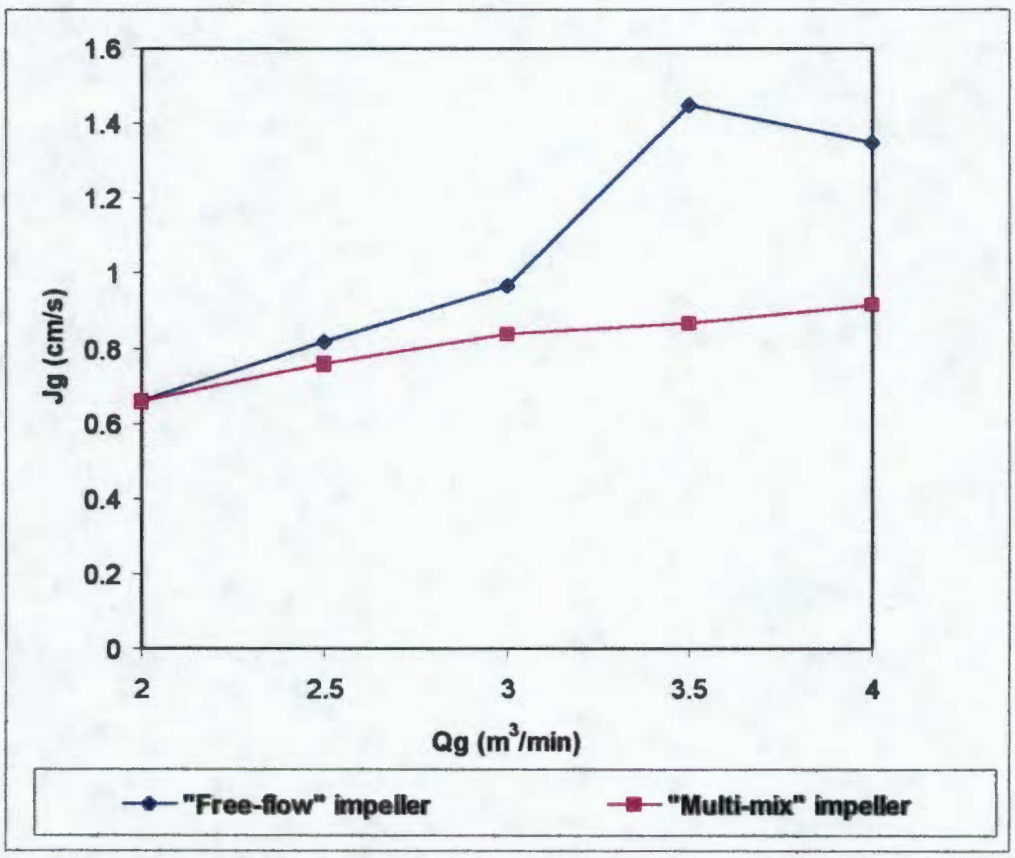

Figure 5.18: Superficial gas velocity (Jg) at different air flowrates (Qg) in the OK 50-m^3 TankCells.

5.2.3.2 Effect of impeller speed

Impeller speed has been shown to have a significant effect on gas dispersion in flotation cells (Gorain, *et al.*, 1995a,b; 1996). The values of superficial gas velocity were compared for the two OK 50-m^3 TankCells in which chemical conditions in the cells remained the same. The only variables were the impeller speed, the impeller type and the air flowrate. A similar comparison was made in the WEMCO 144 standard and high-power cells, in which the difference in motor size provided two impeller speeds for the test.

(a) OK 50-m^3 TankCells

The effect of impeller speed on the superficial gas velocity was studied for the two OK 50-m^3 TankCells, which were operated under similar conditions except for the difference in their impeller speeds, impeller types and air flowrates. The data in Figure 5.19 indicate that the "Multi-mix" impeller rotating at 131 rpm produced a lower superficial gas velocity than the "Free-flow" impeller rotating at 105 rpm.

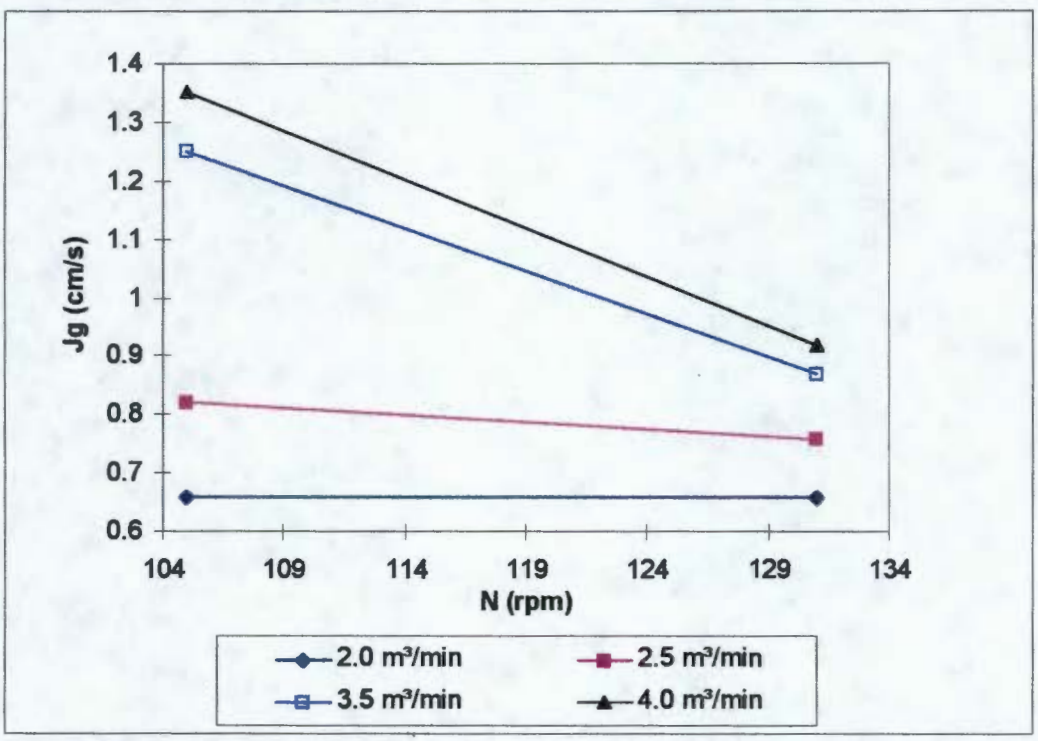

Figure 5.19: Superficial gas velocity (Jg) at different impeller speeds (N) in OK 50-m^3 TankCells (105 rpm = "Free-flow" impeller, 131 rpm = "Multi-mix" impeller).

In principle, varying impeller speed at constant air flowrate should have no effect on the superficial gas velocity, because the smaller bubble sizes produced by the higher impeller speeds should be balanced by the high gas holdup. Any observed change in the superficial gas velocity with changing impeller speed is an indication of the changes in the cell's hydrodynamics, which in turn determine the efficiency of air dispersion in the cell.

Though only two impeller speeds were studied, there was a significant difference in the superficial gas velocity between the two OK 50-m^3 TankCells at the two, higher air flowrates. The differences in the superficial gas velocities in the two cells might be due to the differences in the flow patterns generated in them. The cell with the higher impeller speed had relatively smaller bubbles and a higher pulp circulating velocity, making it likely that a large percentage of the bubbles were trapped in the circulation loop. This would cause a depletion of bubbles in the bulk of the cell and therefore lower measured values of superficial gas velocity. This may explain why the superficial gas velocities measured in the higher-impeller-speed, "Multi-mix" cell were lower than in the lower-impeller-speed, "Free-flow" impeller cell, even though the same amount of air was supplied to each. At the normal operating air flowrate of around 3.5 m^3/min, there was as much as 40 % difference in superficial gas velocity between the two cells (see Table C11 in Appendix C) under similar operating conditions.

(b) WEMCO 144 cells (standard and high-power motor)

It can be seen from Figure 5.20 that, within a similar range of air flowrates, the WEMCO 144 high-power cell had lower superficial gas velocities than the standard cell. Figure 5.20 was plotted from Tables C3 and C4 using the average superficial gas velocity in the quiescent and turbulent zones in the cell within the indicated air flowrates. The differences in the superficial gas velocities in the two cells may be attributed to the differences in the flow patterns generated at the different impeller rotational speeds.

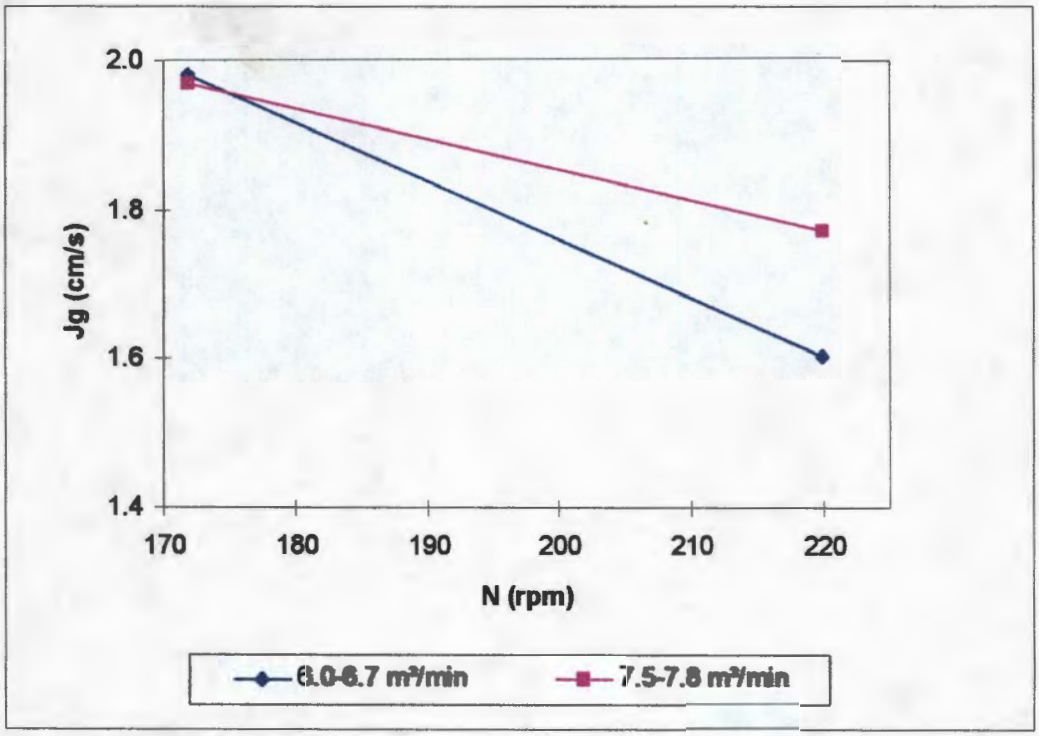

Figure 5.20: Superficial gas velocity (Jg) at different impeller speeds (N) in WEMCO 144 cells.

5.2.3.3 Effect of location

Location in the cell is known to significantly affect the superficial gas velocity measurement. The effect in the OK 16-m^3 and the WEMCO 144 standard and high-power cells is shown in Figure 5.21, and described below.

(a) WEMCO 144 cell (standard and high-power motor)

As is evident from Figure 5.21, there are considerable differences in the superficial gas velocities between the impeller and the quiescent zones. However, the extent to which they differ varies from cell to cell and even within the same cell depending on the conditions that prevail. Thus, while the superficial gas velocity in the WEMCO high-power cell was much lower in the impeller than in the quiescent zones, there was little difference in superficial gas velocity within the standard cell. Figure 5.21 was plotted from Tables C3, C4 and C7, and the

points represent the average superficial gas velocities in the quiescent and turbulent zones at the air flowrates shown.

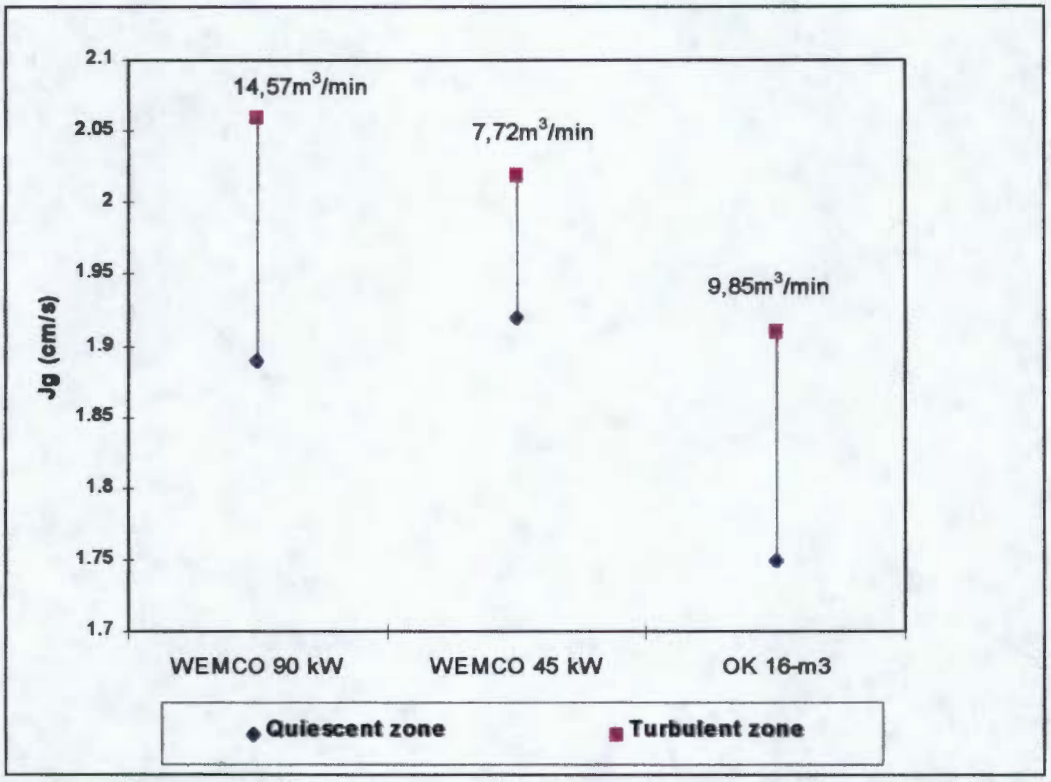

Figure 5.21: Superficial gas velocity (Jg) at different location in WEMCO 144 and OK 16-m^3 cells.

The probable reason for these differences is that the high air rate in the high-power cell (6-15 m^3/min), produces a greater probability of bubble coalescence than in the standard cell (see section 2.3.8 above). As a result of coalescence, the larger bubbles in the upper sections of the cell would acquire high rise velocities and thus influence the superficial gas velocity in there.

Alternatively, the differences in the superficial gas velocity in the high-power cell could be the result of the greater circulation velocity of the pulp in the impeller zone, due to the higher impeller speed. Different superficial gas velocities were measured at different points along the radius in the impeller zone. The measurements shown for this zone therefore may not reflect the true average or the "ideal", superficial gas velocity (defined in Gorain, *et al.*, 1996) in the cell. The superficial gas velocity may thus be lower in the impeller zone due to

circulation and higher in the quiescent zone where recirculation is virtually absent and the flow regime approaches plug flow. It is likely that the circulation in the standard cell is less intense than in the high-power cell. Thus, the differences in superficial gas velocity between zones would be less noticeable in the standard cell.

(b) OK 16-m^3 cell

Figure 5.21 also shows the superficial gas velocities measured in the OK 16-m^3 cell at different locations. A general trend of greater superficial gas velocity in the upper sections of the cell can be deduced from the figure. The reason for this observation is very likely to be the same as that of the WEMCO high-power cell discussed above. A similar observation has been made by Gorain, *et al.*, (1996).

5.2.3.5 Summary

From the discussions above, it can be inferred that the superficial gas velocity in industrial flotation cells has a strong dependence on the air flowrate and the impeller speed, both of which reflect the power dissipation in the cell. The superficial gas velocity was also influenced by the location in the cell, this effect being very sensitive to the prevailing internal conditions.

In each of the cells that showed a maximum in superficial gas velocity with air flowrate, it was observed that this maximum coincided with the maximum Sauter mean bubble size measured in the cell.

5.2.4 Bubble surface area flux

The general behaviour of the bubble surface area flux in the cells was found to be very similar to that of the superficial gas velocity and the bubble size distribution (which together directly determine bubble surface area flux). The bubble surface area flux was calculated as the ratio of the superficial gas velocity and Sauter mean bubble

size, using equation (37) in Section 3.4. Calculated values of the bubble surface area flux for the cells studied are given in Table C1-C18 in Appendix C. Bubble surface area flux was found to vary significantly with air flowrate, impeller power, impeller speed, location in the cell and type of cell. The specific factors that affect the bubble surface area flux in the different types of cells are discussed in the sections that follow.

5.2.4.1 Effect of air flowrate

Figure 5.22 shows the bubble surface area flux versus air flowrate relationship for the WEMCO standard and high-power cells and the OK 16-m^3 cell. The values of the bubble surface area flux from this figure, as in the case of the bubble size and the superficial gas velocity, are the averages of the measurements made at the six, standard locations at each air flowrate.

(a) WEMCO 144 cells (standard and high-power motor)

Figure 5.22 shows a slight increase in bubble surface area flux from lowest to highest with air flowrate. However, the variation at points between the high and low values is considerable, making any generalisation regarding trends impossible. The graphs of the bubble surface area flux are similar in some cases to the graphs of Sauter bubble diameter and superficial gas velocity at similar conditions in the same cell (see Figures 5.12 and 5.17). This is not surprising, as the bubble surface area flux is proportional to the ratio of superficial gas velocity and Sauter mean diameter.

In the WEMCO 144 standard cell, it was found that the optimal bubble surface area flux of 71 m^2/m^2sec occurred at an air flowrate of about 5 m^3/min. This suggests that with chemical and other operational conditions being equal, the air flowrate required for the WEMCO 144 cell to maximise the production of the bubble surface area flux is around 5 m^3/min. A similar trend was found in the case of the WEMCO high-power cell. The maximum bubble surface area flux of 83

m^2/m^2sec was found at the air flowrate of around 8 m^3/min. The bubble surface area flux in the high-power cell showed a decrease when air flowrate increased from 8 to 15 m^3/min. Between these values, there may be a maximum in bubble surface area flux as a function of air flowrate for the high power motor. Unfortunately, no experimental data points were obtained between the air flowrates of 8 and 15 m^3/min, as has been mentioned previously under section 5.2.3.1. Thus the existence of this maximum cannot be proven.

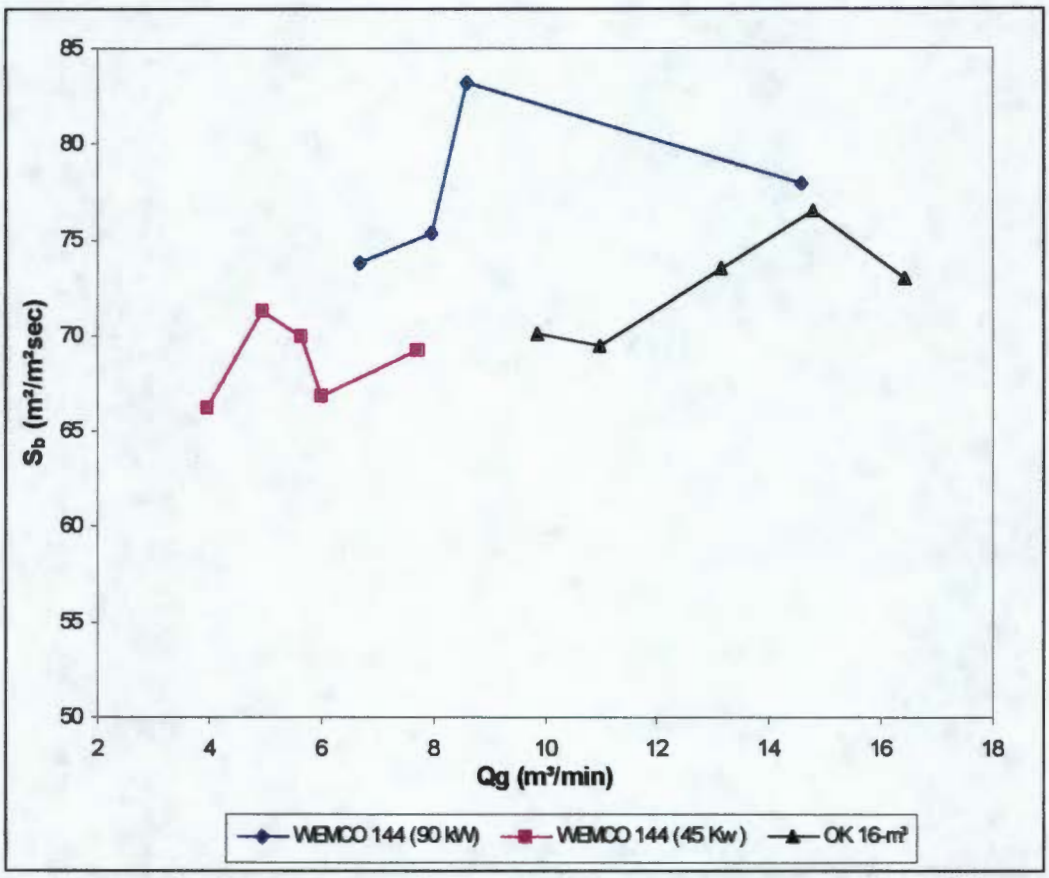

Figure 5.22: Bubble surface area flux (S_b) at different air flowrates (Qg) for the WEMCO 144 and OK 16-m^3 cells.

(b) OK 16-m^3 cell

In the OK 16-m^3 cell, the data are similar to those in the WEMCO 144 cells. The S_b at the highest air flowrate is higher than that at the lowest air flowrate, but the maximum S_b occurs at an intermediate air flowrate value. Whether this maximum is true, optimised value cannot be shown from these data. It can thus be suggested

that within similar experimental conditions, the air flowrate required to optimise the generation of bubble surface area flux is in the region of 15 m^3/min.

It should be noted that a few of the OK 16-m^3 cells were being operated at air flowrates in excess of 17 m^3/min, which was beyond the detection limit of the device used for measuring the air flowrates to the cells. This means that there was no independent corroboration of the air flow measurements, but does not in any way affect the results as the S_b was calculated from the Jg and d_b measurements made in the pulp.

(c) OK 50-m^3 TankCells

In the OK 50-m^3 TankCells, the change in bubble surface area flux with air flowrate varied with the type of mechanism used. The behaviour of bubble surface area flux in the "Free-flow" impeller cell was similar to that of the cells mentioned above, going through an apparent, local maximum at around 3.5 m^3/min air flowrate (Figure 5.23). In the "Multi-mix" impeller system, however, practically no change was observed in the bubble surface area flux with air flowrate. This phenomenon is discussed further in the next section when the effect of impeller speed is considered.

5.2.4.2 Effect of impeller speed

(a) OK 50-m^3 TankCells

In the OK 50-m^3 TankCells it was observed that the different impeller speeds of the "Multi-mix" and "Free-flow" impellers generated significantly different values of bubble surface area flux. The "Multi-mix" impeller, turning at 131 rpm, produced a smaller bubble surface area flux than the "Free-flow" turning at 105 rpm. The difference in impeller speeds in the two mechanisms is due to their different motor sizes. At the manufacturer's recommended air flowrate of 3.5 m^3/min, the "Free-flow" impeller produced a bubble surface area flux value nearly

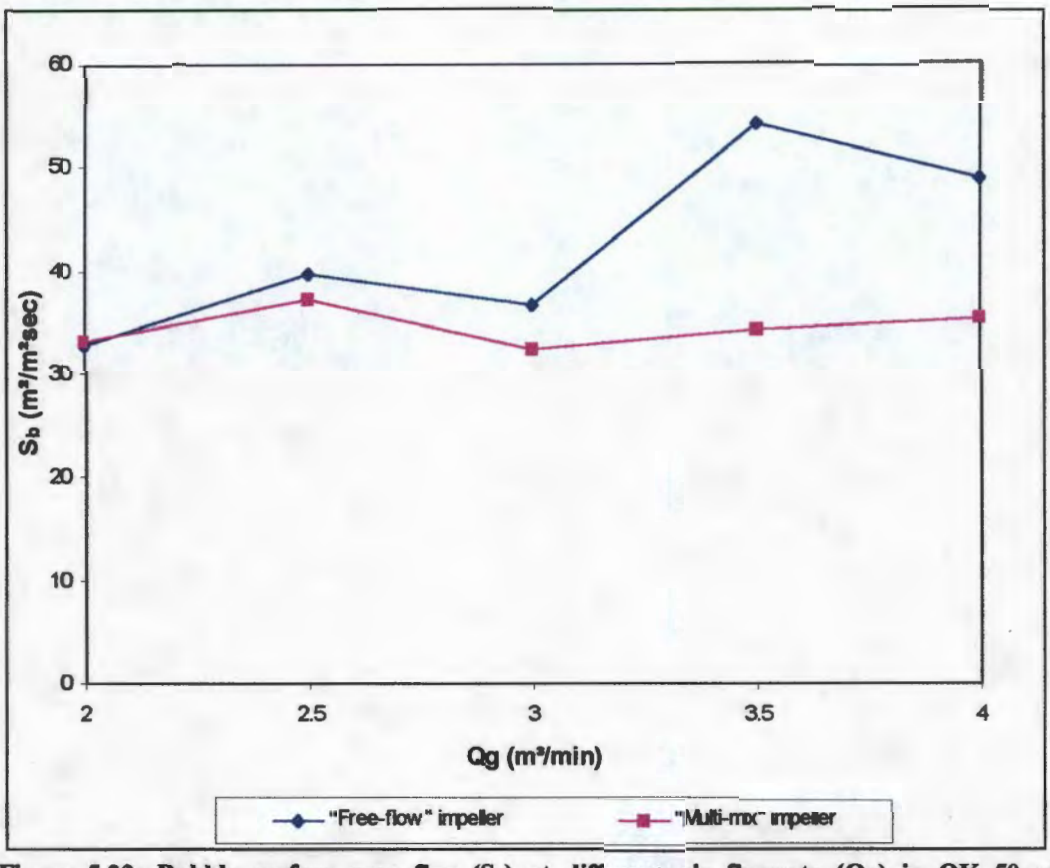

Figure 5.23: Bubble surface area flux (S_b) at different air flowrate (Qg) in OK 50-m^3 TankCells.

20 m^2/m^2sec greater than that produced by the "Multi-mix" impeller at the same air flowrate. It would be expected that, since the "Multi-mix" mechanism has a higher power input, the bubble surface area flux would be greater at the same air flowrate than in the "Free-flow" mechanism cell. On the contrary, the reverse was observed. The most likely reason for this observation is that, since there is a strong pulp recirculation with the "Multi-mix" stator, more bubbles are spread sideways and downwards in the cell, resulting in a low superficial gas velocity measurement at the single location measured (Figure 5.18). Hence bubble surface area flux will probably be lower than in the "Free-flow" mechanism cell.

(b) WEMCO 144 cell (standard and high-power motor)

The effect of impeller speed on bubble surface area flux was also considered for the WEMCO 144 cell at the two speeds provided by the 45 kW and 90 kW

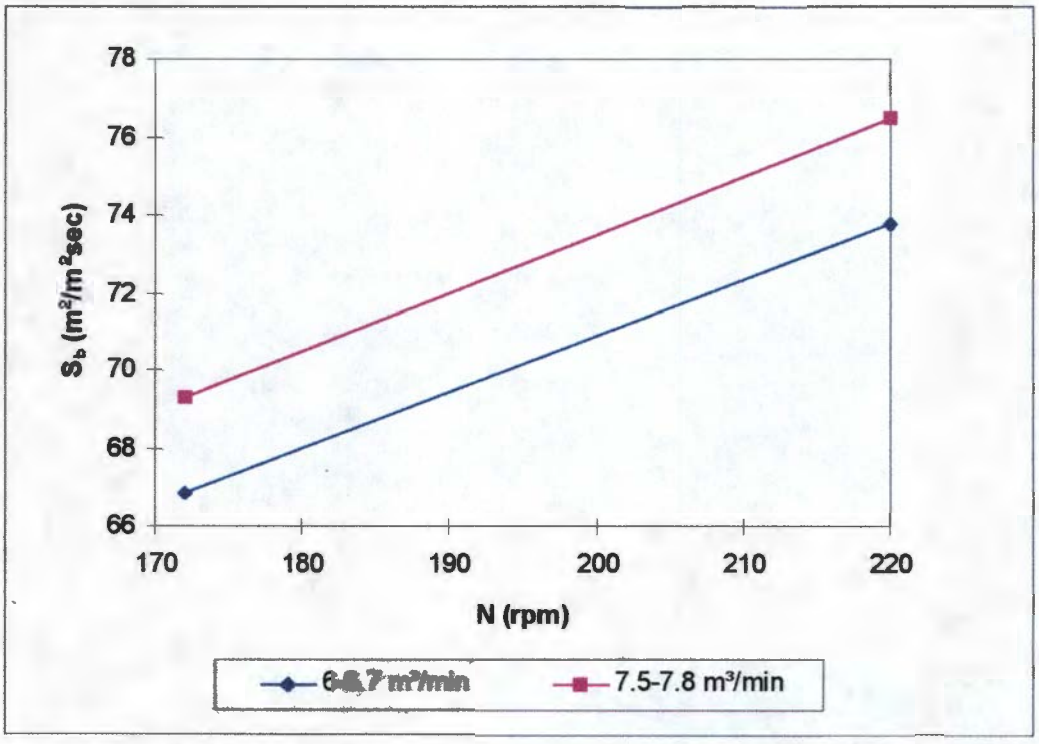

Figure 5.24: Bubble surface area flux (S_b) at different impeller speeds (N) in WEMCO 144 cells.

motors. In the case of the WEMCO 144 cells, the bubble surface area flux was based on the average of measurements of bubble sizes and superficial gas velocities at six different locations in the cell. Figure 5.24 below shows a significant difference in bubble surface area flux produced by the high-power cell rotating at 220 rpm, compared with the standard cell rotating at 172 rpm, within a similar range of aeration rate (6-8 m3/min). The greater bubble surface area flux in the higher power cell may be attributed to the smaller sizes of bubbles it produced. Once again, the lines in Figure 5.24 are intended only to show a trend and not linearity in the in bubble surface area flux/impeller speed relationship.

5.2.4.3 Effect of Location

(a) WEMCO 144 cell (standard and high-power motor)

The variation of bubble surface area flux with location in the flotation cells follows from the considerations already given for the Sauter bubble diameter and

in the quiescent and turbulent zones were more noticeable in smaller cells than in the larger ones.

Bubble size increased with air flowrate and decreased with impeller speed. The size of bubbles produced in flotation cells was inversely related to the power consumption. In the impeller zone bubble sizes were generally smaller than in the quiescent zone.

The superficial gas velocity increased with air flowrate and impeller speed and was affected considerably by location in the cell. Differences in measured superficial gas velocity at the same air flowrate but different impeller speeds arise probably on account of differences in flow patterns in the cells under these conditions.

The bubble surface area flux increased with air flowrate within the limit at which the impeller can effectively disperse the air. In all the cells measured there appeared to be a maximum bubble surface area flux with air flowrate beyond which it decreased. Bubble surface area flux was also affected by the speed of the impeller and the location in the cell.

5.3 GAS DISPERSION – COMPARISIONS AMONG FLOTATION CELLS

The main focus of this section is on differences in gas dispersion among the different types of cells investigated. It entails discussions on how gas dispersion varies between cells of different types and sizes in the same circuits and between cells of different sizes and duties. The latter comparisons bring into play the effects of reagent suite, particle size and solids concentration on gas dispersion. The individual effects of gas holdup, bubble size distribution and superficial gas velocity are discussed in the sections that follow, together with their overall effect on bubble surface area flux in these cells. The detailed results may be found in Tables C9 and C10 in Appendix C.

The extent of errors associated with the individual measurements of gas holdup, bubble size and superficial gas velocity and bubble surface area flux has been shown with error bars on some of the graphs.

the superficial gas velocity at similar locations (sections 5.2.2.5 and 5.2.3.3). In the WEMCO 144 high power cell a distinct profile of lower bubble surface area flux was observed in the impeller region and higher in the quiescent region at low air flowrates. However, as the air flowrate increased, the distinction disappeared and the bubble surface area flux in both sections of the cell approached the same value. It is not surprising to see this trend in bubble surface area flux because the Sauter bubble diameter and the superficial gas velocity, the major characteristic parameters that determine bubble surface area flux, showed similar trends.

In the impeller region, the measured superficial gas velocity was lower than in the quiescent region, on account of strong pulp recirculation (as with the "Multi-mix" impeller in the TankCell, discussed in the previous section). This would explain the lower calculated value of bubble surface area flux obtained. In the quiescent zone, the superficial gas velocity was greater owing to the absence of the recirculation effect, and so a greater bubble surface area flux was obtained than in the turbulent region. As the air flowrate increased, air would begin to escape from the recirculation loop until the distinction between the two zones disappear.

In the case of the WEMCO 144 standard power cell, there was essentially no difference observed at the different sections of the cell at the different air flow rates as the intensity of circulation is perceived to be milder that in the high power cell.

(b) OK 16-m3 cell

In the OK 16-m3 cell, there was no discernible trend in the values of the bubble surface area flux at the various locations within the limit of the air flowrate. As there were only marginal changes in bubble size and the superficial gas velocity, the bubble surface area flux would be expected to show very little variation. At low air flowrates, very close values of bubble surface area flux were found at the six locations in the cell. This suggests that at low air flowrates, with good gas

dispersion, the bubble surface area flux can be said to be uniform throughout the cell.

5.2.4.4 Summary

It can be generalised from the above discussion that the bubble surface area flux in flotation cells is determined by the air flowrate, impeller speed and to a lesser extent the location in the cell. Within the air dispersion capability of a specific impeller, more air will result in higher bubble surface area flux. Higher impeller speed can result in production of smaller bubbles and hence greater bubble surface area flux, but the regime of agitation is of paramount importance. Greater bubble surface area flux will be realised at increased impeller speeds as long as the flow pattern in the cell is not drastically altered. It was found that the "Multi-mix" impeller TankCell, although consuming more power, produced less bubble surface area flux than the "Free-flow" impeller. However, this difference is probably due to the unreliability of the measurement at only one location in the OK 50-m3 TankCells as a result of the flow patterns in relation to the points of measurement. This suggests that in future work the number and location of measurements will have to be considered more carefully and in the light of the flows in the cell.

5.2.5 Overall summary

Gas dispersion characteristics in individual flotation cells have been discussed in the preceding sections. The gas phase properties of air holdup, bubble sizes and superficial gas velocity and bubble surface area flux were used in characterisng these cells. The results of the measurements made have been analysed in terms of factors that affect these cell characteristics such as air flowrate, impeller speed and location in the cell.

Air holdup showed very little response to air flowrate and impeller speed in the cells that were operated under their normal operating conditions. Differences in air holdup

5.3.1 Air holdup

5.3.1.1 Air holdup along the bank

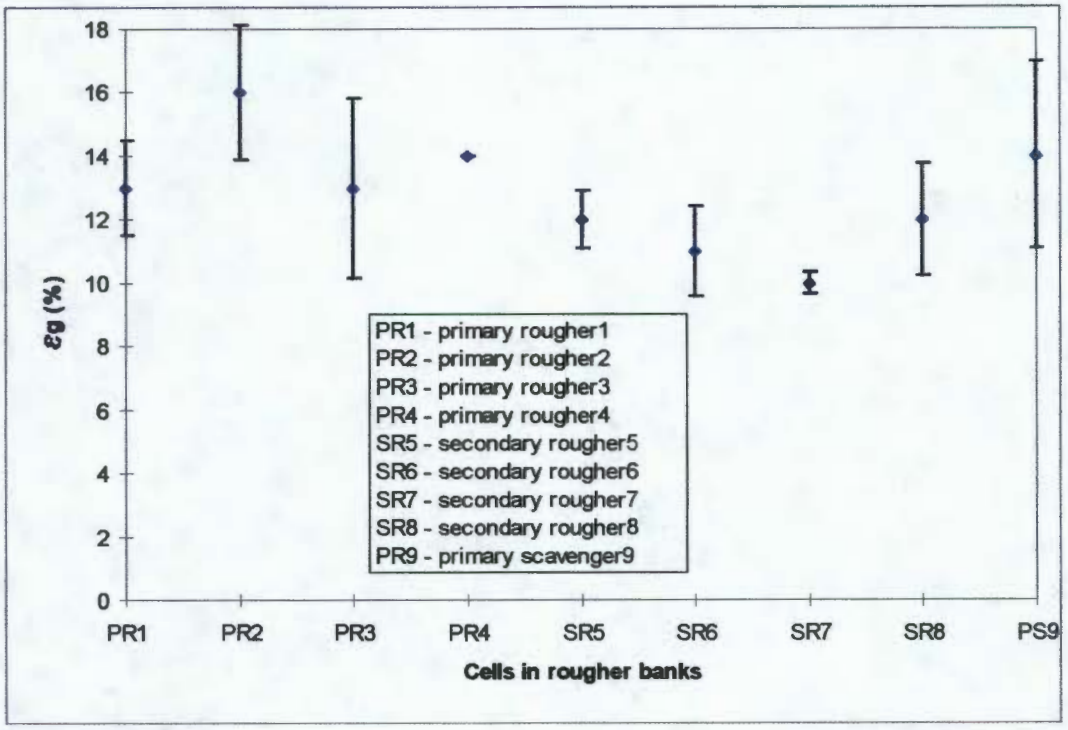

Figure 5.25: Air Holdup ((g) profile along a bank of WEMCO 144 rougher cells.

Figure 5.25 depicts the air holdup profile in a section of nine rougher cells on one of the plants where the tests were done. Each point represents the average of all the data for that particular cell, obtained from Tables C1 and C2. The error bar indicates the standard deviations of the measurement at each point. In the bank of WEMCO 144 cells, there was no obvious trend in holdup moving from cell to cell along the bank. The air holdup observed in all nine cells was between 10 and 16 %, even though they were operated at different air flowrates. It was however observed that slightly greater air holdup corresponded to increased air flowrates; thus the greatest air holdup of 16 % occurred in the cell PR2, with air flowrate of 8.67 m3/min, while the lowest holdup occurred in cells SR6 and SR7 with air flowrates of 5.6 m3/min.

5.3.1.2 Air holdup in different types, sizes and duties of cells

The air holdup in different types and sizes of cells was also compared and plotted from Table C18. As shown in Figure 5.26, the air holdup was not found to depend on either the size or the type of the cell or on the duty it performed. The only factor that appeared to influence the air holdup was the air flowrate per unit volumn of the cell. As in figure 5.25, the greatest holdup value corresponded to the cell with the highest air flowrate per unit volume.

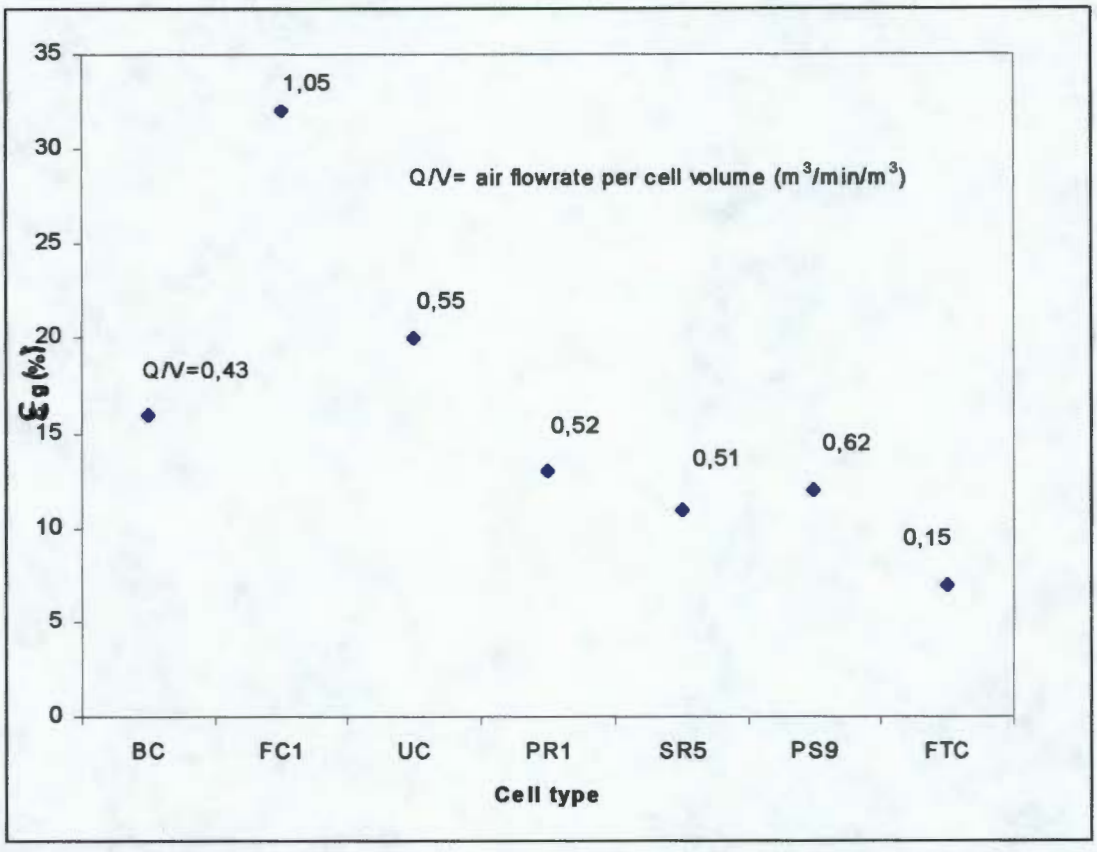

Figure 5.26: Air holdup (εg) profile in different types, sizes and duties of flotation cells.

The largest air holdup of 32% was measured in the WEMCO 120 final cleaner cell with an air flowrate of 1.05 m^3/min per unit volume of pulp. The lowest air holdup was measured in the OK 50-m^3 TankCell with an extremely low air flowrate of about 0.15 m^3/min per unit volume of pulp. Between these extreme holdup values are the intermediate holdup and air flowrate values in the 3-m^3 Bateman cell, used as final cleaner in the TankCell circuit, and the WEMCO 144 (PR, SR, SC) and WEMCO 144 unit cells used for roughing and cleaning duties respectively.

It was observed that in the large cells, usually used for roughing duties, there was virtually no difference in air holdup between the impeller zone and the quiescent zone of the cells. In a number of the cells, the holdup varied erratically with air flowrate. However, it was observed that in the smaller cells, usually used as cleaners and recleaners, the holdup was smaller in the impeller region and greater in the upper sections of the cell. This is, however, not a universal trend as it is not consistent with earlier findings in this work. Further, in the work of Gorain, *et al.*, (1995b), which used a 2.8-m^3 cell with controlled air flowrates, the air holdup profile observed was high in the impeller region and lower in the quiescent region of the cell.

It would appear that the critical factor that determines air holdup in flotation cells is neither the size nor the type of cell, but the air flowrate per unit volume of cell space. It was noted that the difference in holdup between the two regions was a function of the air flowrate per unit volume of the cell: The larger the air flowrate at a given impeller speed, the greater the difference in the holdup between the upper and lower sections of the cell. In the smaller cells, relatively larger bubbles are formed as a result of the greater air flowrate per unit volume of cell compared to the larger rougher cells. While these large bubbles possess high rise velocities in the impeller region, their velocities are considerably reduced as they approach the surface of the cell, by limitations in bubble rise velocities due to particle loading and slow froth removal in the upper sections of these cells. This may explain the low air holdup in the impeller region and the high holdup in the quiescent zone observed in the WEMCO 120 cells.

Extremely large differences in holdup were observed between the turbulent and quiescent zones of the WEMCO 120 cleaner cells: Air holdup, as low as 5 %, was measured in the turbulent zone, while in the quiescent zone a value of 32 % was recorded under the same conditions.

It was also noted that in the cells with air flowrate greater than 1.0 m^3/min per unit volume, there was a significant difference in the holdup profiles, with greater

holdups in the upper sections of the cell. For example, some of the WEMCO 120 cells, which are used for cleaning duty, showed an exceptionally high holdup of 37% in the quiescent zone, compared with 27% in the impeller zone at an air flowrate of 1.18 m^3/min per unit cell volume.

In the 4.25-m^3 WEMCO 84 cell, a similar phenomenon was observed: In some cases, at air flowrates greater than 1.0 m^3/min per unit volume, holdup values of 5% were measured in the impeller region compared to 26% holdup measured in the quiescent zone. In the 3-m^3 Bateman cell, the holdup profile observed did not follow the same trend as in the other cleaner cells: the holdup in the two zones was more or less the same. This was attributed to the smaller air flowrate of 0.45 m^3/min per unit volume.

In the WEMCO 164 rougher cell, the air holdup was found to be insensitive to the location in the cell. Similar observations were made under the discussions of single cells in section 5.2.1.3.

The large differences in air holdup observed in the cleaner cells are possibly due to the fact that with the relatively higher air flowrate to these cells, more air is admitted into the cell than can effectively be dispersed by the impeller. A large proportion of this air leaves the impeller region undispersed, in the form of large bubbles with high rise velocities. This accounts for the lower holdup measurements recorded in the lower regions of the cell, as well as for the extremely high holdups found in the upper regions, where the combined effects of bubble loading and bubble crowding may considerably retard the rise velocities of the bubbles.

5.3.2 Bubble size

5.3.2.1 Bubble sizes along the bank

Figure 5.27 shows the Sauter mean bubble diameter measured along a bank of nine 16-m^3 WEMCO 144 rougher cells. Each point represents the average of all the data for that particular cell, obtained from Tables C1 and C2. The error bars indicate the standard deviations of the Sauter mean bubble diameter at each point. It appears that bubble size is independent of the cell position in the bank, as there is no systematic increase or decrease in bubble size down the bank. This suggests that although frother and solids concentration may decrease down the bank, the effect is not so drastic as to affect bubble size. The slight difference in bubble size between the cells is more likely due to the differences in air flowrate.

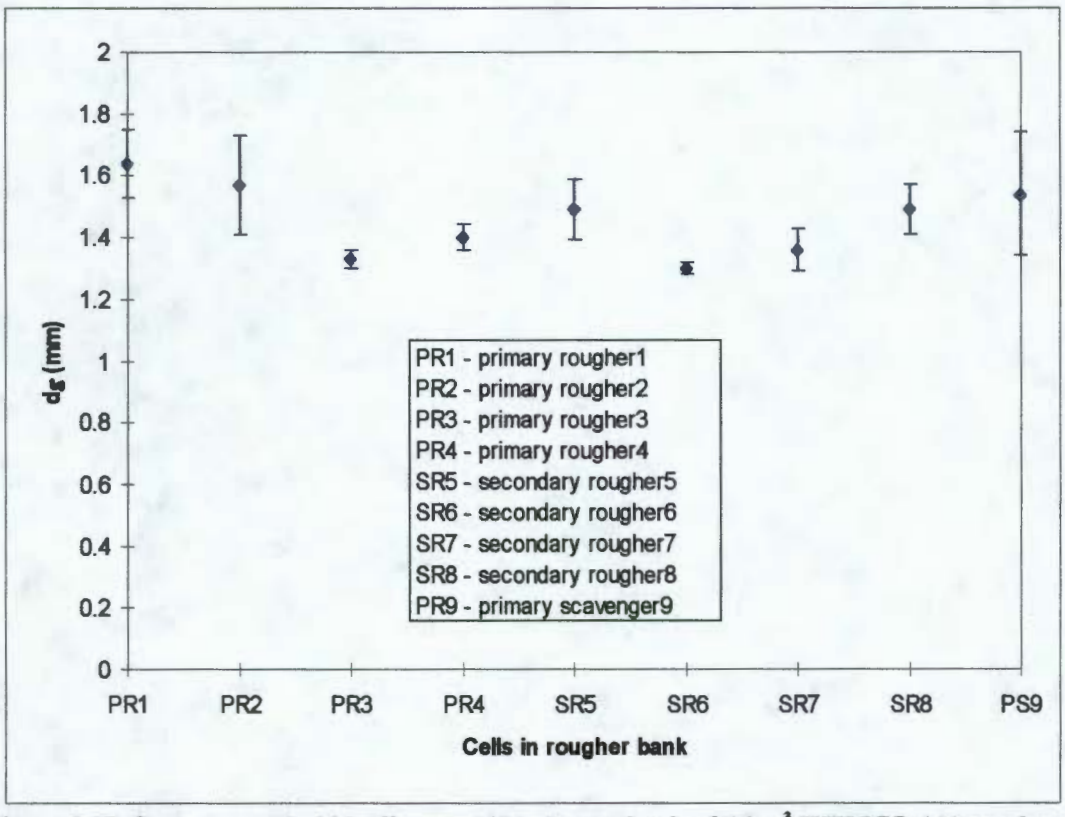

Figure 5.27: Sauter mean bubble diameter (d_S) along a bank of 16-m^3 WEMCO 144 rougher cells.

5.3.2.2 Bubble sizes in different types, sizes and duties of cells

Most of the cells measured in the course of this work belonged to the WEMCO type but a few cells of other types, such as Outokumpu and Bateman, were also studied. Figure 5.28 was plotted from the averages of the bubble sizes in each cell, as listed in Table C18. It shows that the different types and sizes of cells, operating in different circuits from roughers to recleaners, produced similar sizes of bubbles. This is true even with the wide variation in air flowrates existing in the cells but not shown in Figure 5.28. However, it appears that the bubble sizes were slightly larger in the smaller cells, usually used for cleaning, than in the larger cells. This is probably due to the relatively higher, superficial gas velocities in these smaller cells. Bubble size was shown to relate directly to the superficial gas velocity in section 5.4. This is further confirmed in WEMCO 120, WEMCO 84 and Bateman BQ30 cells, in which the range of bubble sizes measured (1.5-2.2 mm) was found to be considerably larger than in the larger cells used as roughers.

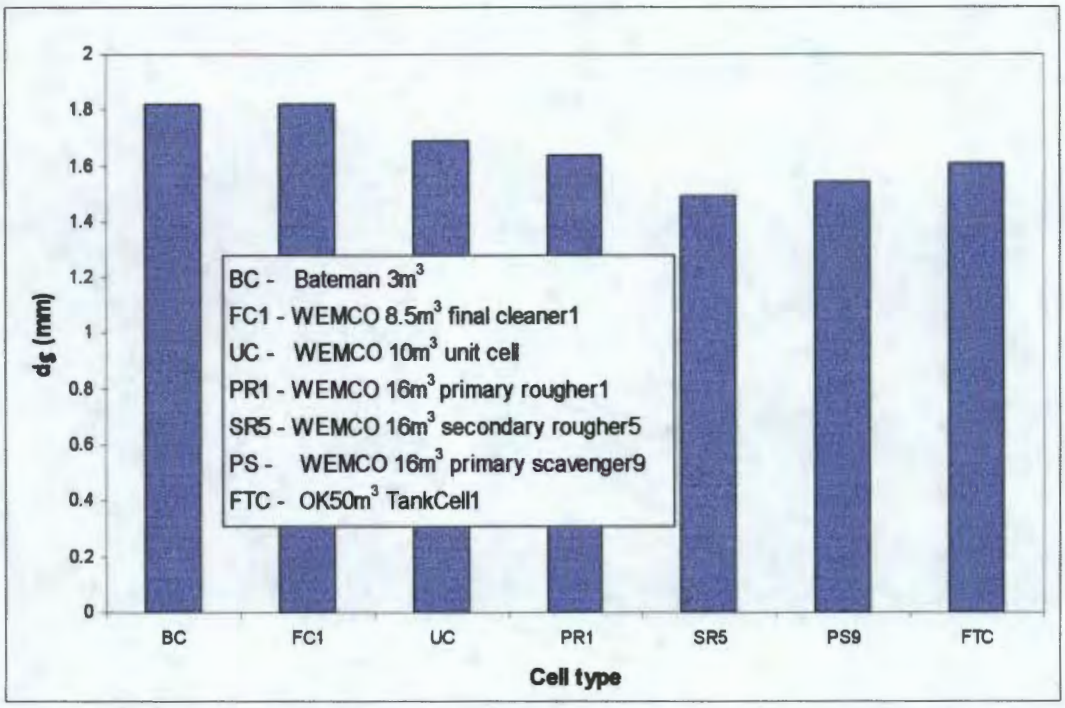

Figure 5.28: Sauter mean bubble diameter (d_S) in different types, sizes and duties of flotation cells.

5.3.2.3 Effect of oversize mechanism on bubble size

In some of the tests the mechanism in the 16-m^3 WEMCO 144 cell was replaced with a 164 mechanism. The 164 mechanism has a bigger impeller and requires a higher power input than the 144 mechanism (see Table 4.3 in Chapter 4). Figure 5.29 shows the Sauter mean diameters of bubbles in the cell with the standard 144 mechanism and a 164 mechanism retrofitted into the same cell. With equivalent power dissipation, the oversize mechanism was found to produce smaller bubbles than the standard, 144 mechanism. It is difficult to generalise this observation since similar measurements carried out in a 144 standard cell with a 164 mechanism earlier in the test programme showed very little difference in bubble size between the two mechanisms (Table C1-C2 in Appendix C). The differences in bubble size observed in (Figure 5.29) are likely to be due to the change in ore type or reagent suite, or possibly to poor functioning of the other 164 mechanisms due to wear.

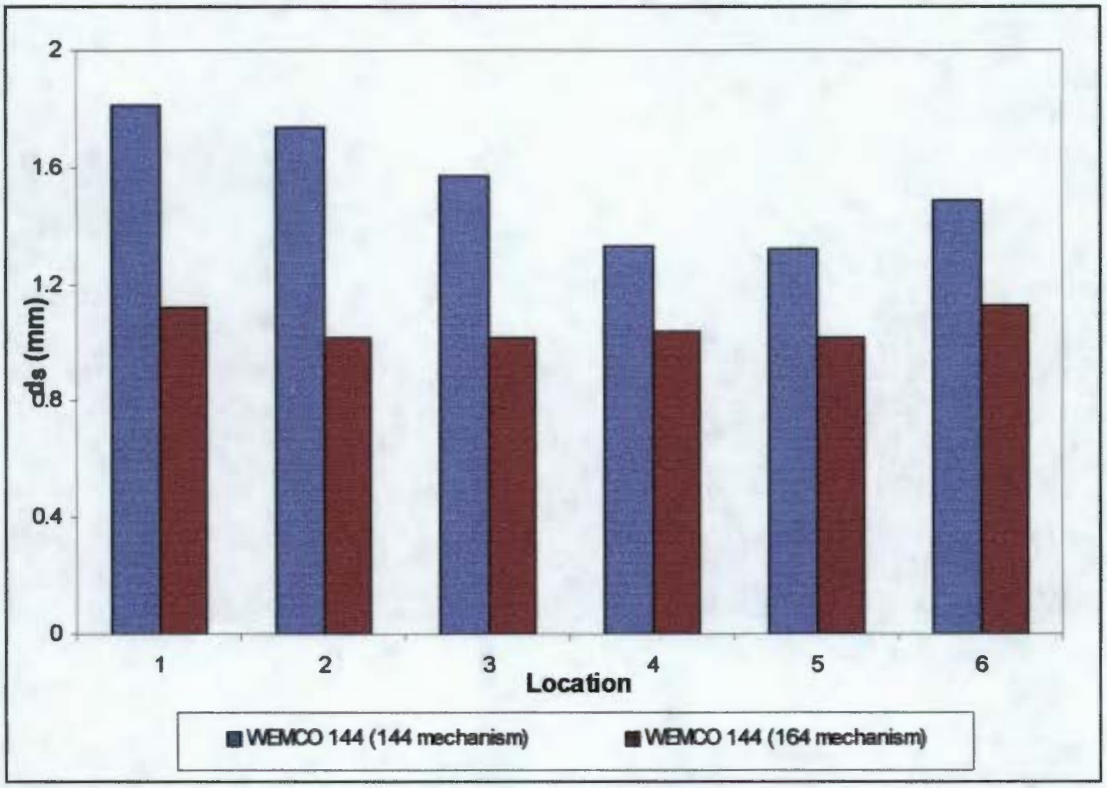

Figure 5.29: Sauter mean bubble diameter (d_S) in 16-m^3 WEMCO 144 cell fitted with standard 144 and 164 mechanisms.

5.3.3 Superficial gas velocity

5.3.3.1 Superficial gas velocity along the bank

The behaviour of superficial gas velocity along a bank of cells is illustrated in Figure 5.30 with reference to a bank of 8.5-m^3, WEMCO 120 cleaner cells. Each point represents the average superficial gas velocity in a particular cell and the data for this graph are found in Table C18. The error bars indicate the standard deviations of the superficial gas velocity measurements in the each cell. It is obvious from this figure that there is little appreciable difference in superficial gas velocity among these cells. The small differences observed may be attributed to the differences in air flowrates; small air flowrates corresponded to lower superficial gas velocities. The position of the cell in the circuit did not appear to have much effect on the superficial gas velocity.

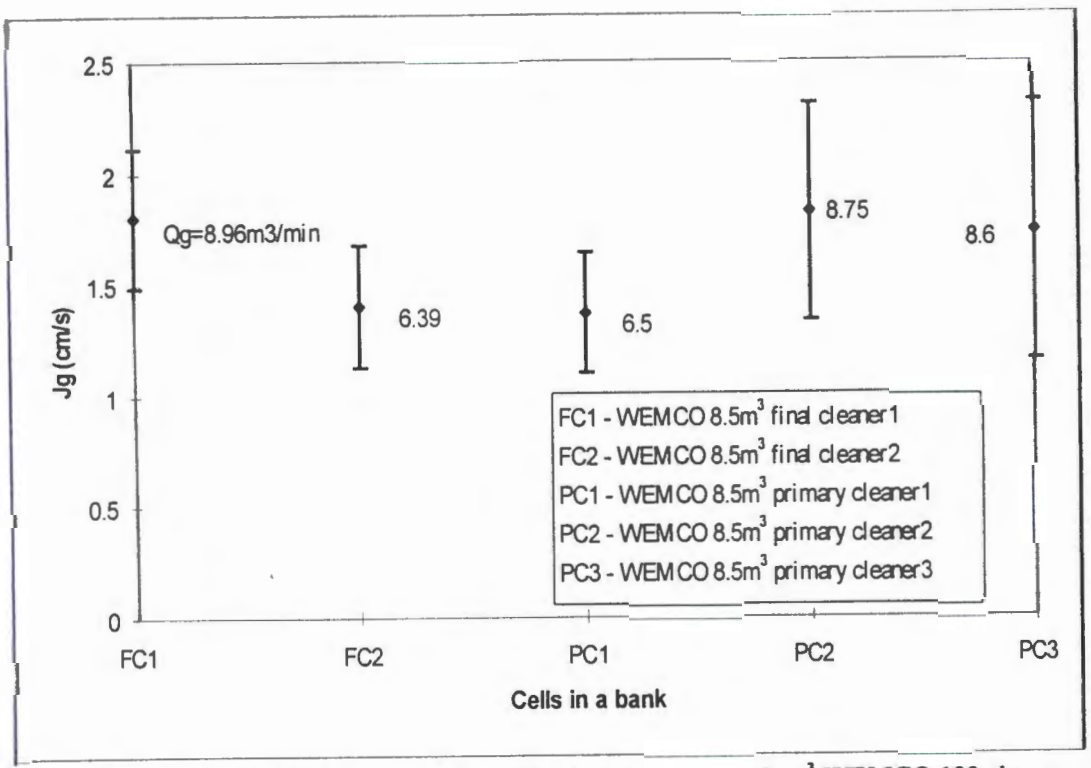

Figure 5.30: Superficial gas velocity (Jg) profile along a bank of 8.5-m^3 WEMCO 120 cleaner cells.

5.3.3.2 Superficial gas velocity in different types, sizes and duties of cell

The effects of different types, sizes and duties of cells on superficial gas velocity is compared in Figure 5.31, plotted from data in Table C18. It may be deduced from this figure that superficial gas velocity does not appear to depend much on cell types, size or duty of the cell.

In the cleaner cells, the superficial gas velocities were found to be greater than in the rougher cells. In the 8.5-m^3, WEMCO 120 cell, average superficial gas velocities of about 1.8 cm/s were measured. For an air flowrate of 1.35 m^3/min, the 3-m^3 Bateman cell produced average superficial gas velocity of 2.22 cm/s in the upper zone and 1.05 cm/s in the lower zone. The average superficial gas velocities in the WEMCO 10-m^3 unit cell were 1.36 cm/s in the impeller zone and 1.98 cm/s near the froth zone, at an air flowrate of about 5.5 m^3/min. The supporting data are found in Tables C1-C18 in Appendix C.

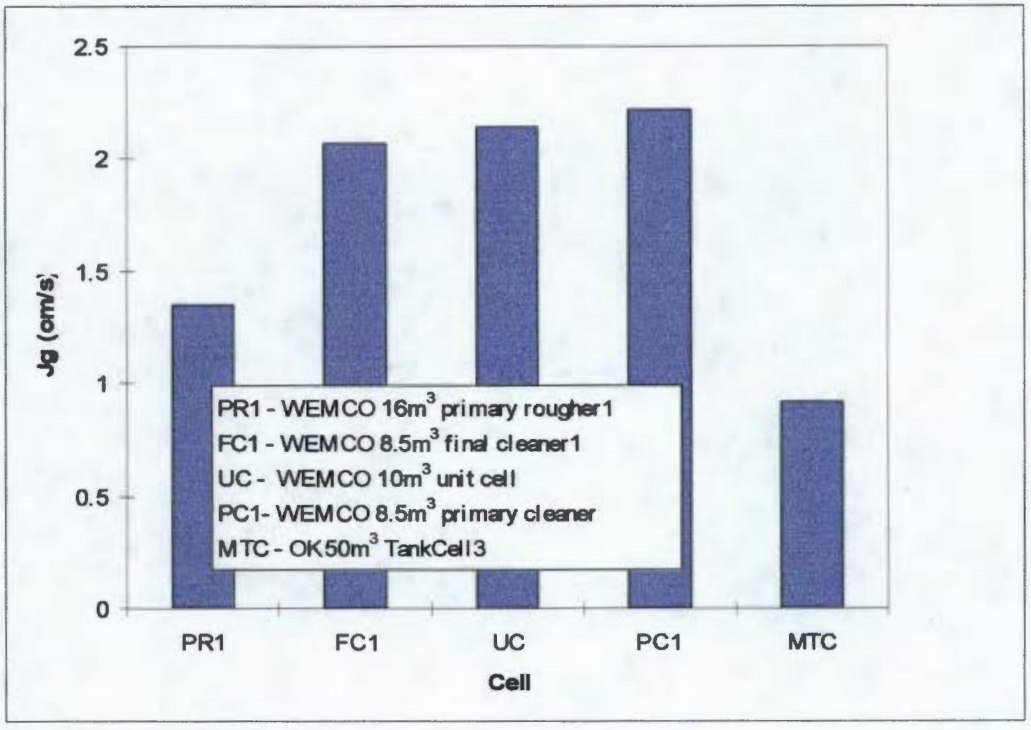

Figure 5.31: Superficial gas velocity (Jg) in different types, sizes and duties of flotation cells

The superficial gas velocities in the WEMCO cells were consistent with the manufacturer's recommended superficial gas velocity of about 2 cm/s. In the WEMCO cells the superficial gas velocity in the turbulent zone was lower than in the quiescent zone. The most likely reasons for this observation have already been discussed in section 5.2.3.3.

The OK 16-m^3 cells show differences in superficial gas velocities between the quiescent and turbulent zones, but they are not as prominent as in the WEMCO 144 high-power cell. The OK 16-m^3 cells had a greater superficial gas velocity (1.4-2.4 cm/s) in the air flow range of 9-17 m^3/min. At air flowrates beyond this range, superficial gas velocities of about 2.8 cm/s were produced. In general, the superficial gas velocities produced in the OK 16-m^3 cells were greater than in the WEMCO 144 cells (compare Tables C5, C6 and C8). This observation is not surprising as the air flowrates in the OK 16-m^3 cells were greater.

Relatively lower, superficial gas velocities were measured in the OK 50-m^3 "Multi-mix" TankCell, with 0.9 cm/s being recorded at the highest air flowrate of 4 m^3/min (Figure 5.31). The extremely low, superficial gas velocities in the TankCell are attributed to the lower air flowrates in the "Multi-mix" system.

5.3.4 Bubble surface area flux

5.3.4.1 Bubble surface area flux along the bank

The variation of bubble surface area flux along a bank of 16-m^3 WEMCO cells is discussed in section 5.3.4.2 below (see Figure 5.33).

5.3.4.2 Bubble surface area flux in different types, sizes and duties of cells

Figure 5.32 depicts values of bubble surface area flux obtained in flotation cells with volumes between 3 and 50-m^3. Despite the enormous variations in cell volume, the value of bubble surface area flux remains within a fairly small range,

between about 45 and 60 m^2/m^2sec. The WEMCO 10-m^3 unit cell had the highest value of bubble surface area flux, though this was only slightly higher than the values measured in several other cells. The high values measured in the WEMCO 10-m^3 unit cell may be due to the fact that it was fitted with an oversize mechanism, resulting in a very high power dissipation per unit volume. The high values measured in WEMCO 8.5-m^3 final cleaner probably resulted from the high air rate per unit volume in that cell.

Most of the gas dispersion measurements performed over the course of the experimental programme were in the WEMCO 84 (4.25 m^3), 120 (8.5 m^3) and 144 (16 m^3) cells. The results from these cell types are of interest as WEMCO cells are used quite extensively in the mining industry. Values of bubble surface area flux were remarkably similar in all the WEMCO cells studied. In Figure 5.32 the values of bubble surface area flux are seen to be almost identical for WEMCO 144 cells, operating in the primary rougher (164 mechanism), secondary rougher (164 mechanism) and scavenger (144 mechanism) applications.

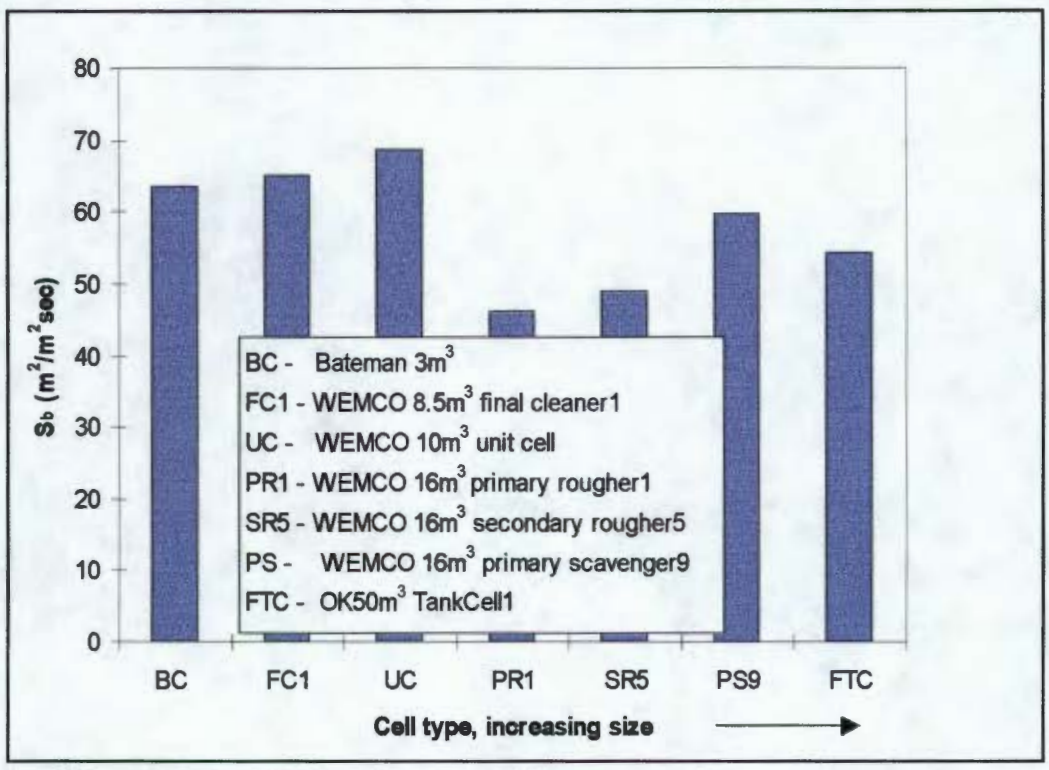

Figure 5.32: Bubble surface area flux (S_b) for different types of cells.

This general observation was confirmed when gas dispersion measurements were performed down an entire bank of WEMCO 144 (some of them with 164 mechanisms) cells as may be seen in Figure 5.33. The data for Figure 5.33, found in Table C18, represent the averages of bubble surface area flux in each cell. The error bars represent the standard deviations of bubble surface area flux measured in each cell. It was found that although that the air flowrate varied widely from 5-10 m^3/min, the values of the bubble surface area flux remained comparatively constant at between 45 and 60 m^2/m^2sec. This suggests that the WEMCO cell type is fairly insensitive to changing operating conditions, generating similar values of bubble surface area flux over a variety of air flowrates and applications.

The bubble surface area flux along the cleaner cells supports this assertion. Within an air flowrate range of 6-9 m^3/min, the bubble surface area flux for all the five cleaner WEMCO 120 cells lay in the range from 52-60 m^2/m^2sec. Data may be found in Tables C9 and C10 in Appendix C.

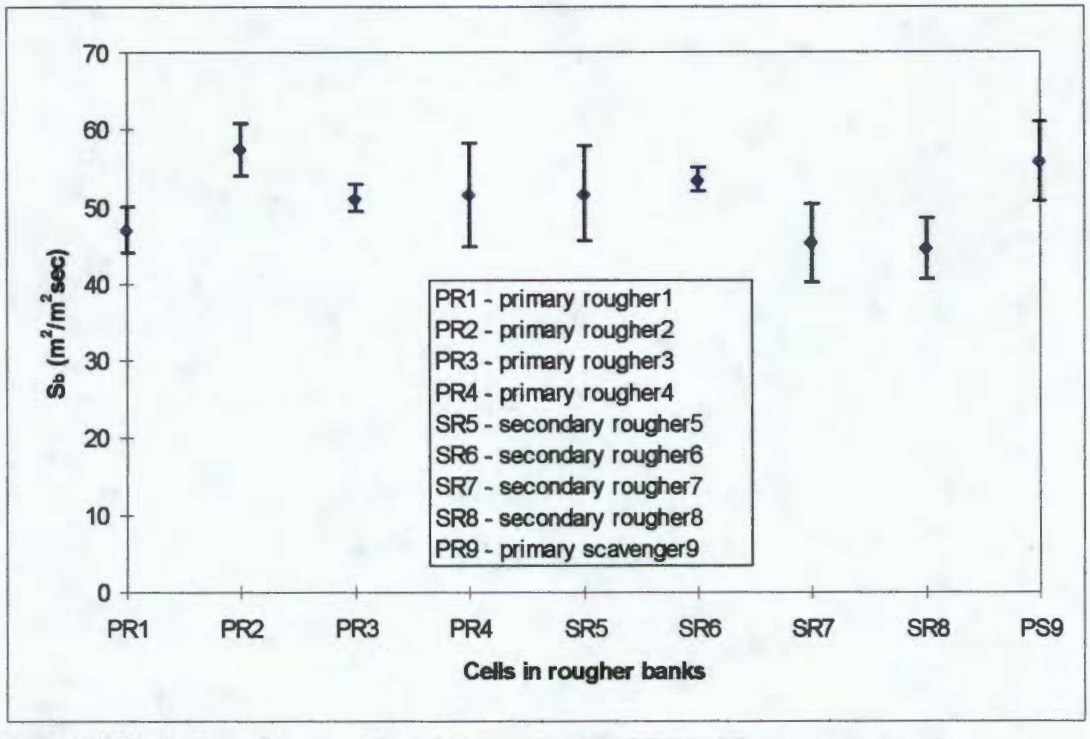

Figure 5.33 Bubble surface area flux (S_b) along banks of WEMCO 144 rougher cells.

Similar bubble surface area flux rates were observed in some of the other cell types. For example, in the OK 50-m^3 TankCells with the "Free-flow" impeller system, at the operating air flowrate of 3.5 m^3/min, a bubble surface area flux of about 55 m^2/m^2sec was produced (see Table C11 in Appendix C). The 3-m^3 Bateman cell, despite its diminutive size, also produced bubble surface area flux comparable to that of the other, larger cells (Table C13 in Appendix C).

5.3.4.3 Effect of oversized mechanism on bubble surface area flux

It has been a general philosophy in platinum processing plants to increase the rate of flotation by using oversized mechanisms and higher power motors in the flotation cells. An additional benefit for the use of an oversize mechanism in this application is that wear is minimised and the life of the mechanism is prolonged. The perceived increase in the flotation rate is thought to be due to better gas dispersion by the upgraded mechanism or motor envisaged.

Figure 5.34 depicts the bubble surface area flux produced in a 16-m^3 WEMCO 144 cell, located in the scavenger circuit, with a standard mechanism and in the same cell retrofitted with an oversized, 164 mechanism. The 164 mechanism is the standard size for WEMCO 30-m^3 cell. It is clear from Figure 5.34 that the use of an oversized mechanism produced a significant increase in bubble surface area flux, even though the impeller speed of the 164 mechanism was calibrated so as to give equivalent power draw to that of the 144 mechanism. The air flowrate obtained using the 164 mechanism was even lower than with the 144 mechanism. The data are found in Table C2 in Appendix C.

It is not clear what contributed to the higher bubble surface area flux with the 164 mechanism in this case. Previous measurements with similar 164 mechanisms were no different from those made with standard 144 mechanisms (see Table C1 in Appendix C). The differences in the bubble surface area flux between the two data sets for the 164 mechanism in a 144 cell, as shown respectively in Tables C1 and C2, may be due to changes in ore type or to wear of the mechanism.

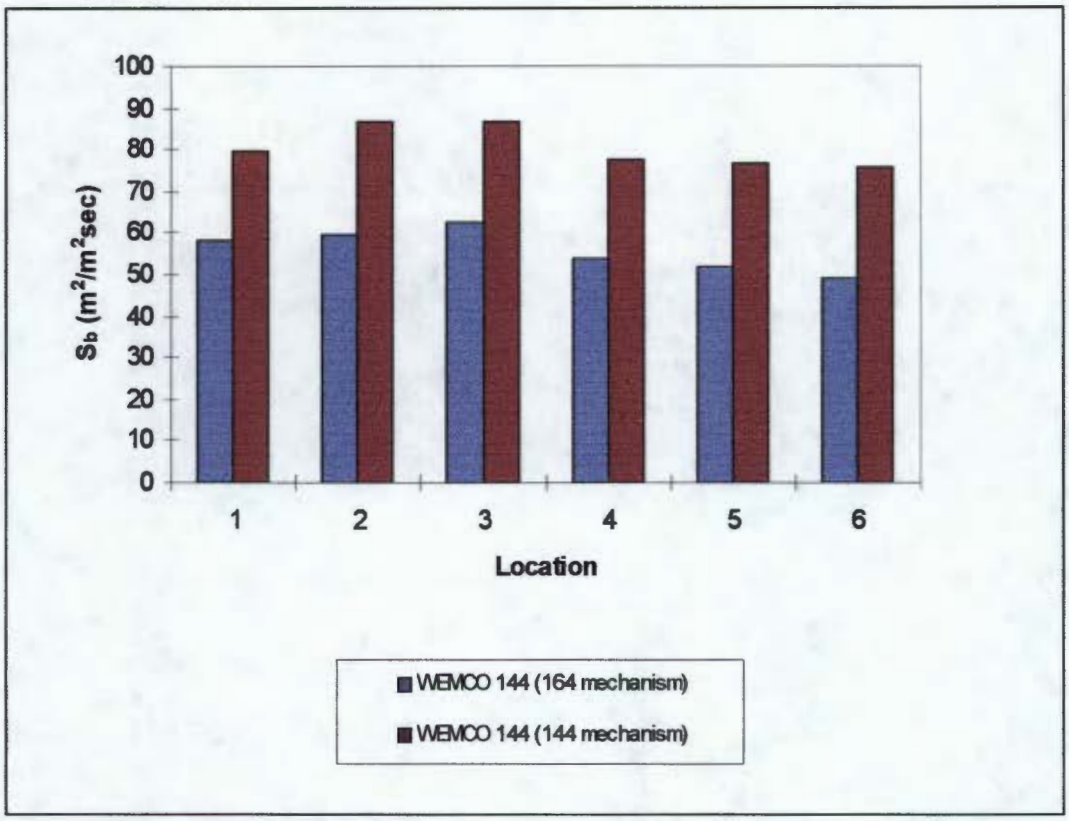

Figure 5.34: Effect of oversize mechanism on bubble surface area flux (S_b)

5.3.4.4 Effect of oversize motor on bubble surface area flux

Figure 5.35 depicts values of bubble surface area flux obtained from Table C4, averaged for all measured locations over a range of air flowrates. Again, these data are for WEMCO 144 cell in a primary rougher circuit powered by a standard (45 kW) motor and a high-power (90 kW) motor. It is clear from this figure that the high power motor generates a substantially higher bubble surface area flux than the standard motor. The high power input results in higher shear, producing smaller bubbles and a consequently higher bubble surface area flux. Similarly, the high-power input to the 10-m^3, WEMCO unit cell explains its superior bubble surface area flux production (Figure 5.32).

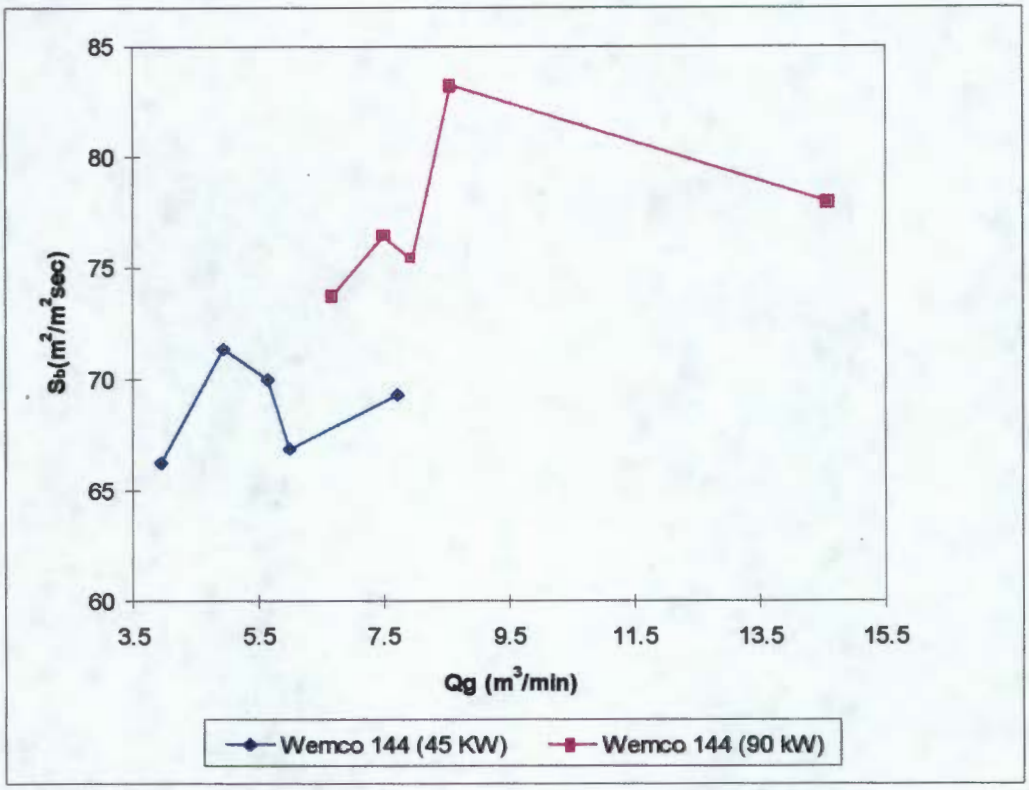

??Figure 5.35: Effect of oversize motor on bubble surface area flux (S_b).

One of the key objectives (Knopjes, 1996) behind installing higher power in the "Multi-mix" impeller system in the TankCell was to improve the performance of the cell by creating a superior air dispersion capacity in the cell. From this work, it would appear that this objective was not realised. However, these conclusions need to be seen in the context of only one measurement point in these cells (see discussion in Section 5.2.4.2) and it is recommended that more readings be taken in these cells for any meaningful conclusions to be drawn.

5.3.4.4 Summary

Air holdup measured in different flotation cells was independent of the type and size of the cell and does not depend on the position of cell in the circuit. The key determining factor was the air flowrate to the cell per unit volume of cell. Cleaner cells, by virtue of their duties, usually operate at higher air flowrate per unit volume and so have higher holdup than cells used for roughing and scavenging.

No significant changes in bubble sizes were noted in the different cell types or in the banks of cells investigated. This is probably due to the narrow range of air flowrates used and the fact that there were no significant changes in particle size and reagent concentration during the testwork or within a bank of cells. Generally, the smaller cells showed slightly larger bubble sizes, probably due to their higher values of air flowrate per unit volume of cell.

The superficial gas velocities were generally greater in the smaller cells, owing to the higher aeration rate into these cells as compared to the larger ones.

Bubble surface area flux did not change to any appreciable extent for the different types, sizes and duties of cells measured. However, increasing the cell motor size showed a great improvement in bubble surface area production. Results using different mechanisms should be checked by more comparative tests.

5.4 GENERAL FINDINGS

The discussion in this chapter has concerned the observations made in the variety of flotation cells surveyed in this test, with respect to solids suspension and gas dispersion, under various conditions of air flowrate, impeller speed, power input and location. It is worth emphasising a few other important findings of this work, which have not been discussed in the preceding sections of the chapter. These findings will be discussed with reference to their relevance to the classical, chemical engineering literature on gas dispersion.

The limiting factor in the flotation process is often thought to be the probability of collision and coalescence of bubbles with the desired ore particles in the cell. Bischofberger and Schubert (1978) have shown that the number of collisions in a flotation cell is directly proportional to the number of bubbles and particles present. Thus the rate of removal of particles from the cell should be related to the number of bubbles. Smaller bubbles have been proposed by many researchers to increase the collision efficiency, since a greater interfacial area of bubbles is produced in the case

of smaller bubbles. Thus the particle removal efficiency should be strongly related to the rate of production of this interfacial area, referred to as bubble surface area flux in this thesis. The discussions below are directly or indirectly related to this characteristic, gas dispersion property called bubble surface area flux, with references from the classical chemical engineering literature. The applicability of these theories to flotation testify to the relevance of the literature to the flotation process.

5.4.1 Sauter mean bubble size versus superficial gas velocity

Figure 5.36 shows a plot of the Sauter mean bubble diameter versus superficial gas velocity for industrial-scale, WEMCO and OK cells of different sizes and performing different duties. It can be seen from this figure that, irrespective of the type, size and duty of the cells there is a fair correlation (R^2= 0.86) between the Sauter mean bubble size and the superficial gas velocity. The bubble surface area flux has a direct and an indirect relationship with the superficial gas velocity and bubble size respectively, while the superficial gas velocity and Sauter mean bubble size have a direct relationship to some extent. The relationship between these two gas-phase properties mitigates any big impact on the bubble surface area flux resulting from changes in a variable such as air flowrate. This may explain why there was no significant change in the bubble surface area flux in the different types of cells that were studied, even though their air flowrates varied significantly. The significance of Figure 5.36 is that such a relationship for typical industrial flotation cells may serve as a useful tool for design and scale-up of flotation cells.

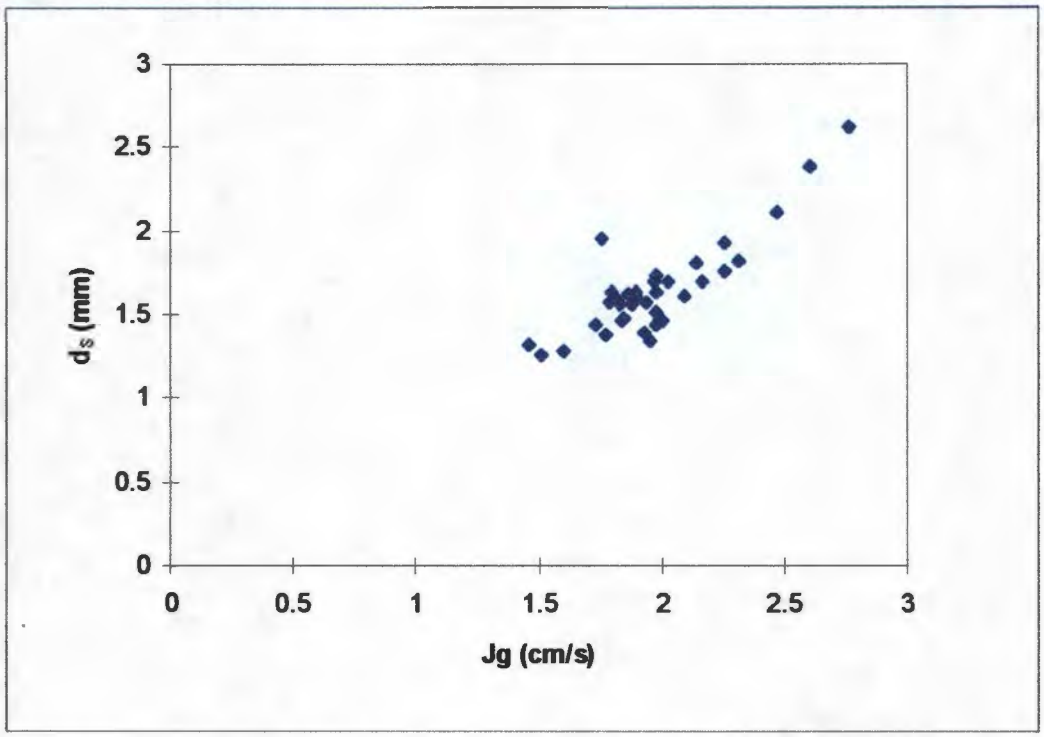

Figure 5.36 Sauter mean bubble diameter (d_S) versus measured superficial gas velocity (Jg) in flotation cells.

5.4.2 Sauter mean bubble size versus power

Figure 5.37 shows the effect of cell power per unit volume on the sizes of bubbles produced in the 16-m^3 WEMCO 144 standard and high-power cells and the OK 16-m^3 cell. The changes in power dissipation in the cells were achieved by varying the air flowrates. It has been shown by a number of researchers (Parthasarathy, *et al.*, 1991) that power input in an aerated system has a big influence on the size of bubbles produced. Figure 5.37 shows that as the power to the cell decreased, bubble sizes increased, in the WEMCO 144 high power and the OK 16-m^3 cells. The WEMCO 144 standard cell did not show any appreciable change in power, probably because of the narrow aeration range at which the tests in it were performed.

Figure 5.38 considers the power only in the volume swept by the impeller axis plus blades. It appears that the power dissipation in the impeller-swept volume is more closely correlated with the mean bubble size than the raw power dissipation. This is

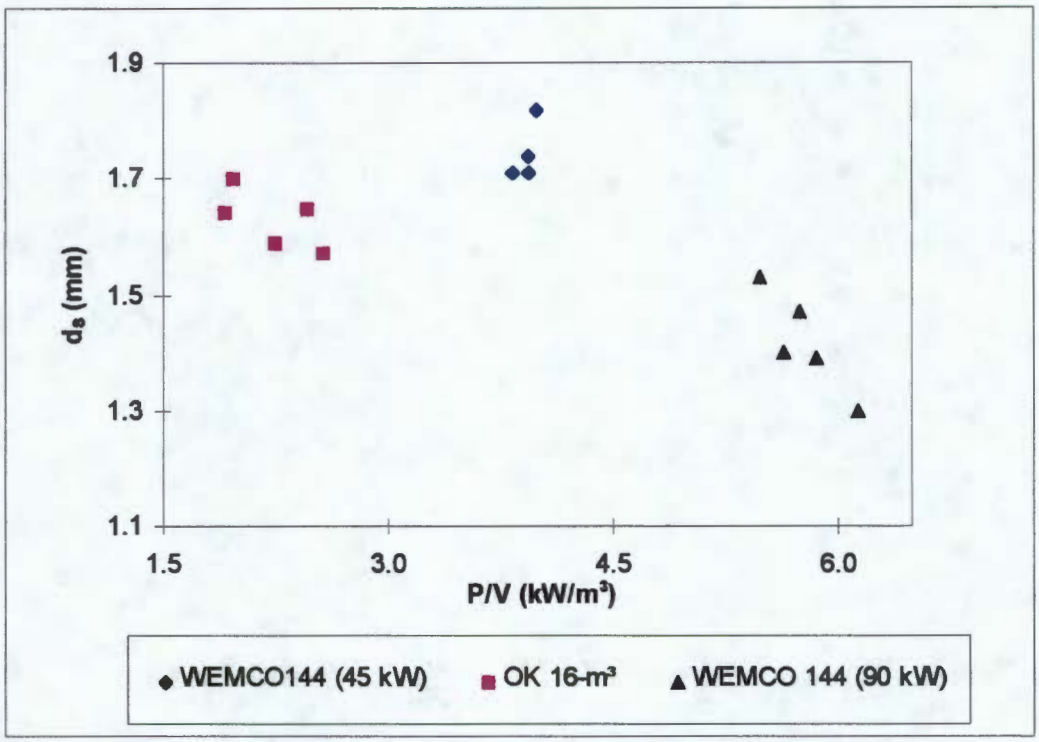

Figure 5.37: Effect of cell power per total cell volume (P/V) on Sauter mean bubble diameter (d_S) for WEMCO 144 and OK 16-m^3 cells.

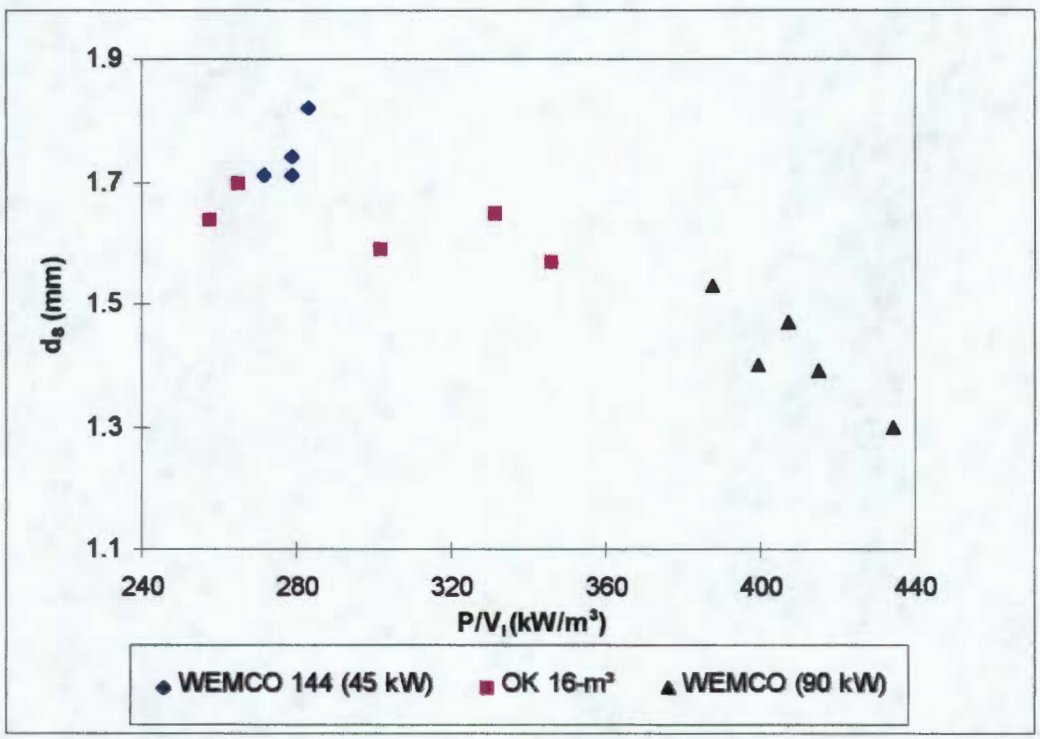

Figure 5.38: Effect of cell power per impeller-swept volume (P/V_I) on Sauter mean bubble diameter (d_S) for WEMCO 144 and OK 16-m^3 cells.

because bubble generation occurs within the impeller zone, and in a non-coalescent system the size of bubbles does not change elsewhere in the cell.

Similar observations have been made by a number of authors. For example, it has been reported (Coste and Couderc, 1988; Okamoto, *et al.*, 1981) that the energy dissipation in a stirred tank varies with location, being very high near the impeller zone and smaller in the bulk of the tank. Van't Riet and Smith (1973) have also shown that in a stirred vessel, bubble break-up occurs in the impeller zone and that bubble size is not expected to change elsewhere in the tank. Therefore in such a system, the energy dissipation rate per impeller-swept volume provides a better estimate of the bubble size. Parthasarathy, *et al.*, (1991) have recently found that there is a greater degree of accuracy in the prediction of bubble sizes based on the energy dissipation in the impeller-swept volume than in the entire volume of the cell.

It is clear from Figure 5.38 that when the power dissipation-bubble size relationship was limited to the impeller swept volume, all the points seem to lie in the same band irrespective of the type of impeller ($R^2 = 0.81$). In each case, the power dissipation per unit volume was found to be about a hundred times that for the entire volume of the cell. This may be a useful finding for designing and scaling-up of mechanical flotation cells.

Although it is not within the scope of the current thesis, it would be interesting to develop correlations to predict bubble sizes in industrial mechanical flotation cells from these findings.

5.4.3 Power versus bubble surface area flux

Power consumption by the impeller was calculated for each cell from the current drawn using equation (60) in Appendix E. Impeller power was varied in the cells by varying the air flowrate. Power has been shown to have an effect on the size of bubbles produced in flotation cells (see section 5.2.2.6). This implies that increasing

the power to a flotation cell should cause an increase in bubble surface area flux, probably because of the good gas dispersion that also occurs. This relationship was not apparent in the data, probably because of the narrow range of power inputs studied, which in turn resulted from restriction in the air flowrates available. As shown in Figure 5.39, there was little correlation between the cell power per impeller-swept volume and the bubble surface area flux in the different cells. A general trend of increasing bubble surface area flux with power was however, discernible. Poorer correlation was observed between the bubble surface area flux and power consumption per the entire cell volume ($R^2 = 0.36$).

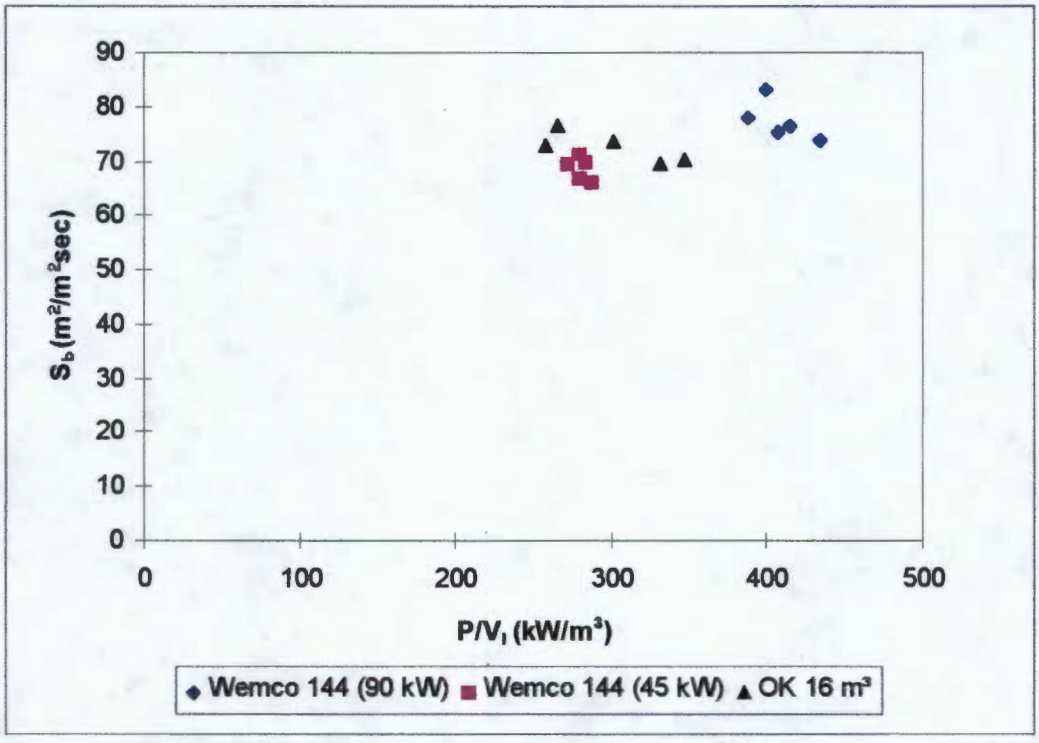

Figure 5.39: Effect of cell power per impeller-swept volume (P/V_I) on bubble surface area flux (S_b).

5.4.4 Summary

The following general observations were made, for typical, industrial flotation cells:

(a) There is a good correlation (R^2=0.86) between the Sauter mean bubble size and the superficial gas velocity, irrespective of the type, size and duty of the cells.

(b) There is a fairly good correlation (R^2=0.81) between Sauter mean bubble size and power per impeller-swept volume; this correlation is better than that between Sauter mean bubble size and power per total cell volume (R^2=0.36).

(c) There is a very weak (R^2=0.30) correlation between bubble surface area flux and power per impeller-swept volume. This poor correlation may be due to the narrow range of power inputs over which the tests were done.

CHAPTER 6

CONCLUSIONS AND RECOMMENDATIONS

6.0 INTRODUCTION

The central objective of this project, was to characterise gas dispersion in industrial, mechanical flotation cells on the basis of a new characteristic parameter - the bubble surface area flux. To do this, the three, gas-phase properties of bubble size, gas holdup and superficial gas velocity were measured in a variety of flotation cells of different types, sizes and duties, using the special devices as discussed in Chapter 4. The bubble surface area flux was then determined from these properties. Experiments were carried out under different conditions of air flowrates, cell power input and impeller speed. Solids suspension in these flotation cells was also considered briefly in the course of the project, at different conditions of air flowrate, cell power and impeller speed. The conclusions drawn from this work are summarised in this chapter, together with some recommendations for future work.

6.1 CONCLUSIONS

(1) The Sauter mean bubble diameter measured in flotation cells in a typical pgm plant was between 1.0 and 2.6 mm (arithmetic mean bubble diameter of 0.5 - 1.3 mm). This range of bubble sizes compares very well with bubble sizes measured in base metal plants with photographic devices. The reliability of the UCT Bubble Size Analyser was therefore corroborated. The sizes of bubbles were found to be different in different regions of the cell, and were generally smaller in the impeller region and larger near the froth zone. Bubble sizes were also found to be different in the different cells. The key factors controlling them were the air flowrate, cell power input and impeller speed.

(2) The range of superficial gas velocity measured was 1.0 - 2.8 cm/s for all the different types, sizes and duties of cell at the different conditions of the tests. This superficial gas range agrees very well with measurements in industrial flotation cells reported by Harris (1976).

Differences in superficial gas velocity values were found between the lower and upper regions of the cells. These differences are attributed to the differences in the flow patterns in the cells. Although the measured superficial gas velocity is a function of air flowrate, it is heavily dependent on the impeller speed and power input. At the same air flowrate, the superficial gas velocity may be different at different impeller speeds, due to the generation of different flow patterns.

(3) Air holdups measured were in the range of 8 - 16%. Extremely high air holdups of almost 32% were measured in some cleaner cells. Power input, impeller speed and air flowrate had very little effect on air holdup in the cells.

(4) The bubble surface area flux in industrial, mechanical flotation cells under standard operating conditions ranged from 50 - 60 m^2/m^2sec. There was very little difference in bubble surface area flux amongst flotation cells of different types, sizes and applications. It did however vary with location in the same cell. The bubble surface area flux in a cell can be improved by manipulating key cell variables such as the air flowrate and impeller speed.

(5) Aspects of the classical, chemical engineering literature are of relevance to gas dispersion in flotation cells.

6.2 RECOMMENDATIONS

Bubble surface area flux has been shown to be a function of air flowrate. More detailed measurements is recommended to identify the optimum air flowrates at which maximum values of S_b occur.

In the OK 50-m^3 TankCells, more measurements are recommended to more fully characterise the gas dispersion and especially bubble surface area flux in the "Multi-mix" and the "Free-flow" mechanisms.

As a follow up to the present work, the experimental data gathered could be used to develop correlations for the prediction of bubble size and gas holdup in flotation cells. This would be very useful in gas dispersion studies in flotation.

This work was subject to several limitations, most notably the inability to control and measure power inputs and air flowrates over a wide ranges. It would be useful to plan and conduct a more comprehensive test, with equipment designed to vary and measure power input and air flowrates to the cells easily and accurately.

The power per impeller-swept volume relationship promises to be a very useful way of predicting bubble sizes in flotation cells. It recommended that this relationship be explored further, from laboratory-scale through pilot-scale to industrial-scale flotation cells.

REFERENCES

Ali, A.M., Yuan, H.H.S., Dicky, D.S. and Tatterson, G.B., Liquid Dispersion Mechanisms in Agitated Tanks, Part 1 - Pitched Blade Turbine, Chem. Eng. Commun., Vol. 10, (205), 1981.

Arbiter, N., Harris, C. C., and Yap, R. F., Hydrodynamics of Flotation Cells, Trans. AIME, Vol. 244, pp. 134-148, March, 1969.

Barigou, M. and Greaves, M., Bubble size in the impeller region of a Rushton turbine, Trans. Inst. Chem. Eng., Vol. 70, Part A, pp. 153-159, March 1992.

Barresi, A. and Baldi, G., Solid Dispersion in Agitated Vessel, Chem. Eng. Sci., Vol. 42, No. 12, pp. 2949-2956, 1987.

Bertrand, J., Coudere, J.P. and Angelino, H., Power Consumption, Pumping Capacity and Turbulence Intensity in Baffled Stirred Tanks - Comparison Between Several Turbines, Chem. Eng. Sci., Vol. 35, (2157), 1980.

Bezuidenhout, G., The Bateman Flotation Machine, Colloquium: Interactions between Communition and Downstream Processing, SAIMM, Mintek, Randburg, South Africa, June, pp. 1-8, 1995.

Bischofberger, C. and Schubert, H., On the Hydrodynamics of Flotation Machines, Int. J. of Miner. Process., Vol. 5, pp. 131-142, 1978.

Bogdanov, O.S., Hainman, V.Y., and Maxomov, I.I., On Certain Physical-Mechanical Factors Determining the Rate of Flotation, 7th Int. Miner. Process. Cong., New York, N. Arbiter (ed.), Gordon and Beach, New York, Part 4, pp. 169-174, 1965.

Bruijn, K., van't Riet, K., and Smith, J.M., Power Consumption with Aerated Rushton Turbine, Trans. Inst. Chem. Eng., Vol. 52, pp. 88-104, 1974.

Calderbank, P. H., Inter-Dispersion of Immiscible Fluid Phases, Trans. Inst. Chem. Eng., Vol. 36, (443), 1958.

Calderbank, P.H., Mixing: Theory and Practice, Vol. 2, Uhl, V.W., and Gray, J.B., (eds.), Academic Press, New York, Chapt. 6, (2), 1967.

Chapman, C.M., Nienow, A.W., Cooke, M., and Middleton, J.C., Particle-Gas-Liquid Mixing in Stirred Vessels: Part 1. Particle-Liquid Mixing, Chem. Eng. Res. Des., Vol. 61, pp. 71-81, 1983a.

Chapman, C.M., Nienow, A.W., Cooke, M., and Middleton, J.C., Particle-Gas-Liquid Mixing in Stirred Vessels: Part 2. Gas-Liquid Mixing, Chem. Eng. Res. Des, Vol. 61, pp. 82-95, 1983b.

Chapman, C.M., Nienow, A.W., Cooke, M., and Middleton, J.C., Particle-Gas-Liquid Mixing in Stirred Vessels: Part 3. Three Phase Mixing, Chem. Eng. Res. Des, Vol. 61, pp. 163-183, 1983c.

Costes, J., and Couderc, J.P., Study by Laser Doppler Anemometry of the Turbulent Flow Induced by a Rushton Turbine in a Stirred Tank: Influence of the Size of the Units – II. Spectral Analysis and Scales of Turbulence, Chem. Eng. Sci., Vol. 43, (2765), 1988.

Diaz-Penafiel, P. and Dobby, G.S., Kinetics Studies in Flotation Columns: Bubble Size Effects, Miner. Eng. Vol. 7, No. 4, pp. 465-478, 1994.

Dobby, G.S., A Fundamental Flotation Model and Flotation Column Scale-up, Ph.D. Thesis, McGill University, Montreal, 1984, in Finch and Dobby, 1990, *op. cit.*

Eby, G.J., WEMCO Large-Capacity Flotation Cells, CIM Bulletin, pp. 50-55, Feb. 1972.

Evans, L.F., Bubble-Mineral Attachment, Ind. Eng. Chem., Vol. 46, pp. 2420-2424, 1954.

Fallenius, K., Outokumpu Flotation Machines, Outokumpu Oy, Tapiola, Finland, 1975.

Fallenius, K., A New Set of Equations for the Scale-up of Flotation Cells, J. Laskowski (ed.), XIII Int. Miner. Process. Cong., Warsaw, pp. 1353-1376, 1979.

Finch, J.A. and Dobby, G.S., Column Flotation, Pergamon Press, Oxford, 1990.

Gaudin, A. M. Flotation, McGraw-Hill Book Co., New York, 1957.

Glembotski, V.A., Klassen, V.I. and Plaksin, I.N., Flotation, translated by and available from Primary Sources, New York, 1963.

Golding, E.W., Electrical Measurements and Measuring Devices, Sir Isaac Pitman & Sons, Ltd., (169), 1941.

Gorain, B.K., Franzidis, J.-P. and Manlapig, E.V., Studies on Impeller Type, Impeller Speed and Air Flowrate in an Industrial Scale Flotation Cell, - Part 1: Effect on Bubble Size Distribution, Miner. Eng., Vol. 8, No. 6, pp. 515-635, 1995a.

Gorain, B.K., Franzidis, J.-P. and Manlapig, E.V., Studies on Impeller Type, Impeller Speed and Air Flowrate in an Industrial Scale Flotation Cell, - Part 2: Effect on Gas Holdup, Miner. Eng., Vol. 8, No. 12, pp. 1557-1570, 1995b.

Gorain, B.K., Franzidis, J.-P. and Manlapig, E.V., Studies on Impeller Type, Impeller Speed and Air Flowrate in an Industrial Scale Flotation Cell, - Part 3: Effect on Superficial Gas Velocity, Miner. Eng., Vol. 9, No. 6, pp. 639-654, 1996a.

Gorain, B.K., Franzidis, J.-P., and Manlapig, E.V., Bubble Surface Area Flux: A New Criterion to Evaluate the Flotation Cell Performance, Minerals and Materials '96, Vol.

1, pp. 326-334, Proceedings of an Int. Conf., 31 July-2 August, 1996, SAIMM, Somerset West, South Africa.

Gorain, B.K., Franzidis, J.-P. and Manlapig, E.V., Studies on Impeller Type, Impeller Speed and Air Flowrate in an Industrial Scale Flotation Cell, - Part 4: Effect of Bubble Surface Area Flux on Flotation Performance, Miner. Eng., Vol. 10, No. 4, pp. 367-379, 1997.

Grainger-Allen, T.J.N., Bubble Generation in Froth Flotation machines, Trans. Inst. of Min. and Metall., Vol. 28, pp. C15-22, 1970.

Greaves, M., and Kobbacy, K. A. H., Fluid Mixing, Inst. Chem. Eng. Sym. Ser., No. 64, Int. Chem. Eng., Warks, England, L1, 1981.

Harris, C.C., and Lepetic, V., Flotation Cell Design, Mining Eng., pp. 67-72, 1966.

Harris, C.C., Gupta, S.C., and McFall, G.K., Aeration, Suspension and Dispersion Characteristics of Flotation Machines, AIME Annual Meeting, New York, February 16-20, 1975.

Harris C.C., Flotation Machines, A.M. Gaudin Memorial Volume, AIME, New York, Vol. 2, M.C. Fuerstenau (ed.), pp. 753-815, 1976.

Hinze, J.O., Fundamentals of the Hydrodynamic Mechanism of Splitting in Dispersion Processes, Amer. Inst.Chem. Eng., J., Vol. 1, No. 3, pp. 289-295, 1955.

Hochreiter, R.C., Kennedy, D.C., Muir, W. and Woods, A.I., Platinum in South Africa, SAIMM J.,Vol. 85, No. 6, pp. 165-185, 1985.

Holmes, D.B., Voncken, R.M., and Decker, J.A., Fluid Flow in Turbine-Stirred, Baffled Tanks - 1: Circulation Time, Chem. Eng. Sci., Vol. 19, (201), 1964.

Jameson, G.J., Nam, S. and Moo Young, M., Physical Factors Affecting Recovery Rates in Flotation, Miner. Sci. Eng., Vol. 9, No. 3, July, pp. 103-118, 1977.

Jameson, G.J., Physics and Hydrodynamics of Bubbles, The Scientific Basis of Flotation, Proceedings of the NATO Advanced Study Institute on the Scientific Basis of Flotation, K.J. Ives (ed.), Cambridge, England, July, 1982, pp. 53-77, 1984.

Jameson, G.J. and Allum, P., A Survey of Bubble Sizes in Industrial Flotation Cells, Report Prepared for AMIRA Ltd., 1984.

Jameson, G.J., Mixing in Mineral Processing - Meeting the Challenges, Australian Mixing Conference, University of Newcastle, 1994.

Joshi, J.B., Mass Transfer and Hydrodynamic Characteristics of Gas Inducing Type of Agitated Contactors, Can. J. Chem. Eng., Vol. 55, (689), 1977.

Joshi, J.B., Axial Mixing in Multiphase Contactors - A Unified Correlation, Trans. Inst. Chem. Eng., Vol. 58, No. 1, pp. 155-165, 1980.

Joshi, J.B., Axial Mixing in Multi-phase Contactors-A Unified Correlation, Trans. Inst. Chem. Eng., Vol. 59, Part 1, pp. 139-143, 1981.

Joshi, J.B., Pandit, A.B., and Sharma, M.M., Mechanically Agitated Gas-Liquid Reactors, Chem. Eng. Sci., Vol. 37, No. 6, (813), 1982.

Kelly, E.G. and Spottiswood, D.J., Introduction to Mineral Processing, John Wiley and Sons, Ltd., New York, 1982.

Khang, S.J. and Levenspiel, O., New Scale-up and Design Method for Stirrer Agitated Batch Mixing Vessels, Chem. Eng. Sci., Vol. 31, pp. 569-577, 1976.

King, R.P., Hatton, T.A. and Hulbert, D.G., Bubble Loading During Flotation Process, Trans. Inst. Min. and Metall., London, Vol. 83, pp. 112-115, 1974.

King, R.P., (ed.), Principles of Flotation, SAIMM, Johannesburg, 1982.

Kirchberg, H. and Topfer, E., The Mineralisation of Air Bubbles in Flotation, New York, Gordon and Breach, Part 4, pp. 157-168, 1965.

Klassen, V.I., and Mokrousov, V.A., An Introduction to the Theory of Flotation, Chapter 5, Butterworths, London, 1963.

Klimpel, R.R., Use of Chemical Reagents in Flotation, Chem. Eng., September, pp. 75-79, 1984.

Knopjes, B., Consulting Metallurgist, Lonrho Platinum Division, Private Communication, 1996.

Laskowski, J., The Relationship between Flotability and Hydrophobicity, Advances in Min. Proc., P. Somasundaran (ed.), SME, Littleton, Colorado, pp. 189-208, 1986.

Levich, V.G., Physicochemical Hydrodynamics, Prentice-Hall, Englewoods Cliffs, New Jersey, 1962.

Levins, D.M., and Glastonbury, J.R., Trans. Inst. Chem. Engrs. Vol. 50, (32), 1972, quoted in Joshi, *et al.*, 1982.

Li, H.C. and De Bruyn, P.L., Electrokinetic and Adsorption Studies on Quartz, Surface Science, Vol. 217, pp. 203-220, 1966.

Lindegger, G., Project Engineer, Supaflo Technologies Pty Ltd., Private Communications, 1993.

Mackenzie, J.M.W., and Matheson, G.H., Kinetic and Dynamic Relationships in Coal Flotation, Trans. Soc. Min. Eng., AIME, Vol. 226, pp. 68-75, 1963.

Mavros, P., Mixing and Hydrodynamics in Flotation Cells, in Innovations in Flotation Technology, Mavros, P. and Matis, K.A. (ed.), Kluver Academic Publishers, Netherlands, pp. 211- 234, 1992.

McManamey, W.J., A Circulation Model for Batch Mixing in Agitated Baffled Vessels, Trans. Inst. Chem. Eng., Vol. 58, (271), 1980.

Mujumdar, A.S., Huang, B., Wolf, D., Weber, M.E. and Douglas W.J.M., Turbulence Parameters in a Stirred Tank, Can. J. Chem. Eng., Vol. 48, (475), 1970.

Nagata, S. Mixing: Principles and Applications, John Wiley and Sons, Ltd., New York, 1975.

Nienow, A.W., Suspension of Solid Particles in Turbine Agitated Baffled Vessels, Chem. Eng. Sci., Vol. 23, pp. 1453-1459, 1968.

Nienow, A.W. and Wisdom, D.J., Flow over Disc Turbine Blades, Chem. Eng. Sci., Vol. 29, pp. 1994-1997, 1974.

Nienow, A.W., and Ulbrecht, J.J., Gas-Liquid Mixing and Mass Transfer in High Viscosity Liquids, in Mixing of Liquids by Mechanical Agitation, Ulbrecht, J.J. and Patterson, G.K., (eds.) Gordon and Breach, New York, 1985.

Nienow, A.W., The Suspension of Solid Particles, Mixing in the Process Industries, (2nd ed.), Butterworth-Heinemann Ltd., Oxford, 1992.

O'Connor, C.T., Randall, E.W., and Goodall, C.M., Measurement of the Effects of Physical and Chemical Variables on Bubble Size, Int. J. Miner. Process., Vol. 28, pp. 139-149, 1990.

O'Connor, C.T., Cilliers, J.J. and Mills, P.J.T., The Prediction of Large Scale Column Flotation Performance using Pilot Plant Data, 4th Meeting of Southern Hemisphere on

Mineral Technology and 3rd Latin American Congress on Froth Flotation, Concepcion, Chile, Vol. 2, pp. 137-147, 1994.

Okamoto, Y., Nishikawa, M. and Hashimoto, K., Int. Chem. Eng., Vol. 21, (88), 1981, quoted in Parthasarathy, *et al.*, 1992.

Oldshue, J.Y., Fluid Mixing Technology, McGraw-Hill Book Co., New York, 1984.

Oyama, Y. and Endoh, K., Power Characteristics of Gas Liquid Contacting Mixers, Chem. Eng., Tokyo, Vol. 19, pp.2-8, 1955.

Pandit, A.B. and Joshi, J.B., Mixing in Mechanically Agitated Gas-Liquid Contactors, Bubble Columns and Modified Bubble Columns, Chem. Eng. Sci., Vol. 38, (1189), 1983.

Parthasarathy, R., Jameson, G.J. and Ahmed, N., Bubble Breakup in Stirred Vessels-Predicting the Sauter Mean Diameter, Trans. Inst. Chem. Eng., Vol. 69, Part A, pp. 295-301, 1991.

Pavlushenko, I.S., Kostin, N.M. and Mateev, S.F., Stirrer Speeds in the Stirring of Suspensions, Journal of Applied Chemistry, U.S.S.R., Vol. 30, pp. 1235-1243, 1957.

Raghav Rao, K.S.M.S., Rewatkar, V.B., and Joshi, J.B., Critical Impeller Speed for Solid Suspension in Mechanically Agitated Solid-Liquid Contactors, Amer.Inst.Chem. Eng. J., Vol. 34, 1988a.

Raghav Rao, K.S.M.S. and Joshi, J.B., Liquid Phase Mixing in Mechanically Agitated Solid-Liquid Reactors, Chem. Eng. J., Vol. 39, (111), 1988b.

Raghav Rao, K.S.M.S., and Joshi, J.B., Liquid Phase Mixing in Mechanically Agitated Vessels, Chem. Eng. Commun., Vol. 74, (1), 1988c.

Raghav Rao, K.S.M.S. and Joshi, J.B., Power Consumption and Gas Phase Dispersion in Mechanically Agitated Gas-Liquid Reactors, Int. J. Eng. Fluid Mechanics, 1989a.

Raghav Rao, K.S.M.S. and Joshi, J.B., Power Consumption and Gas Phase Dispersion in Mechanically Agitated Gas-Liquid Reactors, Int. J. Eng. Fluid Mechanics, Vol. 2, (645), 1989b.

Ranade, V.V. and Joshi, J.B., Flow Generated by Pitched Bladed Turbine-Measurements Using Laser-Doppler Anemometer, Chem. Eng. Commun., Vol. 85, pp. 83-90, 1989.

Rennie, J. and Valentin, F.H.H., Gas Dispersion in Agitated Tanks, Chem. Eng. Sci., Vol. 23, pp. 663-664, 1968.

Rewatkar, V.B., Raghav Rao, K.S.M.S., and Joshi, J.B., Power Consumption in Mechanically Agitated Contactors using Pitched Bladed Impellers, Chem. Eng. Commun., Vol. 88, pp. 69-90, 1990.

Rewatkar, V.B., Deshphande, A.J., Pandit, A.B., and Joshi, J.B., Gas Holdup Behaviour of Mechanically Agitated Gas-Liquid Reactors using Pitched Blade Downflow Turbines, Can. J. of Chem. Eng., Vol. 71, April 1993.

Rushton, J.H., Costich, E.W. and Everett, H.J., Power Characteristics of Mixing Impellers, Chem. Eng. Prog., Vol. 46, pp. 395-404, 467-476, 1950.

Sachs, J. P., and Rushton, J., Discharge Flow from Turbine-Type Mixing Impellers, Chem. Eng. Prog.,Vol. 50, Part 12, (597), 1954.

Sawant, S. B., and Joshi, J. B., Critical Impeller Speed for Onset of Gas induction in Gas Inducing Type of Agitated Contactors, Chem. Eng. J., Vol. 18, (87), 1979.

Schlichting, H., Boundary-Layer Theory, (6th ed.), McGraw-Hill Book Co., New York, 1968.

Schubert, H., On Some Aspects of the Hydrodynamics of Flotation Processes, in K.S.E. Forssberg (ed.), Flotation of Sulphide Minerals, Elsevier, Amsterdam, pp. 337-355, 1985.

Shamlou, P.A. and Koutsakos, E., Solids Suspension and Distribution in Liquid under Turbulent Agitation, Chem. Eng. Sci., Vol. 44, (529), 1989.

Smith, J.M., Dispersion of Gases in Liquids, in Mixing of Liquids by Mechanical Agitation, Ulbrecht, J.J., and Patterson, G.K., (eds.), Gordon and Breach, New York, pp. 139-202, 1985.

Sun, S.C., and Zimmerman, R.E, The Mechanism of Coarse Coal and Mineral Flotation, Trans. Soc. of Min. Engrs., pp. 616-622, May 1950.

Sutherland, K.L., and Wark, I.W., Principles of Flotation, Australasian Inst. of Min. and Metall., Melbourne, 1955.

Taggart, A. F. , Handbook of Mineral Dressing, (2nd ed.), John Wiley and Sons, Ltd., New York, 1945.

Tatterson, G.B., Yuan, H.H.S. and Brodkey, R.S., Stereoscopic Flow Visualisation of the Flows for Pitched Blade Turbine, Chem. Eng. Sci., Vol. 35, pp. 1369-1375, 1980.

Tatterson, G.B., Fluid Mixing and Gas Dispersion in Agitated Tanks, McGraw-Hill, Book Co., New York, 1991.

Tucker, J.P., Deglon, D.A., Franzidis, J.P., Harris, M.C., and O'Connor, C.T., An Evaluation of a Direct Method of Bubble Size Distribution Measurements in a Laboratory Batch Flotation Cell, Miner. Eng., Vol. 7 (5/6), pp. 667-680, 1994.

Uhl, W.V., and Gray, J.B., Mixing: Theory and Practice, Vols. 1 and 2, Academic Press, New York, 1966.

Van't Riet, K., and Smith, J.M., The Behaviour of Gas-Liquid Mixtures Near Rushton Turbine Blades, Chem. Eng. Sci., Vol. 28, pp. 1031-1037, 1973.

Van't Riet, K., Boom, J.M., and Smith, J.M., Power Consumption, Impeller Coalescence and Recirculation in Aerated Vessels, Trans. Inst. Chem. Eng., Vol. 54, (124), 1976.

Van der Molen, K., and Van Mannen, H.R.E., Laser-Doppler Measurements of the Turbulent Flow in Stirred Vessels to Establish Scaling Rules, Chem. Eng. Sci., Vol. 33, (1161), 1978.

Vera, M.A., The Determination of the Collection Zone Rate Constant and Froth Zone Recovery by Column Flotation, M.Sc. Thesis, JKMRC, University of Queensland, Australia, 1995.

Warmoeskerken, M.M.C.G., and Smith, J.M., Flooding of Disc Turbines in Gas-Liquid Dispersions: A New Description of the Phenomenon, Chem. Eng. Sci., Vol. 40, No. 11, pp. 2063-2071, 1985.

Weissman, J., and Efferding, L.E., Suspension of Slurries by Mechanical Mixers, J. Amer. Inst. Chem. Eng., Vol. 6, (419), 1960.

Westerterp, K.R., van Dierendonck, L.L., and De Kraa, J.A., Interfacial Areas in Agitated Gas-Liquid Contactors, Chem. Eng. Sci., Vol. 18, pp. 157-176, 1963.

Wiedmann, J.A., Steiff, A., and Weinspach, P.M., Experimental Investigations of Suspension, Dispersion, Power, Gas Holdup and Flooding Characteristics in Stirred Gas-Liquid-Solid Systems (Slurry Reactors), Chem. Eng. Commun., Vol. 6, (245), 1980.

Willemse, J. and Gruenewal, T., Geology of Bushveld Igneous Complex Largest Repository of Magmatic Ore-Deposits in the World, 1969, quoted in Hochreiter, *et al.*, 1985.

Wills, B.A., Mineral Processing Technology, (3rd ed.), Pergamon Press, Oxford, 1988.

Woodburn, E.T., King, R.P., and Colburn, R.P., The Effect of Particle Size Distribution on the Performance of a Phosphate Flotation Process, Metall. Trans., Vol. 2, pp. 3163-3174, 1971.

Young, P., Flotation Machines, Mining Magazine, pp. 35-59, January, 1982.

Zundelevich, Y., Power Consumption and Gas Capacity of Self-Inducting Turbo Aerators, Amer. Inst. Chem. Eng. J., Vol. 25, (763), 1979.

Zwietereng, Th.N., Suspension of Solid Particles in Liquid by Agitators, Chem. Eng. Sci., Vol. 8, pp. 244-253, 1958.

APPENDIX A

CLASSIFICATION OF FLOTATION COLLECTORS

There are different types of reagents used in flotation. Prominent among these are collectors which have already been discussed in section 2.1.1.1. Collectors are classified according to their functional groups. Such a classification is shown in Figure A1 below.

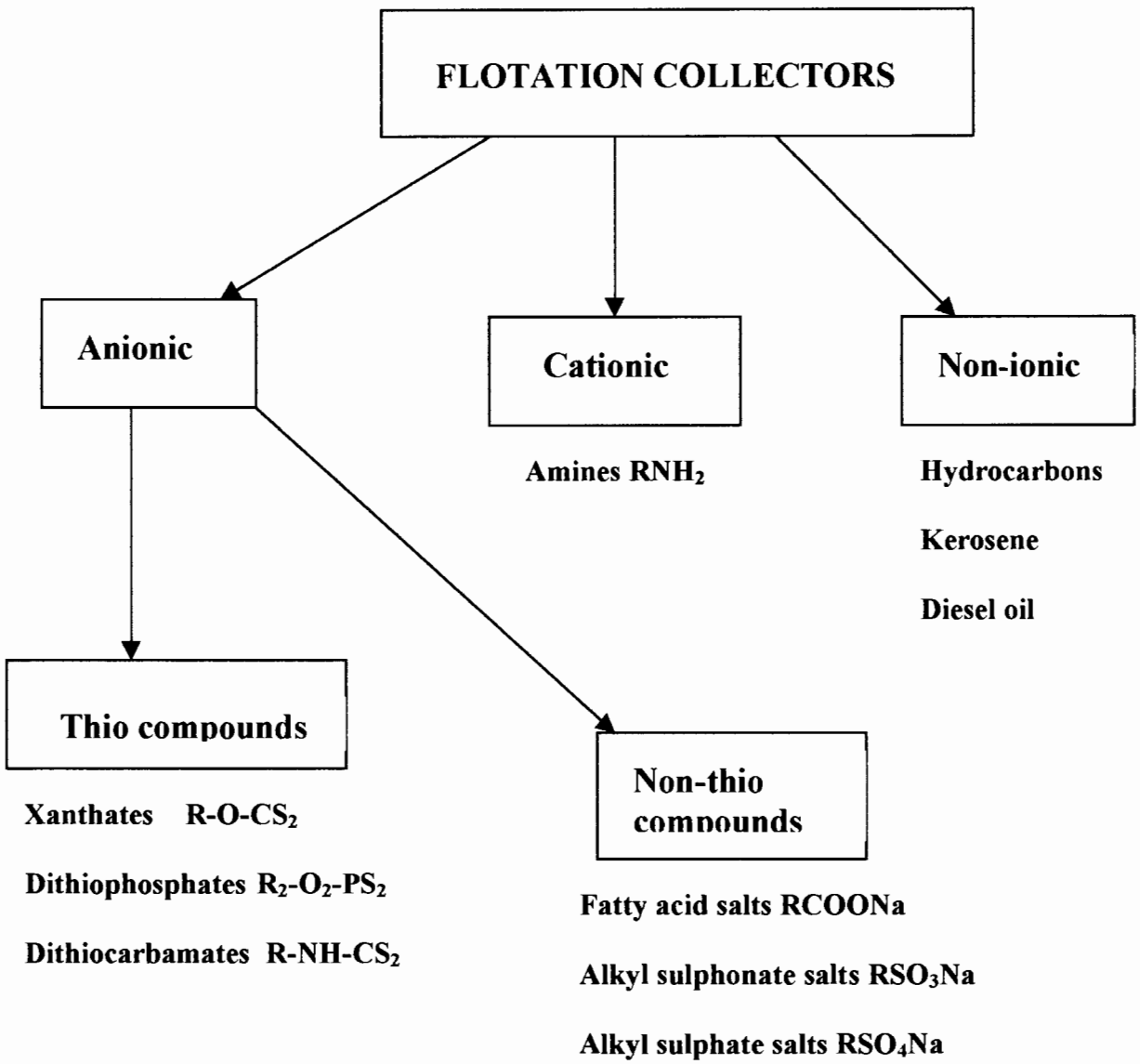

Figure A1: Classification of flotation collectors.

APPENDIX B

SUSPENSION HEIGHT

The constants of the suspension height correlation in equation (25) are shown in Table B1 below (from Arbiter, *et al.*, 1969) for different types of flotation cells.

Table B1: Suspension Height Correlation Data.

Machine	Range of Variables: Tank	T/D	C/D	Glass Spheres Mesh Size (Tyler)	Weight (gms)	Values of Constants in Correlating Eq. 25 $h/T = K[T/D]^a[C/D]^b[P/w]^e d^x$: K	a	b	e	x
Fagergren (manufacturer's impeller)	1	2.28	0.16-0.56	32 x 35	200- 800					
	2	3.08	0.16-0.56	32 x 35	400-1200					
	2	3.08	0.16-0.56	80 x 100	400-1600	21.0×10^{-2}	0	0.20	0.30	-0.18
	2	3.08	0.16-0.56	170 x 200	800-1200					
	2	3.08	0.16-0.56	325 x 400	800					
Denver	2	1.64	0.16-0.56	32 x 35	400-2000					
	2	1.64	0.16-0.56	80 x 100	800-1200	9.1×10^{-2}	0.20	0.30	0.38	-0.30
	3	2.17	0.16-0.46	32 x 35	800-3200					
Agitair (small) (round post impeller) (small)	1	2.07	0.16-0.56	32 x 35	200- 800					
(small)	2	2.80	0.26-0.56	32 x 35	400-1600	1.35×10^{-2}	-0.31	0.40	0.48	-0.58
(small)	2	2.80	0.26-0.56	80 x 100	800-1200					
(large)	2	2.03	0.26-0.56	80 x 100	1200					
Agitair (small) (wedge post impeller) (small)	1	2.07	0.16-0.56	32 x 35	200- 800					
(small)	2	2.80	0.26-0.56	32 x 35	400-1600	3.7×10^{-2}	-0.55	0.30	0.43	-0.45
(small)	2	2.80	0.26-0.56	80 x 100	800-1200					
(large)	2	2.03	0.26-0.56	80 x 100	800					
Weissman and Efferding's data	Diam. 5.5-11.4 inches	2.3-3.1	−0.1-2	140 microns	105-700 gm/lit.	1.4	-0.48	—*	0.20	—†

*C/D = 0.5 (constant) †d = 140 μ (constant)

APPENDIX C

TABLES AND GRAPHS OF MEASURED PARAMETERS

Q_g= volumetric air flowrate, m^3/min; N= impeller speed,rpm; d_b= arithmetic mean bubble size, mm; d_S= Sauter mean bubble diameter, mm; Jg= superficial gas velocity, cm/s; εg= air holdup, %; t= time, s; V= volume of pulp, ml; M= mass of pulp, g; L= location; S_b= bubble surface area flux, $m^2/m^2/sec$.

Table C1: Physical measurements for WEMCO 144L cells along a rougher bank.

WEMCO 144L with 164 mechanism - Rougher cells									
Q_g	L	V	M	S.G.	Jg	εg	d_b	d_S	S_b
				cell1					
8.41	1	1700	2329	1.37	1.19	15	0.84	1.57	45.6
	2	1740	2333	1.34	1.35	13	1.08	1.75	46.2
	3	1710	2323	1.36	1.26	14.5	1.04	1.79	42.3
	4	1760	2380	1.35	1.35	12	0.84	1.63	49.6
	5	1780	2400	1.35	1.18	11	0.94	1.48	47.6
	6	1740	2324	1.34	1.38	13	1.02	1.64	50.5
				cell2					
8.67	2	1680	2215	1.32	1.54	16	1.39	1.68	54.9
	5	1745	2405	1.38	1.45	13	1.02	1.46	59.8
				cell3					
5.13	2	1740	2208	1.27	1.18	13	0.75	1.35	52.4
	5	1820	2422	1.33	1.09	9	0.83	1.31	49.9
				cell4					
6.93	2	1720	2206	1.28	1.28	14	0.79	1.37	56.2
	5	1720	2269	1.32	1.12	14	0.83	1.43	46.8
				cell5					
8.19	1	1750	2203	1.26	1.18	12.5	0.83	1.6	44.12
	2	1760	2207	1.25	1.43	12	0.89	1.54	55.66
	3	1760	2238	1.27	1.38	12	0.84	1.37	60.41
	4	1800	2367	1.32	1.21	10	0.94	1.59	45.51
	5	1780	2328	1.31	1.21	11	0.84	1.37	53.09
	6	1780	2334	1.31	1.23	11	0.9	1.46	50.58
				cell6					
5.59	2	1780	2391	1.34	1.14	11	0.79	1.31	52.34
	5	1820	2491	1.37	1.17	9	0.85	1.28	54.61
				cell7					
5.61	2	1800	2280	1.27	1.07	10	0.74	1.31	48.85
	5	1810	2340	1.29	0.98	9.5	0.67	1.41	41.68
				cell 8					
6.56	2	1760	2282	1.30	1.08	12	0.79	1.55	41.66
	5	1810	2387	1.32	1.13	9.5	0.86	1.43	47.28

Table C2: Physical measurements for WEMCO 144L cells scavenger cells.

WEMCO 144L - Scavenger cell									
Q_g	L	V	M	S.G.	Jg	εg	d_b	d_S	S_b
				cell 9					
10.21	1	1700	2127	1.25	1.75	15	1.15	1.81	58.01
	2	1720	2152	1.25	1.73	14	1.07	1.74	59.66
	3	1700	2164	1.27	1.64	15	0.93	1.57	62.68
	4	1780	2334	1.31	1.19	11	0.78	1.33	53.68
	5	1840	2462	1.34	1.14	8	0.86	1.32	51.82
	6	1800	2379	1.32	1.22	10	0.85	1.49	49.13
WEMCO 144L with 164 mechanism - Scavenger cell									
				cell 9					
6.97	1	1660	2075	1.25	1.49	17	0.74	1.12	79.82
	2	1720	2167	1.26	1.48	14	0.73	1.02	87.06
	3	1760	2235	1.27	1.48	12	0.72	1.02	87.06
	4	1700	2227	1.31	1.35	15	0.71	1.04	77.88
	5	1720	2253	1.31	1.3	14	0.74	1.02	76.47
	6	1740	2279	1.31	1.43	13	0.72	1.13	75.93

Table C3: Physical measurements for WEMCO 144D, 45 kW cell at different air flowrates.

WEMCO 144D (45 kW) - Primary rougher cell									
Q_g	L	V	M	S.G.	Jg	εg	d_b	d_S	S_b
7.72	1	1830	2219	1.21	2	8.5	1.42	1.74	68.97
	2	1830	2191	1.197	2	8.5	1.42	1.8	66.67
	3	1830	2227	1.217	2.05	8.5	1.52	1.89	65.08
	4	1840	2426	1.318	1.94	8	1.31	1.66	70.12
	5	1850	2454	1.326	1.88	7.5	1.24	1.54	73.25
	6	1800	2408	1.338	1.95	10	1.28	1.63	71.78
6.01	1	1860	2285	1.228	1.9	7	1.48	1.81	62.98
	2	1840	2230	1.212	1.92	8	1.48	1.81	63.65
	3	1810	2277	1.258	2.07	9.5	1.49	1.83	67.87
	4	1850	2480	1.341	1.98	7.5	1.38	1.68	70.71
	5	1820	2461	1.352	1.89	9	1.3	1.61	70.43
	6	1840	2509	1.364	1.88	8	1.83	1.72	65.58
5.66	1	1820	2289	1.258	2.22	9	1.54	1.85	72.00
	2	1860	2251	1.21	2.2	7	1.53	1.81	72.93
	3	1850	2272	1.228	2.2	7.5	1.63	1.94	68.04
	4	1810	2404	1.328	2.09	9.5	1.49	1.82	68.90
	5	1810	2398	1.325	2.03	9.5	1.37	1.68	72.50
	6	1790	2362	1.32	2	10.5	1.47	1.83	65.57
4.95	1	1830	2241	1.225	2.14	8.5	1.61	1.87	68.66
	2	1840	2243	1.219	2.12	8	1.54	1.81	70.28
	3	1800	2202	1.223	2.2	10	1.52	1.78	74.16
	4	1820	2398	1.318	1.95	9	1.43	1.7	68.82
	5	1840	2446	1.329	1.95	8	1.28	1.55	75.48
	6	1800	2344	1.302	1.79	10	1.25	1.52	70.66
3.97	1	1820	2192	1.204	1.45	9	0.93	1.25	69.60
	2	1820	2125	1.168	1.5	9	0.93	1.21	74.38
	3	1810	2177	1.203	1.5	9.5	1	1.42	63.38
	4	1800	2357	1.309	1.4	10	0.91	1.46	57.53
	5	1840	2469	1.342	1.43	8	0.91	1.27	67.56
	6	1790	2367	1.322	1.49	10.5	1.02	1.38	64.78

Table C4: Physical measurements for 16-m^3 WEMCO 144D 90 kW cell at different air flowrates.

WEMCO 144D (90 kW) - Primary rougher cell									
Q_g	L	V	M	S.G.	Jg	εg	d_b	d_s	S_b
14.57	1	1650	1949	1.181	2.1	17.5	1.03	1.63	77.30
	2	1650	1972	1.195	1.95	17.5	0.89	1.46	80.14
	3	1640	1950	1.189	2.14	18	0.9	1.5	85.60
	4	1600	2098	1.311	1.89	20	0.81	1.46	77.67
	5	1680	2189	1.3	1.77	16	0.81	1.35	78.67
	6	1630	2175	1.334	2	18.5	0.84	1.75	68.57
8.59	1	1680	1984	1.181	2.02	16	0.89	1.38	87.83
	2	1730	2037	1.177	1.98	13.5	0.93	1.48	80.27
	3	1680	1980	1.179	2.03	16	0.96	1.5	81.20
	4	1610	2113	1.312	1.88	19.5	0.85	1.35	83.56
	5	1670	2167	1.298	1.75	16.5	0.81	1.25	84.00
	6	1620	2201	1.359	1.94	19	0.91	1.41	82.55
7.97	1	1660	1980	1.193	1.95	17	0.92	1.43	81.82
	2	1720	1996	1.16	1.83	14	0.86	1.37	80.15
	3	1700	1996	1.174	1.97	15	0.94	1.64	72.07
	4	1650	2153	1.305	1.78	17.5	0.81	1.46	73.15
	5	1720	2259	1.313	1.73	14	0.82	1.46	71.10
	6	1660	2215	1.33	1.79	17	0.83	1.45	74.07
7.51	1	1650	1944	1.178	1.83	17.5	0.86	1.46	75.21
	2	1680	1959	1.166	1.75	16	0.8	1.3	80.77
	3	1660		1.199	1.98	17	0.8	1.4	84.86
	4	1730	2260	1.306	1.68	13.5	0.79	1.33	75.79
	5	1700	2208	1.299	1.59	15	0.66	1.27	75.12
	6	1660	2189	1.319	1.79	17	0.89	1.6	67.13
6.69	1	1720	2031	1.181	1.69	14	0.75	1.19	85.21
	2	1680	1977	1.177	1.71	16	0.73	1.27	80.79
	3	1700	2007	1.181	1.73	15	0.69	1.41	73.62
	4	1700	2204	1.296	1.56	15	0.73	1.42	65.92
	5	1700	2256	1.327	1.33	15	0.68	1.22	65.41
	6	1670	2207	1.322	1.57	16.5	0.74	1.31	71.91

Table C5: Physical measurements for WEMCO 144D (45 kW) cells along rougher banks.

WEMCO 144D - Primary rougher cells									
Q_g	L	V	M	S.G.	Jg	εg	d_b	d_S	S_b
				cell 1					
8.24	2	1780	2158	1.212	1.73	11	0.92	1.45	71.59
	5	1780	2377	1.335	1.51	11	0.93	1.42	63.80
				cell 3					
7.84	2	1780	2217	1.246	1.51	11	0.86	1.27	71.34
	5	1780	2342	1.316	1.33	11	0.71	1.07	74.58
				cell 8					
6.48	2	1740	2015	1.158	2	13	1.02	1.48	81.08
	5	1760	2227	1.265	1.75	12	0.95	1.46	71.92
WEMCO 144D - Secondary rougher cells									
Q_g	L	V	M	S.G.	Jg	εg	d_b	d_S	S_b
				cell 1					
8.80	2	1780	2164	1.264	1.06	15	0.84	1.27	50.08
				cell 3					
9.15	2	1600	1996	1.234	1.78	15	1.02	1.38	77.39
	5	1820	2287	1.259	1.46	13.5	1	1.34	65.37
				cell 5					
7.96	2	1800	2218	1.232	1.94	10	1.01	1.35	86.22
	5	1840	2274	1.236	0.61	8	0.87	1.2	30.50
				cell 6					
7.54	2	1770	2153	1.216	1.98	11.5	1.06	1.45	81.93
	5	1800	2225	1.236	1.95	10	0.95	1.38	84.78

Table C6: Physical measurements for WEMCO 84 cells along cleaner cell banks.

WEMCO 84 - Primary cleaner cells									
Q_g	L	V	M	S.G.	Jg	εg	d_b	d_S	S_b
				cell 1					
2.93	2	1580	1953	1.23	1.9	21	0.89	1.62	70.37
	5	1760	2107	1.23	1.32	12	0.65	1.04	76.15
				cell 4					
3.07	2	1580	1942	1.229	1.88	21	0.93	1.57	71.85
	5	1700	2084	1.226	1.14	15	0.66	1.11	61.62
				cell3 - Prim. recleaner					
4.07	2	1580	1916	1.213	0.35	21	0.93	1.62	12.96
	5	1980	2436	1.23	2.24	1	0.59	0.9	149.33
				cell 2 - Prim. final cleaner					
4.12	2	1470	1557	1.059	1.86	26.5	1	1.63	68.47
	5	1900	2045	1.076	0.56	5	0.5	1.12	30.00
				cell 2 - Sec. final cleaner					
2.96	2	1620	1697	1.048	2.26	19	1.23	1.77	76.61
	5	1860	1940	1.043	1.46	7	0.79	1.13	77.52
				cell 3- Sec. recleaner					
3.97	2	1700	2098	1.179	2.31	18	1.2	1.83	75.74
	5	1730	2178	1.228	1.28	11	0.67	1.18	65.06
				cell 2 - Sec. cleaner					
3.37	2	1700	2102	1.236	1.8	15	1	1.65	65.45
	5	1840	2307	1.254	1.12	6	0.6	1.43	46.99
				cell 4 - Sec. cleaner					
1.65	2	1600	1996	1.248	1.79	20	0.95	1.58	67.97
	5	1820	2287	1.257	1.09	9	0.6	1.41	46.38

Table C7: Physical measurements for Outokumpu 16-m^3 cell at different air flowrates.

OK 16-m^3 rougher cell									
Q_g	L	V	M	S.G.	Jg	εg	d_b	d_s	S_b
16.42	1	1850	2094	1.132	2.35	7.5	1.33	1.93	73.06
	2	1800	2047	1.137	2.28	10	1.21	1.92	71.25
	3	1880	2113	1.124	1.76	6	0.91	1.29	81.86
	4	1710	2112	1.235	1.86	14.5	1.13	1.76	63.41
	5	1700	2123	1.249	2	15	1.06	1.64	73.17
	6	1860	2118	1.139	1.6	7	0.86	1.28	75.00
14.78	1	1830	2072	1.132	2.4	8.5	1.18	1.7	84.71
	2	1780	2014	1.131	2.47	11	1.46	2.05	72.29
	3	1810	2003	1.107	2.02	9.5	0.95	1.33	91.13
	4	1730	2117	1.224	1.82	13.5	1.18	1.76	62.05
	5	1740	2080	1.195	2.16	13	1.17	1.72	75.35
	6	1770	2105	1.189	2.12	11.5	1.13	1.73	73.53
13.14	1	1840	2026	1.132	2	8	1.04	1.65	72.73
	2	1820	2015	1.137	2.07	9	1.17	1.69	73.49
	3	1800	2014	1.124	1.97	10	1.09	1.52	77.76
	4	1780	2184	1.235	1.78	11	1	1.53	69.80
	5	1770	2282	1.249	1.95	11.5	1.12	1.68	69.64
	6	1780	2206	1.139	1.88	11	0.88	1.45	77.79
10.95	1	1820	2029	1.132	1.85	9	1.13	1.66	66.87
	2	1780	1989	1.137	2.12	11	1.24	1.84	69.13
	3	1840	2011	1.124	2.07	8	0.93	1.57	79.11
	4	1740	2111	1.235	1.68	13	1.02	1.53	65.88
	5	1750	2140	1.249	1.89	12.5	1.02	1.6	70.88
	6	1750	2135	1.139	1.8	12.5	1.12	1.67	64.67
9.85	1	1820	2045	1.124	1.83	9	1.03	1.62	67.78
	2	1780	1990	1.118	2.02	11	1.18	1.75	69.26
	3	1800	2040	1.133	1.89	10	1.02	1.58	71.77
	4	1750	2325	1.329	1.71	12.5	1	1.47	69.80
	5	1750	2455	1.403	1.76	12.5	1.02	1.53	69.02
	6	1760	2348	1.334	1.79	12	0.91	1.47	73.06

Table C8: Physical measurements for Outokumpu 16-m^3 cells in a circuit.

Q_g	L	V	M	S.G.	Jg	εg	d_b	d_s	S_b
OK 16 m^3 Primary rougher cells									
				cell 1					
7.66	2	1920	2169	1.13	1.76	4	1.51	1.96	53.88
	5	1880	2391	1.27	2.33	6	1.34	1.84	75.98
				cell 4					
>17	2	1650	1995	1.209	2.76	17.5	1.91	2.63	62.97
	5	1640	2187	1.334	2.42	18	1.58	2.21	65.70
				cell 6					
>17	2	1720	2061	1.198	2.61	14	1.86	2.4	65.25
	5	1630	2175	1.334	2.76	18.5	1.61	2.21	74.93
				cell 7					
>17	2	1710	1987	1.162	2.47	14.5	1.62	2.12	69.91
	5	1600	2132	1.331	2.14	20	1.48	2.06	62.33
OK 16 m^3 - Secondary rougher cells									
				cell 3					
10.95	2	1720	2035	1.183	2.09	14	1.06	1.62	77.41
	5	1650	2168	1.314	1.92	17.5	1.06	1.72	66.98
				cell 4					
>17	2	1650	2030	1.23	2.26	17.5	1.24	1.94	69.90
	5	1740	2264	1.3	2.16	13	1.07	1.55	83.61
				cell 6					
15.32	2	1780	2061	1.158	1.82	11	0.86	1.6	68.25
	5	1770	2222	1.255	1.69	11.5	0.92	1.47	68.98
				cell 7					
9.3	2	1720	2003	1.165	1.85	14	0.91	1.49	74.50
	5	1750	2171	1.241	1.88	12.5	0.94	1.61	70.06

Table C9: Physical measurements for WEMCO 120 cells in a cleaning circuit.

Q_g	L	V	M	S.G.	εg	Jg	d_b	d_s	S_b
WEMCO 120 - Final Cleaner cells									
				cell 1					
8.96	1	1310	1374	1.05	34.5	1.82	0.93	1.72	63.42
	2	1270	1318	1.04	36.5	2.07	1.12	1.91	64.99
	3	1310	1361	1.04	34.5	1.86	0.90	1.82	61.33
	4	1400	1472	1.05	30	1.51	0.98	1.59	56.96
	5	1380	1431	1.04	31	2.18	1.24	2.13	61.46
	6	1460	1527	1.05	27	1.38	0.98	1.56	53.05
				cell 2					
6.39	2	1360	1423	1.05	32	1.59	0.88	1.67	57.10
	5	1860	1953	1.05	7	1.20	0.68	1.19	60.50

Table C10: Physical measurements for WEMCO 120 cells in a cleaning circuit.

WEMCO 120 Primary cleaner cells									
Q_g	L	V	M	S.G.	εg	Jg	d_b	d_s	S_b
				cell 1					
6.50	1	1480	1562	1.06	26	1.63	1.02	1.77	55.34
	2	1520	1622	1.07	24	1.78	0.93	2.16	49.38
	3	1530	1619	1.06	23.5	1.20	0.81	1.33	54.14
	4	1720	1836	1.07	14	1.30	0.71	1.46	53.60
	5	1800	1897	1.05	10	1.27	0.85	1.46	52.19
	6	1780	1895	1.06	11	1.06	0.8	1.31	48.64
				cell 2					
8.75	2	1480	1564	1.06	26	2.16	1.2	2.08	62.37
	5	1960	2065	1.05	2	1.47	0.91	1.55	57.00
				cell 3					
8.60	2	1400	1486	1.06	30	2.14	1.15	2.17	59.25
	5	1910	2018	1.06	4.5	1.32	0.77	1.75	45.21

Table C11: Physical measurements for Outokumpu 50-m^3 TankCells.

OK 50 m^3 TankCells									
Qg	N	t	V	M	S.G.	εg	Jg	d_s	S_b
Free-flow									
2	105	181	1940	2470	1.27	3	0.66	1.21	32.88
2.5		147	1880	2368	1.26	6	0.82	1.23	39.82
3		124	1880	2310	1.23	6	0.97	1.58	36.75
3.5		82.5	1850	2275	1.23	7.5	1.45	1.61	54.21
4		89	1900	2144	1.13	5	1.35	1.65	49.03
Multi-mix									
2	130	180.5	1840	2358	1.28	8	0.66	1.2	33.24
2.5		158.5	1820	2245	1.23	9	0.76	1.22	37.23
3		143	1840	2171	1.18	8	0.84	1.55	32.48
3.5		138	1800	2201	1.22	10	0.87	1.52	34.32
4		130	1800	2130	1.18	10	0.92	1.56	35.50

Table C12: Physical measurements for WEMCO (10-m^3) unit cell in a cleaning circuit.

WEMCO 10-m^3 unit cell									
Q_g	L	V	M	S.G.	εg	Jg	d_b	d_s	S_b
5.25	1	1620	1843	1.14	19	2.03	1.27	1.88	64.79
	2	1570	1782	1.14	21	2.14	1.36	1.87	68.66
	3	1590	1824	1.15	20	2.02	1.26	1.92	63.13
	4	1600	1845	1.15	20	1.53	0.7	1.39	66.04
	5	1640	1880	1.15	18	1.52	0.79	1.54	59.22
	6	1620	1876	1.16	19	1.48	0.77	1.52	58.42

Table C13: Physical measurements for Bateman (BQ30) cell in a cleaning circuit.

Bateman cell-3-m^3									
Q_g	L	V	M	S.G.	εg	Jg	d_b	d_s	S_b
1.3	2	1680	2008	1.2	16	2.22	1.29	2.1	63.43
	5	1700	2012	1.18	15	1.05	0.98	1.71	40.84

The additional notations used in Tables C14 - C18 are as follows;

P/V= power consumption per the total cell volume, kW/m^3; P/V_I= power consumption per impeller swept volume, kW/m^3; a= bubble surface area per unit volume of pulp, mm^{-1}; H= froth height, mm;

Table C14: Average cell physical measurements at different air flowrates.

Cell Desc.	N	Q_g	S_b	P/V	P/V_I	H	d_s	Jg	εg	a
WEMCO	220	6.69	73.81	6.13	434.3	300	1.3	1.6	15	0.69
(90 kW)		7.97	75.39	5.75	407.2	250	1.47	1.84	16	0.65
		8.59	83.23	5.64	399.4	250	1.4	1.93	17	0.73
		14.57	77.99	5.48	387.8	260	1.53	1.98	18	0.71
WEMCO	172	3.97	66.21	4.05	287	250	1.33	1.46	9	0.41
(45 kW)		4.95	71.34	3.95	279.2	245	1.71	2.03	9	0.32
		5.66	69.99	4	283.1	230	1.82	2.14	9	0.3
		6.01	66.87	3.94	279.2	195	1.74	1.98	8	0.28
		7.72	69.31	3.83	271.4	210	1.71	1.97	9	0.32
OK	160	9.85	70.11	2.57	346.1	230	1.57	1.83	11	0.42
$16m^3$		10.98	69.42	2.46	331.4	230	1.65	1.9	11	0.4
		13.14	73.54	2.25	302	210	1.59	1.94	10	0.38
		14.78	76.51	1.97	265.1	210	1.7	2.17	11	0.39
		16.42	72.96	1.92	257.8	210	1.64	1.98	10	0.37

Table C15: Average cell physical measurements for WEMCO 84 cells in a cleaner and recleaner circuit.

WEMCO 84 cleaner and recleaner cells								
cell type	N	Q_g	εg	d_s	Jg	S_b	P/V	H
PC1	310	2.93	17	1.33	1.61	73	2.58	210
PC4	310	3.07	18	1.34	1.51	67	2.58	210
PR3	310	4.07	21	1.26	1.3	78	2.58	230
PF2	310	4.12	26	1.38	1.21	68	2.58	260
SF2	310	2.96	19	1.45	1.86	77	2.37	250
SR3	310	3.97	18	1.51	1.8	70	2.37	120
SC2	310	3.37	15	1.54	1.46	56	2.47	120
SC4	310	1.65	14	1.5	1.44	57	2.47	150

Table C16: Average physical measurements for WEMCO 144D cells in a rougher circuit.

WEMCO 144D rougher cells								
cell type	N	Q_g	εg	d_s	Jg	S_b	P/V	H
PR1	172	8.24	11	1.44	1.62	68	3.62	240
PR3	172	7.84	11	1.17	1.42	73	3.29	250
PR8	172	6.48	13	1.47	1.88	77	3.12	300
SR1	172	8.8	15	1.27	1.06	50	3.40	210
SR3	172	9.15	14	1.36	1.62	71	3.23	220
SR5	172	7.96	9	1.28	1.28	58	3.62	210
SR6	172	7.54	11	1.42	1.97	83	3.29	210

Table C17: Average physical measurements for Outokumpu cells in a rougher circuit.

OK 16-m^3 cells								
cell type	**N**	**Q_g**	**εg**	**d_s**	**Jg**	**S_b**	**P/V**	**H**
OP1	160	7.66	5	1.9	2.05	65	2.79	480
OP4	160	>18	18	2.42	2.59	64	1.75	300
OP6	160	>18	16	2.31	2.69	70	2.36	250
OP7	160	>18	17	2.09	2.31	66	2.03	250
OS3	160	>18	16	1.67	2.01	72	2.41	250
OS4	160	>18	15	1.75	2.21	77	2.03	280
OS6	160	15.32	11	1.54	1.76	69	2.74	250
OS7	160	9.3	13	1.55	1.87	72	2.19	260

Table C18: Average physical measurements for different types, sizes and duties of cell in a concentrator.

cell type	**N**	**Q_g**	**εg**	**d_s**	**Jg**	**Sb**	**P/V**	**H**
BC	220	1.3	16	1.82	1.62	52	3.07	370
FC1	220	8.96	32	1.82	1.8	59	1.84	n.m.
FC2	220	6.39	20	1.43	1.4	59	2.06	n.m.
PC1	220	n.m.	18	1.6	1.37	52	2.17	n.m.
PC2	220	8.75	26	1.82	1.82	60	2.06	n.m.
SC	220	8.6	30	1.96	1.73	52	2.06	n.m.
UC	220	5.25	20	1.7	1.67	63	10.52	n.m.
PR1	170	8.41	13	1.64	1.28	47	3.34	198
PR2	170	8.67	15	1.57	1.25	57	3.01	203
PR3	170	5.13	11	1.33	1.14	51	2.79	217
PR4	170	6.93	14	1.4	1.15	51	3.01	210
SR5	170	8.19	11	1.49	1.2	51	2.90	257
SR6	170	5.59	10	1.3	1.16	54	2.96	257
SR7	170	5.61	10	1.37	1.03	45	3.12	248
SR8	170	6.56	11	1.49	1.11	45	3.12	268
PS9	210	10.21	12	1.55	1.45	56	n.m.	250
FTC	105	3.5	7	1.61	1.25	54	1.35	412
MTC	131	3.5	10	1.52	0.87	34	1.89	463

Bubble diameter correlations

Tables C22-C24 contain mean bubble and Sauter mean bubble diameters, d_b and d_s respectively, for some specified cells as measured in the experimental campaign. In each case, the mean bubble diameter was obtained from the UCT bubble sizer computer program while the Sauter mean diameter was calculated using equation 44.

Figures C1 and C2 show plots of the correlations between d_S and d_b for the WEMCO cells and other types. Generally, not a very good correlation was found between d_S and d_b (R^2 = 0.8). From these graphs, it may be inferred that d_S is about 1.5 times d_b.

Table C19: Comparison between Sauter and arithmetic mean bubble diameters at different locations in WEMCO 144D (90 kW) flotation cell at different air flowrates.

WEMCO 144 (90 kW)									
Qg	Location	Run1		Run2		Run3		Mean	
		d_b	d_S	db	ds	db	ds	db	ds
14.57	1	1.05	1.63	1.04	1.63	0.99	1.63	1.03	1.63
	2	0.93	1.52	0.88	1.36	0.86	1.49	0.89	1.46
	3	0.82	1.38	0.90	1.47	0.97	1.64	0.90	1.50
	4	0.81	1.42	0.74	1.46	0.88	1.49	0.81	1.46
	5	0.81	1.23	0.85	1.38	0.77	1.43	0.81	1.35
	6	n.m.	n.m.	0.98	1.59	0.89	1.59	0.94	1.59
8.59	1	0.9	1.4	0.89	1.37	0.89	1.37	0.89	1.38
	2	0.88	1.39	0.95	1.44	0.95	1.6	0.93	1.48
	3	0.84	1.34	1.03	1.56	1.01	1.59	0.96	1.5
	4	0.78	1.3	0.91	1.41	0.86	1.33	0.85	1.35
	5	0.81	1.21	0.84	1.29	0.79	1.29	0.81	1.25
	6	0.91	1.48	0.96	1.47	0.86	1.29	0.91	1.41
7.97	1	0.9	1.43	0.98	1.5	0.88	1.37	0.92	1.43
	2	0.86	1.3	0.81	1.33	0.9	1.47	0.86	1.37
	3	0.96	1.58	0.97	1.72	0.89	1.61	0.94	1.64
	4	0.78	1.46	0.83	1.47	0.81	1.44	0.81	1.46
	5	0.82	1.47	0.84	1.56	0.79	1.36	0.82	1.46
	6	0.79	1.31	0.85	1.56	0.85	1.47	0.83	1.45
7.51	1	0.81	1.42	0.91	1.57	0.85	1.39	0.86	1.46
	2	0.73	1.16	0.79	1.31	0.89	1.43	0.8	1.3
	3	0.63	1.25	0.92	1.53	0.85	1.42	0.8	1.4
	4	0.76	1.57	0.77	1.06	0.85	1.35	0.79	1.33
	5	0.64	1.17	0.59	1.4	0.74	1.24	0.66	1.27
	6	0.8	1.47	0.96	1.72	0.9	1.6	0.89	1.6
6.69	1	0.72	1.2	0.74	1.19	0.8	1.18	0.75	1.19
	2	0.72	1.36	0.73	1.21	0.73	1.23	0.73	1.27
	3	0.68	1.17	0.69	1.89	0.71	1.17	0.69	1.41
	4	0.86	1.38	0.76	1.27	0.58	1.6	0.73	1.42
	5	0.68	1.28	0.68	1.19	0.68	1.19	0.68	1.22
	6	0.73	1.16	0.77	1.35	0.73	1.42	0.74	1.31

Table C20: Comparison between Sauter and arithmetic mean bubble diameters at different locations in WEMCO 144D (45 kW) flotation cell at different air flowrates.

WEMCO 144 (45 kW)									
Qg	Location	Run1		Run2		Run3		Mean	
		db	ds	db	ds	db	ds	db	ds
3.97	1	0.95	1.23	0.94	1.3	0.91	1.22	0.93	1.25
	2	0.96	1.22	0.89	1.2	0.93	1.2	0.93	1.21
	3	1.01	1.44	0.99	1.4	1.01	1.43	1	1.42
	4	1.12	1.51	0.74	1.67	0.88	1.2	0.91	1.46
	5	0.92	1.2	0.86	1.34	0.94	1.28	0.91	1.27
	6	1.05	1.46	1.04	1.38	0.97	1.31	1.02	1.38
4.95	1	1.65	1.93	1.63	1.89	1.54	1.8	1.61	1.87
	2	1.59	1.83	1.54	1.86	1.5	1.74	1.54	1.81
	3	1.63	1.89	1.51	1.76	1.42	1.7	1.52	1.78
	4	1.37	1.66	1.5	1.76	1.42	1.69	1.43	1.7
	5	1.27	1.54	1.23	1.46	1.34	1.64	1.28	1.55
	6	1.27	1.55	1.26	1.51	1.22	1.5	1.25	1.52
5.66	1	1.53	1.87	1.53	1.86	1.55	1.81	1.54	1.85
	2	1.48	1.73	1.52	1.81	1.6	1.89	1.53	1.81
	3	1.62	1.99	1.6	1.85	1.68	1.97	1.63	1.94
	4	1.53	1.92	1.51	1.83	1.42	1.71	1.49	1.82
	5	1.46	1.8	1.4	1.69	1.26	1.54	1.37	1.68
	6	1.47	1.87	1.55	1.9	1.4	1.71	1.47	1.83
6.01	1	1.49	1.85	1.51	1.85	1.44	1.73	1.48	1.81
	2	1.45	1.78	1.54	1.88	1.44	1.77	1.48	1.81
	3	1.54	1.94	1.45	1.77	1.48	1.78	1.49	1.83
	4	1.32	1.62	1.46	1.78	1.35	1.64	1.38	1.68
	5	1.28	1.54	1.33	1.68	1.28	1.61	1.3	1.61
	6	1.36	1.7	1.4	1.75	1.38	1.7	1.83	1.72
7.72	1	1.42	1.73	1.43	1.74	1.4	1.75	1.42	1.74
	2	1.38	1.72	1.39	1.8	1.5	1.89	1.42	1.8
	3	1.48	1.86	1.55	1.93	1.52	1.88	1.52	1.89
	4	1.29	1.64	1.31	1.65	1.32	1.69	1.31	1.66
	5	1.27	1.58	1.26	1.56	1.18	1.48	1.24	1.54
	6	1.22	1.6	1.31	1.68	1.3	1.61	1.28	1.63

Table C21: Comparison between Sauter and arithmetic mean bubble diameters at different locations in Outokumpu 16-m^3 flotation cell at different air flowrates.

OK 16-m^3 cell									
Qg	Location	Run1		Run2		Run3		Mean	
		d_b	d_s	d_b	d_s	d_b	d_s	d_b	d_s
9.85	1	n.m.	n.m.	1.06	1.62	1	1.63	1.03	1.62
	2	1.11	1.63	n.m.	n.m.	1.25	1.86	1.18	1.75
	3	0.96	1.5	1.01	1.6	1.08	1.64	1.02	1.58
	4	1.06	1.55	0.98	1.42	0.97	1.44	1	1.47
	5	1.03	1.53	0.99	1.53	1.04	1.53	1.02	1.53
	6	0.91	1.4	0.97	1.48	0.86	1.54	0.91	1.47
10.95	1	1.19	1.65	1.11	1.67	1.09	1.67	1.13	1.66
	2	1.14	1.75	1.26	1.82	1.33	1.94	1.24	1.84
	3	0.92	1.77	0.94	1.37	n.m.	n.m.	0.93	1.57
	4	1.02	1.51	1	1.59	1.04	1.5	1.02	1.53
	5	1.05	1.66	1.07	1.69	0.95	1.44	1.02	1.6
	6	1.13	1.6	1.11	1.74	n.m.	n.m.	1.12	1.67
13.14	1	0.98	1.54	1.08	1.7	1.07	1.7	1.04	1.65
	2	n.m.	n.m.	1.16	1.67	1.18	1.71	1.17	1.69
	3	1.02	1.39	1.04	1.44	1.2	1.72	1.09	1.52
	4	0.99	1.5	1.01	1.54	1	1.55	1	1.53
	5	1.04	1.54	1.15	1.76	1.17	1.74	1.12	1.68
	6	0.89	1.27	0.93	1.4	0.83	1.69	0.88	1.45
14.78	1	1.18	1.84	1.4	2.01	1.42	1.93	1.33	1.93
	2	1.16	1.92	n.m.	n.m.	1.26	1.91	1.21	1.92
	3	0.9	1.1	0.87	1.36	0.97	1.42	0.91	1.29
	4	1.17	1.87	1.12	1.7	1.11	1.71	1.13	1.76
	5	1.05	1.68	1.04	1.56	1.08	1.68	1.06	1.64
	6	0.89	1.23	0.83	1.38	0.87	1.24	0.86	1.28
16.42	1	1.33	1.93	1.23	1.7	0.98	1.47	1.18	1.7
	2	1.21	1.92	1.47	1.99	1.7	2.24	1.46	2.05
	3	0.91	1.29	0.96	1.3	0.98	1.4	0.95	1.33
	4	1.13	1.73	1.2	1.82	1.21	1.73	1.18	1.76
	5	1.06	1.64	1.05	1.5	1.4	2.02	1.17	1.72
	6	0.86	1.28	1.11	1.88	1.12	2.03	1.03	1.73

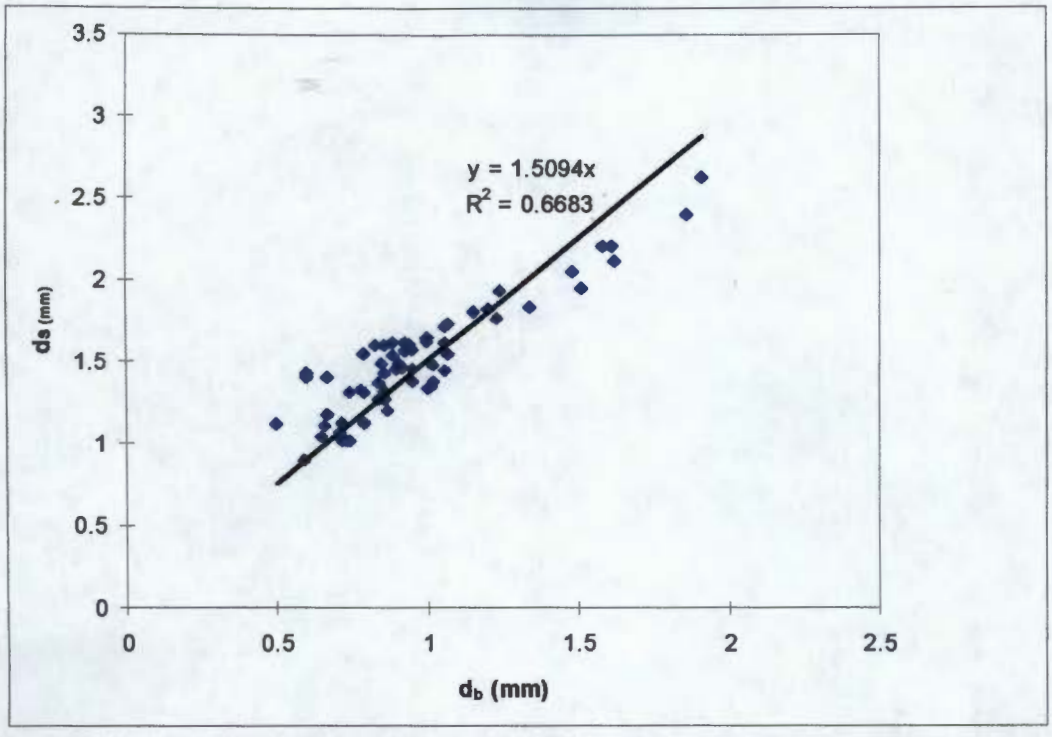

Figure C1: Sauter (d_S) and arithmetic mean (d_b) bubble diameter correlations for different sizes of WEMCO flotation cells.

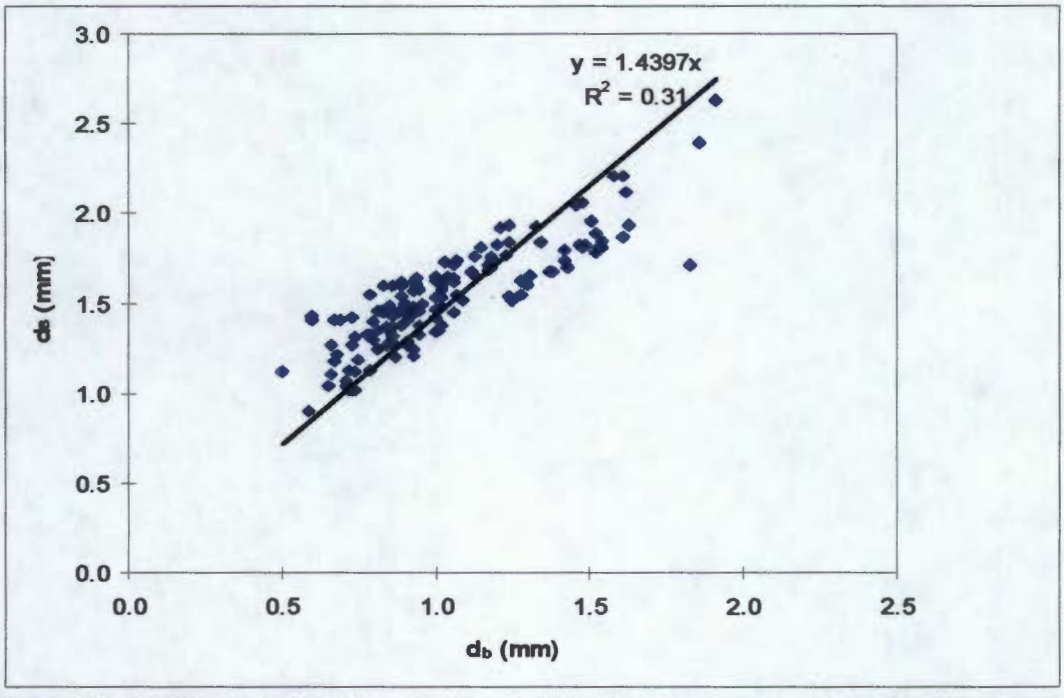

Figure C2: Sauter (d_S) and arithmetic mean bubble diameter (d_b) correlation for different sizes and types of flotation cells.

Reproducibility of bubble size measurement

Table C22 shows the repeatability of bubble size measurements for some selected cells.

Table C22: Reproducibility data for the UCT Bubble Size Analyser.

Description			Sauter mean bubble diameter			
	Cell	Location	Run1	Run2	Run3	S.D
WEMCO 120 (8.5-m^3)	Cell1	1	1.79	1.77	1.75	0.02
Primary cleaner		2	1.63	1.68	1.65	0.03
		3	1.31	1.34	1.34	0.02
		4	1.17	1.5	1.71	0.27
		5	1.27	1.43	1.69	0.21
		6	1.14	1.41	1.38	0.15
	Cell 2	2	2.12	2.07	2.05	0.04
		5	1.59	1.5	1.56	0.05
	Cell 3	2	2.12	2.49	1.91	0.29
		5	1.43	2.31	1.51	0.49
WEMCO 144 (16 m^3)	Cell 5	1	1.53	1.52	1.74	0.12
Secondary rougher		2	1.68	1.43	1.51	0.13
		3	1.29	1.35	1.46	0.09
		4	1.69	1.59	1.5	0.10
		5	1.36	1.35	1.41	0.03
		6	1.33	1.57	1.47	0.12
	Cell 6	2	1.27	1.26	1.4	0.08
		5	1.22	1.32	1.31	0.06
	Cell 7	2	1.47	1.29	1.16	0.16
		5	1.27	1.62	1.35	0.18
	Cell 8	2	1.37	1.49	1.79	0.22
		5	1.44	1.39	1.45	0.03
WEMCO 164 (16 m^3)	cell 1	1	1.51	1.45	1.76	0.16
Primary rougher		2	1.66	1.79	1.8	0.08
		3	1.83	1.85	1.7	0.08
		4	1.35	1.85	1.7	0.26
		5	1.54	1.67	1.24	0.22
		6	1.71	1.59	1.63	0.06
	cell 2	2	1.49	1.74	1.81	0.17
		5	1.45	1.45	1.47	0.01
	cell 3	2	1.37	1.44	1.23	0.11
		5	1.27	1.2	1.47	0.14
	cell 4	2	1.31	1.41	1.4	0.06
		5	1.3	1.65	1.35	0.19
WEMCO 10 m^3 unit cell		1	1.94	1.98	1.73	0.13
		2	1.8	1.84	1.96	0.08
		3	1.97	2.07	1.72	0.18
		4	1.39	1.51	1.28	0.12
		5	1.53	1.46	1.62	0.08
		6	1.53	1.46	1.58	0.06
WEMCO 144L (16 m^3)	cell 9	1	1.69	2.01	1.74	0.17
Scavenger		2	1.84	1.62	1.75	0.11
		3	1.51	1.64	1.55	0.07
		4	1.18	1.31	1.49	0.16
		5	1.29	1.34	1.32	0.03
		6	1.53	1.53	1.42	0.06

Reproducibility of superficial gas velocity measurements

Tables C23-C25 show the repeatability of Jg in WEMCO 144 and OK 16 m^3 cells. In each case, the two measurements are close to one another.

The following notation applies to Tables C23-C25;

Qg=air flowrate, m^3/min; t1=time for test 1, s; t2=time for test 2, s; Jg1=superficial gas velocity based on t1, cm/s; Jg2=superficial gas velocity based on t2, s; R.E.=Relative Error between Jg1 and Jg2, mm.

Table C23: Reproducibility of superficial gas velocity measurements for WEMCO 144 (90 kW) cell.

Q_g	Location	t1	t2	Jg1	Jg2	R.E.
6.69	1	57	57	2.11	2.11	0.00
	2	63	60	1.90	2.00	0.07
	3	56	56	2.14	2.14	0.00
	4	62	65	1.94	1.85	0.06
	5	67	68	1.79	1.76	0.02
	6	59	61	2.03	1.97	0.05
7.51	1	59	60	2.03	2.00	0.02
	2	61	61	1.97	1.97	0.00
	3	57	61	2.11	1.97	0.10
	4	64	64	1.88	1.88	0.00
	5	68	69	1.76	1.74	0.02
	6	63	61	1.90	1.97	0.04
7.97	1	62	61	1.94	1.97	0.02
	2	65	66	1.85	1.82	0.02
	3	61	61	1.97	1.97	0.00
	4	66	69	1.82	1.74	0.06
	5	69	70	1.74	1.71	0.02
	6	66	68	1.82	1.76	0.04
8.59	1	64	67	1.88	1.79	0.06
	2	69	68	1.74	1.76	0.02
	3	62	59	1.94	2.03	0.07
	4	70	73	1.71	1.64	0.05
	5	76	77	1.58	1.56	0.01
	6	67	67	1.79	1.79	0.00
14.57	1	71	71	1.69	1.69	0.00
	2	69	71	1.74	1.69	0.03
	3	71	68	1.69	1.76	0.05
	4	76	78	1.58	1.54	0.03
	5	89	91	1.35	1.32	0.02
	6	75	78	1.60	1.54	0.04

Table C24: Reproducibility of superficial gas velocity measurements for WEMCO 144 (45 kW) cell.

Q_g	Location	t1	t2	Jg1	Jg2	R.E..
3.97	1	84	82	1.43	1.46	0.02
	2	80	80	1.50	1.50	0.00
	3	80	80	1.50	1.50	0.00
	4	86	86	1.40	1.40	0.00
	5	84	84	1.43	1.43	0.00
	6	81	80	1.48	1.50	0.01
4.95	1	56	56	2.14	2.14	0.00
	2	57	56	2.11	2.14	0.03
	3	53	56	2.26	2.14	0.09
	4	61	62	1.97	1.94	0.02
	5	61	62	1.97	1.94	0.02
	6	70	64	1.71	1.88	0.11
6.01	1	63	63	1.90	1.90	0.00
	2	63	62	1.90	1.94	0.02
	3	58	58	2.07	2.07	0.00
	4	60	61	2.00	1.97	0.02
	5	64	63	1.88	1.90	0.02
	6	63	65	1.90	1.85	0.04
7.72	1	60	60	2.00	2.00	0.00
	2	60	60	2.00	2.00	0.00
	3	59	58	2.03	2.07	0.02
	4	62	62	1.94	1.94	0.00
	5	64	64	1.88	1.88	0.00
	6	62	61	1.94	1.97	0.02

Table C25: Reproducibility of superficial gas velocity measurements for OK 16-m^3 conventional cell.

Q_g	Location	t1	t2	Jg1	Jg2	R.E.
9.85	1	64	67	1.88	1.79	0.06
	2	60	59	2.00	2.03	0.02
	3	64	63	1.88	1.90	0.02
	4	71	69	1.69	1.74	0.03
	5	66	70	1.82	1.71	0.07
	6	66	68	1.82	1.76	0.04
10.95	1	65	65	1.85	1.85	0.00
	2	57	56	2.11	2.14	0.03
	3	58	58	2.07	2.07	0.00
	4	73	70	1.64	1.71	0.05
	5	64	63	1.88	1.90	0.02
	6	68	65	1.76	1.85	0.06
13.14	1	60	60	2.00	2.00	0.00
	2	59	57	2.03	2.11	0.05
	3	63	62	1.90	1.94	0.02
	4	68	67	1.76	1.79	0.02
	5	62	61	1.94	1.97	0.02
	6	64	64	1.88	1.88	0.00
14.78	1	50	52	2.40	2.31	0.07
	2	52	53	2.31	2.26	0.03
	3	66	70	1.82	1.71	0.07
	4	65	64	1.85	1.88	0.02
	5	59	61	2.03	1.97	0.05
	6	76	74	1.58	1.62	0.03
16.42	1	51	49	2.35	2.45	0.07
	2	49	48	2.45	2.50	0.04
	3	59	60	2.03	2.00	0.02
	4	67	65	1.79	1.85	0.04
	5	57	56	2.11	2.14	0.03
	6	57	56	2.11	2.14	0.03

APPENDIX D

DEFINITIONS AND DERIVATIONS

a. BUBBLE SURFACE AREA FLUX:

From Jameson (1984),

$$S_b = \frac{a * Jg}{\varepsilon_g} \tag{39}$$

where , $$a = \frac{\sum_i^n \pi d_i}{V_L} \tag{40}$$

and

$$\varepsilon_g = \frac{\sum_i^n \pi d_i^3}{6V_L} \tag{41}$$

The Sauter mean bubble diameter, d_S, is given by;

$$d_S = 6\frac{\sum_i^n \frac{\pi}{6} d_i^3}{\sum_i^n \pi d_i^2} = 6\frac{V_L}{S} \tag{42}$$

where, S_b=bubble surface area flux $m^2/m^2/sec$

Jg=superficial gas velocity (cm/s),

ε_g =air holdup (% v/v),

a=bubble surface area per unit volume of pulp (V), mm^{-1} and

S=total bubble surface area, mm^2

The Sauter mean bubble diameter under Tables and graphs was calculated from equation (42) by using V_L and S values from the UCT Bubble Size Analyser programme summary sheet.

Combining the above equations (39)-(42),

$$S_b = \frac{\sum_i^n \pi d_i^2 * Jg}{\sum_i^n \frac{\pi}{6} d_i^3} = \frac{6 * Jg}{d_s} \qquad (43)$$

S_b was calculated from the experimental data using equation (43) above.

b. SUPERFICIAL GAS VELOCITY:

The superficial gas velocity, Jg, is defined as the volumetric air flowrate per unit cross sectional area of the cell. With the measuring equipment described in Chapter 4, Jg was measured and calculated at the different locations in the cell as follows;

$$Jg = \frac{Q_g}{A_v} = \frac{V_a}{A_v t} = \frac{A_c H_c}{A_v t} \qquad (44)$$

where,

Q_g=air flowrate into the cell (m^3/min),

A_v=cross-sectional area of pinch valve (cm^2),

A_c=cross-sectional area of transparent graduated cylinder (cm^2), and

H_c=height of liquid displaced (cm) within a specified time, t (s).

c. AIR HOLDUP:

The calibrated volume of the measuring device for air holdup was 0.5 ml of water (see Chapter 4). Four volumes of the cylinder of pulp were captured from the flotation cells per measurement and the air holdup was determined from the relation below:

$$\varepsilon g = \frac{2 - V_d}{2} * 100\% \qquad (45)$$

where,

V_d=Volume of de-aerated pulp (ml).

APPENDIX E

POWER EQUATIONS

The power consumed by each cell was calculated from the current shown from the ammeters in each concentrator's motor control centre. Although, the current used in the power calculations was taken from the ammeters, a tong-test of the different phase cables indicated that the current draw were very close to that on the ammeter. A bulk power factor corrector used on both concentrators gave an average factor of 0.92. A brief explanation of industrial power calculation below is intended to enhance easy understanding of the process.

In direct current (d.c.) circuits power may be measured directly by a wattmeter, or by multiplying the readings of an ammeter and a voltmeter.

In alternating current (a.c.) circuits the instantaneous rate at which energy is supplied is equal to the product of the instantaneous voltage and the instantaneous current. Since both of these vary significantly, it is clear that the power consumption varies over each cycle and that some sort of average power must be taken. The average power supplied to any a.c. circuit is equal to the root mean square (rms) voltage times the rms current and multiplied by the cosine of the angle of lag (Golding, 1941);

$$P=VI\cos\varphi \qquad (46)$$

where, P=average power, w,
V=average voltage, v,
I=average current, A,
$\cos\varphi$ =power factor.

The derivation of equation 46 is as follows;

$$p=vi, \qquad (47)$$

where, p= instantaneous power, W,
v= instantaneous voltage, V, and
i= instantaneous current, amps.

Thus if both the current and the voltage waves are sinusoidal, the current lagging in phase by an angle φ, then

$$v= V_{max}Sin\omega t, \tag{48}$$

and

$$i= I_{max}Sin(\omega t-\varphi), \tag{49}$$

The instantaneous power, p, is therefore given by:

$$p= vi, \tag{50}$$

$$= V_{max}I_{max}Sin\omega tSin(\omega t-\varphi), \tag{51}$$

or, writing $\theta=\omega t$,

$$p= V_{max}I_{max}Sin\theta Sin(\theta-\varphi). \tag{52}$$

The mean power, P, is given by:

$$P= \frac{1}{2\pi}\int_0^{2\pi} V_{max}I_{max}Sin\theta Sin(\theta-\varphi)d\theta \tag{53}$$

$$=\frac{V_{max}I_{max}}{4\pi}\int_0^{2\pi} Cos\varphi - Cos(2\theta-\varphi)d\theta \tag{54}$$

$$=\frac{V_{max}I_{max}}{4\pi}\left[\theta Cos\varphi - \frac{Sin(2\theta-\varphi)}{2}\right]_0^{2\pi} \tag{55}$$

$$=\frac{V_{max}I_{max}}{2}Cos\varphi \tag{56}$$

$$=VICos\varphi \tag{57}$$

For a balanced, three-phase system connected either in a star or delta configuration as exist in industrial operations, the power is described by the equation:

$$P = \sqrt{3}VICos\varphi. \quad (58)$$

In this work, it was assumed that all three-phase systems were connected to balanced loads.

Power per total cell volume

Total power dissipation in the cell was calculated from the current shown on the ammeter of the drives and the voltage using equation (58) and the total volume of pulp in the cell. The voltage was assumed to be equal to the nominal line voltage.

$$P/V_p = \sqrt{3}VICos\varphi/V \quad (59)$$

where, V_p=Total volume of pulp in the cell, m^3.

Power per impeller-swept volume

The impeller-swept volume is the volume of the cylinder described by the impeller blade as it rotates and is given by

$$V_i = \pi D^2 W/4, \quad (60)$$

where, D=impeller diameter, m, and
W=impeller blade width, m.

The power per impeller-swept volume is therefore the power dissipated, assuming that all is dissipated in the volume occupied by the impeller described above, and given by

$$P/V_i = \sqrt{3}VICos\varphi/V_i \quad (61)$$

Table D1: Impeller swept volumes for different impellers.

Impeller Type	D, m	W, m	V_i, m^3
Bateman BQ30	0.488	0.314	0.059
WEMCO 84	0.406	0.406	0.053
WEMCO 144	0.660	0.660	0.226
WEMCO 164	0.762	0.762	0.347
WEMCO unit cell	0.762	0.762	0.347
Outokumpu 16-m^3	0.750	0.450	0.199
Outokumpu 50-m^3 (TankCells)	1.050	0.630	0.546

APPENDIX F

AIR FLOWRATE CALCULATIONS

Most Outokumpu cells have control valves for regulation of air. Here the flowrate was varied by adjusting the valve and measured with a hot-wire anemometer inserted, perpendicular to the direction of air, into a hole bored in the pipe. The anemometer fitted so well in the hole that any air losses was prevented.

Most WEMCO cells have an air pipe with an open end usually with no control valves. Here the linear flow velocity was measured with a vane anemometer placed to cover the entire surface of the orifice. The other different air flowrates were obtained by restricting the air flow to the cell with a flat plate and measuring the air velocities in the resultant orifices. The air velocities were noted in all cases and with a knowledge of the diameter of the pipe or the orifice, the air flowrates were calculated:

$$Q_g = V/60 * A, \quad (62)$$

$$= V/60 * \pi * D^2/4, \quad (63)$$

where, V= Velocity of air, m/s,

A=Cross-sectional area of pipe or orifice, m^2, and

D=diameter of pipe or orifice, m.

Table E1: Air flowrate data for the WEMCO 144 and OK 16-m^3 cells.

OK16-m3				
No.	D	A	V	Q_g
1	0.15	0.070686	15	16.42
2	0.15	0.070686	13.8	14.78
3	0.15	0.070686	12	13.14
4	0.15	0.070686	10	10.95
5	0.15	0.070686	9	9.85
WEMCO 144 (45 kW)				
No.	D	A	V	Q_g
1	0.1	0.031416	16.4	3.97
2	0.1	0.031416	12.8	4.95
3	0.1	0.031416	12	5.66
4	0.1	0.031416	10.5	6.01
5	0.1	0.031416	8.4	7.72

WEMCO 144 (90kW)				
No.	D	A	V	Q_g
1	0.13	0.053093	18.29	14.57
2	0.1	0.031416	18.22	8.59
3	0.1	0.031416	16.91	7.97
4	0.1	0.031416	15.93	7.51
5	0.1	0.031416	14.2	6.69